Snow Drought and Streamflow Drought in Western North America in the Context of a Warming Climate

by

Jennifer R. Dierauer

M.Sc., Southern Illinois University, 2011

B.Sc., Winona State University, 2009

Thesis Submitted in Partial Fulfillment of the
Requirements for the Degree of
Doctor of Philosophy

in the
Department of Earth Sciences
Faculty of Science

SIMON FRASER UNIVERSITY

Summer 2018

Approval

Name:	**Jennifer R. Dierauer**
Degree:	**Doctor of Philosophy**
Title:	***Snow Drought and Streamflow Drought in Western North America in the Context of a Warming Climate***
Examining Committee:	**Chair:** Doug Stead Professor
	Diana Allen Senior Supervisor Professor
	Paul Whitfield Supervisor Adjunct Professor
	Pascal Haegeli Internal Examiner Assistant Professor Department of Resource and Environmental Management
	Ulrich Strasser External Examiner Professor Department of Geography University of Innsbruck
Date Defended/Approved:	August 17, 2018

Abstract

In western North America, snowpack supplies much of the water used for irrigation and for municipal and industrial uses, and snowmelt recharges groundwater and provides ecosystem-sustaining baseflow during low flow periods. Continued climate warming is expected to have large impacts on snowmelt hydrology, with subsequent impacts on low flows and snow and streamflow drought regimes. This research combined two separate methodologies, a data-driven (downward) approach and a process-based (upward) approach, to improve our understanding of snow drought and streamflow drought in the context of a warming climate. The data-driven approach combined observed hydroclimatic time series with multiple statistical methods, including bivariate and partial correlation and temporal and spatial analogs. The process-based approach combined climate change projections and hydrological modelling.

The two approaches yielded consistent results that, together, illustrate that snow drought, low flows, and streamflow drought are sensitive to winter climate conditions, particularly precipitation and thawing degrees. In the context of climate warming, increased winter season thawing degrees leads to increased warm (temperature-driven) snow drought, shorter and less severe winter low flows, longer and more severe summer low flows, and increased summer streamflow drought risk. Further, both approaches showed that the response of snowmelt hydrology to climate warming is non-linear, and regions with winter temperatures near 0°C exhibit substantially larger impacts from +2°C of warming compared to regions with winter temperatures far below 0°C.

Temperature-driven shifts in snow drought, low flows, and streamflow drought regimes will have widespread implications for surface water supply security. Increased frequency of warm snow droughts will likely lead to an increased frequency of mid-winter melt events, which will create challenges for water management. As summer low flow periods become more severe and snow-drought related summer streamflow droughts become more frequent, the potential for more severe summer water shortages increases. The most severe shortages will likely occur due to the co-occurrence of warm and dry conditions.

Keywords: streamflow; snow; low flows; climate change; drought

For Laurel

Acknowledgements

First and foremost, I'd like to acknowledge and thank my senior supervisor, Dr. Diana Allen, and my committee member, Paul Whitfield. Their support and unwavering confidence in my abilities has meant so much to me. They provided the perfect balance of guidance and personal freedom.

This research was carried out with scholarship support from Simon Fraser University and through graduate fellowships from the Simon Fraser University Department of Earth Sciences and the Pacific Institute for Climate Solutions.

Finally, the completion of this thesis wouldn't have been possible without the support of my husband Tom, who always believes in me, encourages me, and pulls me back to reality when I start wandering away.

Table of Contents

Approval ii
Abstract iii
Dedication iv
Acknowledgements v
Table of Contents vi
List of Tables ix
List of Figures x

Chapter 1. Introduction 1
1.1. Background and Previous Research 3
1.1.1. Defining Drought 3
Snow drought 4
Hydrological drought 4
1.1.2. Climate Change Impacts on Snowmelt Hydrology 7
1.1.3. Approaches for Investigating Climate Change Impacts on Water Resources 8
Data-driven (downward) approach 8
Process-based (upward) approach 11
1.2. Purpose and Objectives 13
1.3. Scope of Work 13
1.4. Thesis Overview 14
1.5. Significant Contributions 18

Chapter 2. Climate Controls on Runoff and Low Flows in Mountain Catchments of Western North America 20
2.1. Introduction 20
2.2. Data and Methods 22
2.2.1. Streamflow Observations 22
2.2.2. Meteorological Data and Simulated Fluxes 24
2.2.3. Low Flow Regime Characterization 25
2.2.4. Predictor and Response Variables 26
2.2.5. Identification of Dominant Climate Controls 27
2.2.6. Precipitation and Temperature Sensitivity 29
2.3. Results 29
2.3.1. Low Flow Regime Characterization 30
2.3.2. Regional Analysis: Climate Controls on the Low Flow Regime 31
2.3.3. Catchment-scale Analysis: Climate Controls on Inter-annual Variability 33
Mean daily runoff (MDR) 35
Summer low flows 35
Winter low flows 35
2.3.4. Low Flow Sensitivity to Precipitation and Temperature 36
2.3.5. Winter Climate Impacts on SWE, Runoff, and Low Flows 37
2.4. Discussion 40

2.5. Conclusions 42

Chapter 3. Winter Temperature Controls on Snow Drought Risk in Western North America 44
3.1. Introduction 44
3.2. Materials and Methods 46
3.2.1. Data and Domain 46
3.2.2. Snow Drought Classification 47
3.2.3. Precipitation (P) Versus Temperature (T) Sensitivity 50
3.2.4. Temperature Thresholds and SWE Susceptibility Mapping 50
3.3. Results 51
3.4. Discussion 57
3.5. Conclusions 61

Chapter 4. Climate Change Impacts on Snow and Streamflow Drought Regimes 63
4.1. Introduction 63
4.2. Study Locations 64
4.3. Materials and Methods 66
4.3.1. Groundwater - Surface Water (GW-SW) Modelling 66
Land surface data and overland flow 68
Unsaturated and saturated zone 69
MIKE 11 stream network 69
4.3.2. Climate Change Scenario Modelling 70
4.3.3. Evapotranspiration and Snow 71
4.3.4. Assessment of Snow Drought 72
4.3.5. Assessment of Low Flows and Streamflow Drought 73
4.4. Results 74
4.4.1. Climate Change Impacts on the Annual Water Balance 74
4.4.2. Snow Drought 80
4.4.3. Low Flows and Summer Streamflow drought 82
4.5. Discussion 86
4.6. Conclusions 90

Chapter 5. Case Study: Future Water Security in Northeast British Columbia 91
5.1. Introduction 91
5.2. Study Area 93
5.3. Climate Change Projections 94
GCM bias 95
5.4. Hydrologic Modelling 98
5.5. Daily to Hourly Downscaling 102
5.6. Future Water Demand 102
5.7. Results 103
5.7.1. Simulated Versus Observed 103
Snow water equivalent 104

Runoff 105
5.7.2. Dugout Impacts on Runoff 109
5.7.3. Near Future (2021-2050) Versus Historical (1971-2000) Hydrology 111
5.8. Demand Versus Supply 114
5.9. Conclusions 116

Chapter 6. Conclusions 118
6.1. Climate Controls on Low Flows / Hydrological Drought 118
6.2. Climate Controls on Snow Drought 119
6.3. Snow and Streamflow Drought in the Context of a Warming Climate 120
6.4. Contributions 121
6.5. Recommendations for Future Research 122

References 124

Appendix A. Chapter 2 Supplemental Information 148

Appendix B. Chapter 3 Supplemental Information 155

Appendix C. Chapter 4 Supplemental Information 162

Appendix D. Chapter 5 Supplemental Information: Daily to Hourly Climate Time Series Disaggregation 182

Appendix E. Chapter 5 Supplemental Information: Gauge Time Series Comparison 184

List of Tables

Table 2.1 Climate predictor variables and low flow regime response variables used in the analyses. 27

Table 2.2 Streamflow response variable sensitivity to selected climate variables, estimated by standardized regression coefficients. 37

Table 2.3 Effect of winter climate conditions on the median z-scores of runoff and low flows. Significance assessed with the Mann-Whitney U test. 39

Table 3.1 Temperature-related snow drought susceptibility summarized by ecoregion. SWE = mean snow water equivalent; Vol. = mean snowpack water volume. Ecoregion numbering as in Figure 3.1. “Other” includes all grid cells not within the 15 ecoregions. Table S3.5 presents the same data in terms of area as opposed to volume. 57

Table 4.1 Catchment characteristics, including baseline 1980s (1970-1999) mean annual precipitation (P), snow fraction (Sf), mean annual temperature (T), and mean winter (1-Nov to 1-Apr) temperature (T_w). MASL = meters above sea level. 65

Table 4.2 Low flow regime indicators, calculated yearly. Baseline = 1980s (1970-1999). MAR = mean annual runoff. 74

Table 4.3 Risk (severity x frequency) for dry (D), warm (W), and warm and dry (W&D) snow droughts. Baseline 1980s (1970-1999) versus 2050s (2040-2069) and 2080s (2070-2099) for representative concentration pathways (RCPs) 4.5 and 8.5. 82

Table 5.1 Graham and Blueberry headwater catchment Hydrological Response Units (HRUs) 99

Table 5.2 HRU aspect, slope, and elevation. 99

Table 5.3 Modules used in CRHM setups. 100

Table 5.4 Climate stations used to generate hourly time series. 102

Table 5.5 Median monthly and annual runoff estimated by the naturalized model and the dugout model for the Blueberry headwater catchment. Median difference between models was estimated with the Wilcoxon signed-ranks test. 110

List of Figures

Figure 2.1 Study region elevation in meters above sea level (MASL) with the locations of selected hydrometric gauging stations indicated by white circles. Additional station information is included in Appendix A, Table S2.1. 23

Figure 2.2 Example low flow regime classifications: (a) Flathead River, gauge ID 12358500, and (b) Newhalem Creek, gauge ID 12178100. Winter low flow period shown in blue; summer low flow period shown in pink. Dashed horizontal line is equal to the mean daily runoff (MDR) and is used as the upper-bound for defining the low flow periods. The gray areas above the MDR line are equal to the blue and pink areas when not plotted with a logarithmic y-axis. 26

Figure 2.3 Response variable bivariate plots. Spearman's rho reported for significant ($p < 0.05$) correlations. Red (blue) points indicate significant negative (positive) correlation; gray points indicate non-significant results. Abbreviations and units are as in Table 2.1. 30

Figure 2.4 Predictor and response variable bivariate correlation plots. Spearman's rho reported for significant ($p < 0.05$) correlations. Red (blue) points indicate significant negative (positive) correlation; gray points indicate non-significant results. Abbreviations and units are as in Table 2.1. 32

Figure 2.5 Low flow regimes for catchments with different mean annual temperatures (T_a) and mean annual precipitation (P_a) – two each from two level III ecoregions. (a) Cataract Creek, gauge ID 05BL022, (b) Flathead River, gauge ID 12358500, (c) Merced River, gauge ID 11264500, (d) Duncan Canyon Creek, gauge ID 11427700. 33

Figure 2.6 (a) Fraction of stations exhibiting significant correlation (p value < 0.05) between the streamflow response variables and the climate predictor variables. (b) Fraction of stations exhibiting significant partial correlations ($p < 0.05$) – control variable marked with a star. For (a) and (b): Red gradient indicates an increase in the climate predictor variable is associated with a decrease in water quantity (e.g., longer duration low flow season, lower runoff) while blue gradient indicates increased water quantity (e.g., shorter duration low flow season, higher runoff). Color saturation, shown in bottom legend, indicates mean percent variance explained for the subset of stations with significant correlations. Streamflow response variable and climate predictor variable abbreviations are as in Table 2.1, with the addition of preceding year climate variables, as indicated with "-1" postscript. 34

Figure 2.7 Winter season classification based on standardized values (z-scores) for winter precipitation (Pw) and winter thawing degrees (TDw). Number of years in each quadrant indicated by n values. 39

Figure 3.1 Ecoregions (CEC, 2009) and mean peak snow water equivalent (SWE; 1951-2000) for masked analysis domain. Ecoregions are outlined in black and include: (1) Pacific and Nass Ranges, (2) North Cascades, (3) Cascades, (4) Eastern Cascades Slopes and Foothills, (5) Klamath Mountains, (6) Sierra Nevada, (7) Wasatch and Uinta Mountains, (8) Southern Rockies, (9) Middle Rockies, (10) Idaho Batholith, (11) Blue

Mountains, (12) Canadian Rockies, (13) Columbia Mountains / Northern Rockies, (14) Thompson-Okanagan Plateau, (15) Chilcotin Ranges and Fraser Plateau. Glaciated cells as flagged in Livneh et al. (2015). MASL = meters above sea level. 47

Figure 3.2 Frequency, severity, and risk for dry, warm, and warm & dry snow droughts, 1951-2013. 52

Figure 3.3 Snow drought severity, frequency, and risk by ecoregion, 1951-2013. For severity, the gray vertical lines represent individual years, the black horizontal lines span the inter-quartile range, and the symbols coincide with the mean. Ecoregion numbering as in Figure 3.1. See Table S3.4 for values of mean severity, frequency, and risk in table format....53

Figure 3.4 Snow drought risk and peak SWE sensitivities versus mean winter (1-Nov to 1-Apr) temperature [T_W]. Top row: (a) R_D [dry], (b) R_W [warm], and (c) R_{WD} [warm and dry] snow drought risk. Bottom row: Peak SWE sensitivity to (d) temperature [S_T] and (e) precipitation [S_P]. Piecewise linear regression lines are shown in red for variables with strong correlations with temperature (r values shown in top-left corners). Break-points (BPs) from the piecewise regression are shown with black vertical dashed lines. Slopes (S1, S2, S3) and associated standard errors are indicated for each linear regression segment. Model performance indicated by coefficient of determination (R^2). 55

Figure 3.5 Peak SWE temperature-related snow drought susceptibility under (a) historical [1951-2000] and (b) +2°C climate scenario. Ecoregion numbering as in Figure 3.1. Results are summarized by ecoregion in Table 3.1 and Table S3.5. 56

Figure 4.1 Headwater catchment locations and Level I ecoregions (CEC, 2011). ...66

Figure 4.2 Annual climate and water balance components for the 1980s baseline (1970-1999) versus 2050s (2040-2069) and 2080s (2070-2099) for representative concentration pathway (RCP) 4.5 and RCP 8.5, including mean annual temperature (Temp), annual precipitation (Precip), peak snow water equivalent (SWE), annual runoff, annual actual evapotranspiration (AET), and annual groundwater recharge. Blue and orange shading indicate a significant ($p < 0.05$) increase or decrease relative to the baseline period, as assessed with the two-sided Mann-Whitney U test. Arrows are added for clarity where boxplot shading is unclear. Figure S4.1 shows the same data, plotted as absolute values, and Table S4.6 provides the corresponding mean annual values along with the absolute and relative change. 79

Figure 4.3 Frequency (fraction of years) of dry (D), warm (W), and warm and dry (W&D) snow droughts for the baseline 1980s (1970-1999) versus 2050s (2040-2069) and 2080s (2070-2099) for representative concentration pathway (RCP) 4.5 and RCP 8.5. Table S4.7 provides the same data in tabular format. 80

Figure 4.4 Mean severity (fraction below baseline normal) of dry (D), warm (W), and warm and dry (W&D) snow droughts for the baseline 1980s versus 2050s (2040-2069) and 2080s (2070-2099) for representative concentration pathway (RCP) 4.5 and RCP 8.5. Table S4.8 provides the same data in tabular format. Note: Dry snow droughts transition to warm and dry snow

droughts and therefore have no mean severity plotted for some future time periods. 81

Figure 4.5 Summer low flow regime indicators for the 1980s baseline (1970-1999) versus 2050s (2040-2069) and 2080s (2070-2099) for representative concentration pathway (RCP) 4.5 and RCP 8.5. Blue and orange shading indicate a significant ($p < 0.05$) increase or decrease relative to the baseline period, as assessed with the two-sided Mann-Whitney U test. Figure S4.10 shows winter low flow regime indicators. 84

Figure 4.6 Snow drought impacts on summer low flows by snow drought type, including years without snow drought (None) and years with warm (W), dry (D), and warm and dry (W&D) snow droughts. Blue and orange shading indicate the values are significantly ($p < 0.05$) higher or lower relative to years without snow drought, as assessed with the two-sided Mann-Whitney U test. Abbreviations are as in Table 4.2. Arrows are added for clarity where boxplot shading is unclear. Figure S4.15 shows the winter low flow regime indicators. 85

Figure 4.7 Frequency of snow drought propagation into summer streamflow drought, in the absence of summer precipitation deficit, by snow drought type: warm (W), Dry (D), warm and dry (W&D), RCP 8.5. Figure S4.16 shows the same plot for RCP 4.5. 86

Figure 5.1 Study area including (a) Peace River watershed and shale gas plays, (b) Graham and Blueberry watersheds, and current land use and oil and gas industry water source dugout locations in the (c) Graham headwater catchment and (d) Blueberry headwater catchment. 94

Figure 5.2 Boxplots of historical (1971-2000; shown in black) versus near future (2021-2050; shown in gray) climate from model ensemble for the Blueberry headwater catchment. (a) mean daily temperature, (b) monthly precipitation, (c) mean annual temperature, and (d) annual precipitation. Outliers not shown. 95

Figure 5.3 Observed (Wonowon climate station) versus simulated (BCCAQ downscaled data from three GCMs) comparison of (a) monthly precipitation and (b) monthly dry days (precipitation < 0.5 mm). Outliers are not shown. 97

Figure 5.4 Observed (Wonowon climate station) versus simulated (BCCAQ downscaled data from three GCMs) comparison of (a) daily maximum temperature and (b) daily minimum temperature. Outliers are not shown. 98

Figure 5.5 Flowchart of physically based hydrological modules used in the CRHM models. The model structure is the same for the Blueberry and Graham catchments. (abbreviations: Inf: Infiltration; Adj.: Adjusted) 101

Figure 5.6 Projected shale gas industry freshwater demand from Kniewasser and Horne (2015). High, medium, and low development correspond to 5, 3, and 1 Liquid natural Gas (LNG) plants, respectively. The improved water management scenario incorporates 25% water recycling and 25% saline water use. 103

Figure 5.7 Observed versus simulated snow water equivalent (SWE), Wonowon climate station. 105

Figure 5.8 Mean daily snow water equivalent (SWE) observed at the Wonowon climate station versus simulated at the Wonowon climate (forced with observed data), and versus simulated SWE in the Blueberry headwater catchment (forced with downscaled GCM model output). 105
Figure 5.9 Beatton River watershed and gauging station locations. 107
Figure 5.10 Simulated median daily runoff in the Blueberry catchment versus observed median daily runoff from two nearby stream gauges, St. John Creek (Gauge ID: 07FC002) and Blueberry River (Gauge ID: 07FC003). Median daily runoff values are calculated for the observed record period of St. John Creek: 1962-1974 108
Figure 5.11 Monthly mean daily runoff (a) estimated by the North East Water Tool (NEWT) and (b) simulated for the Blueberry headwater catchment and observed at hydrometric gauging stations. Simulated and observed data are summarized for the 1971-2000 period for consistency with NEWT, with the exception of the St. John Creek gauge, which only covers the 1962-1974 period. 109
Figure 5.12 Blueberry headwater catchment (plains) simulated historical (1971-2000) in black and near future (2021-2050) in gray (a) monthly snowfall (represented as mm of snow water equivalent - SWE), (b) mean monthly SWE, (c) monthly actual evapotranspiration (AET), and (d) monthly runoff 112
Figure 5.13 Graham headwater catchment (foothills) simulated historical (1971-2000) in black and near future (2021-2050) in gray (a) monthly snowfall (represented as mm of snow water equivalent - SWE), (b) mean monthly SWE (c) monthly actual evapotranspiration (AET), and (d) monthly runoff. 113
Figure 5.14 (a) Blueberry and (b) Graham headwater catchment annual snowfall, annual peak snow water equivalent (SWE), annual actual evapotranspiration (AET), and annual runoff. Simulated historical (1971-2000) is shown in black and near future (2021-2050) in shown in gray. 114
Figure 5.15 Blueberry headwater catchment fraction of annual runoff required to meet shale gas industry freshwater demands. Results are presented by centered 10-year periods (2020 = 2015-2024, 2030 = 2025-2034, etc.). Boxplots show the fraction allocated for *individual years*; black circles show the fraction allocated based on the 10-year *mean annual runoff*. 115

Chapter 1. Introduction

Drought is one of the main types of weather-related disasters. Unlike other disaster types, which tend to develop quickly and have dramatic visible impacts, drought events develop slowly, often cover extensive areas (trans-national), and can last for months to years (Beran & Rodier, 1985; Sheffield & Wood, 2011). With such large spatial and temporal scales, droughts can have devastating impacts on many economic sectors (Tallaksen & Van Lanen, 2004; Sheffield & Wood, 2011), including drinking water supply, crop production, water transportation, electricity production, and recreation (e.g., Wilhite, 2000; Tallaksen & Van Lanen, 2004; Sheffield & Wood, 2011; van Vliet et al., 2012). Drought is also one of the most damaging natural hazards in terms of societal impacts, such as hunger, mass migration, conflict, and loss of life (Garcia-Herrera et al., 2010; European Environment Agency [EEA], 2012; Hsiang et al., 2013; Emergency Events Database [EM-DAT], 2016).

Droughts can occur anywhere in the world, and because of the growing population and increasing water demands, the adverse impacts of droughts are likely to worsen. Recent drought studies (Sheffield & Wood, 2008; Feyen & Dankers, 2009; Dai, 2011) have shown an increasing trend in drought extent and affected population. Climate change is predicted to lead to more extreme hydrological regimes (Intergovernmental Panel on Climate Change [IPCC], 2013), including a shift from snow-dominated to rain-dominated systems (Laternser & Schneebeli, 2003; Hamlet et al., 2005; Barnett et al., 2008), and, consequently, a shift in snow drought (Harpold et al., 2017) and thus hydrological drought regimes (Feyen & Dankers, 2009; Wanders & Van Lanen, 2015). These factors (increasing population + increasing water demand + climate change) make drought research and management a prominent issue. Indeed, drought and related hazards (heat waves and wildfires) have received increasing attention over the past decade (Sheffield et al., 2012; Dai, 2013; Harpold et al., 2017), but our understanding of drought, especially snow drought, hydrological drought, and the relationship between the two, still has large gaps.

In western North America, snowpack plays a vital role in maintaining streamflow during the relatively warm and dry spring and summer months (Barnett et al., 2008). Snowpack also provides natural storage for water supply and hydropower (Barnett et al.,

2005). Ecosystems (Ficke et al., 2007; Rocca et al., 2014; Service, 2015; Chang & Bonnette, 2016) and economies (Sturm et al., 2017; Hagenstad et al., 2018) depend on the amount of snow that accumulates during the winter and on the timing and rate of melt in the spring and summer. The recent (2014-2015) drought in western United States showed that below-normal winter snow accumulation can lead to below-normal summer streamflow (Harpold et al., 2017); however, there has been limited research on the relationship between snow drought and summer streamflow drought. Gaps in our knowledge of hydrological drought, and its relationship to snow drought, are particularly pressing as many of the adverse impacts of drought are directly related to hydrological drought (drought in rivers, lakes, and groundwater) and only indirectly related to meteorological drought (Dracup et al., 1980; Van Loon, 2015). Understanding the occurrence and variability of hydrological drought events, and their relationship with snow drought events, in both the historic and the future climate, is essential for natural resource management and policy decisions, including managing water allocations for agriculture, municipal, and industrial sectors.

Studies of hydrological drought have traditionally lumped all drought events together; however, recent work by Van Loon & Van Lanen (2012) and Van Loon et al. (2015) propose the classification of hydrological drought into eight distinct types based on climatic causes, including three types related to the timing and magnitude of snow accumulation and melt. Similarly, a recent paper by Harpold et al. (2017) calls for a distinction between “warm” and “dry” snow drought events, and studies of warm versus dry snow drought are just emerging (e.g., Cooper et al., 2016; Sproles et al., 2017; Hatchett & McEvoy, 2018). To my knowledge, no studies have completed a combined analysis of snow drought and streamflow drought in the context of climatic causes, and no studies have undertaken a regional analysis of the historical frequency and severity of warm versus dry snow drought. Additionally, no climate change impact modelling studies have completed a combined analysis of snow drought and hydrological drought. The proposed research aims to close some of the gaps in our knowledge by investigating snow drought, hydrological drought, and the relationship between the two in the context of a warming climate.

1.1. Background and Previous Research

The following sections review the existing literature and provide context for the novel contributions of the proposed research.

1.1.1. Defining Drought

Drought is defined as prolonged, below-average moisture availability (Palmer, 1965). Drought should not be confused with aridity, which is a permanent feature of a dry climate (Mishra & Singh, 2010; Maliva & Missimer, 2012), or with water scarcity, which refers to a below-normal water availability caused fully or in part by human activities (Seneviratne et al., 2012). For purposes of this research, drought is defined as below-normal water availability due to natural causes only.

Drought affects all components of the hydrologic cycle and is typically classified into the following categories (e.g., Changnon, 1980; Tallaksen & Van Lanen, 2004; Mishra & Singh 2010; Sheffield & Wood, 2011), with the addition of the emerging concept of snow drought (Ludlum, 1978; Wiesnet, 1981; Mote et al., 2016; Harpold et al., 2017).

- *Meteorological drought* – precipitation deficiency, possibly in conjunction with increased evapotranspiration.
- *Snow drought* – lack of snow accumulation in winter due to below-normal precipitation and/or above-normal winter temperatures.
- *Soil moisture drought* – soil moisture deficiency which reduces the supply of moisture to vegetation. Soil moisture droughts are closely linked to crop failure and therefore are sometimes referred to as agricultural drought.
- *Hydrological drought* – broad term related to below-normal surface and subsurface water storage and flows.
- *Socioeconomic drought* – associated with the impacts from the four above-mentioned drought types.

The two main classes of drought of direct relevance to this research, snow drought and hydrological drought, are summarized below.

Snow drought

Snow drought (Ludlum, 1978; Wiesnet, 1981) is characterized by below-normal peak or April 1st snow water equivalent (SWE) and can be caused by either a lack of winter precipitation (dry snow drought) or a lack of snow accumulation due to above-normal winter temperatures (warm snow drought) (Harpold et al., 2017). These different snow drought types have different hydrologic and economic impacts. Dry snow droughts reduce streamflow year-round, resulting in low reservoir levels, reduced hydropower production, and, in severe cases, drinking and irrigation water supply shortages. On the other hand, warm snow droughts increase flood risk (Allamano et al., 2009; Harpold et al., 2017) and create a mismatch between water availability and need. Both warm snow droughts and dry snow droughts cause below-normal summer streamflow (Harpold et al., 2017).

The classification of snow droughts into “warm snow drought” and “dry snow drought” is an emerging concept. Mote et al. (2016) showed that exceptionally warm winter conditions prevented snow accumulation in the states of California, Oregon, and Washington during the record low snow season in 2015. Harpold et al. (2017) suggest distinguishing warm versus dry snow droughts based on April 1 SWE and cumulative winter (1-Nov to 1-Apr) precipitation, where winters with below-normal SWE and above-normal precipitation are classified as warm snow droughts and years with below-normal SWE and below-normal precipitation are classified as dry snow droughts. The classification methodology of Harpold et al. (2017), however, does not account for the co-occurrence of warm and dry conditions, which is likely to be the most severe type of snow drought.

Hydrological drought

Hydrological drought is a broad term related to negative anomalies in surface and subsurface water. Hydrological drought may manifest as abnormally low streamflow in rivers and/or abnormally low levels in lakes, reservoirs, and groundwater (Palmer, 1965; Dracup et al., 1980; Tallaksen & Van Lanen, 2004). Hydrological drought is sometimes separated into *groundwater drought*, defined as below-normal groundwater levels (Peters et al., 2003; Peters et al., 2006; Mishra & Singh, 2010), and *streamflow drought*, defined as below-normal river discharge. Streamflow drought should not be confused with low flows, which are a normal, seasonal component of flow regimes

(Smakhtin, 2001); however, low flow periods that are longer and/or more severe than normal are synonymous with streamflow droughts and may have significant impacts on water supply and agricultural production (Wilhite, 2000) and human (Charron et al., 2004) and aquatic ecosystem health (Lake, 2003).

To identify individual hydrological drought events from streamflow time series, a threshold level method is often used (e.g., Dracup et al., 1980; Tallaksen & Van Lanen, 2004; Fleig et al., 2006; Van Loon, 2013). With this method, a drought occurs when the variable of interest falls below the defined threshold level, and the event continues until the threshold is exceeded. Individual hydrological drought events can then be described by several characteristics, including duration, magnitude, and severity. The duration of the drought event is defined as the number of days during which the streamflow is below a predefined threshold level. Drought magnitude is defined as the average streamflow deficit, and drought severity is defined as the cumulative streamflow deficit.

Hydrological drought propagation

Unlike meteorological drought, which is exclusively caused by a precipitation deficiency and controlled by climate, hydrological drought can be caused by precipitation and/or temperature anomalies (Van Loon & Van Lanen, 2012; Van Loon et al., 2015) and is controlled by both climate and catchment characteristics. During the propagation of hydrological drought, the terrestrial part of the hydrological cycle (i.e. the catchment control) acts as a low-pass filter to the meteorological forcing (i.e. the climate control). This low pass filtering results in the following features that characterize the propagation of meteorological drought to hydrological drought (Peters et al., 2003; Tallaksen & Van Lanen, 2004):

- *Pooling* – smaller meteorological drought events are combined into one prolonged hydrological drought.
- *Attenuation* – meteorological droughts are attenuated in surface water and groundwater stores, causing a smoothing of the maximum negative anomaly
- *Lag* – a lag occurs between meteorological, soil moisture, and hydrological drought; the timing of the drought onset is later when moving through the hydrological cycle

- *Lengthening* – droughts increase in length as they move from meteorological drought via soil moisture drought to hydrological drought

Many studies have shown that the propagation of hydrological droughts is dependent on both climate and catchment characteristics (Peters et al., 2003; Van Lanen & Tallaksen, 2007; Vidal et al., 2010; Van Loon, 2012; Van Loon & Van Lanen, 2012; Van Loon et al., 2015); however, the relative importance of different climate and catchment characteristics is not well understood. A global study by Van Lanen et al. (2013) focused on the relative importance of climate versus catchment in the development of hydrological droughts and concluded that catchment control is as important as climate control. In a regional-scale study, Van Loon & Laaha (2014) investigated the relative importance of different climate and catchment characteristics on drought severity and identified catchment storage as the primary catchment control and seasonality as the primary climate control.

Catchment storage is determined by multiple factors including geology, topography, soil, land use, vegetation, and drainage density – the last two of which may change on inter-annual time scales (Van Loon, 2015). According to Van Loon & Laaha (2014), a combination of storage factors must be used to explain the variability of drought severity. Van Loon & Laaha (2014) found that the baseflow index (BFI; ratio of baseflow to total streamflow) provided the best combined measure of catchment storage. While this study added to the knowledge of catchment controls on hydrological drought, the relative importance of individual catchment descriptors in hydrological drought propagation is still poorly understood, and no studies have specifically investigated the role of land use, vegetation, or drainage density in hydrological drought development.

In general, climate controls on hydrological drought are easier to study and therefore are better understood than catchment controls. Seasonality is recognized as the primary climate control (Van Loon & Laaha, 2014; Van Loon, 2015), as hydrological droughts develop differently in climates with low seasonality as compared to climates with high seasonality. In regions with a relatively constant climate, below-normal precipitation and above-normal temperatures are the primary factors in the development of hydrological droughts. In a seasonal climate, additional processes play an important role in hydrological drought development. For example, in climates with snow

accumulation in winter, snow-related processes, including early soil freeze, late/early snowmelt timing, and/or below normal snow accumulation, can lead to a hydrological drought (Van Loon & Van Lanen, 2012; Van Loon et al., 2015). Thus, in catchments with seasonal snow cover, streamflow drought regimes are likely directly related to snow drought regimes.

1.1.2. Climate Change Impacts on Snowmelt Hydrology

Increasing concentrations of greenhouse gases in the atmosphere are expected to lead to an increase in global temperatures and an intensification of the global hydrological cycle (IPCC, 2013). Wet regions, such as the Pacific Northwest, will likely become wetter while drier regions, like southwestern United States, will likely become drier (IPCC, 2013). However, unlike temperature, projections of precipitation show little agreement among climate models (Barnett et al., 2005).

As temperatures rise, precipitation is more likely to fall as rain than to fall as snow. The shift from snow-dominated to rain-dominated systems will have large impacts on hydrologic regimes in catchments with seasonal snow cover. Warming alone is expected to reduce annual snow pack, leading to earlier snowmelt and diminished and potentially warmer late summer flows (Barnett et al., 2008; Wu et al., 2012; Seager et al., 2013; Reynolds et al., 2015; Service, 2015). In western North America, many changes have already been detected, including shifts in the snowmelt season toward earlier spring and subsequent decreases in warm season runoff (Leith & Whitfield, 1998; Whitfield & Cannon, 2000; Adam et al., 2009; Déry et al., 2009; Pederson et al., 2011; among others), decreases in the fraction of rain versus snow (Knowles et al., 2006), and decreasing snowmelt rates (Harpold & Kohler, 2017; Musselman et al., 2017).

While changes in the temporal distribution of streamflow are widely documented and acknowledged, the overall impact of a shift from snow to rain on the long-term mean streamflow is unknown. The general assumption has been that a shift from a snow- to rain-dominated regime will have a negligible impact on the long-term mean streamflow (Barnett et al., 2005; Regonda et al., 2005); however, recent studies by Bosson et al. (2012), Berghuijs et al. (2014), and Zhang et al. (2015) conclude that a warmer climate with less snow will lead to a significant decrease in mean annual streamflow.

Changes in snowmelt hydrology will likely result in shifts in the hydrologic drought regime. While several global-scale studies of climate change impacts on hydrological droughts have been completed (Hirabayashi et al., 2008; Prudhomme et al., 2014; Van Huijgevoort et al. 2014), catchment-scale studies are largely non-existent. In general, frost-season droughts are expected to become less severe and non-frost season droughts are expected to become more severe (Feyen & Dankers, 2009; Wanders & Van Lanen, 2015).

1.1.3. Approaches for Investigating Climate Change Impacts on Water Resources

Climate change impacts on water resources, including snow drought, low flow, and streamflow drought regimes, can be investigated using either a data-driven (downward) approach or a process-based (upwards) approach. These two approaches and relevant past research are summarized in the following two sections.

Data-driven (downward) approach

Data-driven studies assess climate impacts and/or climate sensitivities from observed hydroclimatic time series. Trend analysis is often used as a preliminary step to assess the existence of significant changes in hydroclimatic time series (Merz et al., 2012). Assessing the sensitivity of a hydrologic variables to different climate metrics, e.g., precipitation and temperature, provides insight into how hydrologic regimes may change in the future.

Temporal trend analysis

Snow is an important indicator of climate change because of its sensitivity to temperature, and a common technique for estimating the impact of climate warming on snowpack is temporal trend analysis. While some locations at higher elevations and higher latitudes in western North America exhibit upward trends in snow water equivalent (Hamlet et al., 2005), many studies have shown significant decreases in late season snowpack (Groisman et al., 2004; Mote et al., 2005; Regonda et al., 2005; Barnett et al., 2008; Kapnick & Hall, 2012; Mote et al., 2018). Hamlet et al. (2005) show that the decline in snowpack cannot be explained by changes in total precipitation alone, and it is generally recognized that warming is likely to have played a role in the decrease

of spring snowpack. The Pacific Northwest is particularly sensitive to warming because winter and spring temperatures are near 0°C (Adam et al., 2009).

The magnitude and timing of snowmelt has large impacts on warm season runoff (Barnett et al., 2008), and, unsurprisingly, many temporal trend analyses have documented decreasing summer runoff and decreasing summer minimum flows in catchments across western North America (Aguado et al., 1992; Ehsanzadeh & Adamowski, 2007; Luce & Holden, 2009; Dittmer, 2013; Kormos et al., 2016; among others). Trends in winter flows, however, are less studied and less clear. Novotny and Stefan (2007) documented trends toward less severe winter low flows in Minnesota, attributing the change to more frequent snow melt events. Ehsanzadeh and Adamowski (2007) documented shifts toward earlier winter low flow timing in Canada, suggesting a trend toward shorter winter low flow periods. Kormos et al. (2016) found minimal evidence for significant trends in winter low flows for the Pacific Northwest.

While many other studies have investigated temporal trends in meteorological drought and soil moisture drought (e.g., Cook et al., 2004; Andreadis & Lettenmaier, 2006; Sheffield & Wood, 2008; Dai, 2011; Sheffield et al., 2012; Dai, 2013; among many others), few studies have investigated trends in the severity, duration, or deficit volume of hydrological droughts. Hisdal et al. (2001) completed a pan-European study that included a trend analysis of the severity summer hydrological droughts and found no significant trend in drought severity. Wilson et al. (2010) investigated temporal trends in the duration and deficit volume of summer hydrological droughts in Nordic countries and found a trend toward higher summer drought deficit volumes. Bard et al. (2015) investigated trends in the hydrologic regime of Alpine rivers and found contrasting trends for winter drought severity and a tendency toward earlier summer droughts for snowmelt-rainfall regimes. The only study to analyze temporal trends in hydrological drought characteristics in North America was completed by Wu et al. (2008) for a set of catchments in the State of Nebraska. Like the findings of Hisdal et al. (2001), Wu et al. (2008) found no uniform trend in the duration, magnitude, or severity of streamflow drought.

One of the main assumptions in statistical trend analyses is that the events come from the same population (population homogeneity). The trend studies mentioned in the previous paragraph all grouped drought events into non-frost (i.e. summer) season and

frost (i.e. winter) season droughts; however, hydrological droughts have a variety of causative factors and propagation processes, even within seasons (Van Loon & Van Lanen, 2012). Van Loon (2013) showed that droughts with different propagation processes have different characteristics (e.g., frequency, severity, duration), and Van Loon & Van Lanen (2012) posited that different types of hydrological droughts will respond differently to climate change.

Sensitivity analysis

The sensitivity of processes to shifts in climate has been quantified with a variety of statistical techniques, including path analysis (Kormos et al., 2016) and spatial (Luce et al., 2014) and temporal (Revelle & Waggoner, 1983; Sankarasubramanian et al., 2001; Mote, 2006; Luce et al., 2014) analogs. These methods attempt to isolate the effect of temperature on hydrologic variables from the effect of other variables, such as precipitation.

Path analysis is a special case of structural equation modelling and is used to quantify the direct and indirect influences of correlated predictor variables on response variables (Alwin & Hauser, 1975). Path analysis can be used to help understand the causal structure of the data (Kozak & Kang, 2006); however, it is not very useful at the exploratory stage of research (Zhang et al., 2014). Kormos et al. (2016) and Zhang et al. (2014) both used path analysis to separate temperature effects from precipitation effects on historical streamflow variability. Kormos et al. (2016) focused on low flows and showed that, in the Pacific Northwest, the historical variability of annual summer minimum flows has been more closely related to precipitation than to temperature. Zhang et al. (2014) focused on peak flows and showed that, in the Kaidu River watershed of Xinjiang, China, temperature has a large indirect effect the spring snowmelt peak flow.

Temporal analogs use regression analysis, where, for example, interannual climate data are regressed against a hydrological variable of interest. The general logic behind temporal analogs is that warmer futures will resemble warmer years/days in the historical record (Sankarasubramanian et al., 2001; Mote, 2006; Luce et al., 2014). Temporal analogs have been used to isolate the effects of temperature on April 1 SWE (Howat & Tulaczyk, 2005; Mote, 2006; Casola et al., 2009; Luce et al., 2014) and annual streamflow (e.g., Nash & Gleick, 1991; Ng & Marsalek, 1992; Risbey & Entekhabi, 1996;

Fu et al., 2007) and have also been used to isolate the effect of peak SWE on summer minimum flows (Godsey et al., 2014; Jenicek et al., 2016).

Spatial analogs also rely on regression analysis; however, instead of using interannual data, climatological averages are regressed against a variable of interest. Spatial analogs are sometimes called “space-for-time” substitutions and rely on the logic that a warmer future may look like historically warmer places do now (Luce et al., 2014). Spatial analogs have been used to model the sensitivity of snowpack to precipitation and temperature (Luce et al., 2014) and the sensitivity of streamflow to vegetation expansion (Goulden & Bales, 2014) and snowfall fraction (Berghuijs et al., 2014). Neither temporal analogs or spatial analogs have yet been used to quantify the climate sensitivity of low flows or hydrological drought.

Process-based (upward) approach

Process-based (upward) studies use hydrologic models to simulate future changes to water resources based on outputs from global climate models (GCMs). Many studies have used a process-based approach to study climate change impacts on water resources; however, only a small portion of these studies have analyzed impacts on low flows and/or hydrological drought. Existing process-based studies of climate change impacts on hydrological drought have been completed at the global scale (e.g., Hirabayashi et al., 2008; Prudhomme et al., 2014; Van Huijgevoort et al., 2014), at the continent and nation scale (e.g., Feyen & Dankers, 2009; Prudhomme et al., 2012; Leng et al., 2015), and at the catchment scale (Wanders & Van Lanen, 2015).

The type of hydrological model used for these process-based studies is partially dependent on the scale of the study, and each type of model has its own set of advantages and disadvantages. Hirabayashi et al. (2008), Van Huijgevoort et al. (2014), and Prudhomme et al. (2014) all used global hydrological models (GHMs) and found significant increases in drought for many regions across the globe. While the global-scale studies make it easier to identify large-scale trends, the projections from GHMs are coarser in both the spatial domain and the degree of process realism. Additionally, GHMs are the main source of uncertainty in the global scale studies, with the GCMs providing the second largest source of uncertainty (Hagemann et al., 2013; Prudhomme et al. 2014).

Continent- and nation-scale studies typically use regionalised rainfall-runoff models which are often not specifically parameterised for low flows. Most rainfall-runoff models were designed to simulate average and high flows, and the application of regional rainfall-runoff models to low flow and drought events has been much more limited (Smakhtin, 2001). To my knowledge, Wanders & Van Lanen (2015) is the only study to use catchment scale hydrological models to investigate climate change impacts on hydrological drought. In that study, the authors used lumped conceptual hydrological models of synthetic catchments representing randomly selected locations throughout the world. Results of the study showed a decrease in drought frequency but an increase in average drought duration and deficit volume for all major climates around the world.

Streamflow during low flow and drought events is often dominated by groundwater discharge, i.e. baseflow. Since surface water and groundwater systems exhibit important feedbacks, the modelling procedure used to simulate drought events should take into account both the groundwater and surface water systems. Hewlett & Troendle (1975) stated that accurate prediction of the streamflow hydrograph implies adequate modelling of the sources, flowpaths, and residence time of the water. It follows that adequate modelling requires adequate representation of the physics of water flow, i.e. spatially and temporally distributed deterministic hydrological models.

Freeze & Harlan (1969) provided the first guidelines for what is often considered adequate physics-based hydrological modelling. In the last fifteen years, the guidelines of Freeze & Harlan (1969) have been realised with the development of several physics-based fully integrated (or coupled) surface water-groundwater (GW-SW) models. Examples include InHM (VanderKwaak & Loague, 2001), MODHMS (HydroGeoLogic, 2006), HydroGeoSphere (HGS) (Therrien et al., 2010), ParFlow (Kollet & Maxwell, 2006), and MIKE SHE (Danish Hydraulic Institute [DHI], 2007). Fully integrated (or fully coupled) GW-SW models model water flow through the entire system and should therefore provide an accurate simulation of drought propagation processes. While catchment scale studies using GW-SW models are widespread (e.g., Jones et al., 2008; Goderniaux et al., 2009, 2011; Li et al., 2008), this type of model is typically not used to model streamflow time series, likely due to the high data requirements and long processing times. Previous studies (Li et al., 2008; Partington et al., 2011; Golmohammadi et al., 2014; Foster & Allen, 2015) have shown that GW-SW models can be used to adequately model stream discharge; however, to my knowledge, no studies

have used a fully coupled/integrated GW-SW model to study hydrological droughts, drought propagation, or climate change impacts on drought. Moreover, no studies have used a GW-SW model to complete a combined analysis of climate change impacts on snow drought and hydrological drought.

1.2. Purpose and Objectives

This research aims to test the hypothesis that, in catchments with seasonal snow cover, snow drought regimes are directly related to low flow and streamflow drought regimes, and, consequently, climate warming will have related impacts on snow drought, low flows, and streamflow drought.

The specific objectives of this study are as follows:

1. Identify the dominant climate controls on runoff and low flows in mountain catchments;
2. Quantify the historical frequency, severity, and risk of snow drought over western North America;
3. Develop a methodology for snow drought susceptibility mapping in the context of a warming climate;
4. Estimate how climate change may impact snow drought, low flows, and streamflow drought regimes; and
5. Complete a case study of the potential for water scarcity in the Peace River watershed in the context of future climate change and growing industrial water demand.

1.3. Scope of Work

The following work was undertaken to achieve the research objectives:

- To meet objective 1:
    - Develop and test a methodology for process-based separation of low flows in catchments with seasonal snow cover.
    - Identify the dominant climate controls on the inter-annual variability of runoff and low flows using bivariate and partial correlation analysis.

    - Quantify the relative sensitivity of runoff and low flows to precipitation and temperature using the dominant climate controls identified using the correlation analysis.

- To meet objectives 2 and 3:
    - Develop and test a methodology for classification of snow droughts based on climatic causes.
    - Map the sensitivity of peak snow water equivalent to precipitation and temperature.
    - Quantify the historical frequency, severity, and risk of snow drought at the grid-cell and ecoregion scale.
    - Develop a method for snow drought susceptibility mapping in the context of climate warming using the results of the grid-cell scale quantification of snow drought risk.
- To meet objective 4:
    - Develop generic coupled groundwater-surface water models of headwater catchments in four major ecoregions of British Columbia using the MIKE-SHE modelling code.
    - Use global climate change projections to assess climate change impacts on snow drought, low flows, and snow drought related streamflow droughts.
- To meet objective 5:
    - Develop hydrologic models of two headwater catchments in shale gas region of the Peace River watershed in northeast British Columbia.
    - Use global climate change projections to assess climate change impacts on annual and monthly water quantity and compare to future estimates of shale gas industry freshwater demand.
    - Compare simulated monthly runoff from the hydrologic models to the monthly runoff estimates from the British Columbia Northeast Water Tool.

1.4. Thesis Overview

This thesis is comprised of six chapters.

Chapter 1 introduces the main concepts and outlines the objectives and scope of the research. Chapters 2 through 5 were prepared primarily as papers and have been submitted for publication, as described below. Chapters 2 and 3 present the papers as

submitted, with minor formatting changes. Chapter 4 has been prepared for journal publication but has not yet been submitted. Chapter 5 is an expanded version of a published book chapter, and Chapter 6 summarizes the conclusions and provides recommendations for future research. All papers were co-authored with my thesis supervisors, Dr. Diana Allen and Mr. Paul Whitfield; however, I completed the research and prepared the paper, with Dr. Allen and Mr. Whitfield providing technical input, guidance, and editing. Chapters 2 through 5 are described in more detail below.

Chapter 2 – Climate Controls on Runoff and Low Flows in Mountain Catchments of Western North America.

> In the mountainous regions of western North America (WNA), snowmelt recharges groundwater and provides ecosystem-sustaining baseflow during low flow periods. Continued warming is expected to have large impacts on snowmelt hydrology and on low flow regimes, but the relative impact of temperature and precipitation on low flows is unclear. To address this knowledge gap, the dominant climate controls on summer and winter season low flows in 63 near-natural catchments in mountainous ecoregions of WNA are identified with correlation analysis, and low flow sensitivity to temperature and precipitation is quantified with multiple linear regression analysis. Results show that precipitation is the dominant control on the inter-annual variability of annual runoff and on the duration and severity of summer and winter low flows. The temperature-sensitivity of low flows, however, is up to two times higher than that of annual runoff. Annual runoff and low flows are most sensitive to winter climate conditions, particularly winter precipitation and winter thawing degrees. Warm winters correspond to significantly lower runoff, significantly longer, more severe summer low flows, and significantly shorter winter low flows. This highlights the importance of winter climate conditions for runoff and low flows in these mountain catchments and provides another line of evidence regarding the impacts of climate change on snowmelt hydrology.
>
> This paper was submitted for publication in *Water Resources Research*, authored by J.R. Dierauer, P.H. Whitfield, and D.M. Allen.

Chapter 3 – Winter Temperature Controls on Snow Drought Risk in Western North America.

In western North America (WNA), mountain snowpack supplies much of the water used for irrigation, municipal and industrial uses. Thus, snow droughts (a lack of snow accumulation in winter) can have drastic ecological and socioeconomic impacts. In this study, the historical (1951-2013) frequency, severity, and risk of dry, warm, and warm and dry snow droughts are quantified at the grid-cell and ecoregion scale for the major mountainous regions in WNA. Based on multiple linear regression analysis, relationships between mean winter temperature, snow drought risk, and snow water equivalent (SWE) sensitivity are explored. Piecewise linear regression is used to identify temperature thresholds for mapping temperature-related snow drought susceptibility. Results highlight spatial differences in snow drought regimes across WNA and reveal that a critical temperature-threshold exists, above which the warm snow drought risk increases more rapidly. Three percent of the non-glaciated snow storage in WNA has high susceptibility to temperature-related snow drought, representing 11 km^3 of water. Under a +2°C climate scenario, an additional 8% (28 km^3) of the WNA snow storage volume will transition to high susceptibility.

This paper was submitted for publication in *Water Resources Research*, authored by J.R. Dierauer, D.M. Allen, and P.H. Whitfield.

Chapter 4 – Climate Change Impacts on Snow and Streamflow Drought Regimes.

In many regions with seasonal snow cover, summer streamflow is primarily sustained by groundwater that is recharged during the snowmelt period. Therefore, below-normal snowpack (snow drought) may lead to below-normal summer streamflow (streamflow drought). Summer streamflow is important for supplying human needs and sustaining ecosystems, and while climate change impacts on snow have been widely studied, the relationship between snow drought and streamflow drought is not well understood. In this study, a combined investigation of climate change impacts on snow drought and streamflow drought was completed using generic groundwater – surface water models for four headwater catchments in different ecoregions of British Columbia. Results show

that, in response to increased precipitation and temperature, the snow drought regime changes substantially for all four catchments. Warm snow droughts, which are caused by above-normal winter temperatures, increase in frequency, and dry snow droughts, which are caused by below-normal winter precipitation, decrease in frequency. The shift toward more frequent and severe temperature-related snow droughts leads to decreased summer runoff, decreased summer groundwater storage, and longer, more severe summer low flow periods. Moreover, snow droughts propagate into summer streamflow droughts more frequently in the future time periods (2050s, 2080s) as compared to the baseline 1980s period. Thus, warm snow droughts not only become more frequent and severe in the future but also more likely to result in summer streamflow drought conditions.

This paper is prepared as a manuscript and planned for submission to the journal *Hydrology and Earth System Sciences*.

Chapter 5 – Case Study: Future Water Security in Northeast British Columbia.

In recent decades, the Peace River watershed in Northeast British Columbia (NEBC) has experienced rapid growth in shale gas development activities, resulting in significant increases in surface water and groundwater use and a growing conflict over the use and protection of these water resources. Under a high development scenario, industrial water demand in the Peace River watershed is projected to increase by over 350% by 2030, and future water security in the context of the water-energy nexus is unknown, especially with continued climate warming. In this study, hydrological models are used to simulate the current and future water balance for two headwater catchments of the Peace River watershed, one in the foothills and one in the plains. Both catchments have been impacted by the recent shale gas development, and both contain oil and gas industry water use permits. Climate variables output from three Global Climate Models were used as inputs for the hydrologic models. Water quantity projections for future decades (2020s, 2030s, 2040s, and 2050s) were then compared to the projected water use for low, medium, and high shale gas development scenarios and used to estimate the potential for water scarcity in the region. Results from this study show that areas with high levels of oil and

gas industry development may experience water scarcity if rapid industrial growth continues, and improved water management policies will be needed to mitigate the high industrial water demand.

This chapter is an expanded version of a book chapter that has been published in: Endo, A. and Oh, T. (Eds) Water-Energy-Food Nexus: Human-Environmental Security in the Asia-Pacific Ring of Fire. Springer.

1.5. Significant Contributions

The key findings/contributions of this research include the following:

Chapter 2 – Climate Controls on Runoff and Low Flows in Mountain Catchments of Western North America.

1. Higher mean annual temperatures correspond to longer, more severe summer low flows and shorter, less severe winter low flows.
2. Warm winters correspond to significantly lower runoff, significantly longer, more severe summer low flows, and significantly shorter winter low flows.
3. Compared to annual streamflow, low flows are up to two times more sensitive to temperature, particularly winter temperatures above 0°C.

Chapter 3 – Winter Temperature Controls on Snow Drought Risk in Western North America.

1. Warm and dry winter conditions occurring together produce the most severe snow droughts while warm winter conditions alone produce the least severe snow droughts.
2. The severity and frequency of warm snow droughts is dependent on mean winter (1-Nov to 1-Apr) temperature, and warm snow drought risk increases with increasing mean winter temperatures.
3. The relationship between warm snow drought risk and mean winter temperature is non-linear, and critical temperature thresholds exist, above which warm snow drought risk increases more rapidly.

Chapter 4 – Climate Change Impacts on Snow and Streamflow Drought Regimes.

1. In response to the projected increases in precipitation and temperature, the snow drought regime changes substantially for all catchments. Warm snow droughts increase in frequency, and dry snow droughts decrease in frequency.

2. Snow droughts propagate into summer streamflow droughts more frequently in the future time periods (2050s, 2080s) as compared to the baseline 1980s period. Thus, warm snow droughts not only become more frequent and severe in the future but are also more likely to result in summer streamflow drought conditions.

3. The response of snow drought risk to climate warming is non-linear. A +2°C change in the mean winter (1-Nov to 1-Apr) temperature has a larger impact on the snow drought regime in catchments with winter temperatures near zero compared to catchments with winter temperatures far below zero.

Chapter 5 – Case Study: Future Water Security in Northeast British Columbia.

1. Continued climate warming will likely lead to decreased summer runoff for the plains and foothills regions of the Peace River watershed in northeast British Columbia. Without significant commitment on the part of industry to re-use and recycle water for hydraulic fracturing, this decrease in summer runoff will likely co-occur with substantial increases in oil and gas industry freshwater demand.

2. While larger watersheds will likely have sufficient water quantity to meet future shale gas industry freshwater demands, smaller watersheds in areas with high levels of oil and gas development may experience water scarcity, especially during drought conditions.

3. The Northeast Water Tool (NEWT), a decision support tool that provides guidance on natural water supply and availability, does not capture heterogeneity in the hydrological processes of smaller catchments. Differences between the NEWT-estimated monthly runoff and the actual monthly runoff, especially with regards to runoff timing and earlier than estimated freshet peaks, may result in an over-estimation of summer water supplies in small headwater catchments.

Chapter 2. Climate Controls on Runoff and Low Flows in Mountain Catchments of Western North America

This chapter was submitted as a paper to *Water Resources Research* and is cited in other chapters of this thesis as:

Dierauer, J.R., Whitfield, P.H., & Allen, D.M. (in review-a). Climate controls on runoff and low flows in mountain catchments of western North America. *Water Resources Research*.

Supplemental figures, tables, and text for this chapter are included in Appendix A.

2.1. Introduction

In mountain regions of the western North America (WNA), much of the annual precipitation falls as snow, and thus, snow accumulation and melt are the dominant controls on the within-year distribution of streamflow. Streamflow in these mountain regions is highly seasonal, with low flow periods occurring in winter and/or summer. Winter and summer low flows are generated by different hydrologic processes (Waylen & Woo, 1987; Laaha & Blöschl, 2006; Burn et al., 2008). During the winter season, below freezing temperatures lead to snow accumulation, thus increasing water storage and decreasing flows until the occurrence of the spring freshet. Conversely, summer low flows occur when temperatures are above freezing, snowpack storage is largely depleted, and the evapotranspiration rate exceeds the precipitation rate. Streamflow is often sustained by groundwater discharge during low flow periods. Thus, sustained recharge to the groundwater system is necessary for sustaining streamflow during low flow periods. Depending on climate and physiography, a catchment may have a summer low flow period, a winter low flow period, or both.

While low flow periods are a normal, annually recurring component of the natural flow regime (Smakhtin, 2001), longer and/or more severe low flow periods are synonymous with streamflow droughts and may have significant impacts on water supply, agricultural production (Wilhite, 2000), electricity generation (Wilhite, 2000; van Vliet et al., 2012; Bartos & Chester, 2015), and human (Charron, et al., 2004) and

aquatic ecosystem (Lake, 2003) health. Recent studies (Teuling et al., 2013; Diffenbaugh et al., 2015) have highlighted the role of temperature in streamflow and groundwater droughts, demonstrating that above-average temperatures can increase drought duration and severity. Other studies have shown that above-average temperatures have substantial impacts on snow hydrology, including a shift in the snowmelt season toward earlier spring and, consequently, decreased warm season runoff (Leith & Whitfield, 1998; Whitfield & Cannon, 2000; Adam et al., 2009; Déry et al., 2009; Pederson et al., 2011; among others), as well as decreasing snowmelt rates (Harpold & Kohler, 2017; Musselman et al., 2017).

Despite the documented role of temperature in streamflow and groundwater droughts and the recognized impacts on snowmelt hydrology, the relative impact of temperature and precipitation on summer and winter low flows remains unclear. Kormos et al. (2016) used path analysis to isolate temperature effects from precipitation effects and showed that, in the Pacific Northwest, the historical variability of annual summer minimum flows has been more closely related to precipitation than to temperature. Godsey et al. (2014) and Jenicek et al. (2016) showed that lower peak snow water equivalent corresponds to lower summer minimum flows. These studies, however, only analyzed minimum flows and did not separate the relative impact of precipitation versus temperature on the duration or severity of summer or winter low flows.

Since summer and winter low flows have different causal mechanisms (i.e. high evapotranspiration rates versus below freezing temperatures, respectively), any analysis of the climate controls on low flows must first separate winter low flows from summer low flows. Previous studies have used an arbitrary standard “winter” classification (e.g., Nov 1st to April 30th in Ehsanzadeh & Adamowski, 2007; Nov 16th to May 31st in Kormos et al., 2016) or a “drought year” with an April 1st start (e.g., Douglas et al., 2000). The use of a “drought year” ensures that the low flow period is not split between years but does not separate low flows generated by different hydrological processes. Similarly, a standard winter classification, based upon calendar dates, may effectively separate winter versus summer annual minimum flows, but is ineffective for separating the full summer versus winter low flow periods and ignores the realities of elevation and latitude.

Without a robust methodology for low flow regime classification that includes a process-based separation of summer and winter low flows, the dominant climate

controls and, consequently, the relative impact of precipitation and temperature on low flow generation will likely remain poorly understood. With this in mind, the objectives of this study are to: (1) develop a robust methodology to classify low flow regimes and separate summer and winter low flows, (2) identify the dominant climate controls on low flow regimes and on the inter-annual variability of runoff and low flows, and (3) quantify the relative sensitivity of runoff and low flows to temperature and precipitation.

2.2. Data and Methods

The following sections describe the streamflow observations, meteorological data, and simulated fluxes used (sections 2.2.1 and 2.2.2) as well as the methods employed to characterize the low flow regime (section 2.2.3), define predictor and response variables (section 2.2.4), identify dominant climate controls (section 2.2.5), and quantify the precipitation- and temperature-sensitivity of runoff and low flows (section 2.2.6).

2.2.1. Streamflow Observations

Streamflow records were obtained from the Canadian Reference Hydrometric Basin Network and the United States Hydroclimatic Data Network. These Reference Hydrometric Networks (RHNs) represent a collection of streamflow gauges that have stable conditions and/or a minimum of direct anthropogenic influence (Whitfield et al., 2012). To remove catchments with complex streamflow regimes, catchment size was limited to less than 5,000 km^2. Additionally, in order to have a consistent hydrometeorological dataset for all catchments, the maximum latitude was set to 52°N, matching the northern extent of the Livneh et al. (2015) dataset domain (see section 2.2). A common analysis period of 1983-2012 was chosen to maximize the number of catchments included in the analysis, and only gauges having at least 29 years of flow data with no missing observations were included in the initial subset.

After the initial subset of stations was selected, the streamflow regime for each catchment was visually screened using the R package “FlowScreen” (Dierauer & Whitfield, 2016; Dierauer et al., 2017), and catchments without a recognizable snowmelt peak were removed from the analysis. Remaining catchments were delineated from topographic maps and compared to level III ecoregion polygons for North America

(Commission for Environmental Cooperation [CEC], 2009). Catchments with less than ~90% of their area within a single level III ecoregion were removed from the analysis to avoid mixed catchment types (e.g., half mountains, half plains). Additionally, since the goal of the study was to analyze climate controls on summer low flows and winter low flows, catchments without a substantial (<100 days) summer or winter season (based on the simplified seasonal classification scheme described in section 2.3) were removed from the analysis.

With this selection strategy, the final subset of RHN gauging stations included 12 stations in Canada and 51 stations in the contiguous United States, for a total of 63 stations (Figure 2.1; Appendix A, Table S2.1). The catchments range in size from 9 km^2 to 3354 km^2 and have a wide range of climate conditions. Mean annual precipitation ranges from 486 mm/year to 3100 mm/year. Mean annual temperature ranges from -1.4°C to 6.9°C.

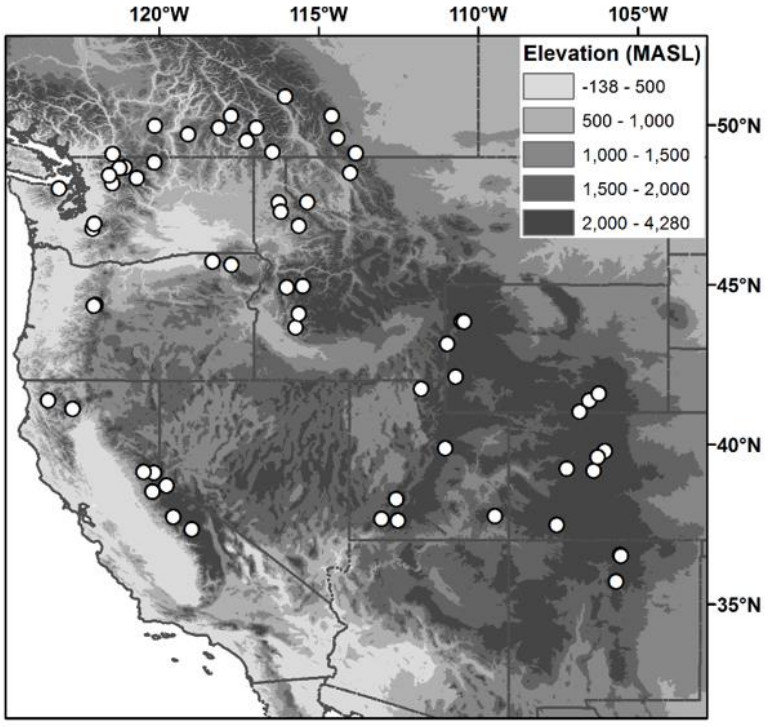

Figure 2.1 Study region elevation in meters above sea level (MASL) with the locations of selected hydrometric gauging stations indicated by white circles. Additional station information is included in Appendix A, Table S2.1.

2.2.2. Meteorological Data and Simulated Fluxes

The climate data used for this analysis were obtained from the Livneh et al. (2015) gridded hydrometeorological dataset. This dataset contains gridded observation-based daily meteorological forcings and simulated Variable Infiltration Capacity (VIC) model states and fluxes at 1/16° resolution for the 1950 to 2013 period. The VIC model (Liang et al., 1994) is a physically based land-surface model capable of simulating energy and water balance. The parameterization and validation of the VIC model is described in Livneh et al. (2015). The Livneh et al. (2015) dataset was chosen because it has a larger domain and finer spatial resolution than previous datasets (e.g., Maurer et al., 2002; Livneh et al., 2013).

In mountainous terrain, gridded datasets may represent over-smoothed topography and thus introduce biases into the climate data. To account for the effects of topography, the Livneh et al. (2015) dataset uses a constant temperature lapse rate of -6.5 °C/km and incorporates orographic scaling across the entire domain. Gridded datasets fail to reproduce station observations completely; however, Behnke et al. (2016) showed that the Livneh et al. (2013) dataset, the domain of which was extended by Livneh et al. (2015), is one of the better-performing gridded climate datasets currently available. Temperature accuracy was an important consideration since the gridded climate data were used to define catchment-specific hydrologic year start days (see section 2.3). The Livneh et al. (2013) dataset has minimal bias (<1°C) for minimum and maximum daily temperatures within ±10° of 0°C (Behnke et al., 2016). With the exception of the Maurer et al. (2002) dataset, other gridded datasets analyzed by Behnke et al. (2016) exhibited higher temperature and precipitation biases. The Livneh et al. (2015) dataset was chosen over the Maurer et al. (2002) dataset because of its higher spatial resolution, and thus the possibility for increased accuracy for data-scarce regions of WNA.

For this study, time series of maximum daily temperature, minimum daily temperature, daily precipitation, and daily snow water equivalent (SWE) from the Livneh et al. (2015) dataset were calculated for each catchment by extracting data for all grid cells within each catchment and calculating the average value per day. Mean daily temperature was calculated as the average between the minimum daily temperature and the maximum daily temperature.

2.2.3. Low Flow Regime Characterization

To separate summer low flows from winter low flows, a catchment-specific seasonal classification was used, where days occurring after the start of the frost season and before the spring freshet peak were classified as “winter”, and days occurring after the spring freshet peak and before the onset of the frost season were classified as “summer”. Low flow periods in the two seasons (summer and winter) were then defined using Mean Daily Runoff (MDR) as the upper bound (Figure 2.2). With this method, the length and timing of the simplified “winter” versus “summer” seasons are unique to each catchment and based on catchment climate. Using the freshet peak (as opposed to an arbitrary date or the end of a temperature-defined frost-season) to separate the “winter” season from the “summer” season effectively separates summer low flows from winter low flows even with inter-annual shifts in freshet timing (Appendix A, Figure S2.1).

Within this catchment-specific seasonal classification scheme, the start of the frost season was defined for each catchment based on the 30-year (1983-2012) average climate, where the start of the frost season was defined as the first day of the year occurring after the warmest day of the year and with a 30-year mean temperature less than 0°C. The catchment-specific frost season start was used to define the start of the hydrologic year for all calculations. In many years, temperatures may oscillate above and below the freezing point for days or weeks, and the actual “boundary” between the summer and winter periods in any one year may be substantially different from the defined boundary. The methodology presented here is based on the average climate of each individual catchment and is applied in the same manner in all catchments. Thus, using these temperature criteria provides a fairer comparison than using an arbitrary calendar date, especially for this large and topographically complex region of WNA, where latitude and elevation strongly affect the timing and duration of the frost season.

For all hydrometric time series, the observed mean daily streamflow values (m^3/s) were converted to daily runoff values (mm/day) and then smoothed with a 15-day centered moving average filter to eliminate day-to-day variations and reduce the effect of individual, potentially spurious values in the raw data. The average timing of the freshet peak, hereafter referred to as the “freshet peak”, for each catchment was defined based on the 30-year (1983-2012) hydrograph, calculated as the mean daily runoff from the smoothed time series. The freshet peak for each catchment was defined as the day of

the year with the highest 30-year mean daily runoff within the set of days occurring after the mid-point of the frost season and before the mid-point of the non-frost season. Defining the freshet peak using this subset of days ensures that the peak is occurring due to snowmelt and not due to late-summer or fall rain.

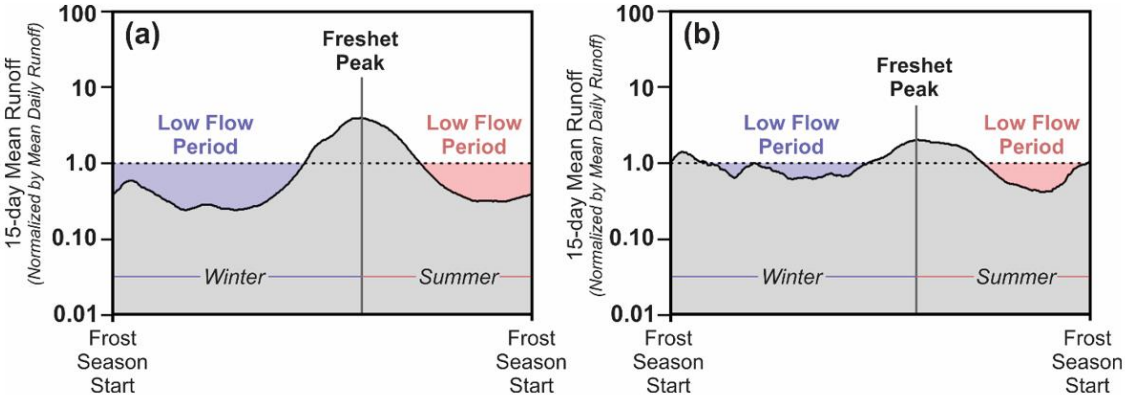

Figure 2.2 **Example low flow regime classifications: (a) Flathead River, gauge ID 12358500, and (b) Newhalem Creek, gauge ID 12178100. Winter low flow period shown in blue; summer low flow period shown in pink. Dashed horizontal line is equal to the mean daily runoff (MDR) and is used as the upper-bound for defining the low flow periods. The gray areas above the MDR line are equal to the blue and pink areas when not plotted with a logarithmic y-axis.**

2.2.4. Predictor and Response Variables

To analyze climate controls on the low flow regimes, nine streamflow response variables and eight climate predictor variables were chosen (Table 2.1). The streamflow response variables include the duration (DUR), average magnitude (MAG), severity (SEV), and maximum deficit (MAX) of the summer (denoted with subscript “s”) and winter (denoted with subscript “w”) low flow periods. DUR was calculated as the cumulative number of days when the smoothed streamflow was less than MDR. SEV was calculated as the cumulative water deficit below MDR, and MAG was calculated as SEV divided by DUR. MAX was calculated as the maximum deviation below MDR and represents the maximum intensity of the low flow period. Low flow duration is directly comparable between catchments and therefore is expressed in units of days. The magnitude, maximum deficit, and severity of the seasonal low flow periods, however, are dependent on the magnitude of catchment MDR. Therefore, to aid in comparison between catchments, magnitude and maximum deficit are normalized by MDR. Severity

is a cumulative value, and therefore is normalized by Mean Annual Runoff (MAR). The full list of streamflow response variables and the associated abbreviations are provided in Table 2.1; equations used to calculate the variables are included in Appendix A, Table S2.2.

The eight chosen climate predictors include both seasonal and annual variables. The seasonal climate variables, summer mean temperature (T_s), summer precipitation (P_s), winter mean temperature (T_w), winter precipitation (P_w), and winter thawing degrees (TD_w), were calculated using the simplified summer versus winter seasonal classification, as defined in section 2.3 and as shown in Figure 2.2. The annual climate variables, mean temperature (T_a), precipitation (P_a), and snow fraction (Sf), were calculated using the catchment specific winter season start (i.e. the start of the frost season, see Figure 2.2) as the start of the hydrologic year. Sf was calculated using a threshold of 0°C, and TD_w was calculated as the sum of mean daily temperatures for all winter days with a mean temperature above 0°C.

Table 2.1 Climate predictor variables and low flow regime response variables used in the analyses.

Predictor variables	Abbreviation	Units
Annual Precipitation	P_a	cm
Mean Annual Temperature	T_a	°C
Summer Precipitation	P_s	cm
Summer Mean Temperature	T_s	°C
Winter Precipitation	P_w	cm
Winter Mean Temperature	T_w	°C
Winter Thawing Degree Days	TD_w	°C
Snow Fraction	Sf	Fraction of P_a
Response variables	**Abbreviation**	**Units**
Mean Daily Runoff	MDR	mm
Summer low flow duration	DUR_s	days
Summer low flow average magnitude	MAG_s	Fraction of MDR
Summer low flow severity	SEV_s	Fraction of MAR
Summer low flow deficit max	MAX_s	Fraction of MDR
Winter low flow duration	DUR_w	days
Winter low flow average magnitude	MAG_w	Fraction of MDR
Winter low flow severity	SEV_w	Fraction of MAR
Winter low flow deficit max	MAX_w	Fraction of MDR

2.2.5. Identification of Dominant Climate Controls

Identification of the dominant climate controls on low flows provides a basis for understanding what might occur under future climate change, particularly separating

responses to changes in temperature from responses to changes in precipitation. In this study, two analyses were completed: (1) a regional analysis of climate controls on low flow regimes and (2) a catchment-scale analysis of climate controls on the inter-annual variability of runoff and low flows. The regional analysis provides insight into how a catchment's low flow regime may change due to an overall shift in the average climate. The catchment-scale analysis reveals which climate conditions lead to more severe summer/winter low flows and/or decreased runoff and is therefore synonymous with the identification of the primary climatic causes of streamflow drought.

For the regional analysis of climate controls on low flow regimes, the predictor and response variables were calculated for each catchment as the mean over the 30-year analysis period (1983-2012). For the catchment-scale analysis of climate controls on the inter-annual variability of runoff and low flows, predictor and response variables were calculated for each hydrologic year, using the same hydrologic year start and seasonal classification scheme as defined by the common 30-year analysis period. The equations used to calculate the 30-year regime values and the yearly values are included in Appendix A, Table S2.2. Godsey et al. (2014) documented significant memory effects in snow-dominated catchments in the Sierra Nevada Mountains; therefore, climate conditions of the preceding year were also included in the catchment-scale correlation analysis and are denoted with a [$^{-1}$] superscript. For the winter low flow season, climate predictors that include information about the following season climate conditions (T_s, P_s, T_a, P_a) were excluded.

Dominant climate controls were identified using correlation analysis. The regional analysis employed bivariate correlation while the catchment-scale analysis employed bivariate and partial correlation. Dominant climate controls on the low flow regime were identified as those exhibiting the strongest correlations with the streamflow response variables. Dominant climate controls on the inter-annual variability of runoff and low flows were identified as those with a high percentage of catchments exhibiting significant correlations and a high mean percent variance explained. The methods used to calculate the percent variance explained by each predictor variable are included in Appendix A, Text S2.1.

2.2.6. Precipitation and Temperature Sensitivity

After using the correlation analysis to identify the dominant predictor (climate) variables, multiple linear regression (MLR) analysis was used to quantify the sensitivity of the streamflow response variables to each of the dominant predictor variables. All predictor and response variables were standardized by subtracting the mean and dividing by the standard deviation (SD). By using standardized values, i.e. z-scores, for all variables, the MLR analysis produces standardized regression coefficients that represent the change in the response variable for every 1 SD change in the predictor variable. Standardized regression coefficients can be directly compared between predictor variables that have different non-standardized units, e.g., precipitation (cm) and temperature (°C), and thus give an indication of the relative sensitivity of a response variable to each of the predictor variables. To isolate the dominant climate controls, only significant variables ($p < 0.05$) with standardized regression coefficients a magnitude larger than the standard error values were kept in the final MLR models. See Appendix A, Text S2.2 for handling of collinearity.

Based on results of the MLR analysis, the Mann-Whitney U test was used to further quantify the impact of the dominant climate controls on runoff and low flows in these catchments. The Mann-Whitney U-test (Mann & Whitney, 1947), also known as the Wilcoxon rank-sum test (Wilcoxon, 1945), is a non-parametric statistical hypothesis test used to determine if there is a significant difference between two independent samples.

2.3. Results

The following sections summarize the main findings of this study. Section 3.1 presents the results of the low flow regime characterization (Objective 1). Sections 3.2 and 3.3 identify the dominant climate controls on low flow regimes and on the inter-annual variability of runoff and low flows, respectively (Objective 2). Sections 3.4 and 3.5 quantify the relative sensitivity of runoff and low flows to temperature and precipitation (Objective 3).

2.3.1. Low Flow Regime Characterization

All catchments exhibit both summer and winter low flow periods. The low flow response variables are inter-related (Figure 2.3). Catchments with longer winter (summer) low flow seasons tend to have shorter summer (winter) low flow seasons, as illustrated by the strong negative correlation (Spearman's rho = -0.81) between DURs and DURw. Additionally, catchments with longer low flow periods, i.e. higher DURs or DURw values, tend to have more severe low flows. Interestingly, catchments with higher runoff (i.e. higher MDR values) tend to have shorter, less severe winter low flow periods but no tendency toward shorter or less severe summer low flow periods.

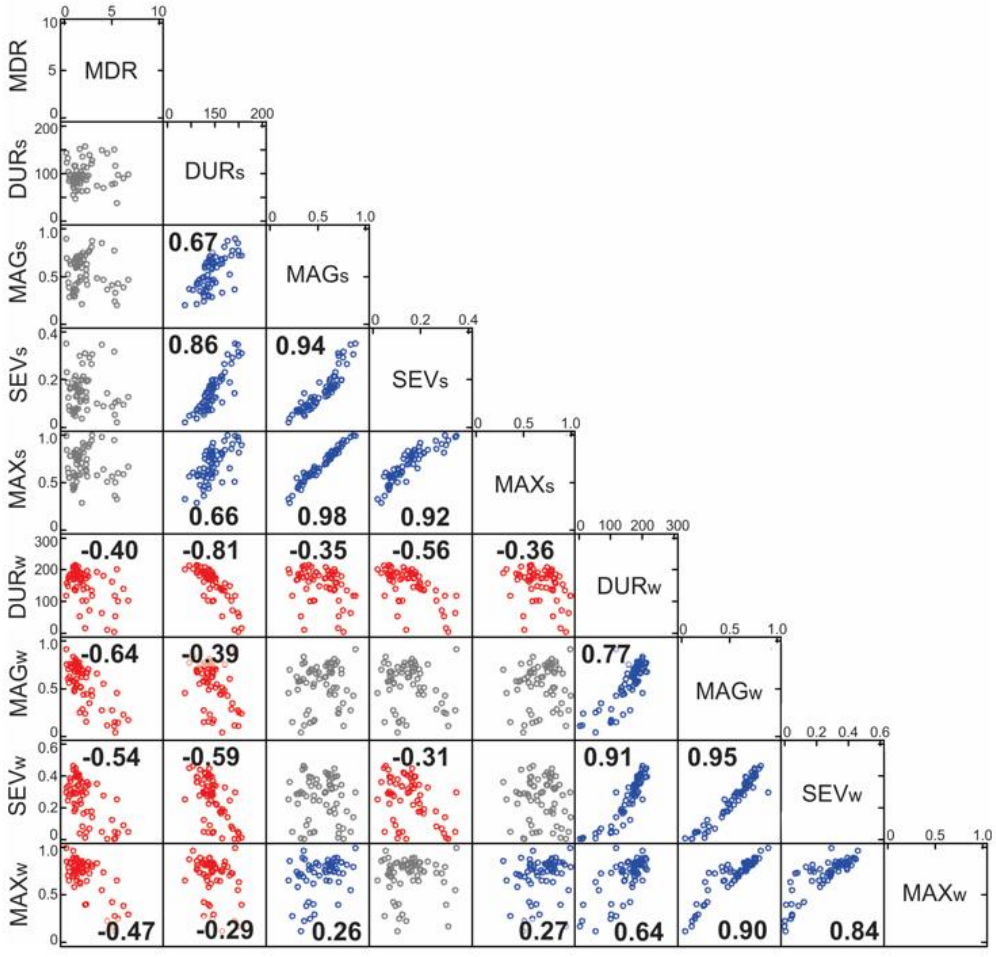

Figure 2.3 Response variable bivariate plots. Spearman's rho reported for significant ($p < 0.05$) correlations. Red (blue) points indicate significant negative (positive) correlation; gray points indicate non-significant results. Abbreviations and units are as in Table 2.1.

2.3.2. Regional Analysis: Climate Controls on the Low Flow Regime

As expected, warmer catchments have longer, more severe summer low flows, and shorter, less severe winter low flows compared to cooler catchments. All seasonal low flow response variables exhibit the highest correlation with temperature-related climate predictors (Figure 2.4). For summer low flows, the correlation is positive, while for winter low flows, the correlation is negative. For example, T_a is positively correlated with the DUR_s and negatively correlated with the DUR_w. Similarly, T_s is positively correlated with SEV_s and negatively correlated with SEV_w.

While MDR is primarily controlled by precipitation, the low flow regime is primarily controlled by temperature. Except for the significant negative correlation (rho = -0.25) between P_s and MAG_s, there are no significant correlations between the summer low flow regime and precipitation (Figure 2.4). Regardless of the magnitude of annual precipitation, warmer catchments have longer, more severe summer low flows. This is further illustrated by Figure 2.5, which shows four catchments (two each from two different ecoregions) with different P_a and T_a values. For both ecoregion pairs, the warmer, wetter catchment exhibits a longer, more severe summer low flow season compared to the cooler, drier catchment.

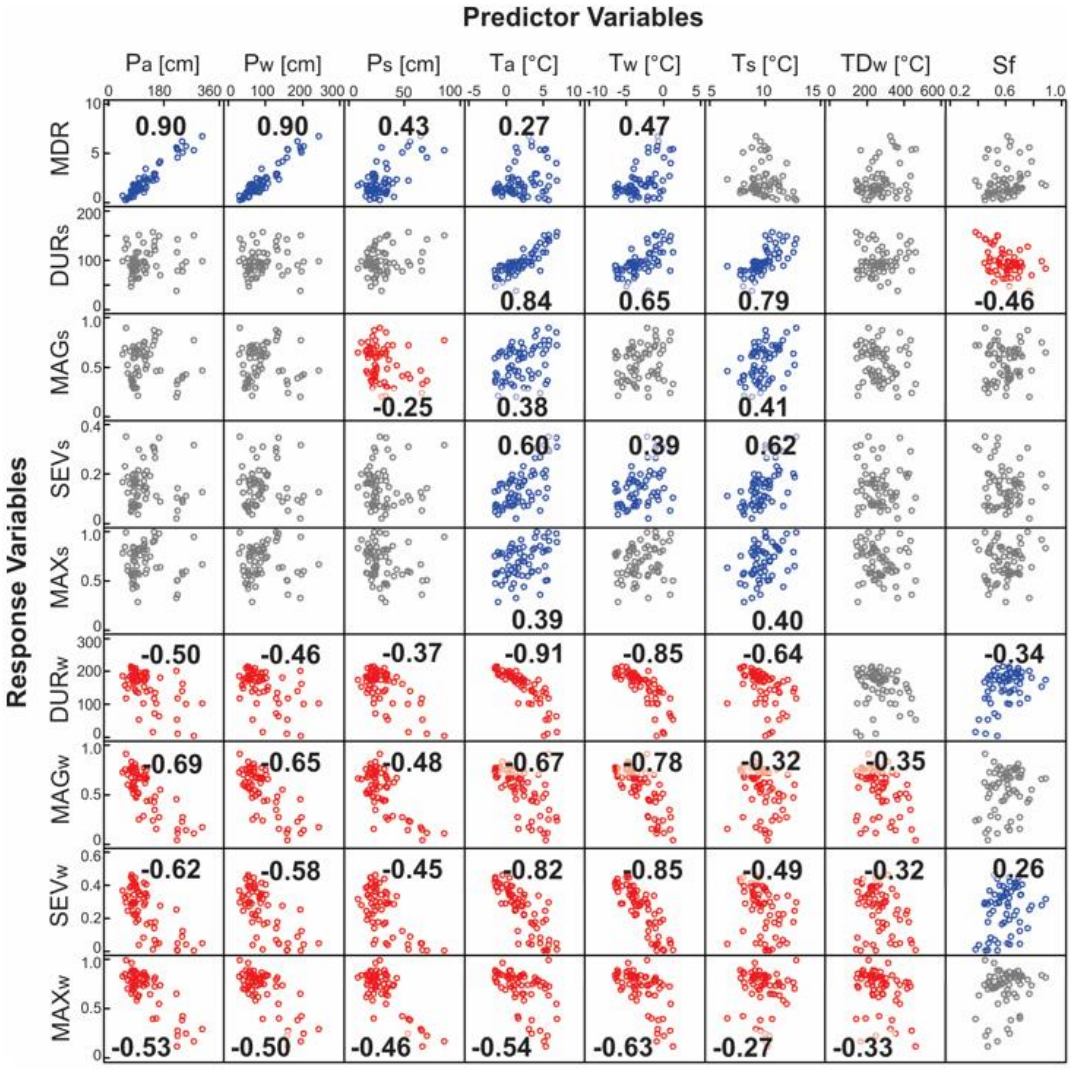

Figure 2.4 **Predictor and response variable bivariate correlation plots. Spearman's rho reported for significant ($p < 0.05$) correlations. Red (blue) points indicate significant negative (positive) correlation; gray points indicate non-significant results. Abbreviations and units are as in Table 2.1.**

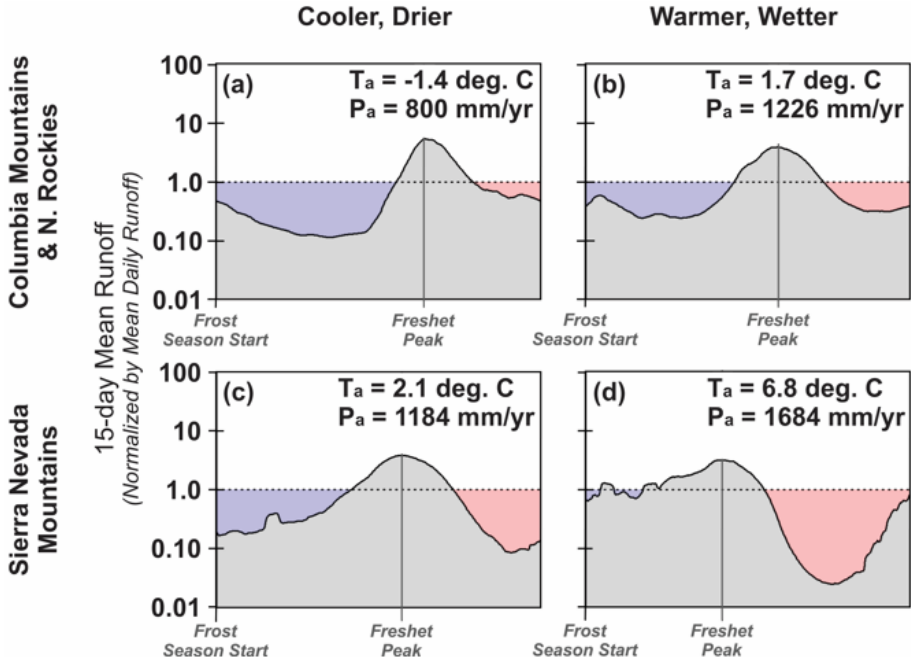

Figure 2.5 **Low flow regimes for catchments with different mean annual temperatures (T_a) and mean annual precipitation (P_a) – two each from two level III ecoregions. (a) Cataract Creek, gauge ID 05BL022, (b) Flathead River, gauge ID 12358500, (c) Merced River, gauge ID 11264500, (d) Duncan Canyon Creek, gauge ID 11427700.**

2.3.3. Catchment-scale Analysis: Climate Controls on Inter-annual Variability

Figure 2.6 shows the relative importance of each climate predictor variable quantified by calculating both the fraction of stations with significant correlations ($p < 0.05$) and the mean percent variance explained by each climate predictor. The mean percent variance explained was calculated using the subset of significant correlations. The dominant climate controls are identified as those with a high fraction of significant correlations and a high mean percent variance explained, i.e. taller bars and with higher color saturation in Figure 2.6.

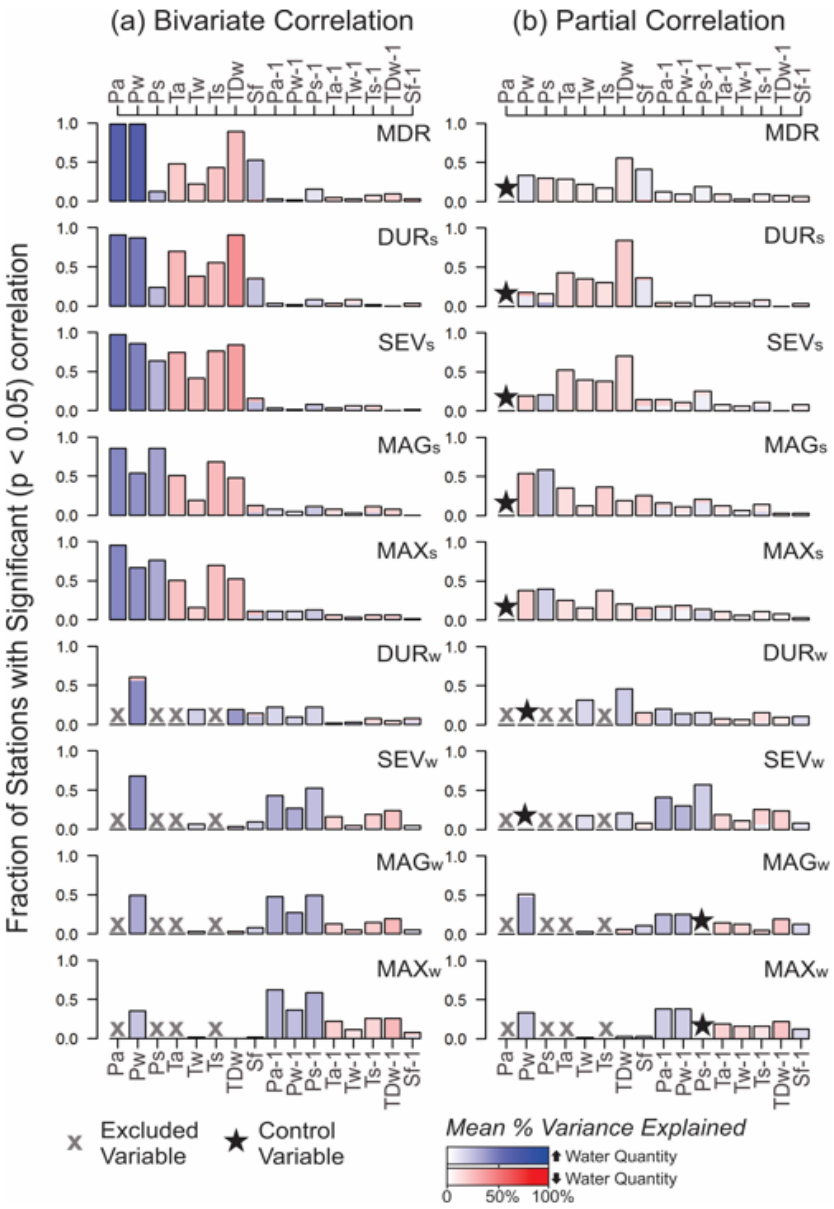

Figure 2.6 **(a) Fraction of stations exhibiting significant correlation (p value < 0.05) between the streamflow response variables and the climate predictor variables. (b) Fraction of stations exhibiting significant partial correlations (p < 0.05) – control variable marked with a star. For (a) and (b): Red gradient indicates an increase in the climate predictor variable is associated with a decrease in water quantity (e.g., longer duration low flow season, lower runoff) while blue gradient indicates increased water quantity (e.g., shorter duration low flow season, higher runoff). Color saturation, shown in bottom legend, indicates mean percent variance explained for the subset of stations with significant correlations. Streamflow response variable and climate predictor variable abbreviations are as in Table 2.1, with the addition of preceding year climate variables, as indicated with "-1" postscript.**

Mean daily runoff (MDR)

Precipitation is the dominant control on the inter-annual variability of MDR (Figure 2.6a). MDR is significantly correlated to P_a in 100% of the catchments and with P_w in 62 out of the 63 catchments. P_s exhibits less control on MDR and is significantly correlated with MDR in less than 24% of catchments (Figure 2.6a). Temperature, particularly winter thawing degrees (TD_w), is a significant secondary control on MDR in the majority (69%) of catchments. Considering two years with equal precipitation (P_a), as represented by the partial correlation analysis (Figure 2.6b), MDR tends to be lower in years with warm winters (i.e. years with high TD_w values). Snow fraction (Sf) is also a significant secondary control in the majority (68%) of catchments. However, Sf cannot be used to isolate the separate roles of temperature and precipitation because the Sf in any one year is dependent on both winter temperatures and precipitation timing.

Summer low flows

Unlike the regional analysis (section 3.2), which indicated that temperature is the dominant control on the low flow regime, the catchment-scale analysis shows that precipitation is the dominant control on the inter-annual variability of summer low flows. Wet years (high P_a values) tend to have shorter, less severe summer low flow periods. However, winter temperature (TD_w) is a significant secondary control on DUR_s and SEV_s in the majority of catchments (90% and 87%, respectively). Considering two years with equal precipitation (P_a), as represented by the partial correlation analysis (Figure 2.6b), the severity and duration of summer low flows tends to be higher in years with warm winters (i.e. years with high TD_w values). Temperature control is higher for DUR_s and SEV_s than for MAG_s and MAX_s, and summer precipitation (P_s) is the dominant secondary control on MAG_s and MAX_s in the majority of catchments (73% and 62%, respectively; Figure 2.6b).

Winter low flows

Like MDR and summer low flows, the inter-annual variability in winter low flows is primarily controlled by precipitation. P_s^{-1} is the strongest control on MAG_w and MAX_w, with 65% and 78% of the catchments exhibiting significant negative correlations between P_s^{-1} and MAG_w and MAX_w, respectively. DUR_w and SEV_w are more strongly controlled by within-season precipitation (P_w; Figure 2.6a). For both predictor variables P_w and P_s^{-1}, higher precipitation corresponds to shorter, less severe winter low flows. A substantial

portion (76%) of stations also exhibit significant partial correlations between DUR_w and TD_w (Figure 2.6b), illustrating that warm winters have shorter low flow periods while cool winters have longer low flow periods. In general, the correlation analysis shows that winter low flows are shorter and less severe in years with warm, wet winters and wet preceding summers than in years with cool, dry winters and dry preceding summers.

2.3.4. Low Flow Sensitivity to Precipitation and Temperature

The MLR models show that temperature-sensitivity of low flows is up to two times higher than the temperature-sensitivity of MDR (Table 2.2). MDR is sensitive to winter season temperatures, with a 1 SD increase in TD_w corresponding to a 0.21 SD decrease in MDR. Summer low flows exhibit the highest sensitivity to temperature, with a 1 SD increase in TD_w corresponding to a 0.42 SD increase in DUR_s and a 0.35 SD increase in SEV_s. For the winter low flow season, DUR_w exhibits the highest temperature-sensitivity (-0.34 SD DUR_w per +1 SD TD_w). For SEV_w, TD_w and TD_w^{-1} act in opposition to one another, and a warm winter (high TD_w) corresponds to a less severe low flow period within the season (lower SEV_w) but longer duration low flows for the following winter season (i.e. higher SEV_w^{+1}).

While the temperature-sensitivity of low flows is higher than the temperature-sensitivity of annual streamflow (represented here by MDR), precipitation is the dominant control on the inter-annual variability of both annual streamflow and low flows (Table 2.2). Summer low flows and annual streamflow are most sensitive to P_a. However, the seasonal distribution of precipitation also matters, especially for MAG_s and MAX_s, and abnormally wet summers (i.e. low P_w) correspond to lower intensity summer low flows (i.e. lower MAG_s and MAX_s). For winter low flows, duration and severity are most sensitive to within-season season precipitation (P_w), while intensity (i.e. MAG_w, MAX_w) is most sensitive to the preceding season precipitation (P_s^{-1}).

Table 2.2 Streamflow response variable sensitivity to selected climate variables, estimated by standardized regression coefficients.

	MDR	DUR_s	SEV_s	MAG_s	MAX_s	DUR_w	SEV_w	MAG_w	MAX_w
P_a	0.71 ±0.02	-0.53 ±0.02	-0.55 ±0.01	-0.48 ±0.02	-0.53 ±0.02	--	--	--	--
P_w [a]	0.13 ±0.02	--	0.19 ±0.01	0.32 ±0.02	0.26 ±0.02	-0.49 ±0.02	-0.49 ±0.02	-0.32 ±0.02	-0.24 ±0.02
P_s^{-1}	--	--	--	--	--	-0.16 ±0.02	-0.29 ±0.02	-0.33 ±0.02	-0.40 ±0.02
TD_w	-0.21 ±0.02	0.42 ±0.02	0.35 ±0.02	0.16 ±0.02	0.19 ±0.02	-0.34 ±0.02	-0.22 ±0.02	--	--
TD_w^{-1}	--	--	--	--	--	--	0.19 ±0.02	0.19 ±0.02	0.21 ±0.02
T_s	--	--	0.14 ±0.01	0.15 ±0.02	0.13 ±0.02	--	--	--	--
y-int.	~0.0 ±0.01	~0.0 ±0.02	~0.0 ±0.01	~0.0 ±0.02	~0.0 ±0.02	~0.0 ±0.02	~0.0 ±0.02	~0.0 ±0.02	~0.0 ±0.02
r^2	0.67	0.59	0.65	0.48	0.52	0.27	0.35	0.27	0.29
F	1282	1372	876.9	437.6	510.3	227	253.3	236.5	252.2
DF	1886	1887	1885	1885	1885	1886	1885	1886	1886

Note: "--" indicates that the variable was not included in regression equation for the corresponding response variable. Standard error values are listed beneath the standardized regression coefficients. Variable abbreviations are as defined in Table 2.1, with [-1] superscripts denoting preceding hydrologic year (see section 3.3). All variables and models are significant at the $p < 0.05$ level. [a] For MDR, DUR_s, MAG_s, SEV_s, and MAX_s, the standardized residuals of $P_w \sim P_a$ are used as input to the regression models (see Text S2.2 for details). For DUR_w, MAG_w, SEV_w, and MAX_w, P_a is not part of the regression models, and the standardized P_w values are used as inputs to the regression models.

2.3.5. Winter Climate Impacts on SWE, Runoff, and Low Flows

The correlation and MLR analyses (sections 3.3 and 3.4) show that, in these mountain catchments, runoff and low flows are sensitive to winter climate conditions, particularly winter precipitation (P_w) and winter thawing degrees (TD_w). To further analyze the impact of winter climate on SWE, runoff, and low flows, particularly the co-occurrence of warm and dry conditions, the winter season was classified into four types based on the standardized P_w and TD_w values (i.e. z-scores) as shown in Figure 2.7. This classification scheme was then used in combination with Mann-Whitney tests to quantify the impact of warm winter conditions (i.e. above average TD_w) on streamflow, runoff, and low flows. Two comparisons for each streamflow response variable were made to isolate the impact of warm winters: 1) years with warm and dry (W-D) winters versus years with cool and dry (C-D) winters, and 2) years with warm and wet (W-W) winters versus years with cool and wet (C-W) winters. Since studies have shown correlations between snow fraction and annual runoff (Berghuijs et al., 2014) and between peak SWE and summer low flows (Godsey et al., 2014; Jenicek et al., 2016),

winter climate impacts on peak and April 1st SWE were also analyzed. Results of the Mann-Whitney U test are presented in Table 2.3.

Results of this analysis show that, in these mountain catchments, W-D winters occur 1.5 times more often than C-D winters (Figure 2.7). Additionally, years with W-D winters and have significantly lower annual runoff, significantly longer, more severe summer low flows, significantly shorter, less severe winter low flows, and significantly lower SWE compared to years with C-D winters (Table 2.3). The lower water quantity in years with W-D winters (compared to years with C-D winters) is at least partially due to significantly lower precipitation (P_a). However, the median absolute difference in P_a (0.06 SD) is substantially smaller than the median absolute difference in annual runoff (0.33 SD) and summer low flow variables (0.37-0.71 SD).

The differences between W-W winters and C-W winters are similar, and years with W-W winters have significantly lower runoff, significantly longer, more severe summer low flows, significantly shorter winter low flows, and significantly lower SWE compared to years with C-W winters (Table 2.3). W-W winters occur approximately half as often as C-W winters (Figure 2.7) and have significantly lower precipitation than C-W winters (Table 2.3). The median absolute difference between W-W and C-W years is highest for DUR_s (0.79 SD), which is in direct agreement with the MLR analysis which showed that, out of all response variables, DUR_s exhibits the highest sensitivity to TD_w.

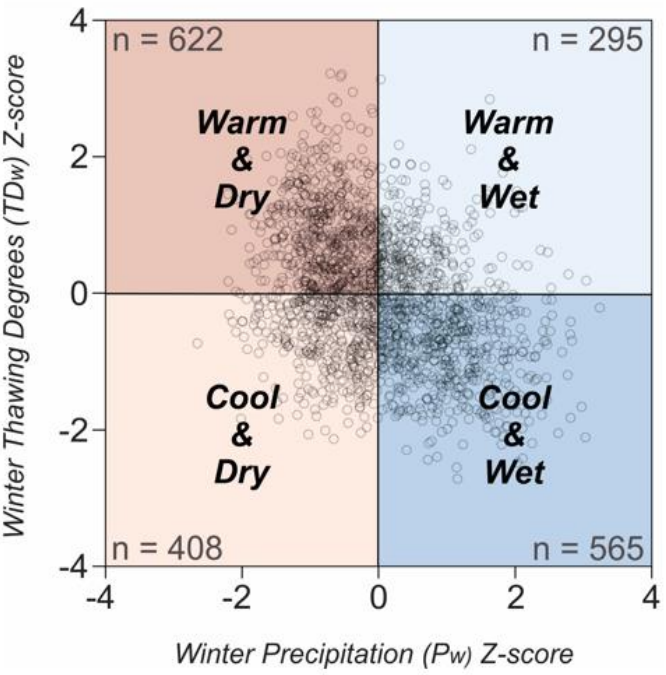

Figure 2.7 **Winter season classification based on standardized values (z-scores) for winter precipitation (Pw) and winter thawing degrees (TDw). Number of years in each quadrant indicated by n values.**

Table 2.3 **Effect of winter climate conditions on the median z-scores of runoff and low flows. Significance assessed with the Mann-Whitney U test.**

	Warm Dry	Cool Dry	Difference	Warm Wet	Cool Wet	Difference
n	*622*	*408*		*295*	*565*	
P_a	-0.71	-0.61	**-0.06**	0.55	0.79	**-0.24**
P_w	-0.71	-0.66	-0.05	0.47	0.94	**-0.36**
Peak SWE	-0.73	-0.56	**-0.17**	0.29	0.94	**-0.59**
April 1 SWE	-0.73	-0.51	**-0.19**	0.32	0.90	**-0.57**
MDR	-0.78	-0.45	**-0.33**	0.25	0.88	**-0.61**
DUR_s	0.79	0.11	**+0.71**	-0.02	-0.84	**+0.79**
SEV_s	0.81	0.11	**+0.69**	-0.14	-0.76	**+0.63**
MAG_s	0.59	0.22	**+0.35**	-0.02	-0.45	**+0.35**
MAX_s	0.63	0.30	**+0.37**	-0.03	-0.46	**+0.37**
DUR_w	0.08	0.60	**-0.48**	-0.50	-0.10	**-0.38**
SEV_w	0.28	0.54	**-0.37**	-0.35	-0.35	-0.01
MAG_w	0.32	0.49	**-0.17**	-0.16	-0.38	**+0.21**
MAX_w	0.37	0.44	**-0.10**	0.02	-0.18	**+0.21**

Note: Abbreviations are as defined in Table 2.1. Winter classification as in Figure 2.7. All tests were one-tailed, in accordance with the alternative hypothesis that the medians of X_1 are either lower ($X_1 < X_2$; negative [-] difference) or higher ($X_1 > X_2$; positive [+] difference) than the medians of X_2. Null hypothesis: the distributions of the two groups are equal. **Bold** values denote Mann-Whitney U Test was significant at the $p < 0.05$ level.

2.4. Discussion

Precipitation as the dominant control on the inter-annual variability of annual runoff has been documented by many previous studies (Fu et al., 2007; Nash & Gleick, 1991; Ng & Marsalek, 1992; Risbey & Entekhabi, 1996; among others). These studies also reported lower, but significant, temperature control on annual runoff, with the temperature-sensitivity of individual catchments ranging from a 1 to 15% decrease in mean annual runoff per 2°C increase in mean annual temperature. In the mountain catchments in this study, annual runoff was found to be more sensitive to winter thawing degrees than to mean annual temperature. To our knowledge, no other studies have quantified runoff sensitivity to thawing degrees, and the higher sensitivity to thawing degrees (relative to mean annual temperature) documented here suggests that the temperature-sensitivity of annual runoff is higher for catchments with seasonal snow cover.

The significant negative relationship between winter thawing degrees and mean daily runoff documented here (Table 2.2) is consistent with recent studies (Berghuijs et al., 2014; Barnhart et al., 2016), which have concluded that a warmer climate with less snow will lead to a significant decrease in mean annual streamflow. Barnhart et al. (2016) argue that lower snowmelt rates lead to lower streamflow, while Berghuijs et al. (2014) show that a decrease in Sf corresponds to a decrease in streamflow. In this study, the control of TD_w on MDR is shown to be stronger than that of Sf, suggesting that temperature deviations above 0°C have a larger impact on streamflow than does a shift from snow towards rain. Further study is needed to clarify which mechanism, TD_w, Sf, or snowmelt rate, has the largest control on annual streamflow. However, TD_w captures the temperature-related snowpack variability due to late frost season onset, mid-season melt events, and early spring melt, and thus is a promising climate metric for exploring the temperature impacts on snowmelt hydrology.

Precipitation as the dominant control on the inter-annual variability of summer minimum flows has also been documented by previous studies (Godsey et al., 2014; Jenicek et al., 2016; Kormos et al., 2016). In this study, precipitation is shown to be the dominant control not only on summer minimum flows, but also on the duration, severity,

and mean magnitude of summer low flows. Further, the seasonal distribution of precipitation is also important, and a shift toward drier summers (with the same annual precipitation amount) will likely lead to a lower summer minimum flows.

Temperature is recognized as an important control on the seasonal distribution of runoff in mountain catchments (Adam et al., 2009; Pederson et al., 2011) and thus is an important control on the inter-annual variability of both summer and winter low flows. As shown in Table 2.2 and Table 2.3, warming, particularly increased winter thawing degrees, increases the duration and severity of summer low flows and decreases the duration of winter low flows. Summer low flow duration is the most temperature-sensitive low flow variable and is directly related to both the timing and magnitude of the snowmelt peak (illustrated in Appendix A, Figure S2.1). The high sensitivity of summer low flow duration to winter thawing degrees is consistent with previous studies (Leith & Whitfield, 1998; Hamlet & Lettenmaier, 1999; Whitfield & Cannon, 2000; Adam et al., 2009; Déry et al., 2009; Pederson et al., 2011; among others), which show that climate warming is leading to earlier snowmelt onset, earlier peak in river runoff (e.g., early spring as opposed to late spring), and decreased warm season runoff.

Temperature exhibits important, but more complicated, controls on winter low flows. Warmer winters correspond to shorter, less severe winter low flows, but more severe, higher intensity winter low flows in the following hydrologic year (i.e. higher SEV_w, MAG_w, MAX_w; Table 2.2). The increased severity and intensity of winter low flows following a warm winter season can be explained by the longer recession period. In years with warm winters, peak snow water equivalent is lower and snowmelt occurs earlier. Thus, the period of groundwater recession is longer, resulting in lower summer low flows and lower winter low flows for the following hydrologic year.

In light of the results presented here, warming temperatures are expected to lead to longer, more severe summer low flows, and shorter winter low flows. In WNA, decreasing summer runoff and decreasing summer minimum flows have already been documented (Aguado et al., 1992; Ehsanzadeh & Adamowski, 2007; Luce & Holden, 2009; Dittmer, 2013; Kormos et al., 2016; among others). Trends in winter flows, however, are less studied and less clear. Novotny and Stefan (2007) documented trends toward less severe winter low flows in Minnesota, attributing the change to more frequent snow melt events. Ehsanzadeh and Adamowski (2007) documented shifts

toward earlier winter low flow timing in Canada, suggesting a trend toward shorter winter low flow periods. Kormos et al. (2016) found minimal evidence for significant trends in winter low flows for the Pacific Northwest.

Detecting trends in winter low flows is more difficult than summer low flows for many mountain watersheds, and the quality of winter low flow measurements may influence the results of low flow analyses (Whitfield & Hendrata, 2006). Daily discharge measurements have greater error during the cold season under ice conditions than during open-water conditions (Moore et al., 2002; Whitfield & Hendrata, 2006; Hamilton, 2008). An in-depth analysis of hydrometric data uncertainty is beyond the scope of this paper. However, the uncertainty in winter and summer low flow measurements was partly overcome by using smoothed time series and the attributes of entire low flow periods rather than only annual minimum flows. Future research on temporal trends in winter low flows may benefit from the low flow period classification scheme presented here, as well as the knowledge that winter warming has confounding effects on winter low flows, causing decreased severity within the winter season, but increased severity and intensity for the winter season in the following hydrologic year.

Overall, the results presented show that runoff and low flows are sensitive to winter climate conditions, particularly winter precipitation and winter thawing degrees. With continued climate warming, winter thawing degrees will increase, resulting in decreased runoff, longer more severe summer low flows, and shorter winter low flows. Compared to annual runoff, low flows, particularly summer low flows, are more sensitive to climate warming. Summer low flow duration is the most temperature-sensitive streamflow response variable analyzed here and thus may represent a useful streamflow metric for future trend detection and attribution studies.

2.5. Conclusions

Climate controls on annual runoff and low flows were investigated using bivariate and partial correlation analysis and standardized multiple linear regression models. Results show that precipitation is the dominant control on the inter-annual variability of annual runoff and on the duration and severity of summer and winter low flows. The temperature-sensitivity of low flows, however, is up to two times higher than the temperature-sensitivity of annual runoff. Annual runoff and low flows are most sensitive

to winter climate conditions, particularly winter precipitation and winter thawing degrees. The results provide another line of evidence regarding the impacts of continued global warming on snowmelt hydrology. An increase in winter temperatures above the 0°C threshold has a much greater impact on the hydrologic regime than just a shift in the snowmelt peak. Warm and dry winters correspond to significantly lower runoff and significantly longer, more severe summer low flows than cool and dry winters. With no change in precipitation, continued warming in these mountain catchments will likely yield longer, more severe summer low flows, shorter winter low flows, and an overall decrease in annual runoff.

Chapter 3. Winter Temperature Controls on Snow Drought Risk in Western North America

This chapter was submitted as a paper to *Water Resources Research* and is cited in other chapters of this thesis as:

Dierauer, J.R., Allen, D.M., & Whitfield, P.H. (in review-b). Winter temperature controls on snow drought risk in western North America. *Water Resources Research*.

Supplemental figures and tables for this chapter are included in Appendix B.

3.1. Introduction

In western North America (WNA), much of the water used for agriculture and human consumption comes from snow. The winter snow accumulation provides natural storage, with the following spring and summer snowmelt filling reservoirs and sustaining streamflow when precipitation is low and evapotranspiration rates are high. Thus, snow drought (i.e. a lack of snow accumulation in winter) can have drastic ecological and socioeconomic impacts. For example, the April 1st snowpack in 2015 in the Pacific Northwest was 50% of normal, and snowpack in the Sierra Nevada – a key water source for much of California – was even lower, at only 5% of normal on 1 April 2015 (Harpold et al., 2017). California's agricultural economy depends on snowpack for water supply, and the 2015 drought resulted in an estimated $1.84 billion in agricultural losses (Howitt et al. 2015).

While both regions (Pacific Northwest and Sierra Nevada) exhibited below-normal 2015 snowpack, the Pacific Northwest received near-normal precipitation (70-120%), while the Sierra Nevada received only 40-80% of the normal precipitation (Harpold et al., 2017). Harpold et al. (2017) labeled the 2015 drought as a "warm snow drought" in the Pacific Northwest and a "dry snow drought" in the Sierra Nevada. These different snow drought types have different hydrologic and economic impacts. Dry snow droughts reduce streamflow year-round, resulting in low reservoir levels, reduced hydropower production, and, in severe cases, drinking and irrigation water supply shortages. Warm snow droughts increase flood risk (Allamano et al., 2009; Harpold et al., 2017) and create a mismatch between water availability and need. Both warm snow

droughts and dry snow droughts cause below-normal summer streamflow (Harpold et al., 2017; Dierauer et al., in review-a). Warm and dry winter conditions occurring together cause the most severe snow droughts and, consequently, the most severe summer streamflow drought conditions (Dierauer et al., in review-a).

The predominance of warm versus dry snow drought is likely related to climate controls on the inter-annual variability of snow water equivalent (SWE). In cold, continental regions, the inter-annual variability of SWE is dominantly controlled by precipitation variability (Cline, 1997; Male & Granger, 1981). In maritime regions, however, the inter-annual variability of SWE is often dominantly controlled by temperature variability (Cooper et al., 2016; Harpold et al., 2012; Harpold & Kohler, 2017). Recent studies (Morán-Tejeda et al., 2013; Sospedra-Alfonso et al., 2015) have shown that elevation thresholds exist above which SWE is temperature-dominated (T-dominated) and below which SWE is precipitation-dominated (P-dominated). Given the documented differences in SWE sensitivity and the existence of elevation thresholds between T-dominated and P-dominated areas, the predominance of dry versus warm snow drought likely varies between ecoregions and with temperature/elevation. Previous studies have mapped snow sensitivity to climate warming (e.g., Nolin & Daly, 2006), but no studies have quantified regional differences in snow drought regimes or investigated the relationship between SWE temperature-sensitivity and snow drought risk.

In this study, the historical (1951-2013) frequency and severity of dry, warm, and warm and dry snow droughts are quantified at the grid-cell and ecoregion scale for the major mountainous regions in WNA. Risk to each snow drought type is quantified, and the temperature-sensitivity (T-sensitivity) and precipitation-sensitivity (P-sensitivity) of peak SWE is quantified. Further, the relationships between mean winter temperature, snow drought risk, and SWE sensitivity are explored. Piecewise linear regression is then used to identify temperature thresholds and map susceptibility to temperature-related snow drought. Results of this study highlight spatial and ecoregion differences in snow drought regimes across WNA and reveal that a critical temperature-thresholds exist, above which the warm snow drought risk and SWE T-sensitivity increase more rapidly.

The region of study and the data used are discussed in section 3.2, including the methodology used to classify snow droughts and quantify peak SWE temperature and

precipitation sensitivity. The results are described and discussed in sections 3.3 and 3.4, and conclusions are provided in section 3.5.

3.2. Materials and Methods

3.2.1. Data and Domain

Daily precipitation, mean daily temperature (calculated as the average between the minimum daily temperature and the maximum daily temperature), and daily SWE data used in this study were obtained from the Livneh et al. (2015) gridded hydrometeorological dataset. This dataset contains gridded observation-based daily meteorological forcings and simulated Variable Infiltration Capacity (VIC) model states and fluxes at 1/16° resolution for the 1950 to 2013 period. The VIC model (Liang et al., 1994) is a physically based land-surface model capable of simulating energy and water balance. Feng et al. (2008) showed that VIC-simulated SWE agreed well with simulated SWE from models with higher complexity. Several recent studies have used (or trained datasets on) the Livneh et al. (2015) dataset to investigate snow hydrology in WNA (Barnhart et al., 2016; Li et al., 2017). The parameterization and validation of the VIC model is described in Livneh et al. (2015).

The Livneh et al. (2015) dataset was chosen over other gridded datasets (e.g., Livneh et al., 2013; Maurer et al., 2002) because of it has a larger domain and finer spatial resolution. To account for the effects of topography, the Livneh et al. (2015) dataset used a constant temperature lapse rate of -6.5 °C/km and incorporated orographic scaling across the entire domain, thereby providing a better representation of precipitation and improving the accuracy of snow estimates in mountain areas (Livneh et al., 2013, 2015).

Grid cells were excluded from the analysis if [1] there was minimal snow cover (< 10 cm mean peak SWE [1951-2000]), [2] the frost season was typically less than 30 days in length, or [3] the cells were flagged within Livneh et al. (2015) for possible unrealistic inter-year SWE accumulations. The flagged cells represent areas where the VIC-simulated SWE “glaciates” and was defined in Livneh et al. (2015) as cells where SWE never reaches 0.0 or where SWE > 6000 mm. The final masked area contained 24,759 VIC simulation grid cells covering an area of more than 824,000 km^2 (Figure 3.1).

To aid in regional analysis, results were further summarized for the 15 level III ecoregions (Commission for Environmental Cooperation [CEC], 2009) with the greatest snow storage (Figure 3.1).

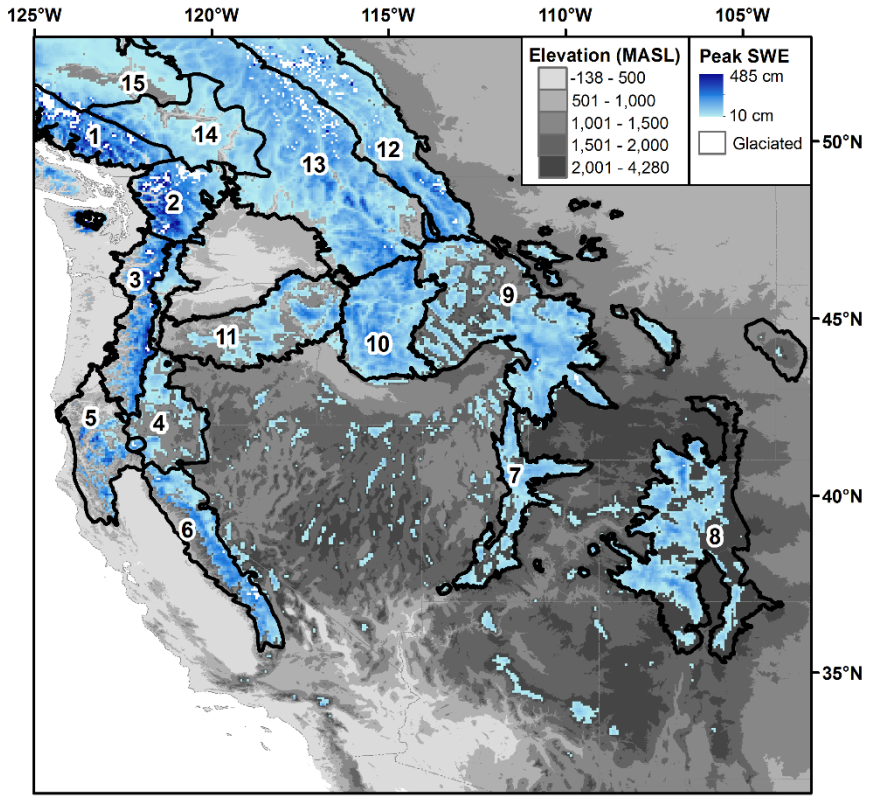

Figure 3.1 **Ecoregions (CEC, 2009) and mean peak snow water equivalent (SWE; 1951-2000) for masked analysis domain. Ecoregions are outlined in black and include: (1) Pacific and Nass Ranges, (2) North Cascades, (3) Cascades, (4) Eastern Cascades Slopes and Foothills, (5) Klamath Mountains, (6) Sierra Nevada, (7) Wasatch and Uinta Mountains, (8) Southern Rockies, (9) Middle Rockies, (10) Idaho Batholith, (11) Blue Mountains, (12) Canadian Rockies, (13) Columbia Mountains / Northern Rockies, (14) Thompson-Okanagan Plateau, (15) Chilcotin Ranges and Fraser Plateau. Glaciated cells as flagged in Livneh et al. (2015). MASL = meters above sea level.**

3.2.2. Snow Drought Classification

To separate warm snow droughts from dry snow droughts, a robust classification scheme is needed – one that works for a range of climate conditions. Harpold et al. (2017) suggest distinguishing warm versus dry snow droughts based on 1-Apr SWE and 1-Nov to 1-Apr cumulative precipitation, where winters with below-normal SWE and

above-normal precipitation are classified as warm snow droughts and years with below-normal SWE and below-normal precipitation are classified as dry snow droughts. While the classification scheme proposed by Harpold et al. (2017) is straightforward and easy to use, it does not account for the co-occurrence of warm and dry conditions, which have been shown to result in significantly more severe summer low flow periods than only dry conditions alone (Dierauer et al., in review-a). Additionally, it doesn't account for spatial and temporal variations in the timing of peak SWE, which varies substantially between and within mountain ranges (Wrzesien et al., 2018).

In this study, winters with below-normal peak SWE are classified as warm, dry, or warm and dry snow droughts based on winter precipitation (P) and winter thawing degrees (TD) using the following conditional statements:

$$if\ \{(SWE_i < \overline{SWE})\ \&\ (P_i < \bar{P})\ \&\ (TD_i < \overline{TD})\}\ D_{type} = DRY \quad [3.1]$$

$$if\ \{(SWE_i < \overline{SWE})\ \&\ (P_i > \bar{P})\ \}\ D_{type} = WARM \quad [3.2]$$

$$if\ \{(SWE_i < \overline{SWE})\ \&\ (P_i < \bar{P})\ \&\ (TD_i > \overline{TD})\}\ D_{type} = WARM\ \&\ DRY \quad [3.3]$$

where SWE_i, P_i, and TD_i are the peak SWE, winter precipitation, and winter thawing degrees in year i, respectively; $\overline{SWE}$, $\bar{P}$, and $\overline{TD}$, are the associated normals for the 1951-2000 period; and D_{type} is the snow drought type. Thawing degrees (TD) were calculated as the sum of mean daily temperatures for all winter days with a mean daily temperature above 0°C. Peak SWE was used (as opposed to 1-April SWE) because of the variability in the date of peak snowpack over the large and topographically complex region of WNA. A 50-year reference period (1951-2000) was used to calculate the climate and peak SWE normals because it spans the range of natural climate variability while excluding the recent extremes.

Using $\overline{SWE}$ as the threshold to define snow droughts results in the identification of many "minor" snow drought events, where winter season peak SWE levels are near-normal. Warm snow droughts are likely to be relatively minor events; therefore, the use of a high threshold, i.e. $\overline{SWE}$, was deemed appropriate, as a lower threshold would likely exclude many temperature-based SWE anomalies.

For the snow drought classification, a grid-cell-based definition of the winter season was used, where "winter" was defined based on the 25th percentile of the mean daily temperature ($\bar{T}_{25}$). With this method, the set of days with a $\bar{T}_{25}$ (1951-2000) less than 0°C was defined as "winter". The start of the winter season was then defined as the first day of the year occurring after the warmest day of the year with a $\bar{T}_{25}$ less than 0°C. The grid-cell-based definition of the winter season is based on the climate of each individual grid-cell and is applied in the same manner across the entire analysis domain. The use of the temperature criteria, $\bar{T}_{25}$, provides a fairer comparison than an arbitrary calendar date and follows recommendations of Cannon (2005) to define seasons based climatological data.

To classify snow droughts, TD was used as the temperature metric, as opposed to mean winter temperature (T_w), because of the non-linear response of SWE to T_w. For example, in regions with a normal T_w near 0°C, a positive T_w anomaly will have a large influence on SWE, while a negative T_w anomaly may have minimal impact on SWE. This grid-cell-based approach using TD as a predictor variable is more complicated than the common 1-Oct/1-Nov to 1-April winter classification used in previous studies (e.g., Luce et al., 2014; Mote, 2003). A methodological comparison showed that a grid-cell-based winter definition with TD and P as predictor variables had the highest predictive ability for peak SWE (Table S3.1). Additionally, the temperature metric (TD) had the highest regression slope (Table S3.2) and lowest standard error (Table S3.3) for the warmer maritime regions, where temperature is expected to play a large role in the snow drought regime.

After classifying each winter season with below-normal peak SWE as a warm, dry, or warm and dry snow drought, the severity, frequency, and risk of each snow drought type was calculated. Severity was calculated from normalized peak SWE as the fraction below the mean. Frequency was calculated as the fraction of total years (n = 63) exhibiting the associated snow drought type. The risk to each snow drought type was then calculated as the mean severity multiplied by the frequency and termed R_D, R_W, and R_{WD}, for warm, dry, and warm and dry snow drought risk, respectively. Thus, risk has units of fractional deficit per year and is equal to the expected annual deficit in peak SWE for each drought type.

To quantify large-scale spatial patterns in snow drought regimes, snow droughts were also classified and quantified at the ecoregion scale. For the ecoregion analysis, time series of average peak SWE, P, and TD were first calculated for each ecoregion as the average for all grid cells within the ecoregion. Snow drought classification and calculation of severity, frequency, and risk were then carried out in the same manner as the grid-cell scale analysis.

3.2.3. Precipitation (P) Versus Temperature (T) Sensitivity

Risk of warm versus dry snow drought is likely related to the temperature and precipitation sensitivity of peak SWE, with regions with higher peak SWE T-sensitivity exhibiting greater risk to warm snow drought. To test this hypothesis, peak SWE sensitivity was quantified using multiple linear regression (MLR) analysis. Variables were kept consistent with the snow drought classification, and the predictor variables (TD and P) were standardized by subtracting the mean and dividing by the standard deviation (SD). Peak SWE was normalized by dividing by the mean. The MLR analysis thus produces regression coefficients that represent the percent change in SWE for every 1 SD change in the predictor variables; the T-sensitivity and P-sensitivity of peak SWE are termed S_T and S_P, respectively. With this method, regression coefficients can be directly compared between grid cells, with results highlighting spatial patterns and ecoregion differences in peak SWE sensitivities, S_T and S_P.

3.2.4. Temperature Thresholds and SWE Susceptibility Mapping

Because of the non-linear relationship between temperature and snowpack, a critical temperature threshold likely exists, above which S_T and R_W increase sharply. To objectively identify such temperature thresholds, piecewise linear regression was implemented with the R package "`segmented`" (Muggeo, 2008). Mean winter (1-Nov to 1-Apr) temperature (T_w) was used as the predictor, with snow drought risk (R_D, R_W, R_{WD}) and peak SWE sensitivities (S_T and S_P) as the response variables. Based on visual assessment of the scatterplots, piecewise regression models with two break-points were investigated, and final models were chosen based on the R^2 values, break-point 95% confidence intervals (< ±0.2°C), and standard error of the piecewise regression slopes (magnitude less than corresponding slope).

Based on the break-points, or "thresholds", identified from this analysis, the susceptibility of peak SWE to temperature-related snow drought was ranked as low, medium, or high. This classification was completed at the grid-cell scale using the following T_w ranges:

$$Low: \quad T_w \leq BP_1 \tag{3.4}$$

$$Medium: \quad BP_1 < T_w \leq BP_2 \tag{3.5}$$

$$High: \quad T_w > BP_2 \tag{3.6}$$

where BP_1 is the dominant break-point separating regression segments 1 and 2 and BP_2 is the dominant break-point separating regression segments 2 and 3. For this analysis, T_w, as opposed to TD, was used to classify susceptibility because it is more easily calculated and requires only widely available climate data, thus allowing for the potential transfer of this susceptibility-mapping methodology to other places. Additionally, this T_w threshold approach allows for the evaluation of temperature-related snow drought susceptibility under simple climate warming scenarios. For example, in this study, the impact of a +2°C climate scenario on the temperature-related snow drought susceptibility was quantified by subtracting 2°C from each of the break-points and reclassifying the grid cells.

3.3. Results

Figure 3.2 shows the spatial variation of snow drought frequency, severity, and risk, and Figure 3.3 shows the snow drought regimes for the major mountainous ecoregions in WNA. Substantial spatial variation exists both between and within ecoregions. Dry, and warm and dry, snow droughts occur throughout the entire analysis domain, while warm snow droughts have a more limited spatial occurrence (Figure 3.2). Warm snow droughts do not occur at some high elevation locations and tend to be more frequent and severe at lower elevations. Similarly, warm and dry snow droughts tend to have higher severity at lower elevations (Figure 3.2).

Overall, warm snow drought is the least frequent and least severe of the three snow drought types, and thus exhibits the least risk. Warm snow droughts are most frequent in the Cascades, Pacific and Nass Ranges, and the Klamath Mountains; least

frequent in the Thompson-Okanagan Plateau and the Chilcotin Ranges and Fraser Plateau; and most severe in the Klamath Mountains. Warm and dry winter conditions occurring together correspond to the most severe snow drought type. Warm and dry snow droughts are also the most frequent drought type in 12 of the 15 ecoregions, with dry snow drought dominating the Pacific and Nass Ranges, Klamath Mountains, and Canadian Rockies. Warm and dry snow droughts exhibit the highest risk of the three drought types in all ecoregions except the Klamath Mountains, where R_D is highest, and the Pacific and Nass Ranges and Canadian Rockies, where R_D and R_{WD} are approximately equal (Figure 3.3). Excluding the Klamath Mountains, R_{WD} increases southward along the coastal mountain ranges (Figure 3.3), and, compared to the other ecoregions, R_{WD} is substantially higher in Sierra Nevada, where the expected annual peak SWE deficit is 14% per year.

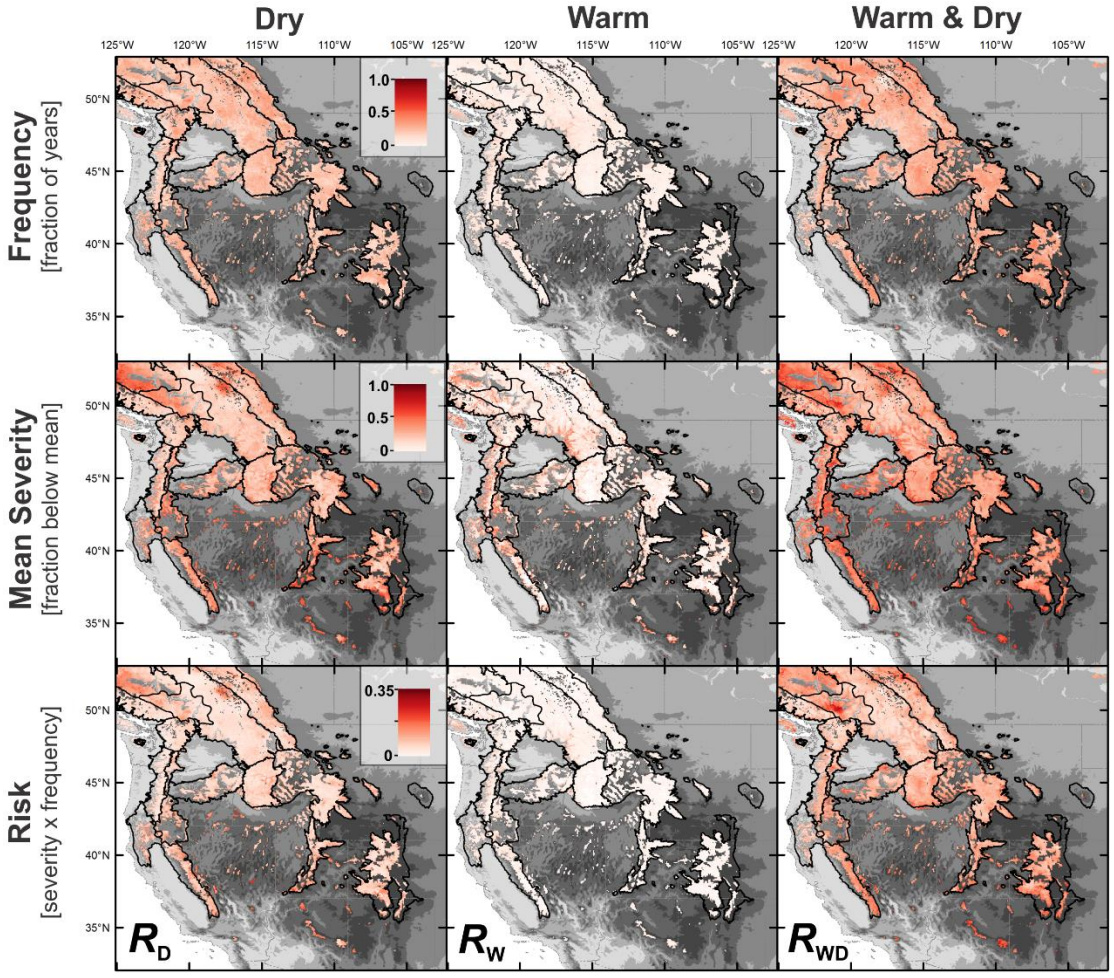

Figure 3.2 Frequency, severity, and risk for dry, warm, and warm & dry snow droughts, 1951-2013.

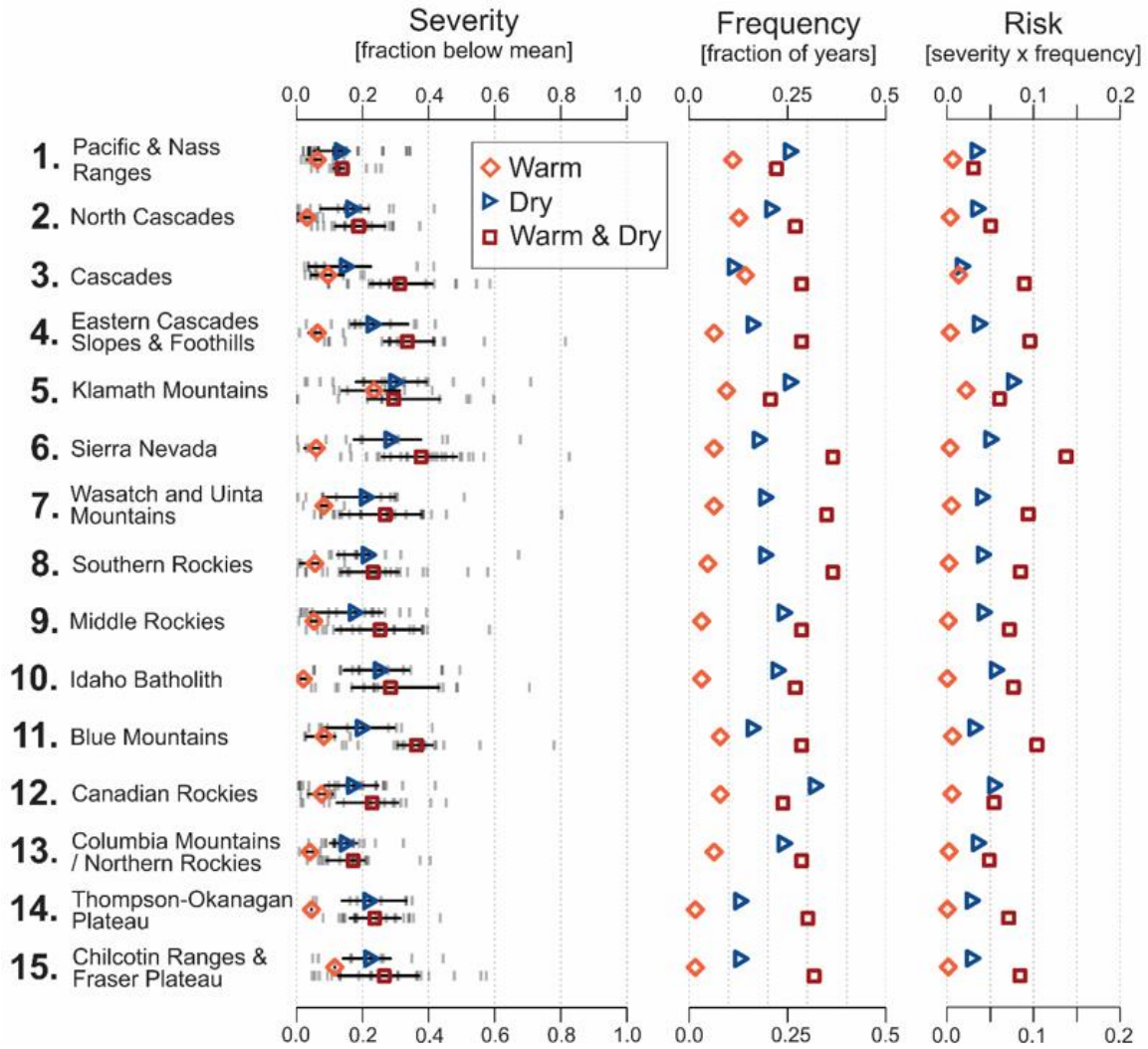

Figure 3.3 Snow drought severity, frequency, and risk by ecoregion, 1951-2013. For severity, the gray vertical lines represent individual years, the black horizontal lines span the inter-quartile range, and the symbols coincide with the mean. Ecoregion numbering as in Figure 3.1. See Table S3.4 for values of mean severity, frequency, and risk in table format.

While Figure 3.2 and Figure 3.3 highlight the large spatial and ecoregion differences in snow drought risk, plots of risk (R_D, R_W and R_{WD}) and SWE sensitivities (S_T and S_P) versus mean winter temperature (T_w; Figure 3.4) reveal that temperature controls R_W and S_T in WNA. Moreover, R_W exhibits a strong positive correlation ($r = 0.91$, $p < 0.01$) with S_T, confirming the hypothesis that regions with higher peak SWE T-sensitivity exhibit greater risk to warm snow drought. Both metrics (R_W and S_T) tend to be higher at lower elevations, as illustrated in Figure 3.2 and in Figure S3.1, respectively. R_D, on the other hand, exhibits no substantial correlation with S_T but is

strongly correlated ($r = 0.67$, $p < 0.01$) with S_P, and regions with higher peak SWE P-sensitivity exhibit greater risk to dry snow drought. As expected from these relationships, and shown in Figure 3.4, temperature-related risk and sensitivity (R_W and S_T) are strongly correlated with T_w, while precipitation-related risk and sensitivity (R_D and S_P) exhibit no substantial correlation with T_w. R_{WD} is related to both precipitation and temperature and exhibits a weak with T_w.

T_w has a non-linear relationship with both R_W and S_T (Figure 3.4). Piecewise linear regression analysis confirms the presence of temperature-thresholds, above which S_T and R_W increase sharply (Figure 3.4b and Figure 3.4d). Linear regression slopes increase substantially at the identified break-points, increasing from 0.1% $°C^{-1}$ to 4.1% $°C^{-1}$ for R_W and from 1.2% $°C^{-1}$ to 13.0% $°C^{-1}$ for S_T at the low (S1) and high slopes (S3), respectively (Figure 3.4b and Figure 3.4d). Both metrics (R_W, S_T) have break-points located between -2.9°C and -2.5°C, showing that temperature has larger negative impacts on SWE in locations where T_w is greater than -2.9°C. R_W and S_T have an additional break-point located at 1.3°C, where the regression slopes of R_W and S_T increase by an order of magnitude. Based on these results, thresholds of -3°C and 1.3°C were chosen for the susceptibility mapping, corresponding to BP_1 and BP_2 in equations 3.4-3.6 (see section 3.2.4), respectively.

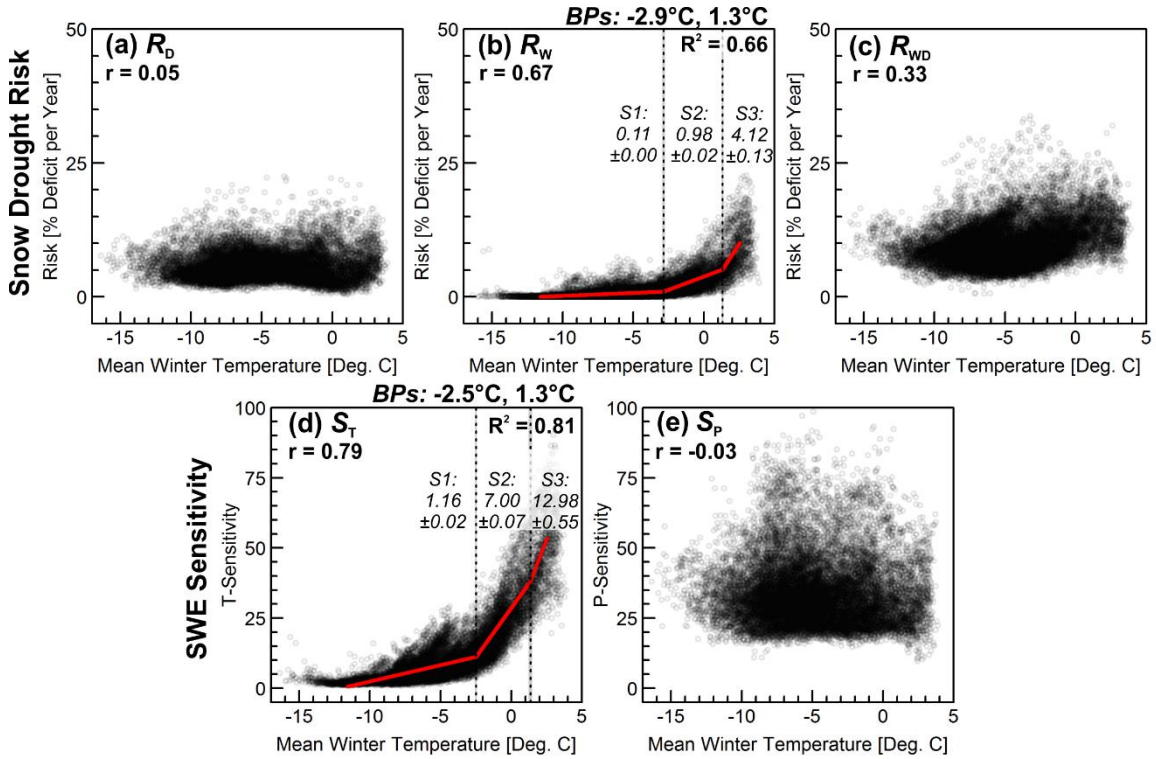

Figure 3.4 **Snow drought risk and peak SWE sensitivities versus mean winter (1-Nov to 1-Apr) temperature [T_W]. Top row: (a) R_D [dry], (b) R_W [warm], and (c) R_{WD} [warm and dry] snow drought risk. Bottom row: Peak SWE sensitivity to (d) temperature [S_T] and (e) precipitation [S_P]. Piecewise linear regression lines are shown in red for variables with strong correlations with temperature (r values shown in top-left corners). Break-points (BPs) from the piecewise regression are shown with black vertical dashed lines. Slopes (S1, S2, S3) and associated standard errors are indicated for each linear regression segment. Model performance indicated by coefficient of determination (R^2).**

Peak SWE susceptibility to temperature-related snow drought is shown in Figure 3.5, and further summarized by ecoregion in Table 3.1 and Table S3.5. The high susceptibility category represents areas with the highest temperature-related snow drought risk (R_W and R_{WD}) and peak SWE T-sensitivity (S_T) and the largest expected increases in risk per increase in T_w (i.e. S3 in Figure 3.4b and Figure 3.4d). Conversely, the low susceptibility category represents areas with the lowest temperature-related snow drought risk and peak SWE T-sensitivity and the lowest expected increases in risk per increase in T_w (i.e. S1 in Figure 3.4b and Figure 3.4d).

The Cascades, Klamath Mountains, and Sierra Nevada have the highest susceptibility to temperature-related snow drought, while the Middle Rockies, Canadian

Rockies, and Chilcotin Ranges/Fraser Plateau have the lowest susceptibility (Table 3.1). Overall, peak SWE is more susceptible to temperature-related snow droughts in the maritime ecoregions (ecoregions 1-6) and less susceptible in the continental ecoregions (ecoregions 7-15). In total, 3% of the non-glaciated snow storage volume in WNA is highly susceptible to temperature-related snow droughts (Table 3.1), representing 11 km^3 of water. Under a +2°C climate scenario, an additional 8% (28 km^3) of the WNA snow storage volume will transition to high susceptibility.

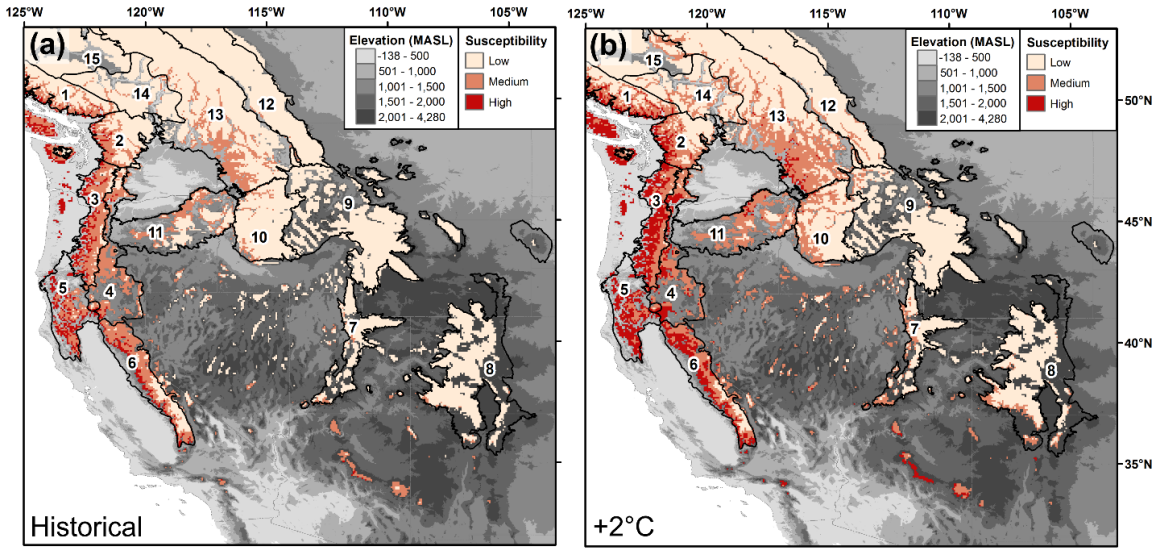

Figure 3.5 **Peak SWE temperature-related snow drought susceptibility under (a) historical [1951-2000] and (b) +2°C climate scenario. Ecoregion numbering as in Figure 3.1. Results are summarized by ecoregion in Table 3.1 and Table S3.5.**

Table 3.1 Temperature-related snow drought susceptibility summarized by ecoregion. SWE = mean snow water equivalent; Vol. = mean snowpack water volume. Ecoregion numbering as in Figure 3.1. "Other" includes all grid cells not within the 15 ecoregions. Table S3.5 presents the same data in terms of area as opposed to volume.

		Historical			+2°C Warming		
Ecoregion	Vol.	Low	Med	High	Low	Med	High
	[km³]	*[% Volume]*			*[% Change]*		
1. Pacific & Nass Ranges	25.8	68%	30%	2%	-26%	+17%	+9%
2. North Cascades	26.2	61%	37%	2%	-25%	+15%	+10%
3. Cascades	26.8	18%	71%	10%	-16%	-15%	+31%
4. Eastern Cascades Slopes & Foothills	8.6	28%	70%	2%	-22%	+1%	+20%
5. Klamath Mountains	10.3	6%	66%	28%	-6%	-31%	+36%
6. Sierra Nevada	20.8	33%	57%	10%	-14%	-7%	+21%
7. Wasatch & Uinta Mountains	8.9	96%	4%	0%	-16%	+16%	0%
8. Southern Rockies	24.8	99%	1%	0%	-6%	+6%	0%
9. Middle Rockies	33.7	100%	0%	0%	-2%	+2%	0%
10. Idaho Batholith	31.1	96%	4%	0%	-13%	+13%	0%
11. Blue Mountains	10.5	67%	33%	0%	-40%	+38%	+2%
12. Canadian Rockies	35.0	100%	0%	0%	-3%	+3%	0%
13. Columbia Mountains / N. Rockies	72.5	89%	11%	0%	-18%	+17%	+1%
14. Thompson-Okanagan Plateau	13.9	98%	2%	0%	-13%	+13%	0%
15. Chilcotin Ranges & Fraser Plateau	8.7	100%	0%	0%	-6%	+6%	0%
Other	18.2	41%	47%	12%	-16%	-6%	+22%
Total	**375.8**	**75%**	**22%**	**3%**	**-15%**	**+7%**	**+8%**

Note: SWE and Vol. are calculated from the study domain (see Figure 3.1) and therefore do not represent the entire ecoregion, rather the masked domain used in this study. Volume (vol.) refers to the mean volume of water stored as snow within the study domain, calculated by multiplying grid-cell mean peak SWE (1951-2000) by the corresponding grid-cell area then summing the result. "Glaciated" cells and cells with less than 10 cm mean peak SWE [1951-2000] were excluded from the analysis domain; therefore, Vol. is an under-estimate of the average volume of water stored as snow/ice in each ecoregion.

3.4. Discussion

Defining snow drought types by climatic causes is a relatively new concept (Harpold et al., 2017). While several recent studies have increased our understanding of snow drought (Cooper et al., 2016; Mote et al., 2016; Sproles et al., 2017; Hatchett & McEvoy, 2018), a regional assessment of snow drought risk has never before been completed. In this study, the dry versus warm snow drought definition proposed by Harpold et al. (2017) was expanded to include snow droughts that are caused by the co-occurrence of warm and dry conditions. A regional scale analysis of historical snow drought severity, frequency, and risk showed that warm and dry snow droughts

dominate the snow drought regime in WNA, while warm snow droughts are the least common and least severe snow drought type. The severity and frequency of warm snow droughts, however, is dependent on mean winter temperature. Temperature-thresholds identified with piecewise linear regression show that the risk of warm snow droughts is substantially higher for locations where the mean winter (1-Nov to 1-Apr) temperature (T_w) is above -3°C, and higher still for locations where T_w is above 1.3°C.

Spatial variation in snow drought risk is primarily driven by elevation, latitude, and proximity to the onshore flow of moisture. Warm snow drought risk (R_W), warm and dry snow drought risk (R_{WD}), and peak SWE T-sensitivity (S_T) all exhibit significant positive correlations with mean winter temperature (T_w), indicating these metrics tend to decrease with increasing elevation. The relationship between these metrics (R_W, R_{WD}, S_T) and elevation, however, is also dependent on latitude, as isotherms increase in elevation as latitude decreases. Dry snow drought risk (R_D) is dominantly controlled by the onshore flow of moisture. The leeward sides of mountain ranges tend to exhibit higher R_D, especially for the interior plateaus of British Columbia and the Eastern Cascades (ecoregions 14, 15, and 4 in Figure 3.1/Table 3.1). The tendency for S_T to decrease with elevation and increase with temperature has been documented by many previous studies (Mote et al., 2005; Mote, 2006; Safeeq et al., 2016; Sospedra-Alfonso et al., 2015; Morán-Tejeda et al., 2013; Sospedra-Alfonso & Merryfield, 2017; Jenicek et al., 2018; among others); however, no previous studies have documented the inter-relationships between S_T, T_w, elevation, and temperature-related snow drought risk (R_W, R_{WD}). The spatial patterns in R_D are consistent with precipitation pathways and anomaly patterns for WNA (e.g., Sellers, 1968; Alexander et al., 2015; Swales et al., 2016).

Snow drought risk in WNA has not been quantified before, nor has risk to any temperature-influenced drought type (e.g., agricultural, hydrologic, socioeconomic) ever been quantified based on climatic causes. Verdon-Kidd & Kiem (2010) call for drought risk assessments that are derived from an understanding of the climate mechanisms that drive periods of elevated risk, pointing out that, in a nonstationary climate, future drought risk may not resemble the past. Using the temperature-thresholds, identified at T_w values of -3°C and 1.3°C, to complete the susceptibility mapping in this study identifies regions that [1] historically exhibit relatively high levels of temperature-related snow drought susceptibility and [2] are likely to exhibit the largest negative impacts on peak SWE from continued climate warming. In the context of climate warming, the historical versus +2°C

susceptibility mapping (Figure 3.5, Table 3.1, and Table S3.5), can be used to identify regions where the snow drought regimes may shift toward more temperature-related snow droughts in the near future. Thus, the methodology presented in this study is a first step toward snow drought risk assessment in the context of a non-stationary climate.

Based on the strong positive correlation between warm snow drought risk (R_W) and mean winter temperature (T_w), it is clear that temperature drives elevated snow drought risk. Moreover, the non-linear relationship between R_W and T_w and the presence of critical temperature-thresholds at -3°C and 1.3°C indicate that the relationship between temperature and snow drought risk changes with increasing temperatures. The temperature thresholds identified in this study differ from previous elevation/temperature thresholds (Morán-Tejeda et al., 2013; Sospedra-Alfonso et al., 2015; Sospedra-Alfonso & Merryfield, 2017) in that they do not separate P-dominated from T-dominated SWE regions, but rather identify break-points at which the relationship between mean winter temperature (T_w) and peak SWE changes. As T_w increases, warm snow drought risk and SWE T-sensitivity increase; however, the rate of increase is not constant. Once a temperature-threshold is crossed, temperature-related decreases in peak SWE can be expected to "accelerate", and a 1°C increase in T_w has a larger negative impact on peak SWE for regions where T_w is above the temperature-thresholds versus regions where T_w is below the temperature-thresholds. This non-linear relationship between temperature and SWE T-sensitivity is stronger than the modest nonlinearity observed by Luce et al. (2014); however, the proposed acceleration of temperature-related changes in SWE at the identified temperature-thresholds is consistent with the near-term acceleration of hydroclimatic change in the western United States documented by Ashfaq et al. (2013).

Shifts in snow drought regimes have large implications for water resources planning, as different types of snow drought have different impacts and thus require different preparation measures and mitigation strategies. Warm snow droughts reduce the annual flood peak due to increased rain versus snow proportion and a lengthening of the melt interval before the peak flow (Rood et al., 2016) but also increase flood risk due to rain on snow events (Allamano et al., 2009; Rood et al., 2016). Hatchett & McEvoy (2018) showed that, in Sierra Nevada watersheds, warm snow droughts correspond to lower snow fractions and often include midwinter flood events. Warm snow droughts and the associated lower snow fractions lead to decreased lower annual runoff (Berghuijs et al., 2014; Dierauer et al., in review-a) and a shift in water supply away from summer and

towards winter (Leith & Whitfield, 1998; Whitfield & Cannon, 2000; Adam et al., 2009; Déry et al., 2009; Pederson et al., 2011; among others), negatively impacting water quantity, water quality, hydropower operations, winter snow sports, and summer recreation (Sproles et al., 2017).

In the context of historical (1951-2000) climate conditions, warm snow drought impacts are likely to be most severe at lower elevations and in the Klamath Mountains ecoregion, where warm snow drought severity and frequency are high. In the context of climate warming, the maritime ecoregions (1-6 in Table 3.1 and Table S3.5) will likely experience the largest increases warm snow drought risk, and thus increased midwinter flood events, decreased annual runoff, and shifts in the seasonal timing of streamflow. This is consistent with the recent study by Mote et al. (2018), which showed that declines in western US snowpack are largely temperature driven, with the largest downward trends in SWE in locations with mild, wet climates.

Unlike warm snow droughts, which often correspond to increased winter streamflow (Dierauer et al., in review-a), dry snow droughts reduce streamflow year-round (Harpold et al., 2017; Dierauer et al., in review-a). Impacts from dry snow droughts include low reservoir levels, reduced hydropower production, and, in severe cases, drinking and irrigation water supply shortages. Regions with higher dry snow drought risk (R_D) would thus have a higher risk of water quantity shortages. With continued climate warming, dry snow droughts are likely to transition, in part, to warm and dry snow droughts, which cause significantly more severe summer low flow periods than only dry conditions alone (Dierauer et al., in review-a), as well as overall reductions in annual runoff (Berghuijs et al., 2014; Dierauer et al., in review-a). Regions with medium or high susceptibility to temperature-related snow drought along with relatively high risk to dry snow drought (i.e. Klamath Mountains and Sierra Nevada) are likely to have the largest risk to water quantity shortages in the near future.

The Livneh et al. (2015) gridded hydrometeorological dataset data used in this study was created using meteorological stations that do not span the full temporal period, and thus the dataset is not suitable for trend analysis. Further study with datasets appropriate for trend analysis are needed to determine if snow drought regimes are changing as our climate continues to warm. Additionally, this study relied entirely on

VIC-simulated snow water equivalent and further study is needed to verify the presence of temperature-thresholds using observed SWE data.

This study presented a novel approach to snow drought classification and to the quantification of SWE temperature sensitivity. While the grid-cell-based winter season definition using thawing degrees (TD) and precipitation (P) as the predictor variables exhibited the greatest predictive ability for peak SWE, the gains in R^2 values were not large (+0.03 R^2 domain wide; Table S3.1) compared to the other, simpler methods (i.e. T, P with 1-Nov to 1-Apr winter season). Thus, it could be argued that the simpler method should be used. Previous work (Dierauer et al., in review-a) using observed streamflow data from mountain catchments in WNA, however, showed that runoff and low flows are more sensitive to TD than T_w. As the duration and severity of low flow periods are highly dependent on snowmelt hydrology in mountain catchments, the observations of Dierauer et al. (in review-a) suggest that snow accumulation and melt are also more sensitive to TD than to T_w. Additionally, SWE T-sensitivities estimated from the grid-cell-based approach using TD and P as the predictors were higher than the other methods in the warmer, maritime ecoregions (Table S3.2) and standard error estimates were lower (Table S3.3), supporting the use of the more complicated methodology and suggesting T-sensitivity may be under-estimated in the warmer maritime regions using the more conventional methods.

3.5. Conclusions

This study provides new detailed insight into the spatial and ecoregion differences in snow drought regimes across WNA. The relationships between mean winter temperature, snow drought risk, and SWE-sensitivity demonstrate that critical temperature-thresholds exist, above which warm snow drought risk and SWE T-sensitivity increase at a greater rate. While previous studies have shown that the T-sensitivity of SWE tends to decrease with elevation and increase with mean winter temperatures, the “acceleration” in hydroclimatic change at distinct temperature-thresholds has not been demonstrated before. Identified temperature-thresholds at mean winter (1-Nov to 1-Apr) temperature values of -3°C and 1.3° were used to map temperature-related snow drought susceptibility, revealing that 3% of the volume of western North America’s non-glaciated snowpack is highly susceptible to warm snow droughts, and an additional 22% exhibits medium susceptibility. The susceptibility

mapping presented in this study is a first step toward a snow drought risk assessment in the context of a non-stationary climate and can be transferred to other mountainous regions and used to inform snow drought mitigation strategies and water resource management planning.

Chapter 4. Climate Change Impacts on Snow and Streamflow Drought Regimes

This chapter has been prepared as a manuscript entitled “Climate change impacts on snow and streamflow drought regimes in four ecoregions of British Columbia” and is planned for submission to *Hydrology and Earth System Sciences*.

Supplemental figures and tables for this chapter are included in Appendix C.

4.1. Introduction

If temperatures rise as expected (Intergovernmental Panel on Climate Change [IPCC], 2013), precipitation will be more likely to fall as rain than to fall as snow. Warming alone is expected to have large impacts on the hydrologic regimes of catchments with seasonal snow cover (Barnett et al., 2005), with decreased annual snowpack leading to earlier snowmelt and diminished and potentially warmer late summer flows (Barnett et al., 2008; Wu et al., 2012; Seager et al., 2013; Godsey et al, 2014; Reynolds et al., 2015; Service, 2015; Jenicek et al., 2016). Compared to rainwater, snowmelt more effectively infiltrates below the root zone (Earman et al., 2006), and snowmelt often compromises a large fraction of groundwater recharge (Winograd et al., 1998; Earman et al., 2006; Ajami et al., 2012). Therefore, in catchments with seasonal snow cover, summer streamflow droughts can be directly related to snow drought, i.e. a lack of snow accumulation in winter.

Snow drought (Ludlum, 1978; Wiesnet, 1981) can be caused by below-normal precipitation and/or above-normal temperatures (Harpold et al., 2017), and both warm snow droughts and dry snow droughts cause below-normal summer streamflow (Harpold et al., 2017; Dierauer et al., in review-a). Streamflow droughts can propagate directly from snow droughts, with warm and dry winter conditions leading to longer, more severe summer low flow periods (Dierauer et al., in review-a). While the role of temperature in snowmelt hydrology has been widely studied (Leith & Whitfield, 1998; Whitfield & Cannon, 2000; Adam et al., 2009; Déry et al., 2009; Pederson et al., 2011; among others), no studies have explicitly quantified the impact of different snow drought types, i.e. dry, warm, or warm and dry, on the severity and duration of summer streamflow

droughts. Moreover, no studies have completed a combined analysis of snow drought and streamflow drought regimes in the context of climate change.

Recent work by Dierauer et al. (in review-b) has highlighted the relationship between mean winter temperature and temperature-related snow drought and identified critical temperature thresholds above which hydroclimatic change "accelerates". As temperatures rise, increased frequency and severity of temperature-related snow drought will likely lead to increased frequency and severity of summer streamflow droughts. The magnitude of these changes, however, will likely depend on a catchment's starting point, i.e. its baseline mean winter temperature. To investigate climate change impacts on snow drought and the subsequent impacts on summer streamflow drought, this study combines climate change projections with generic groundwater surface water models for four headwater catchments located in different ecoregions of British Columbia, Canada. These headwater catchments span a large range of baseline climate conditions, and thus should exhibit different responses to climate warming. The study locations and the reasons for choosing each catchment are discussed in section 4.2. The development of groundwater-surface water models, the choice of climate change scenarios, and the assessment of low flows and snow drought are discussed in section 4.3. Results are presented in section 4.4 and discussed in section 4.5, and conclusions are stated in section 4.6.

4.2. Study Locations

Four headwater catchments spanning a range of climate conditions were chosen for this study – each is located in a different level I ecoregion (Commission for Environmental Cooperation [CEC], 2011) of British Columbia (Table 4.1, Figure 4.1) and each represents a municipal, agricultural, or industrial surface water supply source. The coldest catchment has a mean annual temperature of -0.6°C and is in the Taiga ecoregion in the headwaters of the Fort Nelson River. The second coldest catchment has a mean annual temperature of 0°C and is in the headwaters of the Blueberry River in Northern Forests ecoregion. Both catchments have relatively cold, dry winters, and, on average, receive less than 15 cm of snow per year. Additionally, both catchments are in Northeast British Columbia (NEBC) – an area of rapidly expanding shale gas development where multi-stage hydraulic fracturing operations require large volumes of water over short time periods. In 2015, 45% of the 7.74 million m^3 of water used for

hydraulic fracturing in NEBC was sourced from surface water sources (British Columbia Oil and Gas Commission, 2016), with the highest water demand occurring in the warmer months from May to September.

Whiteman Creek headwater catchment has a mean annual temperature of 2.1°C and is in the Thompson-Okanagan Plateau, which is part of the North American Deserts level I ecoregion. The Okanagan has a dry continental climate and is in the rain-shadow of the Coast and Cascade Mountain Ranges; however, the region supports a strong agricultural industry that has a high irrigation demand, which accounts for 75% of the consumptive water use (Neilsen et al., 2006). Tributary streams, like Whitman Creek, are the main source of water for the Okanagan Valley, and most streams in the Okanagan are fully allocated, with no leeway for further allocations (Brewer et al., 2001).

The warmest catchment in this study has a mean annual temperature of 5.9°C and is in the headwaters of the Capilano River in the North Shore Mountains of the Marine West Coast Forests ecoregion. The North Shore Mountains have a wet maritime climate, and the headwater catchment in this study has a mean annual precipitation of more than 200 cm. The headwaters of the Capilano River fill the Capilano Reservoir, which supplies one-third of the water supply for the 2.5 million Metro Vancouver residents (Metro Vancouver, 2017).

Table 4.1 Catchment characteristics, including baseline 1980s (1970-1999) mean annual precipitation (P), snow fraction (Sf), mean annual temperature (T), and mean winter (1-Nov to 1-Apr) temperature (T_w). MASL = meters above sea level.

Ecoregion	Watershed	Latitude	Longitude	Elevation [MASL]	Slope	P [cm]	T [°C]	T_w [°C]
Taiga	Fort Nelson River	58.45	-123.04	564	2°	45.9	-0.6	-15.1
Northern Forests	Blueberry River	56.97	-121.88	935	3°	49.8	0.0	-11.7
North American Deserts	Whiteman Creek	50.23	-119.69	1572	10°	65.0	2.1	-6.1
Marine West Coast Forests	Capilano River	49.49	-123.17	1320	35°	234.6	5.9	0.0

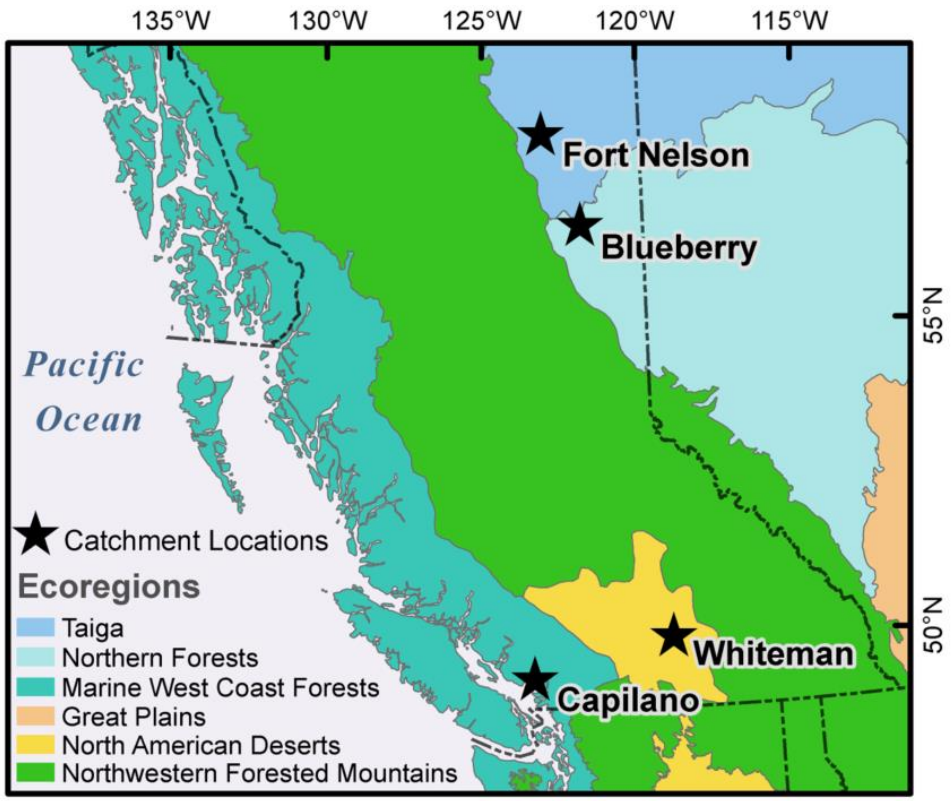

Figure 4.1 Headwater catchment locations and Level I ecoregions (CEC, 2011).

4.3. Materials and Methods

The following sections describe the groundwater-surface water (GW-SW) models that were developed for the study (section 4.3.1), the climate change scenario models that were chosen (section 4.3.2), and the methodology used to assess impacts on the snow drought and low flow regimes.

4.3.1. Groundwater - Surface Water (GW-SW) Modelling

Groundwater discharge during low flow and drought periods is dependent on the amount of snow that accumulates during winter and on the timing and rate of snowmelt and resulting groundwater recharge in the spring and summer (Tague & Grant, 2009; Godsey et al., 2014; Meixner et al., 2016). Therefore, a comprehensive approach for analyzing climate change impacts on snow drought and streamflow drought requires the application of a distributed, physically-based groundwater-surface water model. With this type of model, parameters are directly related to the physical characteristics of the

catchment. Compared to the two other main types of hydrological models, i.e. empirical models and lumped conceptual models, distributed physically based models are more appropriate for simulating ungauged catchments (Refsgaard & Knudsen, 1996) and for use where significant changes in catchment conditions are expected (Klemes, 1985; Refsgaard & Knudsen, 1996), e.g., climate change scenario modelling. Therefore, this study uses the distributed physically based GW-SW modelling code MIKE SHE – MIKE 11 (Danish Hydraulic Institute [DHI], 2007). MIKE SHE has been used in previous climate change scenario modelling studies, including studies in catchments with seasonal snow cover (Liu et al., 2011; Thompson, 2012; Foster & Allen, 2015), and has been compared to other modelling codes and shown to adequately model stream discharge (Vansteenkiste, 2013; Golmohammadi et al., 2014).

MIKE SHE is a deterministic, distributed hydrologic modelling system that can simulate actual evapotranspiration (AET), overland flow, one-dimensional (1D) unsaturated flow, and three-dimensional (3D) variably saturated groundwater flow. Rivers, lakes, and other channels are simulated by the one-dimensional MIKE 11 model, which is coupled directly to the MIKE SHE model through the use of river links (*h*-points). Further details on the comprehensive modelling capabilities of the MIKE SHE software can be found in the user manual (i.e. DHI, 2007).

Model boundary conditions were consistent between all models and consisted of:

1. zero flux boundaries at the catchment boundaries – representing topographical divides;
2. zero flux boundaries at the bottom of the saturated bedrock layer (200 metres below ground surface);
3. closed (zero flux) boundaries at the upstream end of the stream network branches;
4. open (head-dependent flux) boundary defined by a discharge-elevation *(Q-h)* rating curve at the downstream outflow.

The assigned boundary conditions route precipitation onto the model domain and out via evapotranspiration or surface water flow through the downstream flux boundary. Initial groundwater levels were assigned to coincide with the ground surface. The models were run for 150-year periods (1950-2100), using the first 20 years (1950-1969) as the spin up period to achieve a dynamically stable state.

The GW-SW models in this study were developed to explore the relationship between snow drought and hydrological drought in idealized systems, each representing a different ecoregion in British Columbia. While real-world topography, stream networks, etc. were used, all models in this study are generic and were not put through any calibration or validation procedures. The modelling code used in this study meets the guidelines laid out by Freeze & Harlan (1969) for adequate physics-based hydrological modelling and the climate change application criteria of Klemes (1985). Beven (1989) and Grayson et al. (1992), however, warn against the overparameterization of physically based models. Therefore, this study aimed to represent the hydrologic systems in the simplest way possible and used homogenous land cover, soils, and geology for each catchment. Additional details on the model setups, including land surface, saturated zone, and unsaturated zone parameters and stream network data are included in the following sections.

Land surface data and overland flow

Actual transpiration and soil evaporation were calculated using the equations from Kristensen and Jensen (1975). Required inputs include leaf area index (LAI), canopy interception, root characteristics, and empirical coefficients. Leaf area index (LAI) for each catchment was estimated using the 10-day interval LAI dataset from Gonsamo and Chen (2014). The required root characteristics include root depth and a root mass distribution parameter Aroot. Aroot was left at the default value (0.25 m^{-1}; DHI, 2007). Root depth was set at 400 mm for all catchments based on a study by Curt et al. (2001), which showed that the majority of root mass is concentrated within the top 400 mm of soil, regardless of soil quality. The canopy interception parameter C_{int} and the empirical coefficients C1, C2, C3 were left at the default values (0.05 mm and 0.3, 0.2, and 20 mm/day, respectively; DHI, 2007), following Voeckler et al. (2014) and Foster and Allen (2015).

Overland flow occurs when the infiltration capacity of the soil is exceeded or when groundwater discharges to the surface. Within MIKE SHE, overland flow is routed by surface topography at a rate dependent on the diffusive wave approximation of the Saint-Venant equation. The resistance to overland flow is controlled by the roughness of the land surface. Topography for all models was assigned using the Canadian Digital Elevation Model (CDEM; Natural Resources Canada, 2017). Land cover data (DataBC,

2013) were used to define surface roughness values (Manning's *M*). Manning's *M* is the reciprocal of Manning's *n*; therefore, Manning's *n* values from Chow (1959) were used to estimate Manning's *M* values (Table S4.1).

Unsaturated and saturated zone

The unsaturated zone (UZ) within MIKE SHE is the zone through which the water table rises and falls. Vertical flow in the UZ was modelled using Richards' equation (Richards, 1931). Three-dimensional groundwater flow in the saturated zone (SZ) is based on Darcy's equation and is solved implicitly using a finite difference technique. The UZ and SZ are explicitly coupled, and the upper boundary of the SZ is a flux boundary which receives recharge from the SZ. Flux from the unsaturated to the saturated zone varies in time and is computed at the interface of the two zones. Because of the coupling between the two zones, the UZ and SZ must overlap, with the UZ extending to a depth of the lowest possible groundwater head. Depth to groundwater in the catchments is unknown; therefore, to ensure coupling between the UZ and SZ zones, the UZ and SZ zones were assigned the same number of layers, with the same depths, and the same hydraulic properties, extending from ground surface to 200 metres depth.

UZ and SZ layer depths, bulk densities, and vertical and horizontal saturated hydraulic conductivities (K_z, K_{xy}) were assigned based on British Columbia (BC) soil descriptions (Agriculture and Agri-Food Canada, 2013). Textural classes were determined from the BC soil descriptions and used assign values of effective porosity (θ_s), residual porosity (θ_r), and empirical constants α and *n* based on values in Carsel and Parrish (1988). Specific yield values were estimated from Morris and Johnson (1967). Parameters for the organic soil layers in the Fort Nelson (Taiga ecoregion) catchment were based on values from Letts et al. (2000). Soil names, bedrock geology, and the associated parameters are provided in Tables S2 to S5.

MIKE 11 stream network

Stream routing was modelled within MIKE 11 and requires four main components: a stream network, cross-sections, boundary conditions, and hydrodynamic parameters. Stream networks and drainage boundaries were obtained from British Columbia Freshwater Atlas (British Columbia, 2013). Stream cross-sections were

digitized from surface topography (i.e. from the CDEMs). For each catchment, stream network boundary conditions consisted of closed (zero-flux) boundaries at the upstream ends of the stream network branches and an open (head-dependent) flux boundary at the downstream outflow. Rating curves for the downstream head-dependent flux boundaries were calculated using Manning's equation, shown in Equation 4.1.

$$Q = A \times \frac{1}{n} \times R_h^{\frac{2}{3}} \times \sqrt{S} \qquad [4.1]$$

where Q [m^3/s] is the discharge leaving the model domain, A [m^2] is the cross-sectional area, n is Manning's roughness coefficient, R is the hydraulic radius, and S [m/m] is the channel slope. For each catchment, the channel slope was calculated from the CDEM and the hydraulic radius was calculated from the downstream cross-section for a range of possible stream stages spanning low flow to high flow conditions. A value of Q was determined for each stage value using Equation 4.1, thereby creating the rating curve required for the head-dependent flux boundary.

The global bed resistance Manning's roughness coefficient (Manning's n) was set to 0.05 for all catchments based on values in Chow (1959). Conductance values, which control the flow of water between the stream network and the saturated zone, were estimated from the subsurface hydraulic conductivity values (Tables S4.2-S4.5).

4.3.2. Climate Change Scenario Modelling

Statistically downscaled forcing datasets based on three models from Phase 5 of the Coupled Model Intercomparison Project (CMIP5) under representative concentration pathways (RCPs) 4.5 and 8.5 were used for the climate change scenarios in this study. RCPs 4.5 and 8.5 represent different trajectories of anthropogenic radiative forcing, leading to radiative forcing levels of 4.5 and 8.5 W/m^2 by the end of 21st century (van Vuuren et al., 2011). RCP 4.5 represents a medium stabilization scenario, and RCP 8.5 represents a very high baseline emissions scenario (van Vuuren et al., 2011). The three models from the CMIP5 ensemble (CNRM-CM5-1, CanESM2-r1, ACCESS1-0-r1) were selected to capture the widest spread in projected future climate while using a small subset of the full ensemble, following Cannon (2015). Daily climate time series (maximum temperature, minimum temperature, and precipitation) downscaled with the bias-correction/constructed analogues with quantile mapping reordering (BCCAQ)

method were obtained from the Pacific Climate Impacts Consortium (PCIC) data portal (PCIC, 2014) covering the period of 1950 to 2100. Werner and Cannon (2016) showed that, out of the seven downscaling methods tested, BCCAQ performed best for reproducing hydrologically relevant climate extremes. Mean daily temperature was calculated as the average of the minimum and maximum daily temperature and used as the input for MIKE SHE. A comparison of climate data between the baseline 1980s (1970-1999) and two future periods, 2050s (2041-2069) and 2080s (2070-2099) is included in results section 4.4.1.

4.3.3. Evapotranspiration and Snow

In addition to mean daily temperature and daily precipitation, MIKE SHE requires estimates of potential evapotranspiration (PET). Potential evapotranspiration (PET) was calculated with the FAO Penman-Monteith method (Allen et al., 1998) using the R package "`sirad`" (Bojanowski, 2016). Daily solar radiation inputs for the Penman-Monteith method were estimated from daily maximum and minimum temperature using the Hargreaves and Samani (1985) model, following recommendations in Aladenola and Madramootoo (2012). Estimates of daily mean wind speed were unavailable, and a constant wind speed of 5 km/hr was used for all PET calculations, which is within the range of climate normals for the nearby climate stations (Environment and Climate Change Canada, 2018). Wind speed exhibits relatively minor impacts on PET (McKenney & Rosenberg, 1993; Gong et al., 2006; Tabari & Talaee, 2014; Córdova et al., 2015); therefore, the use of a constant wind speed was deemed appropriate.

Within MIKE SHE, snow accumulation and melt are modelled using a threshold melting temperature, a maximum wet snow storage fraction, and a degree-day coefficient. The threshold melting temperature for all catchments was set to 0°C, and the maximum wet snow storage fraction was set to 0.2, which is in the mid-range of values used in previous studies (Wijesekara et al., 2014; Voeckler et al., 2014; Foster & Allen, 2015). A value of 2.74 mm/degree-day C was used for the degree-day coefficient in all models based on recommendations in United States Department of Agriculture (USDA) National Engineering Handbook (Van Mullem & Garen, 2004). The minimum snow storage was set to 0 mm for all catchments.

This snowmelt methodology, referred to as the temperature-index or degree-day method, assumes an empirical relationship between air temperatures and melt rates and has been widely applied due to its simplicity (e.g., Clyde, 1931; Corps of Engineers, 1956; World Meteorological Organization [WMO], 1986; Van Mullem & Garen, 2004). However, the degree-day method does not account for several factors that are important for snowmelt, including wind speed, humidity, topography (slope, aspect, shading), cloud cover, and vegetation (Male & Granger, 1981; Gray & Landine, 1988; Harding & Pomeroy, 1996; Pomeroy et al., 1998; Marks et al., 1999; among others). Despite the over-simplification and documented short-comings of this method, temperature-index methods often perform well at the catchment scale (World Meteorological Organization [WMO], 1986; Sand, 1992; Rango & Martinec, 1995; Hock, 2003) and can match the performance of energy balance models (WMO, 1986). While further study using energy balance models should be completed to investigate within-catchment spatial differences in the response of snow drought regimes to climate warming, the degree-day method was deemed sufficient for modelling the average catchment conditions. Additionally, Rango & Martinec (1995) showed there is little difference in simulated runoff between the degree-day approach and the energy balance approach, and, therefore, the methodology used in this study was deemed appropriate for a combined investigation of snow drought and streamflow drought.

4.3.4. Assessment of Snow Drought

To investigate how different snow drought types impact seasonal low flows, snow droughts were classified using the methodology outlined Dierauer et al. (in review-b). With this method, winters with below-normal peak snow water equivalent (SWE) are classified as warm, dry, or warm and dry snow droughts based on winter precipitation (P_w) and winter thawing degrees (TD_w). Years with below-normal peak SWE, below-normal P_w, and below-normal TD_w are classified as “dry” snow droughts; years with below-normal peak SWE and above-normal Pw are classified as “warm” snow droughts; and years with below-normal peak SWE, below-normal P_w, and above-normal TD_w are classified as “warm and dry” snow droughts. Peak SWE, P_w, and TD_w normals were defined using the baseline 1980s period (1970-1999). For each catchment, the winter season was defined based on the baseline 25th percentile of mean daily temperature ($\bar{T}_{25}$), with days of the year with $\bar{T}_{25}$ <0°C corresponding to “winter”. After classifying

each winter season with below-normal peak SWE as a warm, dry, or warm and dry snow drought, the severity (mean deficit below baseline normal), frequency (fraction of years), and risk (frequency x severity) of each snow drought type were calculated.

4.3.5. Assessment of Low Flows and Streamflow Drought

Winter and summer low flows are generated by different hydrological processes, i.e. below freezing temperatures and snow accumulation versus above freezing temperatures and high evapotranspiration rates (Waylen & Woo, 1987; Laaha & Blöschl, 2006; Burn et al., 2008). To complete a combined analysis of snow drought and streamflow drought, summer low flows must first be separated from winter low flows. Substantial changes in climate occur over the 150-year (1950-2100) simulation period, including large decreases in the length of the snow accumulation period. Thus, a fixed definition of summer versus winter seasons would be ineffective for a process-based separation of low flows, and a flexible classification scheme was needed. To accomplish this, days with a mean daily temperature below 0°C or with ≥ 5 cm of snow cover were classified as “winter” days, and days with a mean daily temperature above 0°C and < 5 cm of snow cover were classified as “summer” days. The hydrologic year start was set to the beginning of the winter season and allowed to vary between years.

After separating the summer versus winter seasons, the severity and duration of low flows were quantified using four low flow regime indicators (Table 4.2). Low flow periods were defined using the baseline (1970-1999) Mean Daily Runoff (MDR) as the upper bound. Low flow duration (DUR) was calculated as the cumulative number of days when runoff was less than the baseline MDR. Low flow severity (SEV) was calculated as the cumulative water deficit below the baseline MDR. To aid in comparison between the catchments, SEV was normalized by the baseline Mean Annual Runoff (MAR). The mean 15-day minimum runoff (MAM15) and the mean 30-day minimum runoff (MAM30) were also calculated and used to quantify the magnitude of summer and winter low flows. Each metric (DUR, SEV, MAM15, and MAM30) was calculated for both the summer and winter season, indicated by “s” and “w” subscripts, respectively.

To evaluate the propagation of snow drought into summer streamflow drought, the frequency and mean severity of summer streamflow droughts following a snow drought were tabulated, considering only years with above-normal (1980s baseline)

summer precipitation. By doing this, summer streamflow droughts caused by a summer precipitation deficit could be separated from summer streamflow droughts caused by snow droughts, and thus the propagation of snow drought into summer streamflow drought could be highlighted. Summer streamflow drought frequency and severity were analysed using each summer low flow regime indicator, using the thresholds indicated in Table 4.2. For DURs and SEVs, a baseline threshold of 20% exceedance frequency was used, i.e. summer low flow duration and severity that was exceeded 20% of the time during the baseline period. For MAM15s and MAM30s, a baseline threshold of 80% exceedance frequency was used, i.e. low flow magnitude that was exceeded 80% of the time during the baseline period. For DURs and SEVs, streamflow drought years occur when the values are above the threshold, and for MAM15s and MAM30s, streamflow drought years occur when values are below the threshold.

Table 4.2 Low flow regime indicators, calculated yearly. Baseline = 1980s (1970-1999). MAR = mean annual runoff.

Winter	Summer	Description	Units	Threshold
DUR_w	DUR_s	Duration of low flow period	days	>20% exceedance
SEV_w	SEV_s	Severity of low flow period	fraction of baseline MAR	>20% exceedance
$MAM15_w$	$MAM15_s$	Mean 15-day minimum runoff	mm/day	<80% exceedance
$MAM30_w$	$MAM30_s$	Mean 30-day minimum runoff	mm/day	<80% exceedance

4.4. Results

The following sections present and discuss the results of the GW-SW climate change scenario modelling, including climate change impacts on the annual and intra-annual water balance (Section 4.4.1) and impacts on snow drought and low flow regimes (Sections 4.4.2 and 4.4.3). Section 4.4.4 analyses the impacts of snow drought on low flows, and section 4.5 provides further discussion of the results.

4.4.1. Climate Change Impacts on the Annual Water Balance

A water balance analysis was completed for each RCP-GCM combination, for a total of six 150-year water balance time series for each headwater catchment. The water balance components of interest for this study include precipitation, snow water equivalent (SWE), runoff, actual evapotranspiration (AET), and groundwater recharge. Groundwater recharge represents water that enters the SZ from the UZ; however, with the MIKE SHE water balance tool, both flux into and out of the SZ are tabulated. Thus,

recharge can be positive (outward flux to UZ) or negative (inward flux to SZ). With no change in groundwater storage, the inward fluxes in recharge zones would be balanced by outward fluxes in discharge zones, and total annual recharge would roughly equal 0. Therefore, a detailed saturated zone water balance was extracted for a small upland region of each catchment to analyse groundwater recharge in a recharge zone only. Runoff for each catchment was calculated as the volume of streamflow leaving the downstream head-dependent flux boundary, converted from m^3/s to mm/day by dividing by catchment area.

Water balance results for individual GCMs are not shown but rather lumped by RCP for simplicity. Results are summarized for a baseline period (1980s) and two future periods (2050s and 2080s) and are presented as both the absolute change (future – baseline) and relative change ([future – baseline] / baseline) for the three-member GCM ensemble (Figure 4.2, Table S4.6). Average annual water balance errors for all models were less than 3%; however, due to transient conditions and changes in subsurface storage, mean annual AET plus mean annual runoff is not equal to mean annual precipitation.

The GCM ensemble projects increases in temperature and precipitation for all four catchments (Figure 4.2, Table S4.6). The relative increase in precipitation is highest in the two northern catchments (Fort Nelson and Blueberry), which have a cold, dry climate. The absolute increase (mm/year) in precipitation, however, is highest in the warmest, wettest catchment – Capilano. The seasonal distribution of precipitation does not change substantially under RCPs 4.5 and 8.5; however, in general, the fall (Sep to Nov) and spring (Mar to May) seasons exhibit the largest relative increases in precipitation (Figure S4.2), and summer (Jun to Aug) and winter (Dec to Feb) exhibit the smallest. Compared to the projected changes in precipitation, changes in temperature are more similar among all catchments (Table S4.6). Projected temperature increases are highest in winter and lowest in fall (Figure S4.3). As expected, increases in the mean annual temperature are greatest for the high emissions scenario (RCP 8.5), and by the 2080s, mean annual temperature is projected to be 5.6 to 6.1 °C higher compared to the baseline 1980s period (Table S4.6).

Annual runoff is projected to increase for all four catchments (Figure 4.2). Relative (%) increases in runoff are largest for the coldest, driest catchment (Fort

Nelson), while absolute (mm/year) increases in runoff are largest for the warmest, wettest catchment (Capilano; Figure 4.2 and Table S4.6). In addition to increases in annual runoff, the within-year distribution of runoff changes substantially. The spring freshet starts earlier for all catchments and decreases in magnitude for all but Fort Nelson (Figure S4.4), which is the northern-most and coldest catchment. In the warmest catchment (Capilano), the spring freshet disappears completely for both future time periods under both RCPs. In all catchments, the slope of the spring freshet rising limb decreases, indicating a lengthening of the melt interval before peak flow (Figure S4.4). These changes (declined spring freshet peak and lengthening of the melt interval) are consistent with observations of Rood et al. (2016), who tied spring flood moderation in Rocky Mountain rivers to winter and spring warming.

In general, changes in the timing and magnitude of the spring freshet are directly related to changes in the length of the snow-covered period and the magnitude and timing of peak SWE (Figure S4.5). While the increased annual precipitation leads to increased peak SWE for the coldest catchment (Fort Nelson), the impact of increased temperatures outweighs the impacts of increased precipitation in the remaining catchments, leading to no significant change in peak SWE (Blueberry) or significant decreases in peak SWE (Whiteman and Capilano; Figure 4.2). The largest absolute and relative decreases in peak SWE occur in the warmest catchment, Capilano, which has a >90% decrease in peak SWE for the 2080s under RCP 8.5. In addition to changes in the magnitude of peak SWE, the average day of peak SWE and melt-out occur earlier, resulting in a shorter snow-covered period for all catchments for both future time periods under both RCPs (Figure S4.5). Additionally, snowmelt is slower for all catchments for both future periods, as illustrated by the shallower slope of the falling limbs (Figure S4.5). The earlier and slower snowmelt is consistent with the Musselman et al. (2017) study, which showed that snow melts more slowly in a warmer world due to an increase in winter and spring melt and longer snow-free periods during times of high energy (i.e. summer).

As expected, the changes in temperature and precipitation, and associated changes in snow accumulation and melt, lead to significant changes in both the total annual AET (Figure 4.2) and the intra-annual patterns in AET (Figure S4.6). AET increases significantly for all catchments except Whiteman, located in the Okanagan Valley, which exhibits no significant change in annual AET (Figure 4.2). Seasonally, AET

increases most in late-winter and spring (Feb to May) and decreases (Whiteman and Capilano) or exhibits no substantial change (Fort Nelson and Blueberry) during summer (Figure S4.6). Decreased AET during the summer can be primarily attributed to the shift toward earlier snowmelt, which decreases summer water availability. This negative feedback between snowmelt timing and evapotranspiration has been discussed by Barnett et al. (2005) and documented by previous climate change modelling studies (e.g., Shrestha et al., 2012). Shifts in vegetation patterns will likely influence catchment response to climate change (Alo & Wang, 2008; Teutschbein et al., 2018); however, it is difficult to project and constrain possible vegetation shifts, and vegetation change was not included in the modelling efforts. Changes in wind speed, either due to climate change or vegetation change, would also impact AET, an effect which was not considered in this study.

Within MIKE SHE, water that reaches the saturated zone (i.e., groundwater recharge) may then exit the saturated zone via evapotranspiration, baseflow to the river, or surface return. Groundwater recharge may be higher or lower than runoff, depending on catchment's physical properties (e.g., soils, geology, vegetation, ground slope) which control the evapotranspiration dynamics and the magnitude of overland flow. In the Fort Nelson catchment, which has high porosity organic soils (Table S4.2) and shallow slope (Table 4.1), groundwater recharge is much higher than runoff (Table S4.6), and a large proportion of the water that reaches the saturated zone then leaves the system through evapotranspiration. In the Capilano catchment, which has lower porosity soils (Table S4.5) and steep slopes (Table 4.1), groundwater recharge is lower than runoff (Table S4.6) and a substantial portion of runoff is generated from overland flow.

At the annual time scale, recharge increases significantly for all but the warmest catchment (Capilano; Figure 4.2). Intra-annually, the patterns in groundwater recharge are primarily affected by changes in the onset of snow accumulation and melt. In all catchments, the spring recharge peak starts earlier in the year and decreases in magnitude (Figure S4.7), resulting in higher winter groundwater storage, an earlier start to the spring/summer groundwater recession period, and thus decreased summer groundwater storage (Figure S4.8). Increased winter-season recharge for regions with seasonal snow cover is consistent with the results of previous climate change modelling studies (e.g., Eckhardt & Ulbrich, 2003; Jyrkama & Sykes, 2007; Kovalevskii, 2007). A shift toward more rain and less snow in combination with slower snow melt would

suggest an overall decrease in groundwater recharge (Earman et al., 2006; Barnhart et al., 2016). While it is difficult to separate the effects of increased temperatures from the effects of increased precipitation, the results of this study show an increasing ratio of recharge to precipitation (R:P ratio) for the Fort Nelson catchment, relatively constant R:P ratios for the Blueberry and Whiteman catchments, and a decreasing R:P ratio for the Capilano catchment (Table S4.6). The different responses of the R:P ratio (increase, no change, decrease) seem to be related to the catchment's starting point (in terms of temperature), as the coldest catchment exhibits an increase in the R:P ratio and the warmest catchment exhibits a decrease in the R:P ratio.

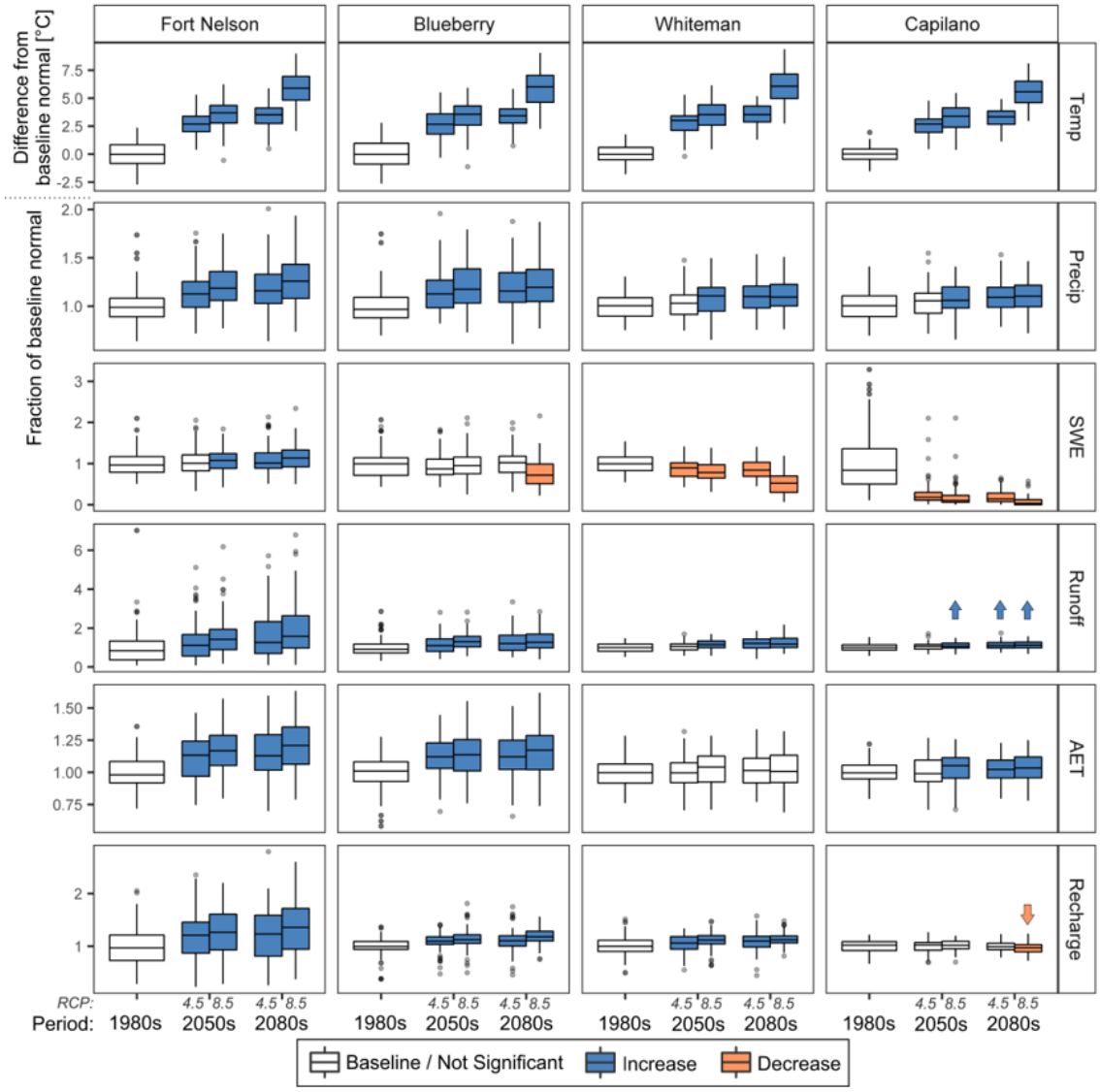

Figure 4.2 **Annual climate and water balance components for the 1980s baseline (1970-1999) versus 2050s (2040-2069) and 2080s (2070-2099) for representative concentration pathway (RCP) 4.5 and RCP 8.5, including mean annual temperature (Temp), annual precipitation (Precip), peak snow water equivalent (SWE), annual runoff, annual actual evapotranspiration (AET), and annual groundwater recharge. Blue and orange shading indicate a significant ($p < 0.05$) increase or decrease relative to the baseline period, as assessed with the two-sided Mann-Whitney U test. Arrows are added for clarity where boxplot shading is unclear. Figure S4.1 shows the same data, plotted as absolute values, and Table S4.6 provides the corresponding mean annual values along with the absolute and relative change.**

4.4.2. Snow Drought

In response to the increased precipitation and temperature (Figure 4.2), the snow drought regime changes substantially for all catchments. Warm snow droughts increase in frequency and dry snow droughts decrease in frequency (Figure 4.3, Table S4.7). Additionally, warm, and warm and dry, snow drought severity increases for the two warmest catchments, Whiteman and Capilano (Figure 4.4, Table S4.8). In general, dry snow droughts transition to warm and dry snow droughts, and, by the 2080s, the frequency of dry snow drought drops to 0 for all catchments (Figure 4.3, Table S4.7). In terms of temperature, the magnitude of change in the snow drought regime is related to the catchment's starting point, with the warmest catchment (Capilano) exhibiting the largest increase in the frequency and severity of snow drought and the coldest catchment (Fort Nelson) exhibiting no substantial increase in the frequency or severity of snow drought (Figure 4.3 and Figure 4.4).

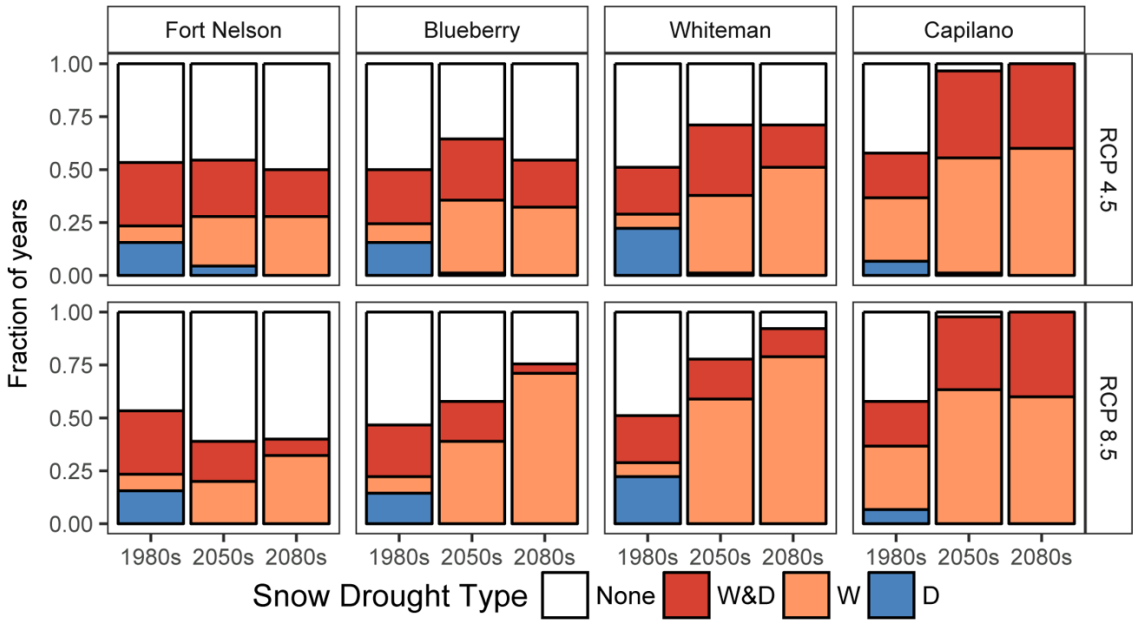

Figure 4.3 **Frequency (fraction of years) of dry (D), warm (W), and warm and dry (W&D) snow droughts for the baseline 1980s (1970-1999) versus 2050s (2040-2069) and 2080s (2070-2099) for representative concentration pathway (RCP) 4.5 and RCP 8.5. Table S4.7 provides the same data in tabular format.**

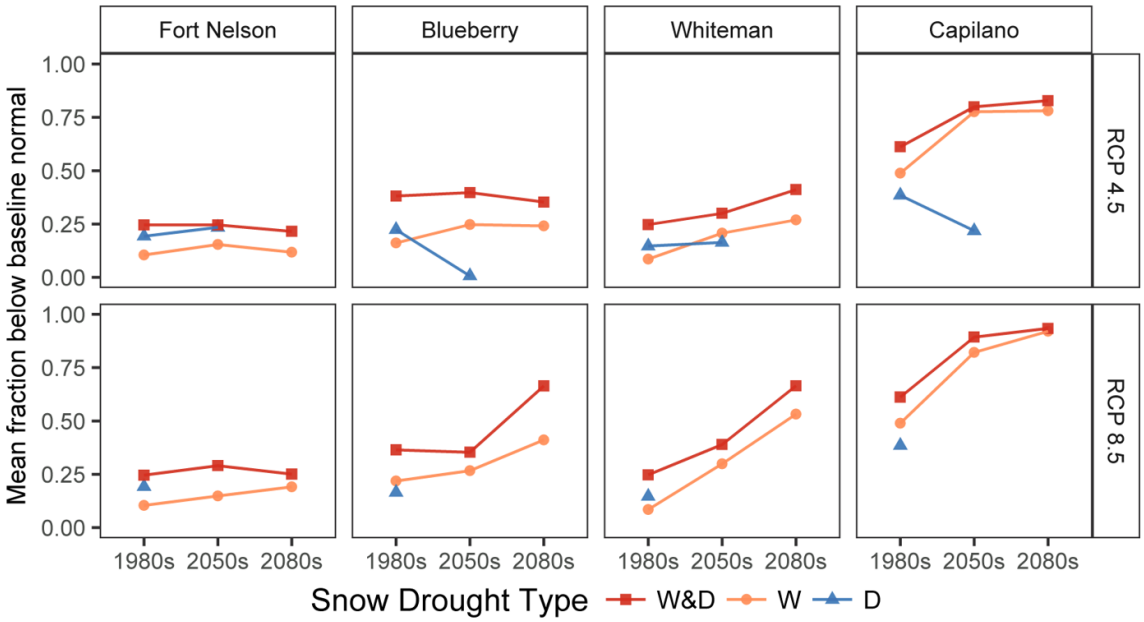

Figure 4.4 **Mean severity (fraction below baseline normal) of dry (D), warm (W), and warm and dry (W&D) snow droughts for the baseline 1980s versus 2050s (2040-2069) and 2080s (2070-2099) for representative concentration pathway (RCP) 4.5 and RCP 8.5. Table S4.8 provides the same data in tabular format. Note: Dry snow droughts transition to warm and dry snow droughts and therefore have no mean severity plotted for some future time periods.**

The increased frequency and severity of snow drought necessarily leads to increased snow drought risk, and overall, the changes in snow drought risk (Table 4.3) mirror the changes in snow drought severity (Figure 4.4). In general, snow drought regimes in all catchments shift toward more frequent, higher severity temperature-related (warm, and warm and dry) snow droughts, and less frequent, lower severity dry snow droughts. However, as documented by Dierauer et al. (in review-b) and shown in Figure S4.9, the response of warm snow drought risk to increased winter temperature is non-linear. A 2°C increase in the mean winter (1-Nov to 1-Apr) temperature corresponds to a substantially larger increase in warm snow drought risk for the Capilano catchment as compared to the Fort Nelson catchment. The two warmest catchments, Whiteman and Capilano, exhibit the largest increases in total snow drought risk. Due to the transition of dry snow droughts to warm and dry snow droughts, dry snow drought risk decreases for all catchments for both future time periods under both RCPs. The coldest catchment, Fort Nelson, exhibits a slight decrease in total snow drought risk.

Table 4.3 Risk (severity x frequency) for dry (D), warm (W), and warm and dry (W&D) snow droughts. Baseline 1980s (1970-1999) versus 2050s (2040-2069) and 2080s (2070-2099) for representative concentration pathways (RCPs) 4.5 and 8.5.

		Fort Nelson		Blueberry		Whiteman		Capilano	
1980s	D	3.0%		3.5%		3.2%		2.6%	
	W	0.8%		1.4%		0.6%		14.6%	
	W&D	7.4%		9.7%		5.5%		12.9%	
	Total	*11.2%*		*14.6%*		*9.3%*		*30.1%*	
	RCP	**4.5**	**8.5**	**4.5**	**8.5**	**4.5**	**8.5**	**4.5**	**8.5**
2050s	D	1.0%	--	<0.1%	--	0.2%	--	0.2%	--
	W	3.6%	3.0%	8.5%	10.4%	7.6%	17.6%	42.2%	52.0%
	W&D	6.5%	5.5%	11.5%	6.7%	10.0%	7.4%	32.9%	30.8%
	Total	*11.1%*	*8.5%*	*20.0%*	*17.1%*	*17.8%*	*25.0%*	*75.5%*	*82.8%*
2080s	D	--	--	--	--	--	--	--	--
	W	3.3%	6.1%	7.8%	29.2%	13.8%	41.9%	46.9%	55.2%
	W&D	4.8%	1.9%	7.8%	3.0%	8.2%	8.9%	33.1%	37.4%
	Total	*8.1%*	*8.0%*	*15.6%*	*32.2%*	*22.0%*	*50.8%*	*80.0%*	*92.6%*

4.4.3. Low Flows and Summer Streamflow drought

As the snow drought regime shifts toward more frequent, higher severity temperature-related (i.e. warm, and warm and dry) snow droughts, the streamflow regime shifts toward shorter, less severe winter low flow periods (Figure S4.10) and longer, more severe summer low flow periods (Figure 4.5). While low flows periods are a normal, annually recurring component of the natural flow regime (Smakhtin, 2001), longer and/or more severe low flows periods are synonymous with streamflow droughts. Thus, a shift toward longer, more severe summer low flows represents an increase in summer streamflow drought severity and duration, and a shift toward shorter, less severe winter low flows represents a decrease in winter streamflow drought severity and duration. The shift in the streamflow drought regime is further illustrated by empirical distribution functions plots (Figures S4.11 to S4.14).

Different snow drought types have different impacts on summer and winter low flows. Consistent with findings of Dierauer et al. (in review-a), warm, and warm and dry, snow droughts lead to significantly longer, more severe summer low flows (Figure 4.6) and significantly shorter and less severe winter low flows (Figure S4.15). In the context of climate warming and considering the documented relationship between snow drought and low flows (Figure 4.6), summer streamflow drought regimes are likely to shift toward more frequent, higher severity snow-drought related events. Using a threshold-based

approach to define summer streamflow drought years for each low flow metric (see section 4.3.4) shows that, in the absence of summer precipitation deficit, snow droughts propagate into summer streamflow droughts more frequently in the future time periods as compared to the baseline 1980s (Figure 4.7 and Figure S4.16). Thus, warm snow droughts not only become more frequent and severe in the future (Figure 4.3 and Figure 4.4) but are also more likely to result in summer streamflow drought conditions. Dry snow droughts, on the other hand, become less frequent in the future (Figure 4.3) and are unlikely to lead to summer streamflow droughts (Figure 4.7 and Figure S4.16).

The warm snow season streamflow drought events identified in this study are strictly temperature-driven, as both winter and summer precipitation are above the baseline 1980s normal. Climate change impacts on the frequency of these events vary between catchments due to the baseline winter air temperature. The Fort Nelson catchment, which has winter air temperatures far below zero, exhibits minimal increase in the occurrence of warm snow season streamflow droughts, while Capilano catchment, which has winter air temperatures near zero, exhibits a large increase in the occurrence of warm snow season streamflow droughts (Figure 4.7 and Figure S4.16).

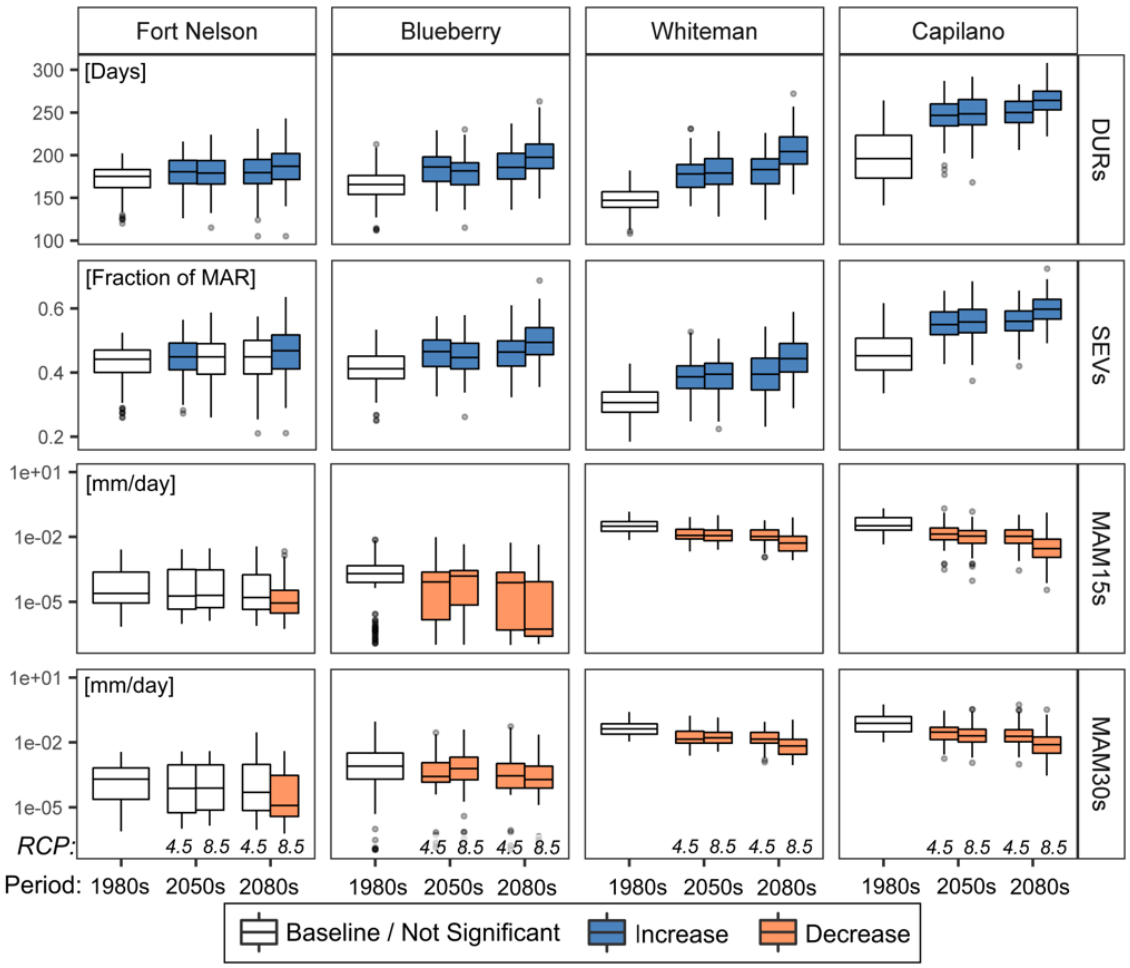

Figure 4.5 **Summer low flow regime indicators for the 1980s baseline (1970-1999) versus 2050s (2040-2069) and 2080s (2070-2099) for representative concentration pathway (RCP) 4.5 and RCP 8.5. Blue and orange shading indicate a significant ($p < 0.05$) increase or decrease relative to the baseline period, as assessed with the two-sided Mann-Whitney U test. Figure S4.10 shows winter low flow regime indicators.**

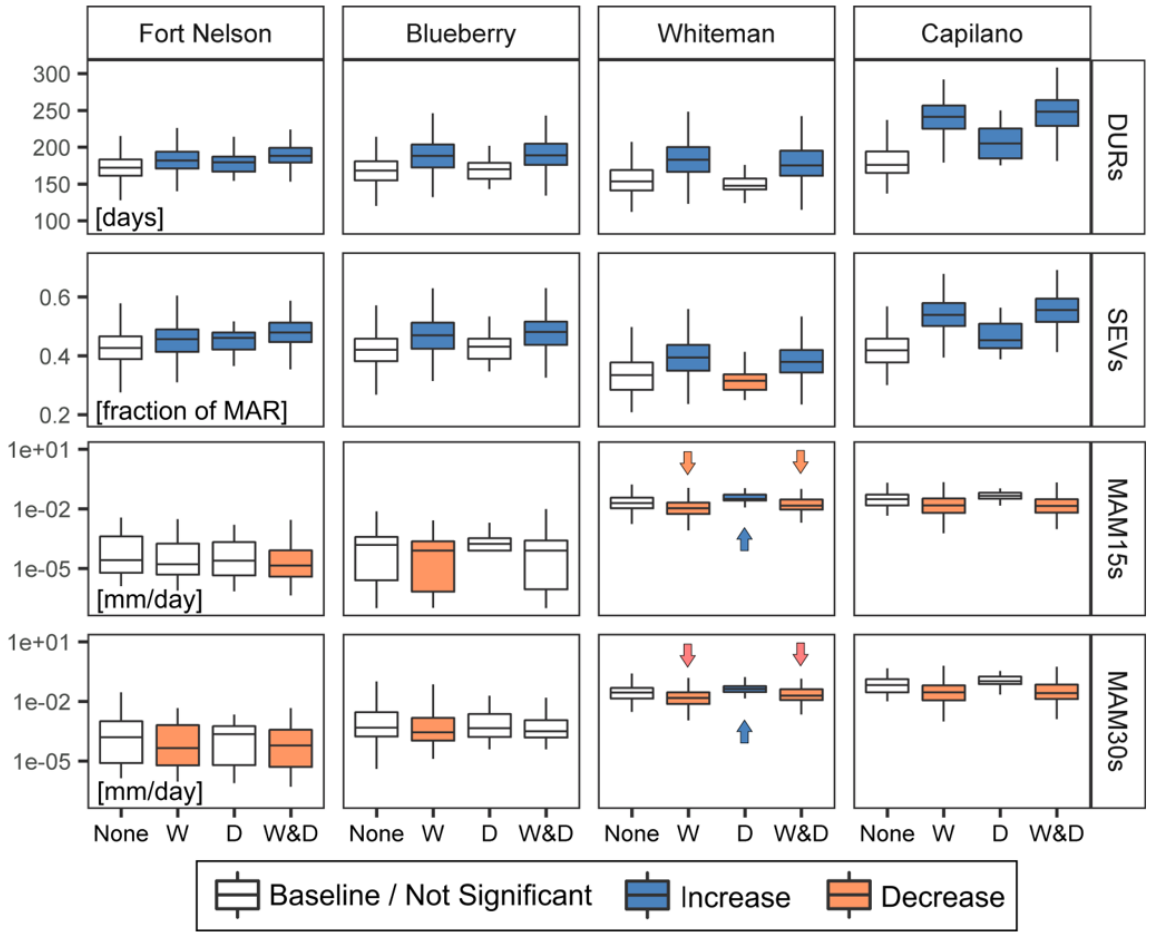

Figure 4.6 **Snow drought impacts on summer low flows by snow drought type, including years without snow drought (None) and years with warm (W), dry (D), and warm and dry (W&D) snow droughts. Blue and orange shading indicate the values are significantly ($p < 0.05$) higher or lower relative to years without snow drought, as assessed with the two-sided Mann-Whitney U test. Abbreviations are as in Table 4.2. Arrows are added for clarity where boxplot shading is unclear. Figure S4.15 shows the winter low flow regime indicators.**

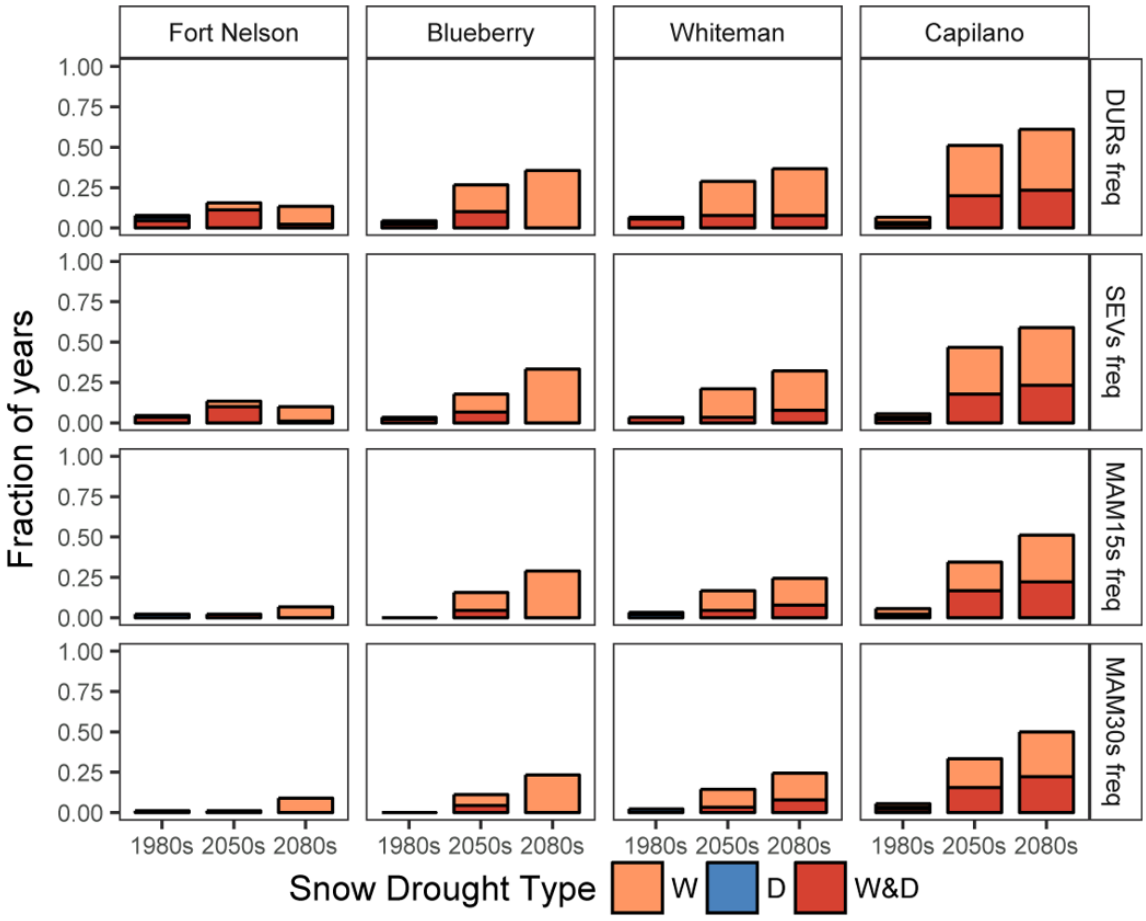

Figure 4.7 **Frequency of snow drought propagation into summer streamflow drought, in the absence of summer precipitation deficit, by snow drought type: warm (W), Dry (D), warm and dry (W&D), RCP 8.5. Figure S4.16 shows the same plot for RCP 4.5.**

4.5. Discussion

While recent studies have increased our understanding of snow drought (Dierauer et al., in review-b; Mote et al., 2016; Harpold et al., 2017) and its hydrological impacts (Cooper et al., 2016; Sproles et al., 2017; Hatchett & McEvoy, 2018), no previous studies have explicitly related climate change impacts on snow drought to subsequent impacts on summer low flows and summer streamflow drought. In this study, generic GW-SW models of headwater catchments were combined with downscaled climate change projections for two different RCPs. Climate change projections show increases in both precipitation and temperature, leading to decreases in the frequency and severity of dry snow droughts and increases in the frequency and severity of warm, and warm and dry, snow droughts. Climate warming and the

subsequent shifts in the snow drought regime result in decreased summer runoff, decreased summer groundwater storage, and longer, more severe summer low flow periods. Climate warming has the opposite effect on the winter season, with model results showing increased winter runoff, increased winter groundwater storage, and shorter, less severe winter low flow periods.

Snow droughts have direct impacts on summer low flows (Figure 4.6), and temperature-related (i.e. warm, and warm and dry) snow droughts not only become more frequent and severe in the future but are also more likely to result in summer streamflow drought conditions (Figure 4.7). The shift to lower severity winter streamflow droughts and higher severity summer streamflow droughts is consistent with the results of previous hydrologic modelling studies (Feyen & Dankers, 2009; Wanders & Van Lanen, 2015) and with the general hypothesis that streamflow droughts with different causative factors will respond differently to climate change (Van Loon and Van Lanen, 2012; Van Loon et al., 2015). In general, increased summer streamflow drought severity and decreased winter streamflow drought severity are consistent with an overall shift in the intra-annual distribution of runoff, an impact of climate warming on snowmelt hydrology which has been documented by many previous studies (Leith & Whitfield, 1998; Whitfield & Cannon, 2000; Adam et al., 2009; Déry et al., 2009; Pederson et al., 2011; among others).

Consistent with the results of Dierauer et al. (in review-b), the response of snow drought risk to climate warming is non-linear (Figure S4.9), and the magnitude of change in the snow drought and low flow regime is related to the catchment's baseline mean winter (1-Nov to 1-Apr) temperature. Due to the non-linear relationship between temperature and snow drought risk, a +2°C change in the mean winter temperature has a larger impact on the snow drought regime in catchments with winter temperatures near zero (e.g., the Capilano catchment) compared to catchments with winter temperatures far below zero (e.g., the Fort Nelson catchment). Because of the impacts of snow drought on summer low flows, warmer catchments also exhibit greater increases in the severity and duration of the summer low flow period compared to colder catchments.

The shift toward more frequent and more severe temperature-related snow droughts and longer, more severe summer low flow periods will have widespread implications for terrestrial and aquatic ecosystems. Earlier snow disappearance will lead

to increased wildfire activity (Westerling et al., 2006), increased tree mortality (Bales et al., 2018), greater water stress for mountain ecosystems (Harpold, 2016), and decreased carbon uptake (Hu et al., 2010; Winchell et al., 2016). Since stream temperatures are positively associated with air temperature and negatively associated with streamflow rates (Hockey et al., 1982; Webb et al., 2003), climate warming and the subsequent shifts in the low flow regime will have compound impacts on stream temperature during the summer low flow period. Summer low flow periods are critical for aquatic ecosystem health (Fleming et al., 2007; Moore et al., 2013), and increased stream temperatures have direct impacts on species distributions and growth rates (Beschta et al., 1987, Eaton & Scheller, 1996). Further, summer low flows that are lower than normal, i.e. drought conditions, correspond to reduced dissolved oxygen levels (Sprague, 2005; van Vliet & Zwolsman, 2008; Ylla et al., 2010), reduced hydrological connectivity and habitat availability (Lake, 2003), and increased pollutant concentrations through decreased dilution capacity (Mosley, 2015).

Shifts in snow drought, low flows, and streamflow drought regimes will also have widespread implications for surface water supply security. Increased frequency of warm snow droughts will likely lead to an increased frequency of mid-winter melt events (Hatchett & McEvoy, 2018), which will create challenges for reservoir management. Winter melt events should be of low intensity (e.g., Musselman et al., 2017); however, climate change may also result in increased rain on snow events and thus high intensity flows, i.e. floods (Yan et al., 2018). Reservoirs may require higher flood control due to the increased winter flows and increased risk to rain on snow events, while simultaneously requiring larger storage capacity to combat decreasing summer flows. As summer low flow periods become more severe and snow-drought related summer streamflow droughts become more frequent, the potential for more severe summer water shortages increases. The most severe shortages will likely occur due to a combination of different drought types (Van Loon et al., 2015) and the co-occurrence of warm and dry conditions (AghaKouchak et al., 2014) – as illustrated by the recent multi-year California drought (AghaKouchak et al., 2014; Howitt et al., 2015).

The GW-SW models in this study are generic, and, therefore, represent interpretive tools (Anderson et al., 2015). Like all GW-SW models, they are simplified numerical representations of natural flow systems and cannot duplicate the natural flow system exactly. However, the models are physically-based, and the documented

consistency with previous studies indicates that the results can provide general insights into future water management challenges. Additionally, this study could be used as a base for identifying areas of interest and designing subsequent snow drought and streamflow drought modelling studies. While the models should not be used to forecast future water availability, results are discussed, in general terms, in relation to regional water management challenges in the following paragraphs.

In NEBC, where the Fort Nelson and Blueberry catchments are located, shifting snow and streamflow drought regimes will likely lead to decreased freshwater security for oil and gas industry. Since 2005, oil and gas industry development in NEBC has expanded rapidly due to technological advancements made in hydraulic fracturing and directional drilling (Rivard et al., 2014). The multi-stage hydraulic fracturing operations put high demands on local watersheds, requiring large volumes of water in concentrated areas over short time periods (Rivard et al., 2014). Without significant commitment on the part of industry to re-use and recycle water for hydraulic fracturing, industrial water demand is likely to increase substantially – with the possibility of a more than 350% increase by 2030 compared to 2015 levels under a high development scenario (Kniewasser & Horne, 2015). Industrial freshwater abstractions are suspended during streamflow drought conditions, and the British Columbia Oil and Gas Commission has issued water use suspensions four times in the last eight years (https://www.bcogc.ca/directives). As summer low flows decrease, water use suspensions are likely to become more frequent, and balancing increasing demand with decreasing security will be a significant challenge for the region in the future.

In the Okanagan Valley, where the Whiteman catchment is located, surface water sources supply 67% of the annual water demand (Summit Environmental Consultants Inc., 2010). Most streams in the Okanagan are fully allocated, with no leeway for further allocations (Brewer et al., 2001). The greatest proportion water is used for agriculture, and irrigation, which accounts for 75% of regional consumptive water use, is expected to increase considerably with continued climate warming (Neilsen et al., 2006). Additionally, average per person water use is high (Summit Environmental Consultants Inc., 2010) and population is expected to grow at a rate of 0.2 to 0.7% per year (BCstats, 2017). Population growth in the Metro Vancouver region, where the Capilano catchment is located, is expected to be even higher at 0.9 to 1.4% per year (BCstats, 2017). Significant opportunities exist for demand-side reductions in water use

for the Okanagan (DHI Water and Environment, 2010; Neale et al., 2007) and Metro Vancouver (Metro Vancouver, 2011) regions. However, water shortages have already occurred both regions (Okanagan Water Stewardship Council, 2008; Metro Vancouver, 2015), and, considering the results presented in this study and others (DHI Water and Environment, 2010; Harma et al., 2012), summer water shortages are likely to occur more widely and frequently in the future.

4.6. Conclusions

Climate change impacts on snow drought, low flows, and summer streamflow drought were investigated using generic coupled GW-SW models for four headwater catchments in British Columbia. Results show that increased precipitation and temperature lead to decreased dry snow drought risk and increased temperature-related (i.e. warm and warm and dry) snow drought risk. Climate warming and the subsequent shifts in the snow drought regime result in decreased summer runoff, decreased summer groundwater storage, and longer, more severe summer low flow periods. Snow droughts have direct impacts on summer low flows, and temperature-related snow droughts not only become more frequent and severe in the future but are also more likely to result in summer streamflow drought conditions.

The response of snow hydrology to climate warming is non-linear, and catchments with winter temperatures near 0°C exhibit substantially larger impacts from +2°C of warming compared to catchments with winter temperatures far below 0°C. The shift toward more frequent and more severe temperature-related snow droughts will decrease water availability during the summer for agricultural and industrial uses – potentially leading to decreased freshwater supply security, and the increased frequency of warm snow droughts will likely lead to an increased frequency of mid-winter melt events that will affect reservoir management. Changes in the low flow regimes will affect the ecology of river systems, and increased rain on snow events may require higher flood control.

Chapter 5. Case Study: Future Water Security in Northeast British Columbia

This chapter is an expanded version of a book chapter that was published as: Dierauer, J.R., Allen, D.M., & Whitfield, P.W. (2018). Exploring future water demand and climate change impacts on water availability in the Peace Region of British Columbia, Canada. In A. Endo & T. Oh (Eds.), *The Water-Energy-Food Nexus: Human-Environmental Security in the Asia Pacific Ring of Fire*. (pp. 45-54). Springer Singapore, ISBN 978-981-10-7383-0

Supplemental information for this chapter is included in Appendices D and E.

5.1. Introduction

Shale gas development in Northeast British Columbia (NEBC) has occurred rapidly in recent decades due to technological advancements made in hydraulic fracturing and directional drilling. Hydraulic fracturing requires large volumes of water – on the order of 2,000-100,000 m^3 per hydraulic fracturing event for well pads in NEBC (Rivard et al., 2014). While the region has abundant water resources, these multi-stage hydraulic fracturing operations put high demands on local watersheds, requiring large volumes of water in concentrated areas over short time periods. With such sporadic high-volume water demand, water availability is a key issue in NEBC. The short-term, high volume water demands by the oil and gas industry are managed by the British Columbia Oil and Gas Commission (BCOGC) through the use of short-term water use approvals (ST-approvals). These ST-approvals have a maximum duration of 2 years. In 2015, there were 294 active ST-approvals with 1027 approved withdrawal locations totaling 19 million m^3 of water – approximately 0.015% of the region's average annual runoff volume (BCOGC, 2016).

These ST-approvals create a fast-changing system of water withdrawals in NEBC. To aid in the management of the region's water resources, the BCOGC developed the Northeast Water Tool (NEWT). NEWT is a Geographic Information System (GIS)-based hydrology decision support tool that combines hydrometric data (estimates of monthly and annual runoff volumes) with water license and permitting records (Chapman et al., 2012). NEWT represents an important step forward in water

resource management for this data-scarce region and is used by the BCOGC to manage water allocations – with the goal of balancing environmental flow needs (EFNs) with other industrial, municipal, and agricultural water demands. The EFNs of a stream are defined as the volume and timing of water flow required for proper functioning of the aquatic ecosystem (British Columbia, 2018).

NEWT is used by decision-makers as a guidance on natural water supply and availability, and it is recognized to have several limitations and uncertainties. The primary limitation is that the estimated runoff volumes represent 30-year averages (Chapman et al., 2012). The hydrologic regime in NEBC is snowmelt-dominated, and streamflow is highly variable. Thus, in any one year, the observed conditions may differ significantly from the 30-year average runoff and from the annual and monthly runoff estimates in NEWT. NEWT also has a large amount of uncertainty associated with the underlying hydrologic modelling used to derive the monthly and annual runoff estimates. Mean error, median error, and mean absolute error for the annual runoff estimates were reported as 5.5%, 3.7%, and 16.1%, respectively, with 42 out of the 53 (77.8%) calibrated basins having annual runoff estimates within ±20% of the observed mean annual runoff values (BCOGC, 2017). Additional uncertainty is present in the monthly runoff estimates from NEWT, which were calculated as a percentage of the estimated annual runoff using a multivariate regression model (Chapman et al., 2012).

These two limitations are inherent to the underlying data and methodology on which NEWT was built. However, NEWT's limitations are partially overcome by the consideration of additional data and the issuance of directives to suspend water withdrawals from lakes, rivers, and streams in specified watersheds during drought conditions. However, if annual runoff in a watershed is over-estimated by 20%, the potential for over-allocation and/or water scarcity is high, especially in the drier plains region of NEBC. The combination of uncertain water quantity combined with the highly variable hydrologic regime makes it difficult to identify reliable surface water sources for the high-volume fracking operations in NEBC – especially during drought conditions when industrial water abstractions from rivers and lakes are often limited or suspended.

Due to the high variability of streamflow, as well as the difficulty in hauling water from streams to well pads, other surface water sources are used to meet the shale gas industry water demands. In NEBC, many oil and gas companies currently rely on water

source dugouts, i.e. ponds or pits where water from snowmelt, rainfall, or groundwater inflow accumulates (BCOGC, 2016). The water source dugouts used by the oil and gas industry store excess precipitation and runoff from wet periods (spring snowmelt) for use in dry periods (late summer) when streamflow is insufficient. Unlike abstractions from streams and lakes, the use of oil and gas industry dugout water is not suspended during drought conditions. While the exact amount of water used by the oil and gas industry from source water dugouts in NEBC is unknown, it was roughly estimated at 2.2 million m^3 for 2015 (Mattison, 2017). The BCOGC reports that 7.74 million m^3 of water was used for hydraulic fracturing in 2015 (BCOGC, 2016); thus, approximately 28% of the water used in 2015 was sourced from dugouts.

With continued climate warming and a shift in the snow-to-rain ratio, the reliability of dugout water sources and summer streamflow in NEBC is uncertain. Continued shale gas industry development may lead to increased freshwater demand, and in the context of this water-energy nexus, future water security in the region is unknown. To address this knowledge gap, this study aims to estimate the potential for water scarcity in the Peace River watershed in the context of future climate change and growing water demand.

5.2. Study Area

The Peace River region of NEBC extends from the Rocky Mountains to the west, through the foothills, to the low-lying plains to the east (Figure 5.1a). Most of the shale gas development is focused in the low-lying plateau area, although some activity extends into the foothills. Of the four major shale gas plays in NEBC, the Montney Play exhibits the highest levels of development (Figure 5.1a).

For this study, two small headwater catchments within the Montney Play area were chosen, the 2.3 km^2 Graham River headwater catchment in the foothills and the 3.2 km^2 Blueberry River headwater catchment in the plains (Figure 5.1b). Both catchments are located upstream of active gauging stations, the watershed boundaries of which are shown in Figure 5.1b. Land use in each catchment was digitized from satellite imagery (Google Earth, 2014, 2015) and is shown in Figure 5.1c,d. At the time of this study, both watersheds contained water source dugouts that were in use by the oil and gas industry. The Blueberry catchment contained 2 dugouts, with a combined total allocated (i.e.

approved abstraction) water volume of 26,136 m^3/year. The Graham catchment contained 1 dugout with a total allocated water volume of 1,500 m^3/year.

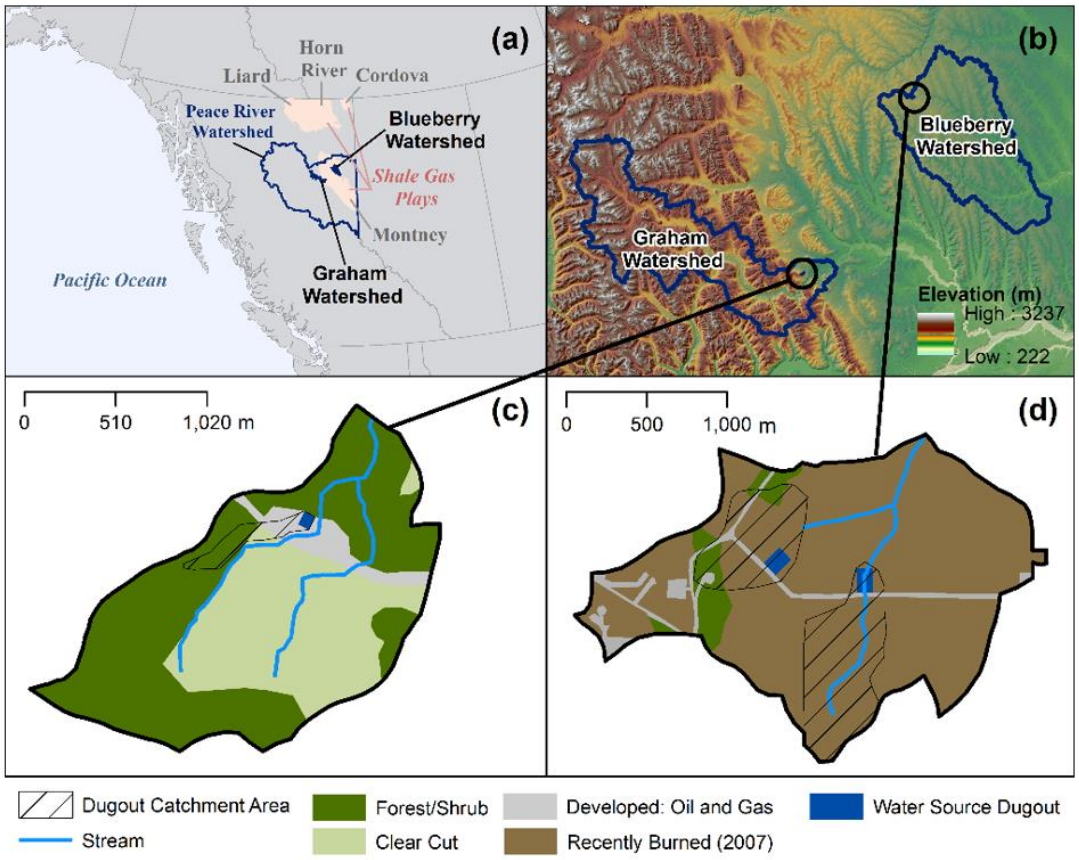

Figure 5.1 Study area including (a) Peace River watershed and shale gas plays, (b) Graham and Blueberry watersheds, and current land use and oil and gas industry water source dugout locations in the (c) Graham headwater catchment and (d) Blueberry headwater catchment.

5.3. Climate Change Projections

Statistically downscaled forcing datasets based on three models from Phase 5 of the Coupled Model Intercomparison Project (CMIP5) under representative concentration pathways (RCPs) 4.5 and 8.5 were used for the climate change scenarios in this study. The three models from the CMIP5 ensemble (CNRM-CM5-1, CanESM2-r1, ACCESS1-0-r1) were selected to capture the widest spread in projected future climate while using a small subset of the full ensemble, following Cannon (2015). Daily climate time series downscaled with the bias-correction/constructed analogues with quantile mapping reordering (BCCAQ) method were obtained from the Pacific Climate Impacts Consortium

(PCIC) data portal (PCIC, 2014) covering the period of 1950 to 2100. Werner & Cannon (2015) showed that, out of the seven downscaling methods tested, BCCAQ performed best for reproducing hydrologically relevant climate extremes.

The global climate model (GCM) ensemble projects increases in temperature and precipitation for both the Blueberry (plains) and Graham (foothills) catchments. For both catchments, the mean annual temperature is projected to be 2°C warmer in the near future (2021-2050) as compared to the historical period (1971-2000). The largest increases in temperature are for the coldest (January) and warmest (July) months. Total annual precipitation is projected to increase by approximately 60 mm/year relative to the historical period. Figure 5.2 shows the historical and near future climate for the Blueberry headwater catchment. Historical and near future climate in the Graham catchment (not shown) exhibits similar seasonal climate patterns and projected changes.

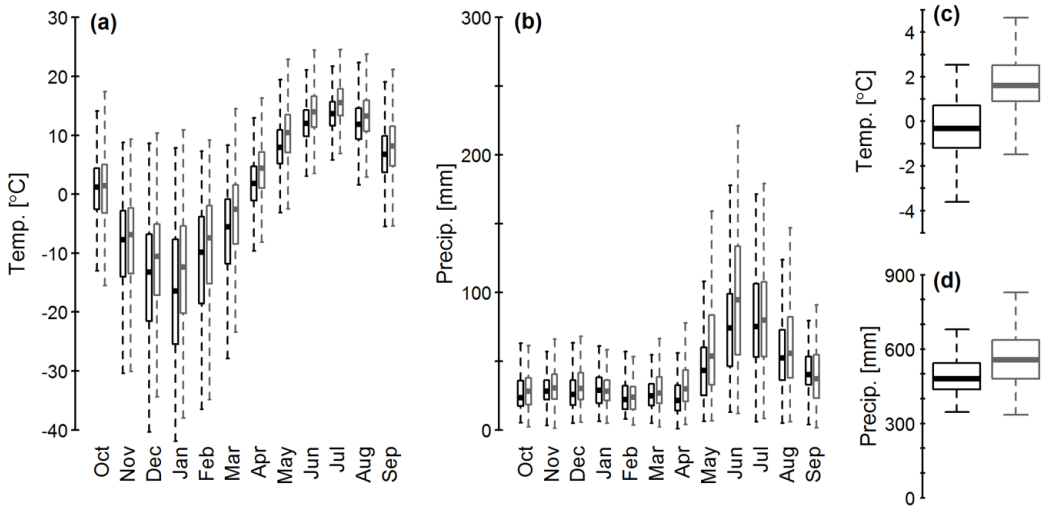

Figure 5.2 Boxplots of historical (1971-2000; shown in black) versus near future (2021-2050; shown in gray) climate from model ensemble for the Blueberry headwater catchment. (a) mean daily temperature, (b) monthly precipitation, (c) mean annual temperature, and (d) annual precipitation. Outliers not shown.

GCM bias

Despite the BCCAQ downscaling, significant bias exists between observed climate and the climate time series obtained from PCIC. To quantify this bias, we compared observed climate data to the downscaled GCM time series. This analysis was completed only for the Wonowon climate station (BC Hydro station, ID: 2509), near the

Blueberry catchment. Climate stations closer to the Graham catchment have insufficient data coverage. The observed data from the Wonowon station were subset to full years with no missing data (1982-2015). The downscaled GCM model output were subset for this date range for comparison. All three GCMs over-estimate January and February precipitation and under-estimate monthly dry days in most months (Figure 5.3). The downscaled GCM model output also under-estimate summer (JJA) daily maximum temperatures (Figure 5.4).

While bias exists between the downscaled GCM model output and the observed climate data, the seasonal patterns closely match. Except for the positively biased January and February precipitation and the negatively biased monthly dry days, the median monthly values from the downscaled GCM model output are all within the inter-quartile range of the observed monthly values. The under-estimation of monthly dry days corresponds to an under-estimation of rainfall intensity, common to GCMs, and may result in lower than expected runoff during summer months.

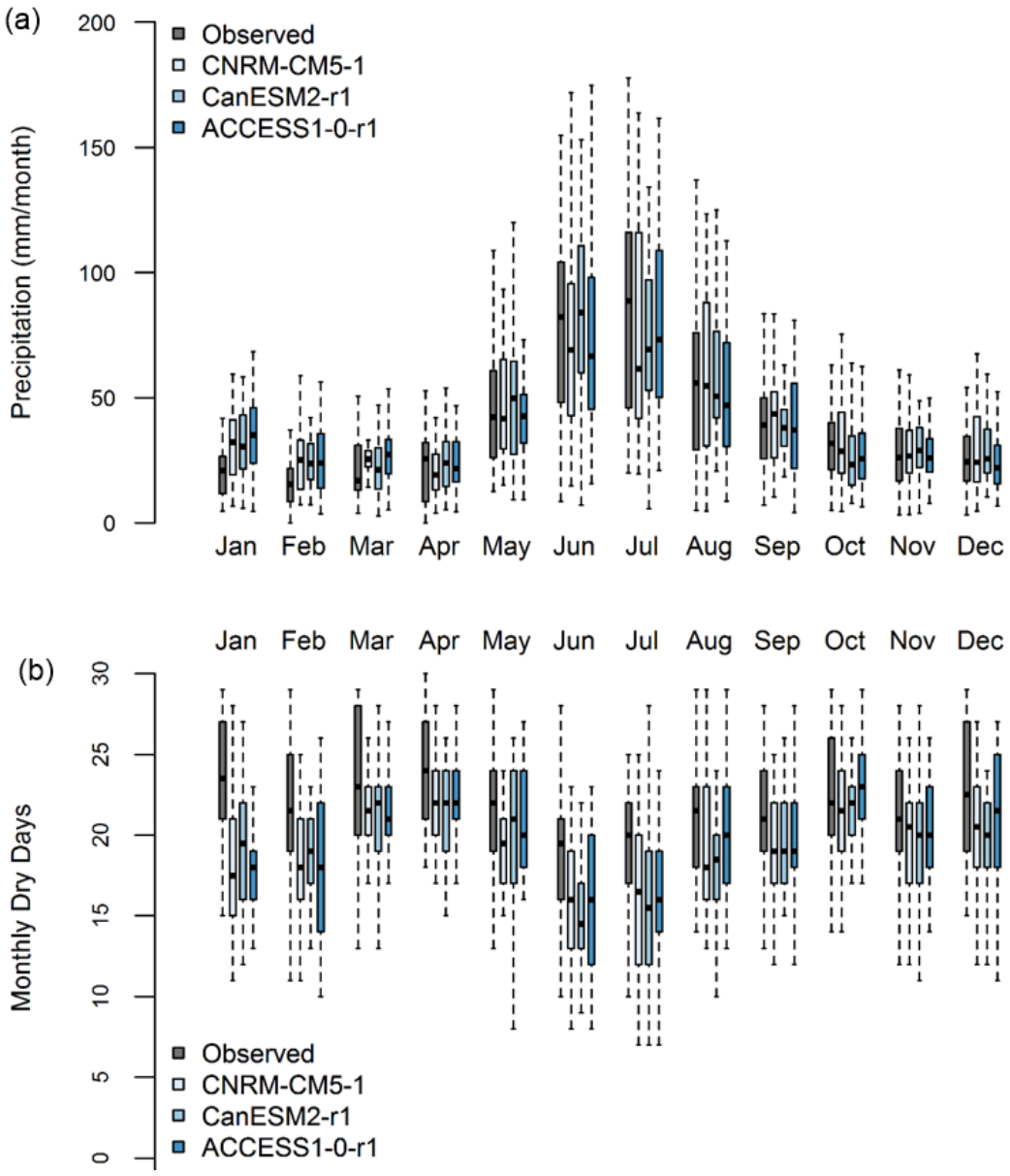

Figure 5.3 **Observed (Wonowon climate station) versus simulated (BCCAQ downscaled data from three GCMs) comparison of (a) monthly precipitation and (b) monthly dry days (precipitation < 0.5 mm). Outliers are not shown.**

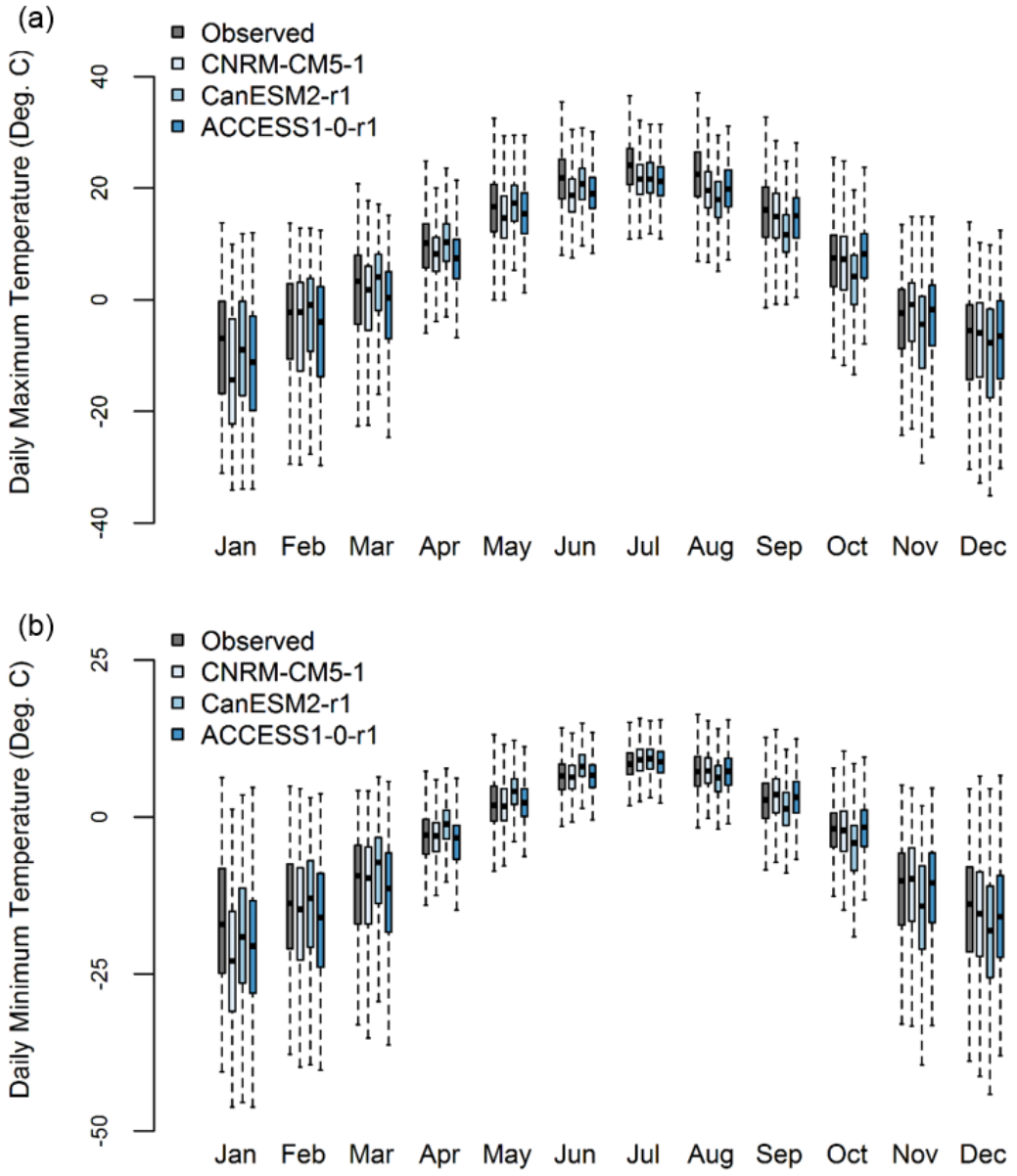

Figure 5.4 **Observed (Wonowon climate station) versus simulated (BCCAQ downscaled data from three GCMs) comparison of (a) daily maximum temperature and (b) daily minimum temperature. Outliers are not shown.**

5.4. Hydrologic Modelling

Frozen soils, snow accumulation, and snowmelt are all important components of the hydrologic cycle in the Peace River region, and as noted above, much of the region is data scarce. The physically based cold regions hydrological modelling (CRHM) platform was chosen as the modelling code for this study because of its proven ability to

simulate snow processes in diverse settings such as prairie (Fang & Pomeroy, 2007; Pomeroy et al., 2007) and alpine basins (Pomeroy et al., 2012). CRHM is a "physically-based, distributed, modular, object-oriented model development system" (Pomeroy et al., 2013). The CRHM models were structured as a set of four Hydrological Response Units (HRUs) corresponding to the major land cover features as listed in Table 5.1.

Table 5.1 Graham and Blueberry headwater catchment Hydrological Response Units (HRUs)

		Blueberry Headwater Catchment		Graham Headwater Catchment	
HRU	**Land Use**	**Area (km^2)**	**% in Dugout Catchment**	**Area (km^2)**	**% in Dugout Catchment**
1	Water Source Dugout	0.030	100%	0.005	100%
2	Developed: Oil & Gas	0.169	21%	0.132	13%
3	Clear Cut / Recent Burn	2.854	23%	0.861	1%
4	Forest	--	--	1.315	3%
5	Shrub	0.164	30%	--	--
	Total	**3.217**	**24%**	**2.314**	**3%**

Within each HRU, physically based modules were sequentially linked to simulate the dominant hydrological processes. Each HRU has a specific combination of vegetation, soils, drainage, and topographic parameters. Elevation, aspect, and slope were calculated from the 0.75 arc second Canadian Digital Elevation Model (CDEM; Natural Resources Canada, 2017). Both watersheds are primarily northeast facing. Aspect and slope values were averaged by land use type (i.e. HRU, see Table 5.2).

Table 5.2 HRU aspect, slope, and elevation.

	Blueberry Headwater Catchment			Graham Headwater Catchment		
HRU	**Aspect**	**Slope**	**Elevation**	**Aspect**	**Slope**	**Elevation**
	degrees	*degrees*	*MASL*[a]	*degrees*	*degrees*	*MASL*[a]
1	63	0	925	69	0	851
2	45	3.2	951	74	6.7	856
3	280	3.1	934	115	10.5	912
4	--	--	--	103	10.5	991
5	60	4.5	948	--	--	--

[a] meters above sea level

Blowing snow, albedo, canopy, and soil parameters were based on the parameterization of HRUs with similar land cover in the Lower Smoky River CRHM model developed by Pomeroy et al. (2013). The modules used are described in Table 5.3, and Figure 5.5 shows the schematic setup of the linked modules.

Table 5.3 Modules used in CRHM setups.

Module	Function/Notes
Radiation	Calculates theoretical global radiation, direct and diffuse solar radiation, and maximum sunshine hours based on latitude, elevation, ground slope, and azimuth (Garnier & Ohmura, 1970).
Observation	Reads forcing meteorological data and provides inputs to other modules. Phase of precipitation was determined by the psychrometric energy balance procedure (Harder & Pomeroy, 2013). Catchments in this study have minimal (<100 m) elevation range; therefore, precipitation and temperature lapse rates were not used.
All-wave radiation	Estimates the net all-wave radiation to snow-free surfaces using the Brunt equation (Brunt, 1932).
Slope radiation	Short-wave radiation is estimated from the theoretical global radiation based on daily maximum and minimum temperatures (Annandale et al., 2001) and then adjusted based on ground slope.
Longwave radiation	Estimates incoming longwave radiation using shortwave radiation on the slope (Sicart et al., 2006).
Canopy	Estimates the snowfall and rainfall intercepted by and sublimated or evaporated from the forest canopy and unloaded or dripped from the canopy (Ellis et al., 2010; 2013).
Blowing snow	Estimates the wind redistribution of snow transport and blowing snow sublimate losses throughout the winter period (Pomeroy & Li, 2000).
Albedo	Estimates snow albedo throughout the winter and into the melt period and indicates the beginning of melt for the energy-balance snowmelt module (Verseghy, 1991).
Energy-balance snowmelt	Estimates snowmelt by calculating the energy balance of radiation, sensible heat, latent heat, ground heat, advection from rainfall, and change in internal energy (Gray & Landine, 1987).
Permafrost	Estimates the ground surface temperature from air temperature, net radiation, and antecedent frost table depth, and tracks the depth of the freezing and thawing fronts (Xie & Gough, 2013).
Infiltration	Estimates infiltration into frozen and unfrozen soils (Ayers, 1959; Zhao & Gray, 1999). Frozen soil infiltration is estimated using a parametric equation (Gray et al., 2001). Unfrozen soil infiltration is estimated with macropores based on soil classification (Ayres, 1959).
Evapotranspiration	The Priestly and Taylor evaporation expression (Priestley & Taylor, 1972) estimates evaporation from saturated surfaces and was used to model actual evapotranspiration (AET) for the dugout HRUs. The Penman-Monteith method was used for all other HRUs and estimates AET from unsaturated surfaces based on available water, stomatal resistance, soil type, soil depth, and leaf area index.
Soil and hillslope	Estimates soil moisture balance, depression storage, surface/sub-surface flows in two soil layers, and groundwater discharge in a groundwater layer. Darcy's Law is used to estimate lateral flow rate in soil layers and the groundwater layer, and the vertical flow rate of excess soil water to groundwater (i.e. groundwater recharge) based on hydraulic conductivity estimates, porosity, pore size distribution, and slope.
Routing	Routes runoff using Clark's lag and route timing estimation method is used to route runoff (Clark, 1945). The catchments simulated in this study are small and runoff lag is minimal. Runoff was routed to the dugout HRUs based on the percentage of each HRU in the dugout catchment (see Table 5.1). The remaining runoff, and any over-flow runoff from the dugout, was routed out of the catchment.

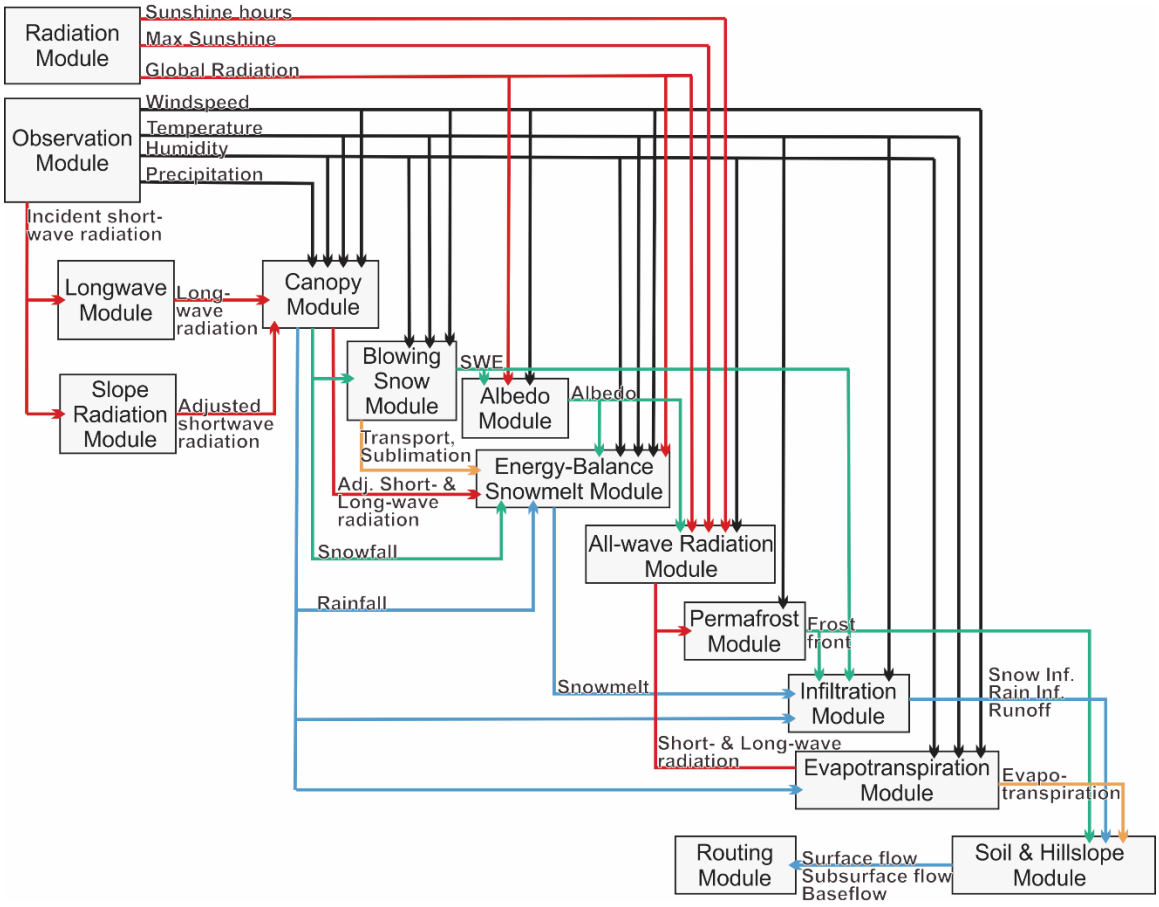

Figure 5.5 Flowchart of physically based hydrological modules used in the CRHM models. The model structure is the same for the Blueberry and Graham catchments. (abbreviations: Inf: Infiltration; Adj.: Adjusted)

Within the CRHM modelling framework, dugout water storage was simulated as detention storage. In both watersheds, the following assumptions regarding dugout water storage and withdrawal were made:

1) Each dugout has a maximum storage volume equal to the total annual allocated water, allowing dugouts to fill completely during the cool winter season. Additional storage to offset expected evaporation during the summer season was not considered. Actual storage volumes of the dugouts are unknown.

2) The allocated water volume is withdrawn at a constant rate over the licensed withdrawal period (May 1st to August 31st). Actual patterns and volumes of withdrawal from the dugouts are unknown.

3) The dugouts are clay-lined and above the groundwater table, allowing for no groundwater discharge to the dugouts to take place. Thus, dugout water is sourced entirely from precipitation and overland flow.

Actual dugout designs are unknown; however, aerial imagery indicates some type of lining material is present.

5.5. Daily to Hourly Downscaling

Required climate forcing data for the CRHM models includes temperature, precipitation, relative humidity, and wind speed at hourly time steps. The statistically downscaled forcing datasets obtained from PCIC included only daily maximum and minimum temperature and daily precipitation. Therefore, hourly time series were generated from the daily observations by resampling observed hourly data from nearby climate stations (Table 5.4). The resampling methodology employed a stochastic technique wherein one day (24 hours) was chosen from a subset of the observed record and used to disaggregate the daily values to hourly. The subset was based on seasonal occurrence (30-day centered window), wet versus dry conditions, and, if wet, quartile matching of the daily precipitation amount. One day (24 hours) was then chosen randomly from the subset. Hourly temperatures were re-scaled to match the projected daily minimum and maximum, and hourly precipitation amounts were re-scaled to match the projected daily precipitation. Humidity and wind values were used without adjustment. This resampling methodology preserves variations in diurnal temperature and relative humidity curves due to seasonality and wet versus dry conditions. Further details on climate disaggregation are included in Appendix D.

Table 5.4 Climate stations used to generate hourly time series.

	Blueberry Catchment	Graham Catchment
Station ID	FLNRO-WMB 1703	FLNRO-WMB 1691
Station Name	Wonowon	Graham
Latitude & Longitude	56.7185, -121.7654	56.4347, -122.4575
Record Start	1-May-1990	19-May-1995
Hourly Variables	Temperature, Precipitation, Wind Speed, Relative Humidity	Temperature, Precipitation, Wind Speed, Relative Humidity

5.6. Future Water Demand

The shale gas industry development scenarios used in this study were developed by the Pembina Institute and correspond to scenario options 1 through 6 in Table 1 of Kniewasser and Horne (2015). These scenarios include current and improved water management policies, and low, medium, and high liquefied natural gas (LNG) development. The improved policy scenarios incorporate 25% water recycling and 25%

deep aquifer saline (non-potable) water use. The LNG development scenarios also assume 1, 3, and 5 LNG terminals (i.e. storage and distribution facilities) for the low, medium, and high development, respectively.

Future shale gas industry freshwater demand is projected to peak in 2030 (Figure 5.6), with the high development scenario exhibiting more than a 350% increase in freshwater demand compared to the 2015 levels. Improved water management policies have the potential to decrease future freshwater demand by almost 50%.

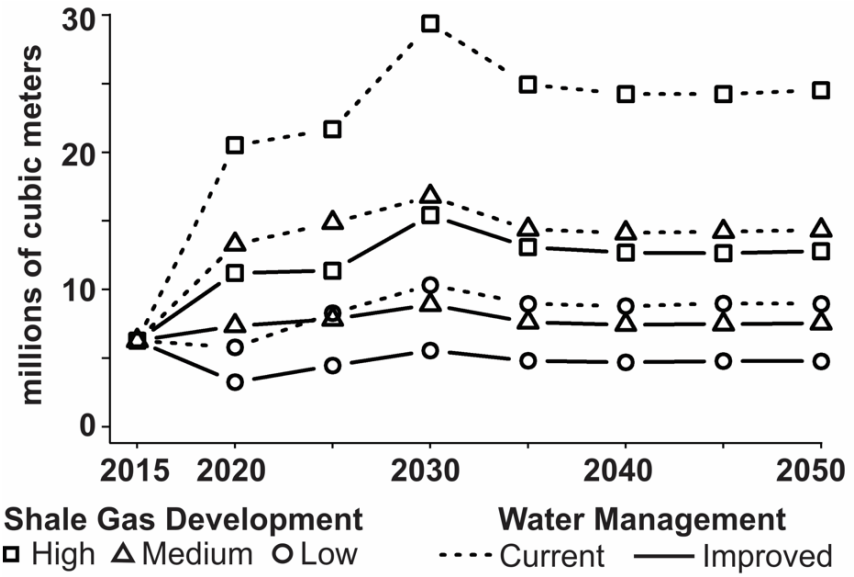

Figure 5.6 Projected shale gas industry freshwater demand from Kniewasser and Horne (2015). High, medium, and low development correspond to 5, 3, and 1 Liquid natural Gas (LNG) plants, respectively. The improved water management scenario incorporates 25% water recycling and 25% saline water use.

5.7. Results

5.7.1. Simulated Versus Observed

No observed snow water equivalent (SWE) or streamflow data exist for the two headwater catchments simulated in this study. Model results for the Blueberry headwater catchment are compared to observed data from a nearby climate station and nearby stream gauges. A comparison between Graham headwater catchment model results and observed data is not completed due to a lack of observations in the foothills region. The results are discussed in the context of the overall purpose of the study which

was to estimate the potential for water scarcity in the Peace River watershed in the context of future climate change and growing water demand.

Snow water equivalent

To evaluate the accuracy of snow accumulation and melt modelling in CRHM (forced with downscaled GCM model output), the simulated Blueberry catchment SWE was compared to observed daily snow depth measurements from the closest climate station (28 km south; Environment Canada Wonowon station; ID 1188973). For location-specific comparison, simulated SWE from a CRHM model forced with the observed data and parameterized to represent the landscape around the Wonowon climate station was also compared to the observed snow depth measurements.

The CRHM-simulated snow is in units of mm of SWE while the observed snow data are in cm of snow depth. The density of the observed snow is unknown, and an assumed snow depth to SWE ratio of 0.2 was used to compare the simulated SWE and observed snow depth measurements. Because of the uncertainty in snow density, the observed versus simulated SWE were visually analyzed for agreement between accumulation onset and melt-out timing rather than SWE magnitude (Figure 5.7 and Figure 5.8). Visual assessment shows that snow is simulated well at the Wonowon climate station, and, despite uncertainty in snow density, statistical performance measures show good agreement with the visual assessment. Between the observed and simulated SWE shown in Figure 5.7, mean absolute error (MAE) is 11.2 mm, root mean square error (RMSE) is 21.9 mm, and the Pearson correlation coefficient is 0.85.

Figure 5.8 shows observed and simulated mean daily SWE values at the Wonowon climate station, highlighting the close agreement between snow accumulation onset and melt-out timing. Figure 5.8 also shows simulated mean daily SWE (1971-2000) for the Blueberry catchment, which was forced with the downscaled GCM model output. Melt-out timing in the Blueberry catchment is later than at the Wonowon climate station; however, the GCM-simulated mean annual temperature at the Blueberry catchment is 1.6°C colder than the observed mean annual temperature at the Wonowon station, and thus later melt-out timing is expected.

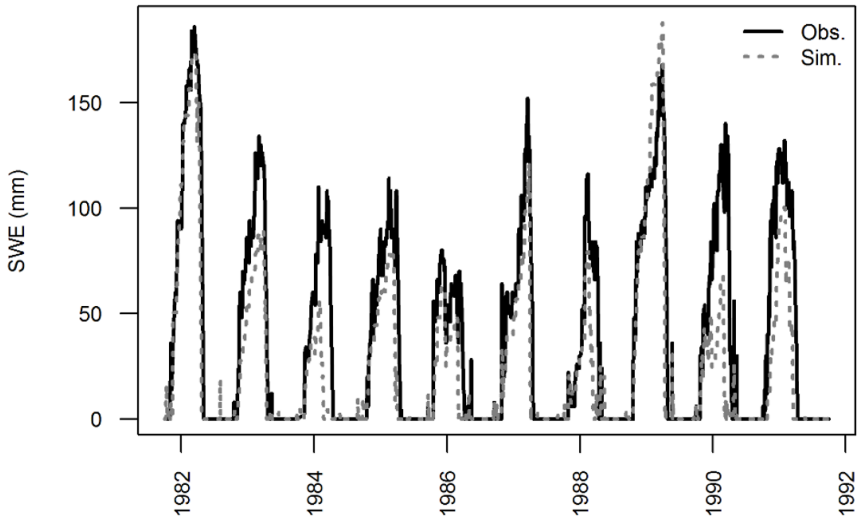

Figure 5.7 Observed versus simulated snow water equivalent (SWE), Wonowon climate station.

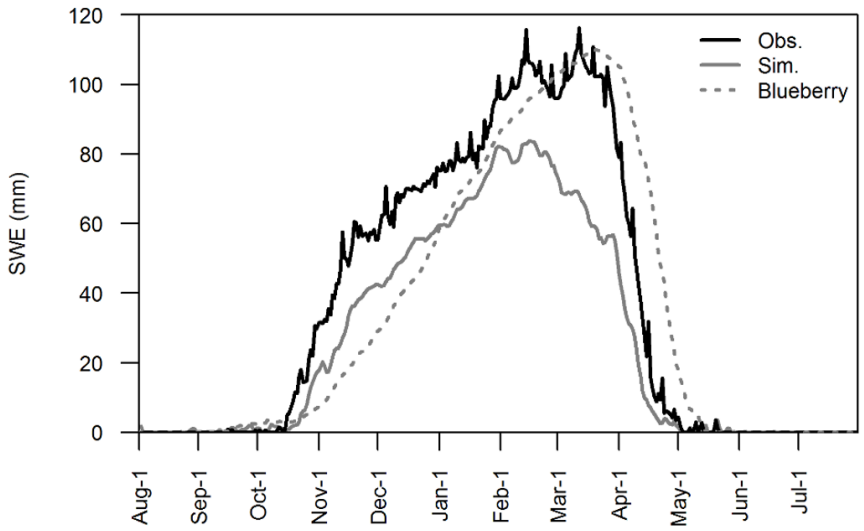

Figure 5.8 Mean daily snow water equivalent (SWE) observed at the Wonowon climate station versus simulated at the Wonowon climate (forced with observed data), and versus simulated SWE in the Blueberry headwater catchment (forced with downscaled GCM model output).

Runoff

To compare the runoff from the simulated Blueberry headwater catchment to observed streamflow data, the CRHM model was run without any dugout storage or water extraction. This was done by changing the dugout (HRU 1) parameters to match the shrubland (HRU 5) parameters.

Mean annual runoff in the naturalized (i.e. no dugouts) Blueberry catchment model was 145 mm/year. This is higher than the long-term mean annual runoff observed in the larger Blueberry watershed (gauge ID: 07FC003) of 95 mm/year. However, the simulated Blueberry headwater catchment is located on the northern edge of the larger gauged Blueberry watershed and thus has a cooler, wetter climate compared to the mean for the entire catchment, and a higher runoff compared to that observed in the entire catchment is expected.

While there are no observed runoff data available for the simulated headwater catchment, estimates of mean annual and mean monthly runoff are available from NEWT. NEWT-estimated mean annual runoff for the Blueberry headwater catchment is 107 mm/year (13% higher than the long-term mean of the larger gauged catchment of 95 mm/year). Therefore, NEWT over-estimates mean annual runoff in the headwater catchment. As well, the simulated runoff is significantly higher than the NEWT-estimated runoff (145 mm/year versus 107 mm/year). These differences in runoff can be explained by the fact that CRHM model uses land use digitized from aerial imagery, including roads, dugouts, and developed areas (oil and gas industry structures), and a recently burned area, as shown in Figure 5.1. In contrast, the NEWT-estimated runoff is based on evapotranspiration (ET) estimates for a primarily (93.2%) shrubland landcover (BCOGC, 2017). Development, road construction, and vegetation changes due to fire are all associated with an increase in runoff, and the +38 mm/yr over the NEWT-estimated mean annual runoff is within the range of documented runoff increases for this type of land use change (see Bosch & Hewlett, 1982, for example).

To quantify the impact of land use on mean annual runoff, the CRHM model was re-run using 100% shrubland (HRU 5) as the land use, and the resulting mean annual runoff was 86 mm/yr. By simply changing land use from mixed to 100% shrubland, the simulated runoff decreased from 107 to 86 mm/year. These results clearly illustrate the importance of accurately representing land use in the model, and that the simplified land use used in NEWT likely underestimates runoff in the headwater catchment.

Further comparison of simulated **median daily runoff** to observed median daily runoff in the gauged Blueberry catchment shows that the simulated Blueberry headwater catchment has an earlier freshet and lower summer (June-August) runoff compared to the larger gauged Blueberry catchment (Figure 5.10). The difference in runoff timing may

be due to scale effects – the gauged Blueberry catchment is much larger than the simulated headwater catchment (1,770 km^2 vs 3.2 km^2). To explore this potential scale effect, the simulated runoff was compared to observed runoff for a smaller (201 km^2) gauged watershed, St. John Creek (ID: 07FC002). All three catchments (simulated Blueberry, gauged Blueberry, and gauged St. John Creek) are located in the plains of the Peace River region within the Beatton River watershed (Figure 5.9).

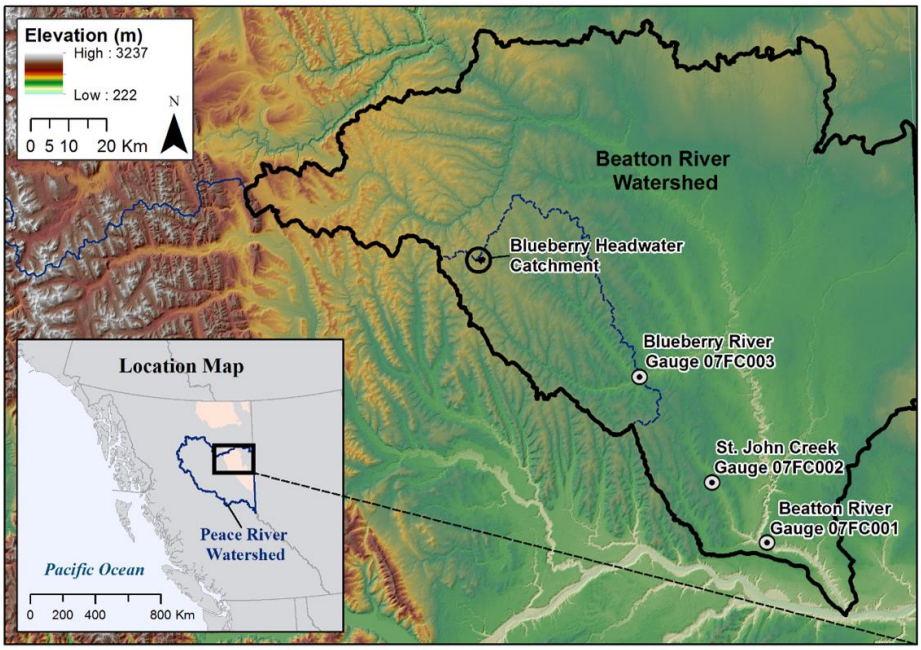

Figure 5.9 Beatton River watershed and gauging station locations.

The spring freshet timing in the simulated Blueberry catchment closely matches the freshet timing in the St. John Creek catchment (Figure 5.10). Comparison of observed daily runoff time series from the Beatton River (15,600 km^2; ID 07FC001), Blueberry River (1,770 km^2; ID 07FC003), and St. John Creek (201 km^2; ID 07FC002) shows that hydrographs of the two sub-watersheds (St. John Creek and Blueberry River) differ significantly from each other and from the Beatton River watershed in which they are contained (see Appendix E for time series plots). St. John Creek, the smallest watershed, consistently exhibits an earlier spring snowmelt peak and lower summer rain event peaks compared to the Blueberry and Beatton watersheds. The hydrographs of the Blueberry and Beatton watersheds are more similar to each other than they are to the St. John Creek hydrographs (see Appendix E - Table S5.1), demonstrating that heterogeneity is larger at the smaller scale.

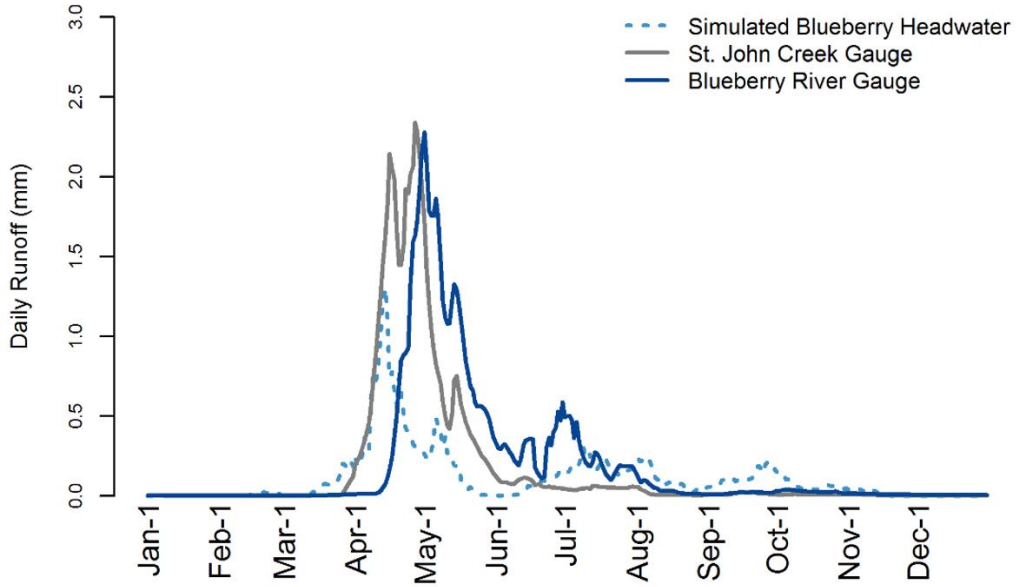

Figure 5.10 Simulated median daily runoff in the Blueberry catchment versus observed median daily runoff from two nearby stream gauges, St. John Creek (Gauge ID: 07FC002) and Blueberry River (Gauge ID: 07FC003). Median daily runoff values are calculated for the observed record period of St. John Creek: 1962-1974.

While the observed data show substantial differences in freshet timing between catchments (see Figure 5.10 and Appendix D), the NEWT-estimated monthly runoff values for the catchments show minimal differences in freshet timing (Figure 5.11a). NEWT-estimated runoff values are a close match to observed values in the Blueberry and Beatton watersheds (Figure 5.11b). NEWT-estimated runoff values differ substantially from the observed values for St. John Creek and from the CRHM-simulated runoff in the Blueberry headwater catchment. NEWT under-estimates April runoff and over-estimates June runoff in all four of the catchments (Figure 5.11b).

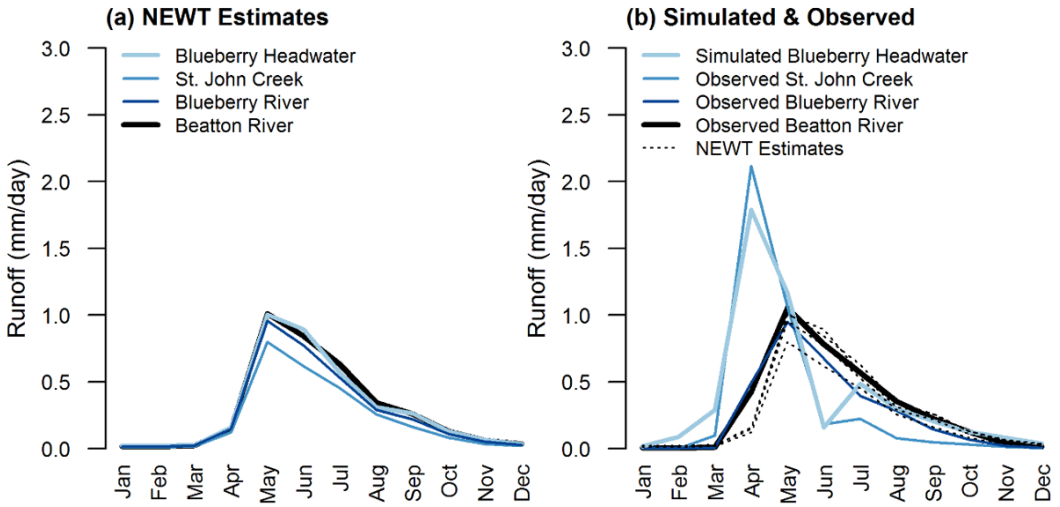

Figure 5.11 Monthly mean daily runoff (a) estimated by the North East Water Tool (NEWT) and (b) simulated for the Blueberry headwater catchment and observed at hydrometric gauging stations. Simulated and observed data are summarized for the 1971-2000 period for consistency with NEWT, with the exception of the St. John Creek gauge, which only covers the 1962-1974 period.

Given the documented heterogeneity in observed runoff between watersheds and the skill of the CRHM for modelling snow accumulation and melt, as demonstrated in this study and in Fang & Pomeroy (2007), Pomeroy et al. (2007), and Pomeroy et al. (2012), the CRHM model results likely represent a reasonable, physically-based estimate of monthly runoff in the Blueberry headwater catchment. The differences between NEWT-estimated runoff and the simulated Blueberry headwater catchment runoff suggest that the NEWT does not capture heterogeneity in the hydrological processes of smaller catchments.

5.7.2. Dugout Impacts on Runoff

Of the two headwater catchments, the Blueberry headwater catchment has the larger percentage of annual runoff allocated for use by the oil and gas industry. Therefore, the impact of dugouts on runoff was analyzed for the Blueberry catchment only. The non-parametric, distribution insensitive, Wilcoxon signed-ranks test was used to determine if there is a significant difference in runoff between the CRHM model with the dugouts (dugout model) and the CRHM model without the dugouts (naturalized model). Results of the Wilcoxon signed-ranks test are presented in Table 5.5.

As stated previously, water is only withdrawn from the simulated dugouts during the licensed withdrawal period (May 1st to August 31st). Correspondingly, runoff in the dugout model is significantly lower than runoff in the naturalized model in all months, except May (Table 5.5). May runoff is higher in the dugout model due to differences in the model parameterization. The clay soils and no vegetation of the dugout HRU result in lower infiltration and reduced early summer evapotranspiration (higher runoff) compared to the loam soils and shrubland vegetation of the naturalized model. The median difference between annual runoff in naturalized model and annual runoff in the dugout model is 8.75 mm/year, which is slightly higher than the total withdrawn/allocated runoff of 8.07 mm/year due to higher (relative to naturalized model) total annual actual evapotranspiration (AET) caused by the dugout water storage.

Table 5.5 Median monthly and annual runoff estimated by the naturalized model and the dugout model for the Blueberry headwater catchment. Median difference between models was estimated with the Wilcoxon signed-ranks test.

	Units	X_1 Naturalized Model	X_2 Dugout Model	Median Difference	Alternative Hypothesis
January	mm/month	0.12	0.06	0.04	a
February	mm/month	0.88	0.83	0.27	a
March	mm/month	3.15	2.42	0.66	a
April	mm/month	54.76	54.15	0.83	a
May	mm/month	8.03	9.93	-1.43	b
June	mm/month	2.03	1.36	0.85	a
July	mm/month	9.85	7.08	2.60	a
August	mm/month	4.56	3.08	1.52	a
September	mm/month	4.67	3.30	1.16	a
October	mm/month	2.70	2.22	0.61	a
November	mm/month	0.97	0.78	0.25	a
December	mm/month	0.17	0.12	0.05	a
Annual	**mm/year**	**134.98**	**125.73**	**8.75**	**a**

Note: All tests were one-tailed. Alternative hypothesis: a) medians of X_1 are higher than the medians of X_2, b) medians of X_2 are higher than the medians of X_1. Null hypothesis: the distributions of the two groups are equal. All tests are significant at the $P < 0.01$ level.

In the small Blueberry headwater catchment simulated here, dugouts have the highest impact on runoff in summer (July-September; Table 5.5) when water demand and ecosystem needs are high. While the combined impact of many dugouts (tens to hundreds) on runoff in larger watersheds in the Peace River region is not known, a recent study by McGee et al. (2012) showed that the cumulative effects of small water diversions on runoff in four larger (158-256 km^2) prairie watersheds in southern Alberta equal or exceed reported effects of climate change. McGee et al. (2012) report a more

than 5% decrease in annual runoff due to small diversions, suggesting that the widespread use of dugouts and stream diversions in Peace River region of NE BC will have a significant impact on annual runoff in the region.

One of the assumptions in this study is that the total dugout storage volume is equal to the total annual ST-approval allocation volume. The reliability of water source dugouts could be improved by increasing the total storage volume to 1.5 or 2 times the total annual allocated volume, allowing for greater storage of snowmelt and spring runoff to use during the drier summer period and possible carry-over storage between wet and dry years. Although not quantified in this study, increased storage volumes would likely have larger impacts on runoff. Additional research is needed to quantify the relationship between dugout volume, water-source reliability, and runoff impacts.

5.7.3. Near Future (2021-2050) Versus Historical (1971-2000) Hydrology

In the simulated Blueberry and Graham headwater catchments, higher temperatures in the near future (relative to the historical period) result in decreased late-season (April-May) snowfall (Figure 5.12a and Figure 5.13a), a shift towards earlier snowmelt as evidenced by reduced snow water equivalent (SWE) in March and April (Figure 5.12b and Figure 5.13b), and increased March runoff (Figure 5.12d and Figure 5.13d). Despite an overall increase in annual precipitation, hydrologic modelling results show no significant changes in total annual runoff in the Blueberry catchment between the historical and near future periods (Figure 5.14a). This is because increases in total annual precipitation in the near future are offset by increased actual evapotranspiration (AET; Figure 5.14a), resulting in no net change in total annual runoff at the annual time scale. In the Graham catchment, however, precipitation increases are larger than AET increases, resulting in an increase in total annual runoff in the near future compared to the historical period (Figure 5.14a).

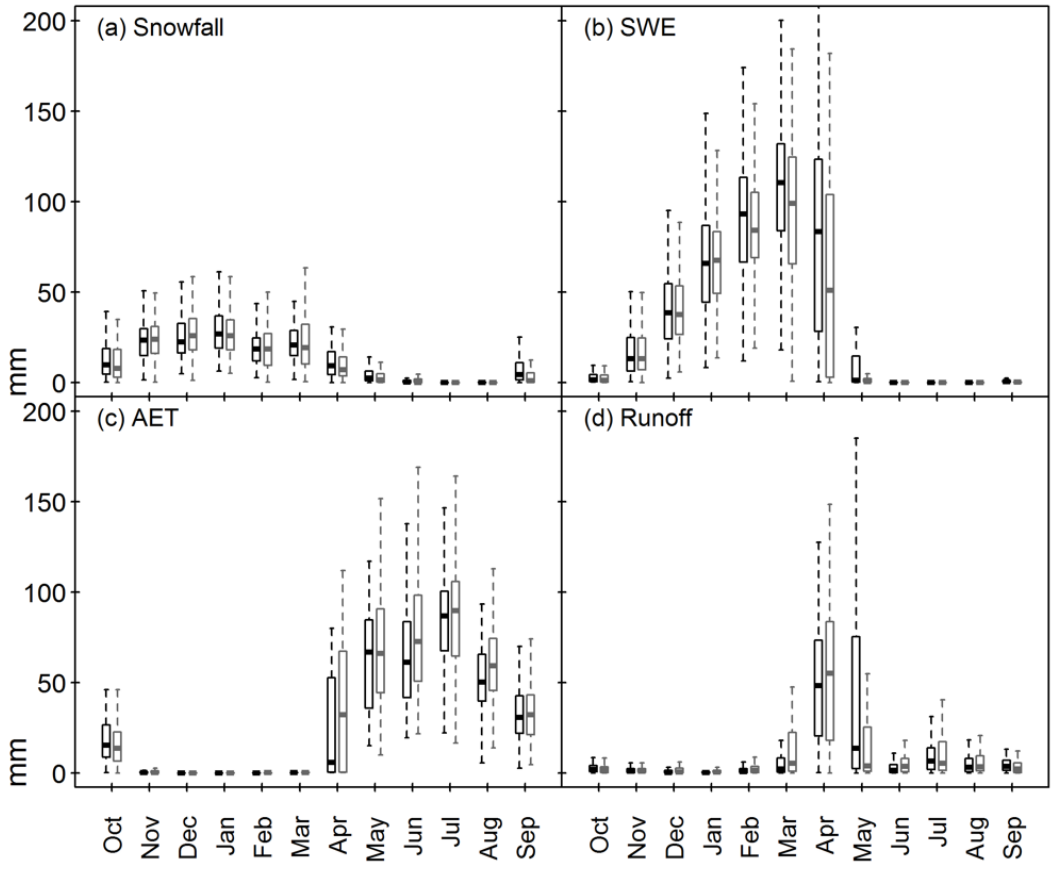

Figure 5.12 **Blueberry headwater catchment (plains) simulated historical (1971-2000) in black and near future (2021-2050) in gray (a) monthly snowfall (represented as mm of snow water equivalent - SWE), (b) mean monthly SWE, (c) monthly actual evapotranspiration (AET), and (d) monthly runoff.**

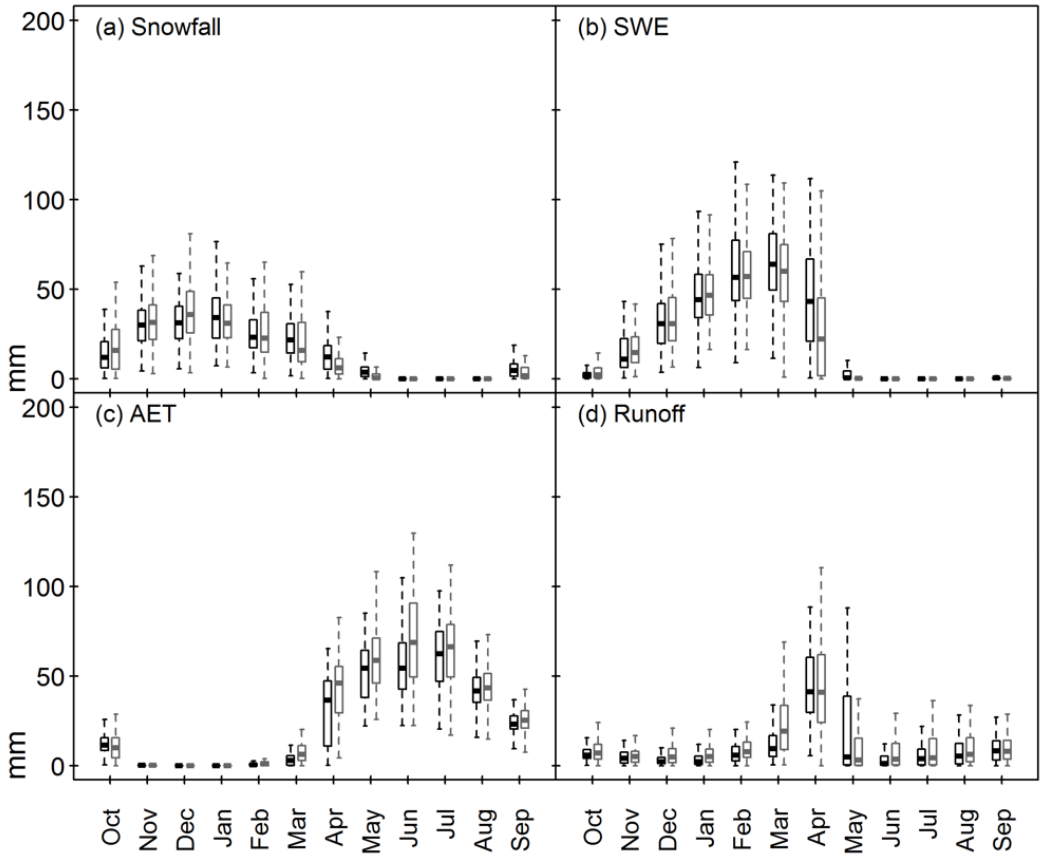

Figure 5.13 **Graham headwater catchment (foothills) simulated historical (1971-2000) in black and near future (2021-2050) in gray (a) monthly snowfall (represented as mm of snow water equivalent - SWE), (b) mean monthly SWE (c) monthly actual evapotranspiration (AET), and (d) monthly runoff.**

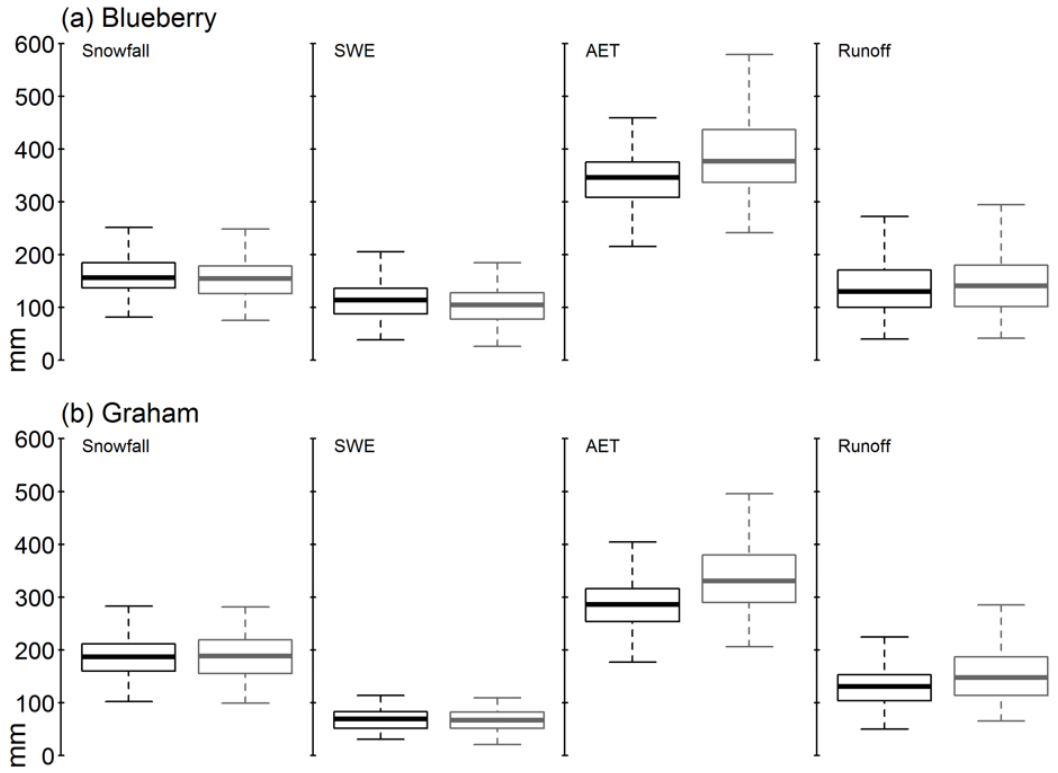

Figure 5.14 (a) Blueberry and (b) Graham headwater catchment annual snowfall, annual peak snow water equivalent (SWE), annual actual evapotranspiration (AET), and annual runoff. Simulated historical (1971-2000) is shown in black and near future (2021-2050) in shown in gray.

5.8. Demand Versus Supply

To determine the potential for future water scarcity, the simulated annual runoff from the naturalized model was compared to future water demand from the six shale gas development scenarios. Future water demand volumes were calculated by multiplying the 2015 allocation volumes by the projected percent change in water use relative to 2015. The fraction of allocated runoff was then calculated as projected future water demand (converted to mm of runoff) divided by the simulated annual runoff. Currently, the BCOGC sets the maximum amount of water available for allocation at 15% of the MAR. Therefore, the fraction of mean annual runoff (MAR) needed to meet shale gas industry demands was also calculated using 10-year periods as shown in Figure 5.15.

Without improved water management, allocation levels in the Blueberry headwater catchment exceeded 15% of MAR (over-allocation) for all time periods under the high development scenario (Figure 5.15). Moreover, in dry years, the fraction of annual runoff allocated exceeded 15% under the current water management practices with even the low development level, as illustrated by the upper quartile and upper outliers of boxplots in the left-most panel of Figure 5.15.

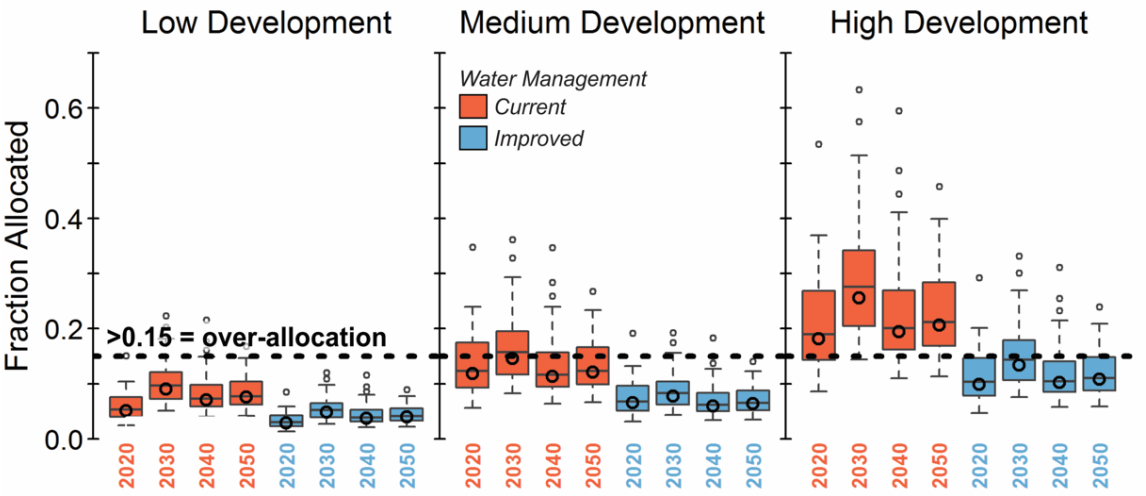

Figure 5.15 Blueberry headwater catchment fraction of annual runoff required to meet shale gas industry freshwater demands. Results are presented by centered 10-year periods (2020 = 2015-2024, 2030 = 2025-2034, etc.). Boxplots show the fraction allocated for *individual years*; black circles show the fraction allocated based on the 10-year *mean annual runoff*.

The hydrological modelling results show no significant change in the total annual runoff for the Blueberry headwater catchment (Figure 5.14a). Therefore, the observed annual runoff from the Blueberry watershed gauge (ID: 07FC003) was used to estimate future water supply at the annual scale. Assuming mean total annual runoff will remain constant through the near future, allocation levels within the 1770 km^2 Blueberry watershed do not exceed 3% under any of shale development scenario combinations. While the Blueberry water supply will likely be sufficient to meet demand at the annual time scale, water scarcity may occur during the warmer months following the spring freshet (May-August) when water demand is high. Modelling results show a decrease in summer (May-August) runoff (relative to historical) in the near future (Figure 5.12d) for the Blueberry headwater catchment. Median summer runoff in the historical and near future periods are 64.6 mm and 55.0 mm (a reduction of 14.8%) in the Blueberry

headwater catchment and 40.6 mm and 35.5 mm (a reduction of 12.6%) in the Graham headwater catchment, respectively.

During drought periods, the BCOGC suspends shale gas industry water use from streams and lakes, but water stored in dugouts remains available for industrial use. With the projected decrease in summer streamflow volumes, dependency on water source dugouts may increase. Therefore, the future reliability of water source dugouts was analyzed by tabulating the CRHM-simulated monthly minimum dugout water levels (results not shown). During the 2020-2050 period, the simulated water source dugout maintained a minimum water level of at least 20% volume in the Graham catchment; however, minimum August dugout water levels decreased by up to 41% relative to the historic period. During late summer (August) in drought years, the dugout water supplies were exhausted in the Blueberry catchment in both the historical and near future periods. Low dugout water levels (less than 20% volume) occur 24% more frequently in the near future period than they do in the historical period.

5.9. Conclusions

Continued global warming will likely result in decreased summer runoff for the plains and foothills physiographic regions of the Peace River watershed in NEBC. This decrease in summer runoff will likely co-occur with increased oil and gas industry freshwater demand. Future increases in water demand may be met by water source dugouts or stream diversion points distributed throughout the shale gas development area and not focused only where development already exists. Thus, water quantity in larger watersheds in the Peace Region of NEBC will likely be adequate to meet the demands of the shale gas industry. Smaller watersheds in areas with high levels of oil and gas industry development may experience water scarcity, especially during drought conditions and under high development scenarios. If the shale gas industry in NEBC continues to expand, improved water management policies, e.g., water recycling and saline water use, will be needed to meet water demands, especially when competing interests (e.g., agricultural, domestic) are accounted for – which was not done in this study.

Water source dugouts may not provide a reliable summer water source during drought years, and the reliability of water source dugouts is likely to decrease in the

future. A substantial portion (~28% in 2015) of short-term water use in this region is sourced from dugouts located in headwater catchments like the ones simulated in this study. Differences between the expected (i.e. NEWT-estimated) monthly runoff and the actual monthly runoff, especially with regards to runoff timing and earlier than estimated freshet peaks, may result in an over-estimation of summer dugout water supplies for the region. Additionally, the CRHM simulations completed in this study show that water extraction from dugouts has the largest negative impact on summer and early fall runoff, when water demand and ecosystem needs are highest.

Chapter 6. Conclusions

This study tested and confirmed the hypothesis that, in catchments with seasonal snow cover, snow drought regimes are directly related to low flow and streamflow drought regimes, and, consequently, climate warming will have related impacts on snow drought, low flows, and streamflow drought. Two main research methodologies were employed: 1) a data-driven (downward) approach (Chapters 2 and 3) and 2) a process-based (upward) approach (Chapters 4 and 5). Together, these two different approaches showed that snow drought, low flows, and streamflow drought are sensitive to winter climate conditions, particularly precipitation and thawing degrees. In the context of a warming climate, increased winter season thawing degrees leads to increased warm (temperature-driven) snow drought, shorter and less severe winter low flows, longer and more severe summer low flows, and increased summer streamflow drought risk in catchments with seasonal snow cover. The following sections summarize the major conclusions and contributions of this research and discuss recommendations for future research.

6.1. Climate Controls on Low Flows / Hydrological Drought

Two analyses were completed to identify the dominant climate controls on low flows: (1) a regional analysis of climate controls on low flow regimes and (2) a catchment-scale analysis of climate controls on the inter-annual variability of runoff and low flows. The regional analysis provides insight into how a catchment's low flow regime may change due to an overall shift in the average climate. The catchment-scale analysis, on the other hand, reveals which climate conditions lead to more severe summer/winter low flows and/or decreased runoff, i.e. identifies the primary climatic causes of streamflow drought.

At the regional-scale in western North America, the low flow regimes of mountain catchments with seasonal snow cover are dominantly controlled by temperature. Catchments with higher mean annual temperatures have longer, more severe summer low flow periods and shorter, less severe winter low flow periods compared to catchments with lower mean annual temperatures. Total annual runoff, however, is

dominantly controlled by precipitation, and catchments with higher mean annual precipitation have higher mean annual runoff.

Conversely, at the catchment-scale, the inter-annual variability of runoff and low flows in mountain catchments with seasonal snow cover is dominantly controlled by precipitation. However, temperature plays an important secondary role. Annual runoff and summer low flows are dominantly controlled by annual precipitation and secondarily controlled by winter temperatures, particularly winter thawing degrees. Winter low flows are dominantly controlled by the preceding summer precipitation and the within-season (i.e. winter) precipitation and secondarily controlled by winter thawing degrees. For both winter and summer, higher precipitation corresponds to shorter, less severe low flow periods. Winter and summer low flows exhibit opposite responses to temperature, with warm winters corresponding to significantly longer, more severe summer low flows and significantly shorter, less severe winter low flows.

6.2. Climate Controls on Snow Drought

Based on multiple linear regression analysis, winter precipitation and winter thawing degrees were identified as the dominant climate controls on peak snow water equivalent (SWE) and thus determined to be the dominant climate controls on snow drought. The definition of the winter season was also important, and a climatologically based definition of winter, using the 25th percentile of mean daily temperature, had a higher predictive ability for peak SWE compared to a strictly calendar based winter season definition (e.g., 1-Oct/1-Nov to 1-Apr). Using winter precipitation and winter thawing degrees, snow drought years, i.e. years with below-normal peak snow water equivalent (SWE), can be classified into three categories based on climatic causes: 1) dry snow drought, caused by below-normal winter precipitation alone, 2) warm snow drought, caused by above-normal winter thawing degrees alone, and 3) warm and dry snow drought, caused by the co-occurrence of above-normal winter temperatures and below-normal winter precipitation. In western North America, warm and dry snow droughts are the most severe type, while warm snow droughts are the least severe. The severity and frequency of warm snow droughts, however, has a non-linear relationship with mean winter (1-Nov to 1-Apr) temperature, and warm snow drought risk is substantially higher for locations with mean winter temperatures above -3°C.

6.3. Snow and Streamflow Drought in the Context of a Warming Climate

Two methods were used to investigate the impacts of climate warming on low flows, streamflow drought, and snow drought. The data-driven (downward) approach (Chapters 2 and 3) combined observed hydroclimatic time series with multiple statistical methods, including bivariate and partial correlation and temporal and spatial analogs. The process-based (upward) approach (Chapters 4 and 5) combined climate change projections and hydrological modelling. These approaches yielded consistent results and provide insight into the impacts of continued climate warming on snowmelt hydrology.

The data-driven approach showed that low flow regimes and warm snow drought risk are strongly controlled by temperature. Thus, continued climate warming will likely lead to a shift in snow drought and low flow regimes, including increased frequency and severity of both warm snow droughts and summer streamflow droughts and decreased frequency and severity of winter streamflow droughts. The process-based approach confirmed these results, and showed that, in response to the projected increases in temperature, warm snow droughts and summer streamflow droughts increase in frequency and severity. Moreover, climate warming and the subsequent shifts in the snow drought regime result in decreased summer groundwater storage and a higher frequency of warm snow drought propagation into summer streamflow drought.

Both approaches showed that the response of snow hydrology to climate warming is non-linear, and catchments with winter temperatures near 0°C exhibit substantially larger impacts from +2°C of warming compared to catchments with winter temperatures far below 0°C. This non-linear response is documented by the data-driven approach in Chapter 3, which showed that, as mean winter (1-Nov to 1-Apr) temperatures increase, warm snow drought risk and peak SWE temperature-sensitivity increase in a non-linear fashion. Critical temperature thresholds exist at -3°C and 1.3°C, and, once crossed, temperature-related decreases in peak SWE can be expected to "accelerate". The non-linear response was further documented by the process-based approach in Chapter 4, which showed that the magnitude of change in the snow drought and low flow regimes is related to the catchment's starting point, i.e. its baseline mean winter (1-Nov to 1-Apr) temperature. Consistent with the data-driven findings of Chapter 3, the process-based approach in Chapter 4 showed that a 2°C increase in mean winter

temperature had a larger impact on the snow drought regime in the headwater catchment with winter temperatures near zero compared to the headwater catchment with winter temperatures far below zero.

6.4. Contributions

The main contributions of this research include the following:

1. *Development and testing of a methodology for the separation of winter low flows from summer low flows in catchments with seasonal snow cover.* Previous studies have used an arbitrary standard "winter" classification based on calendar dates (Ehsanzadeh & Adamowski, 2007; Kormos et al., 2016) or a "drought year" (Douglas et al., 2000) to separate summer low flows from winter low flows. However, these methodologies do not effectively separate low flows generated by different hydrological processes, i.e. high evapotranspiration rates (summer low flows) versus below freezing temperatures (winter low flows). This research is the first to develop a robust methodology to classify low flow regimes and separate summer versus winter low flows based on catchment climatology, allowing for improved understanding of climate controls on summer versus winter low flows.

2. *Quantification of precipitation- versus temperature-sensitivity of summer and winter low flows.* Previous work has documented the role of temperature in streamflow and groundwater droughts (Teuling et al., 2013; Diffenbaugh et al., 2015) and the impact of temperature on snowmelt hydrology (Leith & Whitfield, 1998; Whitfield & Cannon, 2000; Adam et al., 2009; Déry et al., 2009; Pederson et al., 2011; among others); however, the relative impact of precipitation versus temperature on summer and winter low flows remained unclear. This research shows that, while the inter-annual variability of low flows is dominantly controlled by precipitation, temperature, particularly winter temperatures above 0°C, plays an important secondary role.

3. *Development and testing of a methodology for classifying snow drought based on climatic causes.* Harpold et al. (2017) called for the distinction between warm snow drought and dry snow drought but did not account for the co-occurrence of warm and dry winter conditions. No previous studies have tested snow drought classification methodologies at the regional scale, and no previous studies have accounted for the co-occurrence of warm and dry winter conditions. The snow drought classification methodology developed in this study uses winter precipitation and winter thawing degrees to classify years with below-normal peak SWE as dry, warm, or warm and dry snow drought years. The methodology is robust and transferrable to other regions where snow is an important part of the hydrologic cycle.

4. *Development of snow drought risk and susceptibility maps for western North America.* Previous studies have investigated snow sensitivity to climate warming (Nolin & Daly, 2006; Brown & Mote, 2009; Casola et al., 2009; Minder, 2010). However, no studies have completed regional mapping of snow drought risk based on climatic causes, and no previous studies have developed snow drought susceptibility maps. The snow drought susceptibility maps developed in this study are based on temperature-thresholds, above which the relationship between mean winter temperature and peak SWE changes. These susceptibility maps can be easily produced using widely available climate data, and, therefore, this methodology can be transferred to other regions where snow is important for regional water supplies.

5. *Combined analysis of climate change impacts on snow drought, low flows, and streamflow drought.* While previous studies have investigated snow drought and its hydrological impacts (Cooper et al., 2016; Mote et al., 2016; Harpold et al., 2017; Sproles et al., 2017; Hatchett & McEvoy, 2018), no previous studies have explicitly related climate change impacts on snow drought to subsequent impacts on summer low flows and summer streamflow drought. This research completed climate change scenario modelling using generic groundwater-surface water models for four headwater catchments in different ecoregions of British Columbia and explicitly focused on snow drought and its relationship with low flows and summer streamflow drought.

6. *Insight into future surface water quantity versus industrial freshwater demand in the Peace River shale gas region of northeast British Columbia.* Previous research has estimated future shale gas industry freshwater demand in northeast British Columbia (Kniewasser & Horne, 2015) and others (Schnorbus et al., 2014) have completed hydrologic modelling of climate change impacts for a large portion of the Peace River watershed. However, no previous studies have completed a combined analysis of future shale gas industry freshwater demand versus future streamflow quantity. Further, no previous studies have focused on future freshwater supply security in small headwater catchments – the scale at which the shale gas industry sources at least 28% of the water used for hydraulic fracturing.

6.5. Recommendations for Future Research

This research provides important contributions to this field of study; however, further research that may improve, refine, or build upon this work include the following:

- *Non-linear regression methods.* This research employed multiple linear regression analysis to 1) quantify the relative control of precipitation and temperature on the inter-annual variability of winter and summer low flows and annual runoff, and 2) identify the dominant climate controls on peak SWE.

While variables were standardized for all analyses, the relationships between predictor and response variables likely exhibit non-linearities, which were not quantified in this research. Future work could explore the use of non-linear regression methods, such as multivariate adaptive regression splines or generalized non-linear models.

- *Observation-based study of snow drought risk.* The snow drought analysis and susceptibility mapping completed in this research relied entirely on VIC-simulated SWE time series. While the gridded meteorological time series used to force the VIC model were created from observed data, further study using observed snow time series is needed to verify the utility of the snow drought classification methodology developed in this research and to verify the presence of the temperature thresholds that were used for the susceptibility mapping.

- *Temporal trend analysis*. Snow drought, low flow, and streamflow drought regimes have likely already been impacted by climate warming. While many previous studies have completed temporal trend analyses on snow and streamflow metrics, no studies have completed separate trend analyses for different snow and streamflow drought types and few studies have investigated trends in low flows. A combined analysis of trends in snow drought and low flows, using long-term records of observed data and the classification methodologies developed in this research, would provide additional confirmation of the relationships between snow drought, low flows, and climate warming identified in this study.

- *Broader scale analysis of climate change impacts on snow drought regimes.* This research investigated climate change impacts on snow drought regimes for four headwater catchments in British Columbia. Further analysis of climate change impacts on snow drought regimes should be completed. Specifically, a companion study to Chapter 3 using CMIP5 climate change modelling results would be a logical next step in this line of research.

- *Snow drought impacts on seasonal patterns of water balance components.* This research quantified the impact of different snow drought types on winter and summer low flows. However, different snow drought types likely also have different impacts on the seasonal patterns of actual evapotranspiration (AET), soil moisture, groundwater recharge/storage, and streamflow. This further research could be completed using the existing model outputs from the climate change modelling presented in Chapter 4 and would be a useful extension of the snow drought and streamflow drought research theme by providing insight into the relationships between snow drought and soil moisture and groundwater drought. Further, it would help understand the role of temperature on the water balance during snow drought events through the analysis of seasonal patterns in AET.

References

Adam, J.C., Hamlet, A.F., & Lettenmaier, D.P. (2009). Implications of global climate change for snowmelt hydrology in the twenty-first century. *Hydrological Processes*, 23, 962-972. doi:10.1002/hyp.7201

AghaKouchak, A., Chen, L., Mazdiyasni, O., & Farahmand, A. (2014). Global warming and changes in risk of concurrent climate extremes: insights from the 2014 California drought. *Geophysical Research Letters*, 41, 8847-8852. doi:10.1002/2014GL062308

Agriculture and Agri-Food Canada. (2013). *Soil Name and Profile Data – Soils of British Columbia.* Retrieved from Agriculture and Agri-Food Canada website http://sis.agr.gc.ca/cansis/soils/bc/soils.html

Aladenola, O.O. & C.A. Madramootoo. (2014). Evaluation of solar radiation estimation methods for reference evapotranspiration estimation in Canada. *Theoretical and Applied Climatology*, 118(3), 377-385.

Aguado, E., Cayan, D., Riddle, L., & Roos, M. (1992). Climatic fluctuations and the timing of West Coast streamflow. *Journal of Climate*, 5, 1468-1483. doi:10.1029/2005GL023410

Ajami, H., Meixner, T., Dominguez, F., Hogan, J., & Maddock, T. (2012). Seasonalizing mountain system recharge in semi-arid basins – climate change impacts. *Groundwater*, 50, 585-597.

Alexander, M.A., Scott, J.D., Swales, D., Hughes, M., Mahoney, K., & Smith, C.A. (2015). Moisture pathways into the U.S. Intermountain West associated with heavy precipitation events. *Journal of Hydrometeorology*, 16, 1184-1204. doi:10.1175/JHM-D-14-0139.1

Allamano, P., Claps, P., & Laio, F. (2009). Global warming increases flood risk in mountainous areas. *Geophysical Research Letters*, 36, L24404. doi:10.1029/2009GL041395

Allen, R.G., Pereira, L.S., Raes, D., & Smith, M. (1998). Crop Evapotranspiration: Guidelines for computing crop water requirement. FAO Irrigation and Drainage Paper, 56. Rome, Italy: FAO.

Alo, C.A. & Wang, G.L. (2008). Hydrological impact of potential future vegetation response to climate changes projected by 8 GCMs. *Journal of Geophysical Research – Biogeosciences*, 113(G3), G03011. doi:10.1029/2007JG000598

Alwin, D.F. & Hauser, R.M. (1975). The decomposition of effects in path analysis. *American Sociological Review*, 40(1) 37-47. doi:10.2307/2094445

Anderson, M.P., Woessner, W.W., & Hunt, R.J. (2015). *Applied groundwater modeling: simulation of flow and advective transport*. Elsevier Academic Press.

Andreadis, K.M. & Lettenmaier, D.P. (2006). Trends in 20th century drought over the continental United States. *Geophysical Research Letters*, 33(10), L10403. doi:10.1029/2006GL025722

Annandale, J.G., Jovanovic, N.A., Benadé, N., & Allen, R.G. (2001). Software for missing data analysis of Penman-Monteith reference evapotranspiration. *Irrigation Science*, 21, 57-67.

Ashfaq, M., Ghosh, S., Kao, S., Bowling, L.C., Mote, P., Touma, D., et al. (2013). Near-term acceleration of hydroclimatic change in the western U.S. *Journal of Geophysical Research Atmospheres*, 118(19), 10,676-10,693. doi:10.1002/jgrd.50816

Ayers, H.D. (1959). Influence of soil profile and vegetation characteristics on net rainfall supply to runoff. *Proceedings of Hydrology Symposium No. 1: Spillway Design Floods*, NRCC: Ottawa; 198-205.

Bales, R.C., Goulden, M.L., Hunsaker, C.T., Conklin, M.H., Hartsough, P.C., O'Geen, A.T. … Safeeq, M. (2018). Mechanisms controlling the impact of multi-year drought on mountain hydrology. *Scientific Reports*, 8, 690. doi:10.1038/s41598-017-19007-0

Bard, A., Renard, B., Lang, M., Giuntoli, I., Korck, J., Koboltschnig, G., et al. (2015). Trends in the hydrologic regime of Alpine rivers. *Journal of Hydrology*, 529, 1823-1837. doi:10.1016/j.jhydrol.2015.07.052

Barnett, T.P., Adam, J.C., & Lettenmaier, D.P. (2005). Potential impacts of a warming climate on water availability in snow-dominated regions. *Nature*, 438, 303-309. doi:10.1038/nature04141

Barnett, T.P., Pierce, D.W., Hidalgo, H.G., Bonfils, C., Santer, B.D., Das, T., et al. (2008). Human-induced changes in the hydrology of the western United States. *Science*, 319, 1080-1083. doi:10.1126/science.1152538

Barnhart, T.B., Molotch, N.P., Livneh, B., Harpold, A.A., Knowles, J.F., & Schneider, D. (2016). Snowmelt rate dictates streamflow. *Geophysical Research Letters*, 43(15), 8006-8016. doi:10.1002/2016GL069690

Bartos, M.D. & Chester, M.V. (2015). Impacts of climate change on electric power supply in the Western United States. *Nature Climate Change*, 5, 748-752. doi:10.1038/nclimate2648

BCstats. (2017). *Sub-Provincial Population Projections – P.E.O.P.L.E. 2017*. [Table]. Retrieved from http://www.bcstats.gov.bc.ca/apps/PopulationProjections.aspx

Behnke, R., Vavrus, S., Allstadt, A., Albright, T., Thogmartin, W.E., & Radeloff, V.C. (2016). Evaluation of downscaled, gridded climate data for the conterminous United States. *Ecological Applications*, 26(5), 1338-1351. doi:10.1002/15-1061

Beran, M.A. & Rodier, J.A. (1985). Hydrological aspects of drought: a contribution to the International Hydrological Programme. UNESCO-WMO *Studies and Reports in Hydrology*, 39, 149 pp.

Berghuijs, W.R., Woods, R.A., & Hrachowitz, M. (2014). A precipitation shift from snow towards rain leads to a decrease in streamflow. *Nature Climate Change*, 4, 583-586. doi:10.1038/nclimate2246

Beschta, R.L., Bilby, R.E., Brown, G.W., Holtby, L.B., and Hofstra, T.D. (1987). Stream temperature and aquatic habitat: Fisheries and forestry interactions. In E.O. Salo & T.W. Cundy (Eds.), *Streamside Management: Forestry and Fishery Interactions* (pp. 191-232). Washington, Seattle: University of Washington.

Beven, K. (1989). Changing ideas in hydrology – the case of physically based models. *Journal of Hydrology*, 105, 157-172.

Bojanowski, J.S. (2016). Functions for calculating daily solar radiation and evapotranspiration. Version 2.3-3. Retrieved from https://cran.r-project.org/web/packages/sirad/sirad.pdf

Bosch, J.M. & Hewlett, J.D. (1982). A review of catchment experiments to determine the effect of vegetation changes on water yield and evapotranspiration. *Journal of Hydrology*, 55(1-4), 3-23.

Bosson, E., Sabel, U. Gustafsson, I.G., Sassner, M., & Destouni, G. (2012). Influences of shifts in climate, landscape, and permafrost on terrestrial hydrology. *Journal of Geophysical Research: Atmospheres*, 117(5), 1-12. doi:10.1029/2011JD016429

Brewer, R., Cohen, S., Embley, E., Hamilton, S., Julian, M., Kulkarni, T. et al. (2001). Water Management and Climate Change in the Okanagan Basin. S. Cohen & T. Kulkarni (Eds.). Environment Canada & University of British Columbia.

British Columbia. (2013). *British Columbia Freshwater Atlas*. Retrieved from ftp://ftp.geobc.gov.bc.ca/sections/outgoing/bmgs/FWA_Public

British Columbia. (2018). *Water sustainability act*. Retrieved from Government of British Columbia website http://www.bclaws.ca/civix/document/id/complete/statreg/14015

British Columbia Oil and Gas Commission (BCOGC). (2016). *Water Management for Oil and Gas Activity 2015 Annual Report*. Retrieved from https://www.bcogc.ca/node/13261/download.

British Columbia Oil and Gas Commission (BCOGC). (2017). Northeast Water Tool. Accessed December 14, 2017, from https://water.bcogc.ca/newt

Brown, R.D. & Mote, P.W. (2009). The response of northern hemisphere snow cover to a changing climate. *Journal of Climate*, 22, 2124-2145. doi:10.1175/2008JCLI2665.1

Brunt, D. (1932). Notes on radiation in the atmosphere. *Quarterly Journal of the Royal Meteorological Society*, 58, 389-418.

Burn, D.H., Buttle, J.M., Caissie, D., MacCulloch, G., Spense, C., & Stahl, K. (2008). The processes, patterns, and impacts of low flows across Canada. *Canadian Water Resources Journal*, 33(2), 107-124.

Cannon, A.J. (2015). Selecting GCM scenarios that span the range of changes in a multimodel ensemble: application to CMIP5 climate extremes indices. *Journal of Climate*, 28(3), 1260-1267.

Cannon, A.J. (2005). Defining climatological seasons using radially constrained clustering. *Geophysical Research Letters*, 32, L14706. doi:10.1029/2005GL023410

Carsel, R.F. & Parrish, R.S. (1988). Developing joint probability distributions of soil water retention characteristics. *Water Resources Research*, 24(5), 755-769. doi: 10.1029WR024i005p00755

Casola, J.H., Cuo, L., Livneh, B., Lettenmaier, D.P., Stoelinga, M.T., Mote, P.W., & Wallace, J.M. (2009). Assessing the impacts of global warming on snowpack in the Washington Cascades. *Journal of Climate*, 22, 2758-2772.

Chang, H. & Bonnette, M.R. (2016). Climate change and water-related ecosystem services: impacts of drought in California, USA. *Ecosystem Health and Sustainability*, 2(12), e01254. doi:10.100s/ehs2.1254

Changnon, S.A. (1980). Removing the confusion over droughts and floods – The interface between scientists and policy makers. *Water International, 1*(10), 10-18.

Chapman, A., Kerr, B., & Wilford, D. (2012). Hydrological modelling and decision-support tool development for water allocation, Northeastern British Columbia. In *Geoscience BC Summary of Activities 2011*, Geoscience BC, Report 2012-1, 81-86.

Charron, D.F., Thomas, M.K., Waltner-Toews, D., Aramini, J.J., Edge, T., Kent, R.A. … Wilson, J. (2004). Vulnerability of waterborne diseases to climate change in Canada: A review. *Journal of Toxicology and Environmental Health, Part A*, 67(20-22), 1667-1677. doi:10.1080/15287390490492313

Chow, V.T. (1959). *Open-channel hydraulics*. New York, NY: McGraw-Hill, Inc.

Clark, C. (1945). Storage and the unit hydrograph. *Transactions of the American Society of Engineers*, 110(1), 1419-1446.

Cline, D.W. (1997). Snow surface energy exchanges and snowmelt at a continental, midlatitude Alpine site. *Water Resources Research*, 33(4), 689-701. doi:10.1029/97WR00026

Clyde, G.D. (1931). Snow-melting characteristics. *Utah Agricultural Experiment Bulletin*, 231, 1-23.

Commission for Environmental Cooperation. (2011). *North American Terrestrial Ecoregions—Level III*. Montreal, Canada: Commission for Environmental Cooperation.

Cook, E.R., Woodhouse, C.A, Eakin, C.M., Meko, D.F., & Stahle, D.W. (2004). Long-term aridity changes in the western United States. *Science*, 5(5698), 1015-1018. doi:10.1126/science.1102586

Cooper, M.G., Nolin, A.W., & Safeeq, M. (2016). Testing the recent snow drought as an analog for climate warming sensitivity of Cascades snowpacks. *Environmental Research Letters*, 11, 084009. doi:10.1088/1748-9326/aa/8/084009

Córdova, M., Carrillo-Rojas, G., Crespo, P., Wilcox, B., & Célleri, R. (2015). Evaluation of the Penman-Monteith (FAO 56 PM) method for calculating reference evapotranspiration using limited data. *Mountain Research and Development*, 35(3), 230-239. doi:10.1659/MRD-JOURNAL-D-14-0024.1

Corps of Engineers. (1956). Summary report of the snow investigations, snow hydrology. Portland, Oregon: US Army Engineer Division.

Criss, R.E. & Winston, W.E. (2008). Do Nash values have value? Discussion and alternate proposals. *Hydrologic Processes*, 22, 2723-2725. doi:10.1002/hyp.7072

Curt, T., Lucot, E., & Bouchaud, M. (2001). Douglas-fir root biomass and rooting profile in relation to soils in a mid-elevation area (Beaujolais Mounts, France). *Plant and Soil*, 233(1), 109-125.

Dai, A. (2011). Drought under global warming: A review. *Wiley Interdisciplinary Reviews: Climate Change*, *2*(1), 45-65. doi:10.1002/wcc.81

Dai, A.G. (2013). Increasing drought under global warming in observations and models. *Nature Climate Change*, *3*(1), 52-58. http://doi.org/10.1038/nclimate1633

Danish Hydraulic Institute (DHI). (2007). MIKE SHE User Manual: Reference Guide, vol. 2. Denmark: Danish Hydraulic Institute.

DataBC. (2013). *Baseline thematic mapping present land use version 1 spatial layer*. Retrieved from https://apps.gov.bc.ca/pub/geometadata/metadataDetail.do?recordUID=43171&recordSet=ISO19115.

Déry, S.J., Stahl, K., Moore, R.D., Whitfield, P.H., Menounos, B., & Burford, J.E. (2009). Detection of runoff timing changes in pluvial, nival, and glacial rivers of western Canada. *Water Resources Research*, 45, W04426. doi:10.1029/2008WR006975

DHI Water and Environment. (2010). *Okanagan Basin water accounting model. Final Report*. Retrieved from https://www.obwb.ca/obwrid/docs/338_2010_OBWAM%20Final%20Report.pdf

Dierauer, J.R. & Whitfield, P.H. (2016). FlowScreen: Daily streamflow trend and change point screening (version 1.3), R Foundation for Statistical Computing, Vienna, Austria. Available at https://CRAN.R-project.org/package=FlowScreen.

Dierauer, J.R., Whitfield, P.H., & Allen, D.M. (in review-a). Climate controls on runoff and low flows in mountain catchments of western North America. *Water Resources Research*.

Dierauer, J.R., Allen, D.M., & Whitfield, P.H. (in review-b). Winter temperature controls on snow drought risk in western North America. *Water Resources Research*.

Dierauer, J.R., Whitfield, P.H., & Allen, D.M. (2017). Assessing the suitability of hydrometric data for trend analysis: The FlowScreen package for R. *Canadian Water Resources Journal*, 42(3), 269-275. doi:10.1080/07011784.2017.1290553

Diffenbaugh, N.S., Swain, D.L., & Touma, D. (2015). Anthropogenic warming has increased drought risk in California. *Proceedings of the National Academy of Sciences*, 112(13), 3931-3936.

Dittmer, K. (2013). Changing streamflow on Columbia basin tribal lands – climate change and salmon. *Climatic Change*, 120(3), 627-641.

Douglas, E.M., Vogel, R.M., & Kroll, C.N. (2000). Trends in low flows in the United States: impact of spatial correlation. *Journal of Hydrology*, 240, 90-105.

Dracup, J.A., Lee, K.S., Paulson, E.G. (1980). On the definition of droughts. *Water Resources Research*, 16(2), 297-302.

Earman, S., Campbell, A.R., Phillips, F.M., Newman, B.D. (2006). Isotopic exchange between snow and atmospheric water vapor: estimation of the snowmelt component of groundwater recharge in the southwestern United States. *Journal of Geophysical Research-Atmospheres*, 111(D9), D09302.

Eaton, J.G. & Scheller, R.M. (1996). Effects of climate warming on fish thermal habitat in streams of the United States. *Limnology and Oceanography*, 41(5) 1109-1115. doi:10.4319/lo.1996.41.5.1109

Eckhardt, K. & Ulbrich, U. (2003). Potential impacts of climate change on groundwater recharge and streamflow in a central European low mountain range. *Journal of Hydrology*, 284(2-4), 244-252. doi:10.1016/j.jhydrol.2003.08.005

Ehsanzadeh, E. & Adamowski, K. (2007). Detection of trends in low flows across Canada. *Canadian Water Resources Journal*, 32(4), 251-264. doi:10.4296/cwrj3204251

Ellis, C., Pomeroy, J., Brown, T., & MacDonald, J. (2010). Simulation of snow accumulation and melt in needleleaf forest environments. *Hydrology and Earth System Sciences*, 14(6): 925-940.

Ellis, C., Pomeroy, J., & Link, T. (2013). Modeling increases in snowmelt yield and desynchronization resulting from forest gap-thinning treatments in a northern mountain headwater basin. *Water Resources Research*, 49(2), 936-949.

Emergency Events Database (EM-DAT). (2016). *Disasters in numbers.* [Table]. Retrieved from www.emdat.be/

Environment and Climate Change Canada. (2018). *1971-2000 Climate Normals & Averages*. [Table]. Retrieved from http://climate.weather.gc.ca/climate_normals/index_e.html

European Environment Agency (EEA). (2012). Urban adaptation to climate change in Europe, Challenges and opportunities for cities together with supportive national and European policies. Report No 2/2012. Copenhagen, Denmark: EEA.

Fang, X. & Pomeroy, J.W. (2007). Snowmelt runoff sensitivity analysis to drought on the Canadian prairies. *Hydrological Processes*, 21, 2594-2609.

Feng, X., Sahoo, A., Arsenault, K., Houser, P., Luo, Y., & Troy, T.J. (2008). The impact of snow model complexity at three CLPX sites. *Journal of Hydrometeorology*, 9, 1464-1481. doi:10.1175/2008JHM860.1

Feyen, L. & Dankers, R. (2009). Impact of global warming on streamflow drought in Europe. *Journal of Geophysical Research: Atmospheres*, 114(17), 1-17. doi:10.1029/2008JD011438

Ficke, A.D., Myrick, C.A., Hansen, L.J. (2007). Potential impacts of global climate change on freshwater fisheries. *Reviews in Fish Biology and Fisheries*, 17(4), 581-613.

Fleig, A.K., Tallaksen, L.M., Hisdal, H., & Demuth, S., (2006). A global evaluation of streamflow drought characteristics. *Hydrology and Earth System Sciences*, 10(4), 535-552. doi:10.5194/hess-10-535-2006.

Fleming, S.W., Whitfield, P.H., Moore, R.D., & Quilty, E.J. (2007). Regime-dependent streamflow sensitivities to pacific climate modes cross the Georgia-Puget transboundary region. *Hydrological Processes*, 21, 3264-4287. doi:10.1002/hyp.6544

Foster, S.B. & Allen, D.M. (2015). Groundwater-surface water interactions in a mountain-to-coast watershed: effects of climate change and human stressors. *Advances in Meteorology*, 2015. doi:20.1155/2015/861805

Freeze, R.A., & Harlan, R.L. (1969). Blueprint for a physically-based, digitally-simulated hydrologic response model. *Journal of Hydrology*, 9, 237-258. doi:10.1016/0022-1694(69)90020-1

Fu, G., Charles, S.P., & Chiew, F.H.S. (2007). A two-parameter climate elasticity of streamflow index to assess climate change effects on annual streamflow. *Water Resources Research*, 43, W11419. doi:10.1029/2007WR005890.

Garcia-Herrera, R., Daz, J., Trigo, R.M., Luterbacher, J., & Fischer, E.M., (2010). A review of the European summer heat wave of 2003. *Critical Reviews in Environmental Science and Technology*, 40(4), 267-306.

Garnier, B. & Ohmura, A. (1970). The evaluation of surface variations in solar radiation income. *Solar Energy*, 13(1), 21-34.

Goderniaux, P., Brouyère, S., Fowler, H. J., Blenkinsop, S., Therrien, R., Orban, P., & Dassargues, A. (2009). Large scale surface-subsurface hydrological model to assess climate change impacts on groundwater reserves. *Journal of Hydrology*, 373(1-2), 122-138. doi:10.1016/j.jhydrol.2009.04.017

Godsey, S.E., Kirchner, J.W., & Tague, C.L. (2014). Effects of changes in winter snowpacks on summer low flows: Case studies in the Sierra Nevada, California, USA. *Hydrological Processes*, 28, 5048-5064. doi:10.1002/hyp.9943

Golmohammadi, G., Prasher, S., Madani, A., & Rudra, R. (2014). Evaluating three hydrological distributed watershed models: MIKE-SHE, APEX, SWAT. *Hydrology*, 1(1), 20-39. doi:10.3390/hydrology1010020

Gong, L., Xu, C., Chen, D., Halldin, S., & Chen, Y.D. (2006). Sensitivity of the Penman-Monteith reference evapotranspiration to key climatic variables in the Changjiang (Yangtze River) basin. *Journal of Hydrology*, 329(3-4), 620-629. doi:10.1016/j.jhydrol.2006.03.027

Gonsamo, A. & Chen, J.M. (2014). Improved LAI algorithm implementation to MODIS data by incorporating background, topography, and foliage clumping information. *IEEE Transactions on Geoscience and Remote Sensing*, 52, 1076-1088.

Google Earth 7.1.8.3036 (32-bit). July 11, 2014. Blueberry River watershed, British Columbia, Canada. 56.96°N, 121.89°W, http://www.google.com/earth/index.html, Accessed March 13, 2017.

Google Earth 7.1.8.3036 (32-bit). December 30, 2015. Graham River watershed, British Columbia, Canada. 56.42°N, 122.51°W, http://www.google.com/earth/index.html, Accessed March 13, 2017.

Goulden, M.L. & Bales, R.C. (2014). Mountain runoff vulnerability to increased evapotranspiration with vegetation expansion. *Proceedings of the National Academy of Sciences*, 111(39), 14071-14075.

Gray, D.M. & Landine, P.G. (1988). An energy-budget snowmelt model for the Canadian Prairies. *Canadian Journal of Earth Sciences*, 25(8): 1292-1303.

Gray, D., Toth, B. Zhao, L., Pomeroy, J. & Granger, R. (2001). Estimating areal snowmelt infiltration into frozen soils. *Hydrological Processes*, 15(16): 3095-3111.

Grayson, R.B., Moore, I.D., & McMahon, T.A. (1992). Physically based hydrologic modeling, 2. Is the concept realistic? *Water Resources Research*, 26(10), 2659-2666.

Groisman, P.Y., Knight, R.W., Karl, T.R., Easterling, D.R., Sun, B., & Lawrimore, J.H. (2004). Contemporary changes of the hydrological cycle over the contiguous United States: Trends derived from in situ observations. *Journal of Hydrometeorology*, 5, 64-85.

Hagemann, S., Chen, C., Clark, D.B., Folwell, S., Gosling, S.N., Haddeland, I., et al. (2013). Climate change impact on available water resources obtained using multiple global climate and hydrology models. *Earth System Dynamics*, 4(1), 129-144. doi:10.5194/esd-4-129-2013

Hagenstad, M., Burakowski, E., & Hill, R. (2018). The economic contributions of winter sports in a changing climate. Prepared for Protect Our Winters (POW) and Recreational Equipment, Inc. (REI) Co-op. Retrieved from https://protectourwinters.org/download/5778/?uid=e5ec966af9

Hamilton, A.S. (2008). Sources of uncertainty in Canadian low flow hydrometric data. *Canadian Water Resources Journal*, 33(2), 125-136.

Hamlet, A.F., Mote, P.W., Clark, M.P., & Lettenmaier, D.P. (2005). Effects of temperature and precipitation variability on snowpack trends in the western United States. *Journal of Climate*, 18(21), 4545–4561. doi:10.1175/JCLI3538.1

Harder, P. & Pomeroy, J. (2013). Estimating precipitation phase using a psychrometric energy balance method. *Hydrological Processes*, 27(13), 1901-1914. doi:10.1002/hyp.9799

Harding, R.J. & Pomeroy, J.W. (1996). The energy balance of the winter boreal landscape. *Journal of Climate*, 9, 2778-2787.

Hargreaves, G.H. & Samani, Z.A. (1985). Reference crop evapotranspiration from temperature. *Applied Engineering in Agriculture*. 1(2): 96-99.

Harma, K.J., Johnson, M.S. & Cohen, S.J. (2012). Future water supply and demand in the Okanagan Basin, British Columbia: a scenario-based analysis of multiple, interacting stressors. *Water Resources Management*, 26, 667-689. doi:10.1007/s11269-011-9938-3

Harpold, A.A. (2016). Diverging sensitivity of soil water stress to changing snowmelt timing in the western US. *Advances in Water Resources*, 92, 116-129. doi:10.1016/j.advwatres.2016.03.017

Harpold, A.A. & Kohler, M. (2017). Potential for changing extreme snowmelt and rainfall events in the mountains of western United States. *Journal of Geophysical Research: Atmospheres*, 122, 13,219-13,228. doi:10.1002/2017JD027704

Harpold, A., Brooks, P., Rajagopal, S., Heidbuchel, I., Jardine, A., & Stielstra, C. (2012). Changes in snowpack accumulation and ablation in the intermountain west. *Water Resources Research*, 48, W11501. doi:10.1029/2012WR011949

Harpold, A.A., Dettinger, M., & Rajagopal, S. (2017). Defining snow drought and why it matters. *Eos, Transactions, American Geophysical Union*, 98. doi:10.1029/2017EO068775

Hatchett, B.J. & McEvoy, D.J. (2018). Exploring the origins of snow drought in the northern Sierra Nevada, California. *Earth Interactions*, 22. doi:10.1175/EI-D-17-0027.1

Hewlett, J.D. & Troendle, C.A. (1975). Non-point and diffuse water sources: A variable source area problem. *In Proceedings of the Watershed Management Symposium*, ISBN 0-939970-88-0, Logan, UT, August 1975, pp. 21-46.

Hirabayashi, Y., Kanae, S., Emori, S., Oki, T., & Kimoto, M. (2008). Global projections of changing risks of floods and droughts in a changing climate. *Hydrological Sciences Journal*, 53(4), 754–772. doi:10.1623/hysj.53.4.754

Hisdal, H., Stahl, K., Tallaksen, L. M., & Demuth, S. (2001). Have streamflow droughts in Europe become more severe or frequent? *International Journal of Climatology*, 21(3), 317-333. doi:10.1002/joc.619

Hock, R. (2003). Temperature index melt modelling in mountain areas. *Journal of Hydrology*, 282, 104-115. doi:10.1016/S0022-1694(03)00257-9

Hockey, J.B., Owens, I.F., & Tapper, N.J. (1982). Empirical and theoretical models to isolate the effect of discharge on summer water temperatures in the Hurunui River. *Journal of Hydrology (New Zealand)*, 21(1), 1-12.

Howat, I.M. & Tulaczyk, S. (2005). Climate sensitivity of spring snowpack in the Sierra Nevada. *Journal of Geophysical Research*, 110, F04021. doi:10.1029/2005JF000356

Howitt, R., MacEwan, D., Medellín-Azuara, J., Lund, J., & Sumner, D. (2015). Economic analysis of the 2015 drought for California agriculture. UC Davis Center for Watershed Science, Davis, California. Retrieved from https://watershed.ucdavis.edu/files/biblio/Final_Drought%20Report_08182015_Full_Report_WithAppendices.pdf

Hsiang, S.M., Burke, M., & Miguel, E. (2013). Quantifying the influence of climate on human conflict, *Science*, 341, 1235367. doi:10.1126/science.1235367.

Hu, J., Moore, D.J.P, Burns, S.P., & Monson, R.K. (2010). Longer growing seasons lead to less carbon sequestration by a subalpine forest. *Global Change Biology*, 16, 771-783. doi:10.1111/j.1365-2486.2009.01967.x

HydroGeoLogic Inc. (2006). MODHMS: a comprehensive MODFLOW based hydrologic modeling system, Version 3.0. Code documentation and user's guide, HydroGeoLogic Inc. Herndon, VA.

Intergovernmental Panel on Climate Change (IPCC). (2013). Climate Change 2013: The Physical Science Basis. Contribution of Working Group I to the Fifth Assessment Report of the Intergovernmental Panel on Climate Change [Stocker, T.F., D. Qin, G.-K. Plattner, M. Tignor, S.K. Allen, J. Boschung, A. Nauels, Y. Xia, V. Bex and P.M. Midgley (eds.)]. Cambridge University Press, Cambridge, United Kingdom and New York, NY, USA, 1535 pp.

Jenicek, M., Seibert, J., Zappa, M., Staudinger, M. & Jonas, J. (2016). Importance of maximum snow accumulation for summer low flows in humid catchments. *Hydrology and Earth System Sciences*, 20, 859-874. doi:10.5194/hess-20-859-2016

Jones, J. P., Sudicky, E. A., & McLaren, R. G. (2008). Application of a fully-integrated surface-subsurface flow model at the watershed-scale: A case study. *Water Resources Research*, 44(3), 1-13. doi:10.1029/2006WR005603

Jyrkama, M.I. & Sykes, J.F. (2007). The impact of climate change on spatially varying groundwater recharge in the grand river watershed (Ontario). *Journal of Hydrology*, 338(3-4), 237-250. doi:10.1016/j.jhydrol.2007.02.036

Kapnick, S. & Hall, A. (2012). Causes of recent changes in western North American snowpack. *Climate Dynamics*, 38(9-10), 1885-1899. doi:10.1007/s00382-011-1089-y

Klemes, V. (1985). Sensitivity of water-resource systems to climate variations. WCP Report No. 98. Geneva, Switzerland: World Meteorological Organization.

Kniewasser, M. & Horne, M. (2015). B.C. Shale Scenario Tool Technical Report. Prepared for Pembina Institute, pp. 30. Retrieved from http://www.pembina.org/reports/pembina-bc-shale-scenario-tool-technical-report-20150618.pdf

Kollet, S.J., & Maxwell, R.M. (2006). Integrated surface–groundwater flow modeling: A free-surface overland flow boundary condition in a parallel groundwater flow model. *Advances in Water Resources*, 29(7), 945–958. http://doi.org/10.1016/j.advwatres.2005.08.006

Kormos, P.R., Luce, C.H., Wenger, S.J., & Berghuijs, W.R. (2016). Trends and sensitivities of low streamflow extremes to discharge timing and magnitude in Pacific Northwest mountain streams. *Water Resources Research*, 52, 4990-5007. doi:10.1002/2015WR018125

Koutsoyiannis, D. & Montanari, A. (2007). Statistical analysis of hydroclimatic time series: Uncertainty and insights. *Water Resources Research*, 43(5), 1–9. http://doi.org/10.1029/2006WR005592

Kovalevskii, V.S. (2007). Effects of climate changes on groundwater. *Water Resources*, 34(2), 140-152. doi:10.1134/S0097807807020042

Kozak, M. & Kang, M. (2006). Note on modern path analysis in application to crop science. *Communications in Biometry and Crop Science*, 1(1), 32-34.

Kristensen, K.J. & Jensen, S.E. (1975). A model for estimating actual evapotranspiration from potential evapotranspiration. *Hydrology Research*, 6(3), 170-188.

Laaha, G. & Blöschl, G. (2006). Seasonality indices for regionalizing low flows. *Hydrological Processes*, 20, 3851-3878. doi:10.1002/hyp.6161

Lake, P.S. (2003). Ecological effects of perturbation by drought in flowing waters. *Freshwater Biology*, 48, 1161-1172. doi:10.1046/j.1365-2427.2003.01086.x

Laternser, M. & Schneebeli, M. (2003). Long-term snow climate trends of the Swiss Alps (1931-99). *International Journal of Climatology*, 23(7), 733–750. http://doi.org/10.1002/joc.912

Leith, R.M.M. & Whitfield, P.H. (1998). Evidence of climate change effects on hydrology of streams in south-central BC. *Canadian Water Resources Journal*, 23(3), 219-230. doi:10.4296/cwrj2303219

Letts, M.G., Roulet, N.T., Comer, N.T., Skarupa, M.R., & Verseghy, D.L. (2000). Parameterization of peatland hydraulic properties for the Canadian land surface scheme. *Atmosphere-Ocean*, 38(1), 141-160. doi:10.1080/07055900.2000.9649643

Leng, G., Tang, Q., & Rayburg, S. (2015). Climate change impacts on meteorological, agricultural and hydrological droughts in China. *Global and Planetary Change*, 126(0), 23-34. doi:10.1016/j.gloplacha.2015.01.003

Li, Q., Unger, A. J. A., Sudicky, E. A., Kassenaar, D., Wexler, E. J., & Shikaze, S. (2008). Simulating the multi-seasonal response of a large-scale watershed with a 3D physically-based hydrologic model. *Journal of Hydrology*, 357(3-4), 317-336. doi:10.1016/j.jhydrol.2008.05.024

Li, D., Wrzesien, M.L., Durand, M., Adam, J., & Lettenmaier, D.P. (2017). How much runoff originates as snow in the western United States, and how will that change in the future? *Geophysical Research Letters*, 44, 6163-6172. doi:10.1002/2017GL073551

Liang, X., Lettenmaier, D.P., Wood, E.F., & Burges, S.J. (1994). A simple hydrologically based model of land surface water and energy fluxes for general circulation models. *Journal of Geophysical Research*, 99 (D7), 14415-14428. doi:10.1029/94JD00483

Liu, T., Willems, P., Pan, X.L., Bao, A.M., Chen, X, Veroustraete, F., & Dong, Q.H. (2011). Climate change impact on water resource extremes in a headwater region of the Tarim basin in China. *Hydrology and Earth System Sciences Discussions*, 8, 6593-6637. doi:10.5194/hessd-8-6593-2011

Livneh, B., Bohn, T.J., Pierce, D.W., Munoz-Arriola, F., Nijssen, B., Vose, R., et al. (2015). A spatially comprehensive, hydrometeorological data set for Mexico, the U.S., and Southern Canada 1950-2013. *Scientific Data*, 2, 150042. doi:10.1038/sdata.2015.42

Livneh, B., Rosenberg, E.A., Lin, C., Nijssen, B., Mishra, M., Andreadis, K.M., et al. (2013). A long-term hydrologically based dataset of land surface fluxes and states for the conterminous United States: Update and extensions. *Journal of Climate*, 26, 9384-9392.

Luce, C.H. & Holden, Z.A. (2009). Declining annual streamflow distributions in the Pacific Northwest United States, 1948-2006. *Geophysical Research Letters*, 36, L16401. doi:10.1029/2009GL039407

Luce, C.H., Lopez-Burgos, V., & Holden, Z. (2014). Sensitivity of snowpack storage to precipitation and temperature using spatial and temporal analog models. *Water Resources Research*, 50, 9447-9462. doi:10.1002/2013WR014844

Ludlum, D.M. (1978). The snowfall season of 1976. *Weatherwise*, 31, 20-23.

Male, D.H. & Granger, R.J. (1981). Snow surface energy exchange. *Water Resources Research*, 17(2), 609-627. doi:10.1029/WR017i003p00609

Maliva, R. & Missimer, T. (2012). *Arid Lands Water Evaluation and Management*. Berlin: Springer-Verlag.

Mann, H.B. & Whitney, D.R. (1947). On a test of whether one of two random variables is stochastically larger than the other. *Annals of Mathematical Statistics*, 18(1), 5-60.

Marks, D., Domingo, J., Susong, D., Link, T., & Green, D. (1999). A spatially distributed energy balance snowmelt model for application in mountain basins. *Hydrological Processes*, 13, 1935-1959.

Mattison, J.S. (2017). *Dugouts: Report on managing dugouts in northeastern British Columbia*. Prepared for Ministry of Forests Lands and Natural Resource Operations. Retrieved from https://www2.gov.bc.ca/assets/gov/environment/air-land-water/water/dam-safety/dugouts_mattison_july_final.pdf

Maurer, E.P., Wood, A.W., Adam, J.C., Lettenmaier, D.P, & Nijssen, B. (2002). A hydrologically-based data set of land surface fluxes and states for the conterminous United States. *Journal of Climate*, 15, 3237-3251.

McGee, D., Boon, S., & van Meerveld H.J. (2012). Impacts of rural water diversions on prairie streamflow. *Canadian Water Resources Journal*, 37(4), 415-424. doi:10.4269/cwrj2012-911

McKenney, M.S. & Rosenberg, N.J. (1993). Sensitivity of some potential evapotranspiration estimation methods to climate change. *Agricultural and Forest Meteorology*, 64, 81-110.

Meixner, T., Manning, A.H., Stonestrom, D.A., Allen, D.M., Ajami, H., Blash, K.W., et al. (2016). Implications of projected climate change for groundwater recharge in the western United States. *Journal of Hydrology*, 534, 124-138. doi:10.1016/j.jhydrol.2015.12.027

Merz, B., Vorogushyn, S., Uhlemann, S., Delgado, J., & Hundecha, Y. (2012). More efforts and scientific rigour are needed to attribute trends in flood time series. *Hydrology and Earth System Sciences*, 16(5), 1379-1387. doi:10.5194/hess-16-1379-2012

Metro Vancouver. (2011). *Metro Vancouver drinking water management plan*. Retrieved from http://www.metrovancouver.org/services/water/WaterPublications/DWMP-2011.pdf

Metro Vancouver. (2015, September 9). *Metro Vancouver returns to stage two water restrictions* [Press release]. Retrieved from http://www.metrovancouver.org/media-room/media-releases/water/419/Metro%20Vancouver%20Returns%20to%20Stage%20Two%20Water%20Restrictions

Metro Vancouver. (2017). *Watersheds & Reservoirs*. Retrieved from http://www.metrovancouver.org/services/water/sources-supply/watersheds-reservoirs/Pages/default.aspx

Minder, J.R. (2010). The sensitivity of mountain snowpack accumulation to climate warming. *Journal of Climate*, 23, 2634-2650. doi:10.1175/2009JCLI3263.1

Mishra, A.K. & Singh, V.P. (2010). A review of drought concepts. *Journal of Hydrology*, 391(1-2), 202-216. doi:10.1016/j.jhydrol.2010.07.012

Moore, R.D., Hamilton, A.S., & Scibek, J. (2002). Winter streamflow variability, Yukon Territory, Canada. *Hydrological Processes*, 16, 763-778.

Moore, R.D., Nelitz, M., & Parkinson, E. (2013). Empirical modelling of maximum weekly average stream temperature in British Columbia, Canada, to support assessment of fish habitat suitability. *Canadian Water Resources Journal*, 38(2), 135-147.

Morán-Tejeda, E., López-Moreno, J.I., & Beniston, M. (2013). The changing roles of temperature and precipitation on snowpack variability in Switzerland as a function of altitude. *Geophysical Research Letters*, 40, 2131-2136. doi:10.1002/grl.50463

Morris, D.A. & Johnson, A.I. (1967). Summary of hydrologic and physical properties of rock and soil materials as analyzed by the Hydrologic Laboratory of the U.S. Geological Survey, U.S. Geological Survey Water-Supply Paper 1839-D, 42p.

Mosley, L.M. (2015). Drought impacts on the water quality of freshwater systems; review and integration. *Earth-Science Reviews*, 140, 203-214. doi:10.1016/j.earscirev.2014.11.010

Mote, P.W. (2003). Trends in snow water equivalent in the Pacific Northwest and their climatic causes. *Geophysical Research Letters*, 30, 1601. doi:10.1029/2003GL017258

Mote, P.W. (2006). Climate-driven variability and trends in mountain snowpack in western North America. *Journal of Climate*, 19, 6209-6220. doi:10.1175/JCLI3971.1

Mote, P.W., Hamlet, A.F., Clark, M.P., & Lettenmaier, D.P. (2005). Declining mountain snowpack in western North America. *Bulletin of the American Meteorological Society*, 86, 1-39. doi:10.1175/BAMS-86-1-39

Mote, P.W., Li, S., Lettenmaier, D.P., Xiao, M., & Engel, R. (2018). Dramatic declines in snowpack in the western US. *Climate and Atmospheric Science*, 1, 1-6. doi:10.1038/s41612-018-0012-1

Mote, P.W., Rupp, D.E., Li, S., Sharp, D.J., Otto, F., Uhe, P.F., et al. (2016). Perspectives on the causes of exceptionally low 2015 snowpack in the western United States. *Geophysical Research Letters*, 43(20), 10,980-10,988. doi:10.1002/2016GL069965

Muggeo, V.M.R. (2008). Segmented: An R package to fit regression models with broken-line relationships. *R News*, 8(1), 20-25.

Musselman, K.N., Clark, M.P., Liu, C.L., Ikeda, K., & Rasmussen, R. (2017). Slower snowmelt in a warmer world. *Nature Climate Change*, 7, 214-220. doi:10.1038/NCLIMATE3225

Nash, L.L. & Gleick, P.H. (1991). Sensitivity of streamflow in the Colorado Basin to climatic changes. *Journal of Hydrology*, 125, 221-241.

Natural Resources Canada. (2017). 0.75 arcsecond Canada Digital Elevation Model. Edition 1.1. Sherbrooke, Quebec, Canada: Government of Canada, Natural Resources Canada, Map Information Branch. Retrieved from http://maps.canada.ca/czs/index-en.html

Neale, T., Carmicheael, J., & Cohen, S. (2007). Urban water futures: a multivariate analysis of population growth and climate change impacts on urban water demand in the Okanagan Basin, BC. *Canadian Water Resources Journal*, 32(4), 315-330.

Neilsen, D., Smith, C.A.S., Frank, G., Koch, W., Alila, Y., Merritt, W.S., et al. (2006). Potential impacts of climate change on water availability for crops in the Okanagan Basin, British Columbia. *Canadian Journal of Soil Science*, 86(5), 921-936. doi:10.4141/S05-113

Ng, H.Y.F. & Marsalek, J. (1992). Sensitivity of streamflow simulation to changes in climatic inputs. *Hydrology Research*, 23(4), 257-272.

Nolin, A.W. & Daly, C. (2006). Mapping “at risk” snow in the Pacific Northwest. *Journal of Hydrometeorology*, 7, 1164-1171. doi:10.1175/JHM543.1

Novotny, E.V. & Stefan, H.G. (2007). Stream flow in Minnesota: Indicator of climate change. *Journal of Hydrology*, 334(3-4), 319-333.

Okanagan Water Stewardship Council. (2008). *Okanagan sustainable water strategy: action plan 1.0*. Retrieved from https://www2.gov.bc.ca/assets/gov/farming-natural-resources-and-industry/agriculture-and-seafood/agricultural-land-and-environment/water/okanagan_sustainable_water_strategy_osws_action_plan.pdf

Pacific Climate Impacts Consortium (PCIC). (2014). *Statistically Downscaled Climate Scenarios*. [Table]. Retrieved from http://tools.pacificclimate.org/dataportal/downscaled_gcms/map/ September 2016.

Palmer, W.C. (1965). United States Department of Commerce. *Meteorological Drought*. (Research Paper No. 45). Washington, D.C.: U.S. Government Printing Office.

Partington, D., Brunner, P., Simmons, C.T., Therrien, R., Werner, A.D., Dandy, G.C., & Maier, H.R. (2011). A hydraulic mixing-cell method to quantify the groundwater component of streamflow within spatially distributed fully integrated surface water-groundwater flow models. *Environmental Modelling and Software*, 26(7), 886–898. doi:10.1016/j.envsoft.2011.02.007

Pederson, G.T., Gray, S.T., Ault, T., Marsh, W., Fagre, D.B., Bunn, A.G., et al. (2011). Climate controls on snowmelt hydrology of the Northern Rocky Mountains. *Journal of Climate*, 24, 1666-1687. doi:10.1175/2010JCLI3729.1

Peters, E., Torfs, P.J.J.F., van Lanen, H.A.J., & Bier, G. (2003). Propagation of drought through groundwater – a new approach using linear reservoir theory. *Hydrological Processes*, 17(15), 3023-3040. doi:10.1002/hyp.1274

Peters, E., Bier, G., van Lanen, H. a J., & Torfs, P. J. J. F. (2006). Propagation and spatial distribution of drought in a groundwater catchment. *Journal of Hydrology*, 321(1-4), 257-275. doi:10.1016/j.jhydrol.2005.08.004

Pomeroy, J., Fang, X. & Ellis, C. (2012). Sensitivity of snowmelt hydrology in Marmot Creek, Alberta, to forest cover disturbance. *Hydrological Processes*, 26, 1891-1904.

Pomeroy, J.W., Gray, D.M., Brown, T., Hedstrom, N.R., Quinton, W.L., Granger, R.J. & Carey, S.K. (2007). The Cold Regions Hydrological Model: a platform for basin process representation and model structure on physical evidence. *Hydrological Processes*, 21, 2650-2667.

Pomeroy, J.W., Gray, D.M., Shook, K.R., Toth, B., Essery, R.L.H., Pietroniro, A., & Hedstrom, N. (1998). An evaluation of snow accumulation and ablation processes for land surface modelling. *Hydrological Processes*, 12, 2339-2367.

Pomeroy, J. & Li, L. (2000). Prairie and Arctic areal snow cover mass balance using a blowing snow model. *Journal of Geophysical Research*, 105(D21), 26619-26634.

Pomeroy, J.W., Shook, K., Fang, X., Brown, T., & Marsh, C. (2013). *Development of a Snowmelt Runoff Model for the Lower Smoky River, Centre for Hydrology Report No. 13*. Saskatoon, Saskatchewan: Centre for Hydrology, University of Saskatchewan.

Priestley, C. & Taylor, R. (1972). On the assessment of surface heat flux and evaporation using large-scale parameters. *Monthly Weather Review*, 100(2): 81-92.

Prudhomme, C., Giuntoli, I., Robinson, E. L., Clark, D. B., Arnell, N. W., Dankers, R., et al. (2014). Hydrological droughts in the 21st century, hotspots and uncertainties from a global multimodel ensemble experiment. *Proceedings of the National Academy of Sciences of the United States of America*, 111(9), 3262-7. doi:10.1073/pnas.1222473110

Prudhomme, C., Young, A., Watts, G., Haxton, T., Crooks, S., Williamson, J., et al. (2012). The drying up of Britain? A national estimate of changes in seasonal river flows from 11 Regional Climate Model simulations. *Hydrological Processes*, 26(7), 1115-1118. doi:10.1002/hyp.8434

Rango, A. & Martinec, J. (1995). Revisiting the degree-day method for snowmelt computations. *Water Resources Bulletin*, 31(4), 657-669.

Refsgaard, J.C. & Knudsen, J. (1996). Operational validation and intercomparison of different types of hydrological models. *Water Resources Research*, 32(7), 2189-2202.

Regonda, S.K., Rajagopalan, B., Clark, M., & Pitlick, J. (2005). Seasonal cycle shifts in hydroclimatology over the western U.S. *Journal of Climate*. 18, 372-284.

Revelle, R.R. & Waggoner, P.E. (1983). Effects of carbon dioxide induced climatic change on water supplies in the western United States. *Changing Climate*, 419-432.

Reynolds, L.V., Shafroth, P.B., & Poff, N.L. (2015). Modeled intermittency risk for small streams in the Upper Colorado River Basin under climate change. *Journal of Hydrology*, 523, 768-780. doi:10.1016/j.jhydrol.2015.02.025

Richards, L.A. (1931). Capillary conduction of liquids through porous mediums. *Physics*, 1, 318-333.

Risbey, J.S. & Entekhabi, D. (1996). Observed Sacramento Basin streamflow response to precipitation and temperature changes and its relevance to climate impact studies. *Journal of Hydrology*, 184, 209-223.

Rivard, C., Lavoie, D., Lefebvre, R., Séjourné, S., Lamontagne, C., & Duchesne, M. (2014). An overview of Canadian shale gas production and environmental concerns. *International Journal of Coal Geology*, 126, 64-76.

Rocca, M.E., Brown, P.M., MacDonald, L.H., & Carrico, C.M. (2014). Climate change impacts on fire regimes and key ecosystem services in Rocky Mountain forests. *Forest Ecology and Management*, 327, 290-305. doi:10.1016/j.foreco.2014.04.005

Rood, S.B., Foster, S.G., Hillman, E.J., Luek, A., & Zanewich, K.P. (2016). Flood moderation: declining peak flows along some Rocky Mountain rivers and the underlying mechanism. *Journal of Hydrology*, 536, 174-182. doi:10.1016/j.jhydrolo.2016.02.043

Sand, K. (Ed.) (1992). *Snow modelling, water resources, climate change*. Trondheim, Norway: Norwegian Hydrotechnical Laboratory.

Sankarasubramanian, A., Vogel, R.M., & Limbrunner, J.F. (2001). Climate elasticity of streamflow in the United States. *Water Resources Research*, 37(6), 1171-1781. doi:10.1029/2000WR900330

Schnorbus, M., Werner, A., & Bennett, K. (2014). Impacts of climate change in three hydrologic regimes in British Columbia, Canada. *Hydrological Processes*, 28, 1170-1189. doi:10.1002/hyp.9661

Seager, R., Ting, M., Li, C., Naik, N., Cook, B., Nakamura, J., & Liu, H. (2013). Projections of declining surface-water availability for the southwestern United States. *Nature Climate Change*, 3, 482-486. doi:10.1038/NCLIMATE1787

Sellers, W.D. (1968). Climatology of monthly precipitation patterns in the western United States, 1931-1966. *Monthly Weather Review*, 96(9), 585-595.

Seneviratne, S., Nicholls, N., Easterling, D., Goodess, C., Kanae, S., Kossin, J., et al. (2012). Changes in climate extremes and their impacts on the natural physical environment. Managing the Risk of Extreme Events and Disasters to Advance Climate Change Adaptation. A Special Report of Working Groups I and II of the IPCC, Annex Managing the Risks of Extreme Events and Disasters to Advance Climate Change Adaptation, 109–230.

Service, R.F. (2015). Meager snows spell trouble ahead for salmon. *Science*, 348(6232), 268-269. doi:10.1126/science.348.6232.268

Sheffield, J., Wood, E.F., & Roderick, M.L. (2012). Little change in global drought over the past 60 years. *Nature*, 491(7424), 435–8. doi:10.1038/nature11575

Sheffield, J. & Wood, E.F. (2011). Drought; Past Problems and Future Scenarios, Earthscan, London, UK, Washington DC, USA.

Sheffield, J. & Wood, E.F. (2008). Global Trends and Variability in Soil Moisture and Drought Characteristics, 1950–2000, from Observation-Driven Simulations of the Terrestrial Hydrologic Cycle, *Journal of Climate*, 21(3), 432-458. doi:10.1175/2007JCLI1822.1

Shrestha, R.R., Schnorbus, M.A., Werner, A.T., & Berland, A.J. (2012). Modelling spatial and temporal variability of hydrologic impacts of climate change in the Fraser River basin, British Columbia, Canada. *Hydrological Processes*, 26, 1840-1860. doi:10.1002/hyp.9283

Sicart, J.E., Pomeroy, J., Essery, R., & Bewley, D. (2006). Incoming longwave radiation to melting snow: observations, sensitivity, and estimation in northern environments. *Hydrological Processes*, 20(17): 3697-3708.

Smakhtin, V.U. (2001). Low flow hydrology: A review. *Journal of Hydrology*, 240(3-4), 147-186. doi:10.1016/S0022-1694(00)00340-1

Sospedra-Alfonso, R. & Merryfield, W.J. (2017). Influences of temperature and precipitation on historical and future snowpack variability over the Northern Hemisphere in the second generation Canadian Earth System Model. *Journal of Climate*, 30, 4633-4655. doi:10.1175/JCLI-D-16-0612.s1

Sospedra-Alfonso, R., Melton, J.R., & Merryfield, W.J. (2015). Effects of temperature and precipitation on snowpack variability in the Central Rocky Mountains as a function of elevation. *Geophysical Research Letters*, 42, 4429-4438. doi:10.1002/2015GL063898

Sprague, L.A. (2005). Drought effects on water quality in the South Platte River Basin, Colorado. *Journal of the American Water Resources Association*, 41(1), 11-24. doi:10.1111/j.1752-1688.2005.tb03713.x

Sproles, E.A., Roth, T.R., & Nolin, A.W. (2017). Future snow? A spatial-probabilistic assessment of the extraordinarily low snowpacks of 2014 and 2015 in the Oregon Cascades. *Cryosphere*, 11, 331-341. doi:10.5194/tc-11-331-2017

Sturm, M., Goldstein, M.A., & Parr, C. (2017). Water and life from snow: A trillion dollar science question. *Water Resources Research*, doi:10.1002/2017WR020840

Summit Environmental Consultants Inc. (2010). *Okanagan water supply and demand project: phase 2 summary report*. Retrieved from http://www.obwb.ca/wsd/wp-content/uploads/2011/02/339_2011_summary_report.pdf

Swales, D., Alexander, M., & Hughes, M. (2016). Examining moisture pathways and extreme precipitation in the U.S. Intermountain West using self-organizing maps. *Geophysical Research Letters*, 43, 1727-1735. doi:10.1002/2015GL067478

Tabari, H. & Talaee, P.H. (2014). Sensitivity of evapotranspiration to climatic change in different climates. *Global and Planetary Change*, 115, 16-23. doi:10.1016/j.gloplacha.2014.01.006

Tague, C. & Grant, G.E. (2009). Groundwater dynamics mediate low-flow response to global warming in snow-dominated alpine regions. *Water Resources Research*, 45, W07421. Doi:10.1029/2008WR007179

Tallaksen, L.M., & Van Lanen, H.A.J. (Eds.). (2004). *Hydrological drought: processes and estimation methods for streamflow and groundwater, Developments in water science*. Vol. 48. Amsterdam, the Netherlands: Elsevier Science B.V.

Teuling, A.J., Van Loon, A.F, Seneviratne, S.I., Lehner, I., Aubinet, M., Heinesch, B., … Spank, W. (2013). Evapotranspiration amplifies European summer drought. *Geophysical Research Letters*, 40, 2071-2075. doi:10.1002/grl.50495

Teutschbein, C., Grabs, T., Laudon, H., Karlsen, R.H., & Bishop, K. (2018). Simulating streamflow in ungauged basins under a changing climate: The importance of landscape characteristics. *Journal of Hydrology*, 561, 160-178. doi:10.1016/j.jhydrol.2018.03.060

Therrien, R., McLaren, R. G., Sudicky, E.A., & Panday, S. M. (2010). *HydroGeoSphere A Three-dimensional Numerical Model Describing Fully-integrated Subsurface and Surface Flow and Solute Transport*. Waterloo, Ontario: Groundwater Simulations Group, University of Waterloo.

Thompson, J.R. (2012). Modelling the impacts of climate change on upland catchments in southwest Scotland using MIKE SHE and the UKCP09 probabilistic projections. *Hydrology Research*, 43(4), 507-530. doi:10.2166/nh.2012.105

VanderKwaak, J.K. & Loague, K. (2001). Hydrological-response simulations for the R-5 catchment with a comprehensive physics-based model. *Water Resources Research*, 37(4): 999-1013. doi:10.1029/2000WR900272.

Van Huijgevoort, M.H.J., Van Lanen, H.A.J., Teuling, A.J., & Uijlenhoet, R. (2014). Identification of changes in hydrological drought characteristics from a multi-GCM driven ensemble constrained by observed discharge. *Journal of Hydrology*, 512, 421-434. doi:10.1016/j.jhydrol.2014.02.060

Van Lanen, H.A.J., Wanders, N., Tallaksen, L.M., & Van Loon, A.F. (2013). Hydrological drought across the world: impact of climate and physical catchment structure. *Hydrology and Earth System Sciences*, 17(5), 1715–1732. doi:10.5194/hess-17-1715-2013.

Van Lanen, H.A.J. & Tallaksen, L.M. (2007). Hydrological drought, climate variability and change. In M. Heinonen (Ed.) *Climate and Water: Proceedings of the third International Conference on Climate and Water*. Helsinki, 3-6 September 2007, 488-493.

Van Loon, A.F. (2013). *On the propagation of drought. How climate and catchment characteristics influence hydrological drought development and recovery*. Ph.D. thesis, Wageningen University.

Van Loon, A. F. (2015). Hydrological drought explained. *Wiley Interdisciplinary Reviews: Water*, 2, 359-392. doi:10.1002/wat2.1085

Van Loon, A. F., Ploum, S. W., Parajka, J., Fleig, A. K., Garnier, E., Laaha, G., & Van Lanen, H. A. J. (2015). Hydrological drought types in cold climates: quantitative analysis of causing factors and qualitative survey of impacts. *Hydrology and Earth System Sciences*, 19(4), 1993-2016. doi:10.5194/hess-19-1993-2015

Van Loon, A.F. & Van Lanen, H.A.J. (2012). A process-based typology of hydrological drought. *Hydrology and Earth System Sciences*, 16(7), 1915-1946. doi:10.5194/hess-16-1915-2012.

Van Loon, A. F., & Laaha, G. (2014). Hydrological drought severity explained by climate and catchment characteristics. *Journal of Hydrology*, 526, 3-14. doi:10.1016/j.jhydrol.2014.10.059

Van Mullem, J.A. & Garen, D. (2004). Chapter 11: Snowmelt, In *Part 630: Hydrology of the National Engineering Handbook*. Washington, D.C.: U.S. Dept. of Agriculture Natural Resources Conservation Service.

Vansteenkiste, T., Tovakoli, M., Ntegeka, V., Willems, P., De Smedt, F., & Batelaan, O. (2013). *Hydrological Processes*, 27, 3649-3662. doi:10.1002/hyp.9480

van Vliet, M.T.H., Yearsley, J.R., Ludwig, F., Vogele, S., Lettenmaier, D.P, & Kabat, P. (2012). Vulnerability of US and European electricity supply to climate change. *Nature Climate Change*, 2, 676-681. doi:10.1038/nclimate1546

van Vliet, M.T.H. & Zwolsman, J.J.G. (2008). Impact of summer droughts on the water quality of the Meuse river. *Journal of Hydrology*, 353, 1-17. doi:10.1016/j.jhydrol.2008.01.001

van Vuuren, D.P., Edmonds, J., Kainuma, M., Riahi, K., Thomson, A., Hibbard, K., et al. (2011). The representative concentration pathways: an overview. *Climatic Change*, 109, 5-31. doi: 10.1007/s10584-011-0148-z

Verdon-Kidd, D.C. & Kiem, A.S. (2010). Quantifying drought risk in a nonstationary climate. *Journal of Hydrometeorology*, 11, 1019-1031. doi:10.1175/2010JHM1215.1

Verseghy, D.L. (1991). Class-a Canadian land surface scheme for GCMs. I. Soil model. *International Journal of Climatology*, 11(2): 111-113.

Vidal, J.P., Martin, E., Franchistéguy, L., Habets, F., Soubeyroux, J.M., Blanchard, M., & Baillon, M. (2010). Multilevel and multiscale drought reanalysis over France with the Safran-Isba-Modcou hydrometeorological suite. *Hydrology and Earth System Sciences*, 14(3), 459–478. doi:10.5194/hess-14-459-2010

Voeckler, H.M., Allen, D.M., & Alila, Y. (2014). Modeling coupled surface water – Groundwater processes in a small mountainous headwater catchment. *Journal of Hydrology*, 517, 1089-1106. doi:10.1016/j.jhydrol.2014.06.015

Wanders, N. & Van Lanen, H.A.J. (2015). Future discharge drought across climate regions around the world modelled with a synthetic hydrological modelling approach forced by three general circulation models. *Natural Hazards and Earth System Science*, 15(3), 487-504. doi:10.5194/nhess-15-487-2015

Waylen, P.R. & Woo, M.K. (1987). Annual low flows generated by mixed processes. *Hydrological Sciences Journal*, 32(3) 371-383. doi:10.1080/02626668709491195

Webb, B.W., Clack, P.D., & Walling, D.E. (2003). Water-air temperature relationships in a Devon river system and the role of flow. *Hydrological Processes*, 17, 2069-3084.

Werner, A.T. & Cannon, A.J. (2016). Hydrologic extremes – an intercomparison of multiple gridded statistical downscaling methods. *Hydrology and Earth System Sciences,* 20(4), 1483-1508. doi:10.5194/hess-20.1483-2016

Westerling, A.L., Hidalgo, H.G., Cayan, D.R., & Swetnam, T.W. (2006). Warming and earlier spring increase western U.S. forest wildfire activity*. Science*, 313(5789), 940-943. doi:10.1126/science.1128834

Whitfield, P.H., Burn, D.H., Hannaford, J., Higgins, H., Glenn, A., Marsh, T., et al. (2012). Reference hydrologic networks I. The status and potential future directions of national reference hydrologic networks for detecting trends. *Hydrological Sciences Journal*, (April 2013), 37-41. http://doi.org/10.1080/02626667.2012.728706

Whitfield, P.H. & Cannon, A.J. (2000). Recent variations in climate and hydrology in Canada. *Canadian Water Resources Journal*, 25(1), 19-65. doi:10.4296/cwrj2501019

Whitfield, P.H. & Hendrata, M. (2006). Assessing detectability of changes in low flows in future climates from stage discharge measurements. *Canadian Water Resources Journal*, 31(1), 1-12.

Wiesnet, D. (1981). Winter snow drought. *Eos, Transactions, American Geophysical Union*, 62(14), 137-137.

Wijesekara, G.N., Farjad, B., Gupta, A., Qiao, Y., Delaney, P., & Marceau, D.J. (2014). A comprehensive land-use/hydrological modelling system for scenario simulations in the Elbow River watershed, Alberta, Canada. *Environmental Management*, 53(2), 357-381. doi:10.1007/s00267-013-0220-8

Wilcoxon, F. (1945). Individual comparisons by ranking methods. *Biometrics Bulletin*, 1(6), 80-83.

Wilhite, D.A. (2000). Chapter 1 Drought as a Natural Hazard: Concepts and Definitions. In *Drought: A Global Assessment*, pp 3-18. London: Routledge.

Wilson, D., Hisdal, H., & Lawrence, D. (2010). Has streamflow changed in the Nordic countries? – Recent trends and comparisons to hydrological projections. *Journal of Hydrology*, 394(3-4), 334–346. doi:10.1016/j.jhydrol.2010.09.010

Winchell, T.S., Barnard, D.M., Monson, R.K., Burns, S.P., & Molotch, N.P. (2016). Earlier snowmelt reduces atmospheric carbon uptake in midlatitude subalpine forests. *Geophysical Research Letters*, 43(15), 8160-8168. doi:10.1002/2016GL069769

Winograd, I.J., Riggs, A.C., & Coplen, T.B. (1998). The relative contributions of summer and cool-season precipitation to groundwater recharge, Spring Mountains, Nevada, USA. *Hydrogeology Journal*, 6(1), 77-93.

World Meteorological Organization (WMO). (1986). Intercomparison of models for snowmelt runoff. *Operational Hydrology Report 23* (WMO No. 646).

Wrzesien, M.L., Durand, M.T., Pavelsky, T.M., Kapnick, S.B., Zhang, Y., Guo, J., & Shun, C.K. (2018). A new estimate of North American mountain snow accumulation from regional climate model simulations. *Geophysical Research Letters*, 45, 1423-1432. doi:10.1002/2017GL076664

Wu, H., Soh, L. K., Samal, A., & Chen, X. H. (2008). Trend analysis of streamflow drought events in Nebraska. *Water Resources Management*, 22(2), 145-164. doi:10.1007/s11269-006-9148-6

Xie, C. & Gough, W.A. (2013). A simple thaw-freeze algorithm for a multi-layered soil using the Stefan equation. *Permafrost and Periglacial Processes*, 24(3), 252-260.

Yan, H., Sun, N., Wigmosta, M., Skaggs, R., Hou, Z. & Leung, R. (2018). Next-generation intensity-duration-frequency curves for hydrologic design in snow-dominated environments. *Water Resources Research*, 54(2), 1093-1108. doi:10.1002/2017WR021290

Ylla, I., Sanpera-Calbet, I., Vazquez, E., Romani, A.M., Munoz, I., Butturini, A., & Sabater, S. (2010). Organic matter availability during pre- and post-drought periods in a Mediterranean stream. *Hydrobiologia*, 657(1), 217-232. doi:10.1007/s10750-010-0193-z

Zhang, F.Y., Li, L.H., Ahmad, S., & Li, X.M. (2014). Using path analysis to identify the influence of climatic factors on spring peak flow dominated by snowmelt in an alpine watershed. *Journal of Mountain Science*, 11(4). doi:10.1007/S11629-013-2789-z

Zhao, L. & Gray, D.M. (1999). Estimating snowmelt infiltration into frozen soils. *Hydrological Processes*, 13(12-13), 1827-1842.

Appendix A.

Chapter 2 Supplemental Information

Supplementary information, in text form, is included to provide additional details on the methods used to calculate the percent variance explained by climate predictor variables (Text S2.1) and to account for collinearity of predictor variables in the multiple linear regression analysis (Text S2.2).

Supplementary information, in schematic form, is provided to illustrate the classification of summer and winter low flow periods with inter-annual shifts in the freshet peak (Figure S2.1).

Supplementary information, in tabular form, is included to provide additional hydrometric station attributes (Table S2.1) and the equations used to calculate the streamflow response and climate predictor variables (Table S2.2). Mean annual temperature and mean annual precipitation for each catchment (Table S2.1) were calculated from the Livneh et al. (2015) hydrometeorological dataset (see section 2.2). Elevation, in meters above sea level (MASL), is indicated for the stream gauge location in Table S2.1.

Text S2.1

The two-tailed Spearman's correlation was used to assess the significance of all correlation tests as it provides a measure of the monotonic relationship between the variables and is robust to outliers. However, the conversion to ranked data makes Spearman's rho inappropriate for deriving coefficients of determination. Therefore, the Pearson correlation coefficient was used to determine the percent variance explained by each predictor variable. For the bivariate correlation analysis, the percent variance explained by each predictor variable was calculated as the square of the Pearson correlation coefficient and is thus equal to the coefficient of determination. For the partial correlation analysis, the percent variance explained by each predictor variable is dependent on the variance explained by the control variable. For example, for the partial correlation analysis between a predictor variable (X) and a response variable (Y) with a control variable (Z), the percent of total variance in Y that is explained by X (and not explained by Z) is calculated as follows:

$$Percent\ of\ Total\ Variance\ in\ Y\ Explained\ by\ X\ =\ R^2_{XY.Z}\ \times\ (1\ -\ R^2_{YZ}\ )$$

where $R^2_{XY.Z}$ is the coefficient of determination from the partial correlation of X and Y with control variable Z, and R^2_{YZ} is the coefficient of determination from the bivariate correlation of Y and Z.

Text S2.2

In MLR analysis, collinearity between independent variables can create inaccurate estimates of regression coefficients, inflate standard errors, and give false nonsignificant p-values. Bivariate correlation tests between the dominant climate predictor variables showed that P_a and P_w are very strongly correlated ($r > 0.8$) in 98% of the catchments. To remove the collinearity, the Pw residuals from the linear regression of P_w and P_a were used in place of P_w in the MLR models that had both P_a and P_w as predictor variables. The P_w residuals ($P_{w,r}$) represent the variance in winter precipitation that is not explained by the variance in total annual precipitation. With this control for collinearity, the variance inflation factors for all models were less than 3.2.

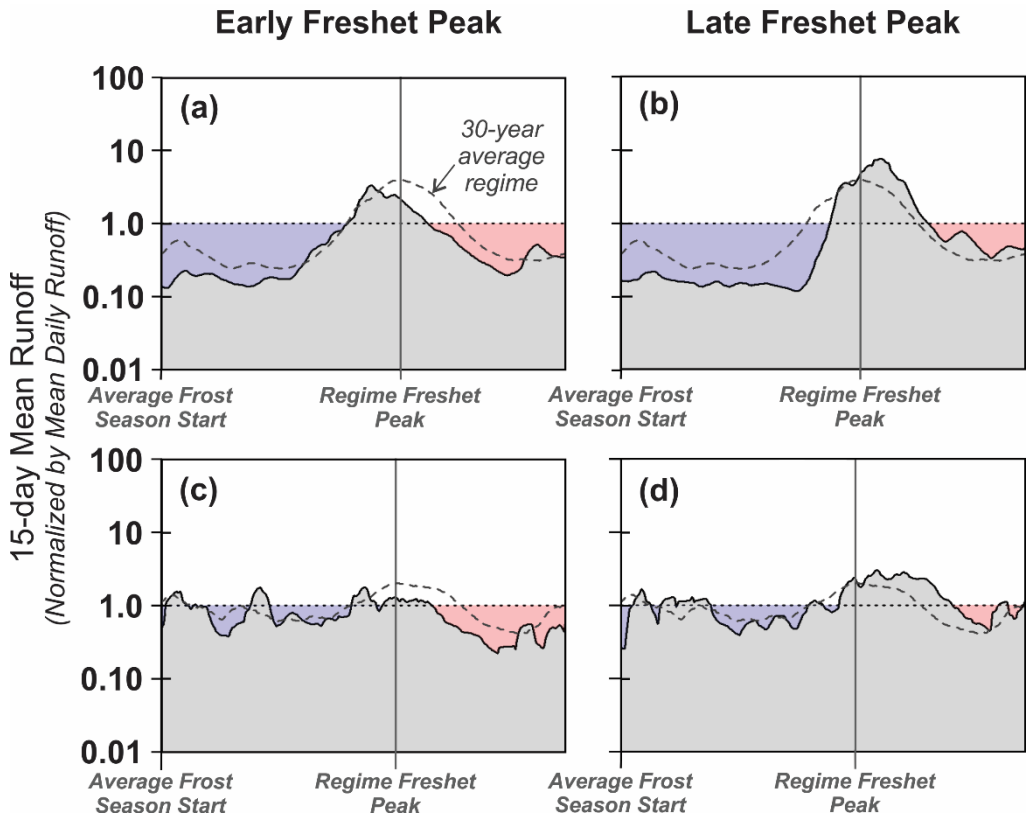

Figure S2.1 **Low flow period separation under shifts in freshet peak timing. Winter low flow period shown in blue; summer low flow period shown in pink. Dashed horizontal line is equal to the mean daily runoff (MDR) and is used as the upper-bound for defining the low flow periods.**

Table S2.1 Hydrometric gauging station information.

ID	Name	Lat.	Lon.	Area [km^2]	Elevation [MASL]	$\overline{T}$ [°C]	$\overline{P}$ [mm]	Ecoregion [CEC, 2009]
05AA008	CROWSNEST RIVER AT FRANK	49.60	-114.41	402.7	1473	0.8	815	Canadian Rockies
05AD003	WATERTON RIVER NEAR WATERTON PARK	49.11	-113.84	612.7	1268	0.8	1281	Canadian Rockies
05BL022	CATARACT CREEK NEAR FORESTRY ROAD	50.29	-114.59	165.5	1671	-1.4	800	Canadian Rockies
08LG016	PENNASK CREEK NEAR QUILCHENA	49.97	-120.14	87	1442	1.9	485	Thompson-Okanogan Plateau
08MH016	CHILLIWACK RIVER AT OUTLET OF CHILLIWACK LAKE	49.08	-121.46	329	685	1.6	2454	North Cascades
08NE006	KUSKANAX CREEK NEAR NAKUSP	50.28	-117.75	337	706	0.4	1247	Columbia Mountains /Northern Rockies
08NE077	BARNES CREEK NEAR NEEDLES	49.91	-118.13	201	603	2.5	846	Columbia Mountains /Northern Rockies
08NF001	KOOTENAY RIVER AT KOOTENAY CROSSING	50.89	-116.04	420	1194	-0.4	775	Canadian Rockies
08NH005	KASLO RIVER BELOW KEMP CREEK	49.91	-116.95	453	693	0.3	1011	Columbia Mountains /Northern Rockies
08NH084	ARROW CREEK NEAR ERICKSON	49.16	-116.45	78.7	854	2.1	841	Columbia Mountains /Northern Rockies
08NJ130	ANDERSON CREEK NEAR NELSON	49.50	-117.26	9.1	761	1.3	1180	Columbia Mountains /Northern Rockies
08NN015	WEST KETTLE RIVER NEAR MCCULLOCH	49.70	-119.09	230	1050	0.6	837	Thompson-Okanogan Plateau
10109001	COM F LOGAN R AB ST D AND LO HP AND SM C N LO UT	41.74	-111.78	555.6	1510	2.4	951	Wasatch and Uinta Mountains
10173450	MAMMOTH CREEK ABV WEST HATCH DITCH, NEAR HATCH, UT	37.62	-112.52	268.5	2223	4.4	648	Wasatch and Uinta Mountains
10234500	BEAVER RIVER NEAR BEAVER, UT	38.28	-112.57	236.4	1916	2.2	784	Wasatch and Uinta Mountains
10242000	COAL CREEK NEAR CEDAR CITY, UT	37.67	-113.03	208.7	1828	5.3	643	Wasatch and Uinta Mountains
10308200	E F CARSON R BL MARKLEEVILLE C NR MARKLEEVILLECA	38.71	-119.76	716.4	1645	5.4	1000	Sierra Nevada
10336660	BLACKWOOD C NR TAHOE CITY CA	39.11	-120.16	29.8	1921	4.0	1542	Sierra Nevada
11230500	BEAR C NR LAKE THOMAS A EDISON CA	37.34	-118.97	135.5	2262	1.7	1024	Sierra Nevada
11264500	MERCED R A HAPPY ISLES BRIDGE NR YOSEMITE CA	37.73	-119.56	468	1227	2.1	1184	Sierra Nevada
11315000	COLE C NR SALT SPRINGS DAM CA	38.52	-120.21	54	1831	4.2	1521	Sierra Nevada
11427700	DUNCAN CYN C NR FRENCH MEADOWS CA	39.14	-120.48	25.5	1607	6.8	1684	Sierra Nevada
11522500	SALMON R A SOMES BAR CA	41.38	-123.48	1943.1	188	6.9	1477	Klamath Mountains
11523200	TRINITY R AB COFFEE C NR TRINITY CTR CA	41.11	-122.71	382.9	791	5.8	1539	Klamath Mountains

ID	Name	Lat.	Lon.	Area [km^2]	Elevation [MASL]	$\bar{T}$ [°C]	$\bar{P}$ [mm]	Ecoregion [CEC, 2009]
12048000	DUNGENESS RIVER NEAR SEQUIM, WA	48.01	-123.13	405	174	1.7	1590	North Cascades
12082500	NISQUALLY RIVER NEAR NATIONAL, WA	46.75	-122.08	350	441	5.4	2265	Cascades
12092000	PUYALLUP RIVER NEAR ELECTRON, WA	46.90	-122.04	240.9	511	4.6	2278	Cascades
12175500	THUNDER CREEK NEAR NEWHALEM, WA	48.67	-121.07	273.8	395	1.3	2244	North Cascades
12178100	NEWHALEM CREEK NEAR NEWHALEM, WA	48.66	-121.24	69.7	372	3.5	2431	North Cascades
12186000	SAUK RIVER AB WHITECHUCK RIVER NEAR DARRINGTON, WA	48.17	-121.47	398.4	284	3.1	3100	North Cascades
12189500	SAUK RIVER NEAR SAUK, WA	48.42	-121.57	1855.3	83	3.5	2568	North Cascades
12358500	Middle Fork Flathead River nr West Glacier MT	48.50	-114.01	2939.2	957	1.7	1226	Canadian Rockies
12390700	Prospect Creek at Thompson Falls MT	47.59	-115.36	470.2	743	5.0	919	Columbia Mountains /Northern Rockies
12413000	NF COEUR D ALENE RIVER AT ENAVILLE ID	47.57	-116.25	2325.2	677	4.6	1168	Columbia Mountains /Northern Rockies
12414500	ST JOE RIVER AT CALDER ID	47.27	-116.19	2679	667	3.6	1278	Columbia Mountains /Northern Rockies
12447390	ANDREWS CREEK NEAR MAZAMA, WA	48.82	-120.15	58.1	1323	-1.0	1177	North Cascades
12451000	STEHEKIN RIVER AT STEHEKIN, WA	48.33	-120.69	830.6	355	1.2	1713	North Cascades
13011500	PACIFIC CREEK AT MORAN WY	43.85	-110.52	404.1	2055	-0.8	908	Middle Rockies
13011900	BUFFALO FORK AB LAVA CREEK NR MORAN WY	43.84	-110.44	851.8	2078	-1.4	901	Middle Rockies
13023000	GREYS RIVER AB RESERVOIR NR ALPINE WY	43.14	-110.98	1161.9	1757	0.0	834	Middle Rockies
13185000	BOISE RIVER NR TWIN SPRINGS ID	43.66	-115.73	2154.4	996	2.4	889	Idaho Batholith
13235000	SF PAYETTE RIVER AT LOWMAN ID	44.09	-115.62	1163.2	1155	1.2	978	Idaho Batholith
13240000	LAKE FORK PAYETTE RIVER AB JUMBO CR NR MCCALL ID	44.91	-116.00	125.6	1564	0.8	1195	Idaho Batholith
13313000	JOHNSON CREEK AT YELLOW PINE ID	44.96	-115.50	561.9	1439	0.5	1060	Idaho Batholith
13331500	MINAM RIVER NEAR MINAM, OR	45.62	-117.73	618.9	795	3.9	838	Blue Mountains
13340600	NF CLEARWATER RIVER NR CANYON RANGER STATION ID	46.84	-115.62	3354.6	512	3.4	1391	Columbia Mountains /Northern Rockies
14020000	UMATILLA RIVER ABOVE MEACHAM CREEK, NR GIBBON, OR	45.72	-118.32	341.4	578	5.8	1011	Blue Mountains
14158500	MCKENZIE RIVER AT OUTLET OF CLEAR LAKE, OR	44.36	-122.00	237.1	948	5.6	2282	Cascades

ID	Name	Lat.	Lon.	Area [km^2]	Elevation [MASL]	$\overline{T}$ [°C]	$\overline{P}$ [mm]	Ecoregion [CEC, 2009]
14158790	SMITH R AB SMITH R RES NR BELKNAP SPRGS, OREG.	44.33	-122.05	40.6	869	5.2	2820	Cascades
6622700	NORTH BRUSH CREEK NEAR SARATOGA, WY	41.37	-106.52	98.7	2463	0.8	929	Southern Rockies
6623800	ENCAMPMENT RIVER AB HOG PARK CR, NR ENCAMPMENT, WY	41.02	-106.82	187.7	2520	0.1	1249	Southern Rockies
6632400	ROCK CREEK AB KING CANYON CANAL, NR ARLINGTON, WY	41.59	-106.22	163	2375	0.5	891	Southern Rockies
7083000	HALFMOON CREEK NEAR MALTA, CO.	39.17	-106.39	60.8	3012	-1.4	755	Southern Rockies
8267500	RIO HONDO NEAR VALDEZ, NM	36.54	-105.56	96.3	2400	1.1	795	Southern Rockies
8271000	RIO LUCERO NEAR ARROYO SECO, NM	36.51	-105.53	43.8	2460	-0.6	883	Southern Rockies
8378500	PECOS RIVER NEAR PECOS, NM	35.71	-105.68	445	2288	2.9	852	Southern Rockies
9035900	SOUTH FORK OF WILLIAMS FORK NEAR LEAL, CO.	39.80	-106.03	72.8	2732	-1.2	753	Southern Rockies
9066000	BLACK GORE CREEK NEAR MINTURN, CO.	39.60	-106.27	32.4	2802	-1.5	831	Southern Rockies
9081600	CRYSTAL RIVER AB AVALANCHE C, NEAR REDSTONE, CO.	39.23	-107.23	432.9	2109	0.4	950	Southern Rockies
9223000	HAMS FORK BELOW POLE CREEK, NEAR FRONTIER, WY	42.11	-110.71	333.2	2275	-0.5	726	Middle Rockies
9312600	WHITE RIVER BL TABBYUNE C NEAR SOLDIER SUMMIT, UT	39.88	-111.04	195.3	2214	2.4	562	Wasatch and Uinta Mountains
9352900	VALLECITO CREEK NEAR BAYFIELD, CO.	37.48	-107.54	188.2	2422	-1.0	980	Southern Rockies
9378630	RECAPTURE CREEK NEAR BLANDING, UT	37.76	-109.48	10.4	2209	5.7	595	Southern Rockies

Table S2.2 Climate predictor and low flow response variable equations.

	Equation for 30-year regime values	Equation for yearly values
P_a	$\bar{P}_a = \frac{1}{30}\sum_{j=1983}^{2012}\sum_{i=1}^{n} P_{i,j}$	$P_{a,j} = \sum_{i=1}^{n} P_{i,j}$
T_a	$\bar{T}_a = \frac{1}{30}\sum_{j=1983}^{2012}\frac{1}{n}\sum_{i=1}^{n} T_{i,j}$	$T_{a,j} = \frac{1}{n}\sum_{i=1}^{n} T_{i,j}$
P_s	$\bar{P}_s = \frac{1}{30}\sum_{j=1983}^{2012}\sum_{[i\ in\ S]} P_{i,j}$	$P_{s,j} = \sum_{[i\ in\ S]} P_{i,j}$
T_s	$\bar{T}_s = \frac{1}{30}\sum_{j=1983}^{2012}\frac{1}{n_s}\sum_{[i\ in\ S]} T_{i,j}$	$T_{s,j} = \frac{1}{n_s}\sum_{[i\ in\ S]} T_{i,j}$
P_w	$\bar{P}_w = \frac{1}{30}\sum_{j=1983}^{2012}\sum_{[i\ in\ W]} P_{i,j}$	$P_{w,j} = \sum_{[i\ in\ W]} P_{i,j}$
T_w	$\bar{T}_w = \frac{1}{30}\sum_{j=1983}^{2012}\frac{1}{n_w}\sum_{[i\ in\ W]} T_i$	$T_{w,j} = \frac{1}{n_w}\sum_{[i\ in\ W]} T_i$
TD_w	$\overline{TD}_w = \frac{1}{30}\sum_{j=1983}^{2012}\sum_{[i\ in\ W]} T_{i,j}\ \ [T_{i,j} > 0]$	$TD_{w,j} = \sum_{[i\ in\ W]} T_{i,j}\ \ [T_{i,j} > 0]$
Sf	$\overline{Sf} = \frac{1}{30}\sum_{j=1983}^{2012}\frac{\sum_{i=1}^{n} P_{i,j}\ [T_{i,j} < 0]}{\sum_{i=1}^{n} P_{i,j}}$	$Sf_j = \frac{1}{\sum_{i=1}^{n} P_{i,j}}\sum_{i=1}^{n} P_{i,j}\ [T_{i,j} < 0]$
MDR	$MDR = \frac{1}{30}\sum_{j=1983}^{2012}\frac{1}{n}\sum_{i=1}^{n} RO_{i,j}$	$MDR_j = \frac{1}{n}\sum_{i=1}^{n} RO_{i,j}$
DUR_s	$DUR_s = \sum_{[i\ in\ W]} 1\,[\overline{RO}_{15i} < MDR]$	$DUR_{s,j} = \sum_{[i\ in\ S]} 1\,[RO_{15i,j} < MDR]$
MAG_s	$MAG_s = \frac{\sum_{[i\ in\ W]} MDR - \overline{RO}_{15i}[\overline{RO}_{15i} < MDR]}{DUR_s \times MDR}$	$MAG_{s,j} = \frac{\sum_{[i\ in\ S]} MDR - RO_{15i,j}[RO_{15i,j} < MDR]}{DUR_{s,j} \times MDR}$
SEV_s	$SEV_s = \frac{\sum_{[i\ in\ S]} MDR - \overline{RO}_{15i}[\overline{RO}_{15i} < MDR]}{MAR}$	$SEV_{s,j} = \frac{\sum_{[i\ in\ S]} MDR - RO_{15i,j}[RO_{15i,j} < MDR]}{MAR}$
MAX_s	$MAX_s = \frac{max(MDR - \overline{RO}_{15i}[i\ in\ S])}{MDR}$	$MAX_{s,j} = \frac{max(MDR - RO_{15i,j}[i\ in\ S])}{MDR}$
DUR_w	$DUR_w = \sum_{[i\ in\ W]} 1\,[\overline{RO}_{15i} < MDR]$	$DUR_{w,j} = \sum_{[i\ in\ W]} 1\,[RO_{15i,j} < MDR]$
MAG_w	$MAG_w = \frac{\sum_{[i\ in\ W]} MDR - \overline{RO}_{15i}[\overline{RO}_{15i} < MDR]}{DUR_w \times MDR}$	$MAG_{w,j} = \frac{\sum_{[i\ in\ W]} MDR - RO_{15i,j}[RO_{15i,j} < MDR]}{DUR_{w,j} \times MDR}$
SEV_w	$SEV_w = \frac{\sum_{[i\ in\ W]} MDR - \overline{RO}_{15i}[\overline{RO}_{15i} < MDR]}{MAR}$	$SEV_{w,j} = \frac{\sum_{[i\ in\ W]} MDR - RO_{15i,j}[RO_{15i,j} < MDR]}{MAR}$
MAX_w	$MAX_w = \frac{max(MDR - \overline{RO}_{15i}[i\ in\ W])}{MDR}$	$MAX_{w,j} = \frac{max(MDR - RO_{15i,j}[i\ in\ W])}{MDR}$

Note: j = hydrologic year, i = day of the hydrologic year, RO = daily runoff, and RO_{15} = 15-day mean runoff. n is the number of days in year j, n_s is the number of days in the set of summer days $[i\ in\ S]$, and n_w is the number of days in the set of winter days $[i\ in\ W]$. The classification of winter versus summer days is unique to each catchment and consistent between years. The 30-year mean daily smoothed runoff is calculated as $\overline{RO}_{15i} = \frac{1}{30}\sum_{j=1983}^{2012} RO_{15i,j}$.

Appendix B.

Chapter 3 Supplemental Information

Supplementary information, in schematic form (Figure S3.1), is provided to illustrate spatial patterns in peak SWE precipitation-sensitivity (Figures S3.1a and S3.1c) and peak SWE temperature-sensitivity (Figures S3.1b and S3.1d).

Supplementary information, in tabular form (Tables S3.1 –S3.3), is provided to summarize six different linear regression models and compare (a) their predictive ability for peak SWE (Table S3.1), (b) the slope magnitude for the temperature predictors (Table S3.2), and (c) the standard error estimates for the temperature predictors (Table S3).

Supplementary information, in tabular form (Table S3.4), is included as the tabular version of Figure 3.3.

Supplementary information, in tabular form (Table S3.5), is provided as an alternative to the *volume-based* ecoregion summary (Table 3.1 in the main text), showing an *area-based* ecoregion summary of peak SWE susceptibility to temperature-related snow drought.

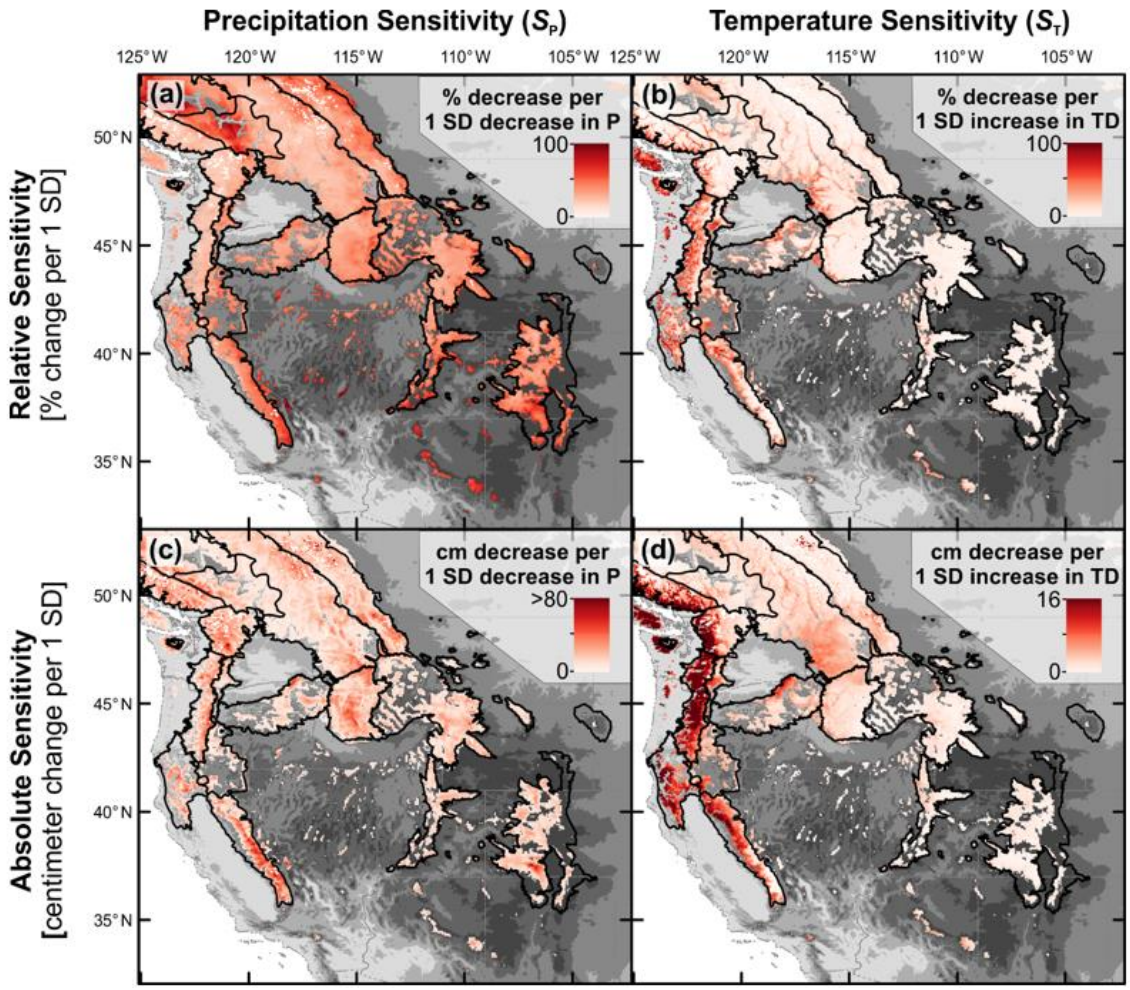

Figure S3.1 Relative and absolute sensitivity of peak SWE to precipitation [S_P; plots (a) and (c)] and temperature [S_T; plots (b) and (d)], using grid-cell based winter season definition and thawing degrees (TD) as the temperature metric. Relative sensitivity is expressed as percent decrease in peak SWE per 1 standard deviation (SD) decrease in precipitation and per 1 SD increase in TD; absolute sensitivity is expressed as the centimeter (cm) decrease in peak SWE per 1 SD decrease in precipitation and per 1 SD increase in TD. *Note:* Glaciated cells are shown in white, and the scale in the bottom row is different between the precipitation and temperature sensitivity maps.

Table S3.1 Peak snow water equivalent (SWE) mean linear model R^2 value by ecoregion based on winter season definition (grid-cell-based versus 1-Nov to 1-Apr) and predictor variables (TD = thawing degrees, P = precipitation, T = temperature). **Bold** values highlight values within 0.01 of the maximum R^2 for each ecoregion. Ecoregion numbering as in Figure 3.1.

	Definition of winter season:	**Grid-cell-based**			**1-Nov to 1-Apr**		
	Predictors:	*TD, P*	*T, P*	*P*	*TD, P*	*T, P*	*P*
1	Pacific & Nass Ranges	**0.85**	0.82	0.60	0.83	0.81	0.58
2	North Cascades	**0.91**	0.89	0.78	0.88	0.87	0.76
3	Cascades	**0.78**	0.74	0.47	0.76	0.73	0.48
4	Eastern Cascades Slopes & Foothills	**0.73**	**0.72**	0.58	**0.72**	**0.72**	0.59
5	Klamath Mountains	**0.64**	**0.64**	0.38	0.54	0.58	0.38
6	Sierra Nevada	**0.81**	**0.82**	0.69	0.78	**0.81**	0.69
7	Wasatch & Uinta Mountains	**0.86**	**0.87**	0.84	0.86	0.86	0.83
8	Southern Rockies	**0.89**	**0.90**	0.88	0.85	0.85	0.83
9	Middle Rockies	**0.87**	**0.88**	0.85	0.84	0.82	0.81
10	Idaho Batholith	**0.93**	**0.92**	0.90	0.91	0.90	0.88
11	Blue Mountains	**0.81**	**0.81**	0.71	**0.82**	0.81	0.71
12	Canadian Rockies	**0.92**	0.89	0.84	0.87	0.86	0.81
13	Columbia Mountains / N. Rockies	**0.90**	**0.90**	**0.89**	**0.89**	0.87	0.86
14	Thompson-Okanagan Plateau	**0.95**	**0.94**	0.92	**0.94**	0.93	0.91
15	Chilcotin Ranges & Fraser Plateau	**0.93**	**0.92**	0.89	0.91	0.91	0.88
	Entire Domain:	**0.87**	**0.86**	0.79	0.85	0.84	0.77

Table S3.2 Peak snow water equivalent (SWE) mean linear model slope, i.e. temperature-sensitivity, for different temperature predictors (TD = thawing degrees, T = temperature) and winter season definition (grid-cell-based versus 1-Nov to 1-Apr). P = precipitation. Slope units are % decrease in peak SWE per 1 SD increase in the associated temperature predictor, consistent with Figure S3.1b. **Bold** values highlight maximum value for each ecoregion. Ecoregion numbering as in Figures 3.1. Mean winter temperature (T_w) is included to illustrate relationship between peak SWE T-sensitivity and temperature.

	Definition of winter season:	Grid-cell-based		1-Nov to 1-Apr		T_w
	Predictors:	*TD, P*	*T, P*	*TD, P*	*T, P*	[°C]
1	Pacific & Nass Ranges	**17.5**	16.4	17.0	16.4	-3.9
2	North Cascades	**11.2**	9.8	10.2	9.5	-4.3
3	Cascades	**25.8**	24.2	24.6	23.5	-0.3
4	E. Cascades Slopes & Foothills	**20.1**	20.0	19.6	19.5	-1.4
5	Klamath Mountains	**31.2**	31.0	23.5	26.1	0.9
6	Sierra Nevada	17.6	**19.0**	16.4	17.8	-1.4
7	Wasatch & Uinta Mountains	4.4	**7.8**	6.3	6.2	-6.3
8	Southern Rockies	3.6	**7.0**	6.0	5.6	-7.7
9	Middle Rockies	3.9	6.0	**6.6**	4.2	-8.6
10	Idaho Batholith	5.0	4.6	**5.2**	4.2	-6.4
11	Blue Mountains	13.6	13.5	**14.3**	13.4	-3.3
12	Canadian Rockies	**7.9**	6.0	6.8	5.7	-9.6
13	Columbia Mtns. / N. Rockies	4.3	5.0	**5.7**	3.3	-6.3
14	Thompson-Okanagan Plateau	**7.0**	5.7	5.5	4.8	-6.5
15	Chilcotin Ranges & Fraser Plateau	**8.4**	7.5	7.1	6.3	-7.6
	Entire Domain:	9.9	**10.2**	10.0	9.2	-5.8

Table S3.3 As Table S3.2, but with standard error values. Bold values highlight minimum standard error for each ecoregion. Ecoregion numbering as in Figure 3.1.

	Definition of winter season:	Grid-cell-based		1-Nov to 1-Apr		T_w
	Predictors:	*TD, P*	*T, P*	*TD, P*	*T, P*	[°C]
1	Pacific & Nass Ranges	**1.82**	1.99	1.91	2.03	-3.9
2	North Cascades	**1.34**	1.45	1.55	1.59	-4.3
3	Cascades	**2.93**	3.14	3.06	3.16	-0.3
4	E. Cascades Slopes & Foothills	**3.73**	3.76	3.80	3.79	-1.4
5	Klamath Mountains	4.72	**4.67**	5.16	4.95	0.9
6	Sierra Nevada	3.28	**3.11**	3.47	3.28	-1.4
7	Wasatch & Uinta Mountains	2.48	**2.36**	2.40	2.42	-6.3
8	Southern Rockies	2.18	**2.05**	2.34	2.39	-7.7
9	Middle Rockies	1.96	**1.89**	2.13	2.27	-8.6
10	Idaho Batholith	1.33	**1.32**	1.47	1.52	-6.4
11	Blue Mountains	2.46	2.49	**2.41**	2.48	-3.3
12	Canadian Rockies	**1.14**	1.30	1.42	1.51	-9.6
13	Columbia Mtns. / N. Rockies	**1.70**	1.73	1.84	2.05	-6.3
14	Thompson-Okanagan Plateau	**1.20**	1.27	1.39	1.40	-6.5
15	Chilcotin Ranges & Fraser Plateau	**1.80**	1.83	2.04	2.07	-7.6
	Entire Domain:	**2.08**	2.10	2.23	2.29	-5.8

Table S3.4 Snow drought severity [fraction below mean], frequency [fraction of years], and risk [severity x frequency], 1951-2013, for dry [D], warm [W], and warm & dry [WD] snow droughts. Ecoregion numbering as in Figure 3.1. Bold values highlight the snow drought type with the maximum severity, frequency, and risk by ecoregion.

	Mean Severity			**Frequency**			**Risk**		
Snow Drought Type:	*D*	*W*	*WD*	*D*	*W*	*WD*	*D*	*W*	*WD*
1. Pacific & Nass Ranges	0.13	0.06	**0.14**	**0.25**	0.11	0.22	**0.03**	0.01	0.03
2. North Cascades	0.17	0.03	**0.19**	0.21	0.06	**0.27**	0.03	0.00	**0.05**
3. Cascades	0.15	0.10	**0.31**	0.11	0.11	**0.29**	0.02	0.01	**0.09**
4. Eastern Cascades Slopes & Foothills	0.23	0.06	**0.34**	0.16	0.05	**0.29**	0.04	0.00	**0.10**
5. Klamath Mountains	**0.30**	0.24	0.29	**0.25**	0.10	0.21	**0.08**	0.02	0.06
6. Sierra Nevada	0.28	0.06	**0.38**	0.17	0.03	**0.37**	0.05	0.00	**0.14**
7. Wasatch & Uinta Mountains	0.21	0.08	**0.27**	0.19	0.06	**0.35**	0.04	0.01	**0.09**
8. Southern Rockies	0.21	0.06	**0.23**	0.19	0.03	**0.37**	0.04	0.00	**0.08**
9. Middle Rockies	0.17	0.05	**0.25**	0.24	0.03	**0.29**	0.04	0.00	**0.07**
10. Idaho Batholith	0.25	0.02	**0.28**	0.22	0.03	**0.27**	0.06	0.00	**0.08**
11. Blue Mountains	0.20	0.08	**0.36**	0.16	0.06	**0.29**	0.03	0.01	**0.10**
12. Canadian Rockies	0.17	0.08	**0.23**	**0.32**	0.06	0.24	0.05	0.01	**0.05**
13. Columbia Mountains / Northern Rockies	0.15	0.04	0.17	0.24	0.03	**0.29**	0.03	0.00	**0.05**
14. Thompson-Okanagan Plateau	0.22	0.05	**0.24**	0.13	0.02	**0.30**	0.03	0.00	**0.07**
15. Chilcotin Ranges & Fraser Plateau	0.22	0.12	**0.27**	0.13	0.02	**0.32**	0.03	0.00	**0.08**

Table S3.5 Temperature-related snow drought susceptibility summarized by ecoregion. SWE = mean snow water equivalent. Ecoregion numbering as in Figure 3.1. "Other" includes all grid cells not within the 15 ecoregions. *Note:* Values may not add up to 100% due to rounding.

		Historical			+2°C Warming		
Ecoregion	Area	Low	Med	High	Low	Med	High
	[km²]		*[% Area]*			*[% Change]*	
1. Pacific & Nass Ranges	27,689	53%	39%	8%	-22%	+6%	+16%
2. North Cascades	28,784	60%	34%	6%	-21%	+9%	+11%
3. Cascades	35,822	11%	63%	27%	-10%	-24%	+34%
4. Eastern Cascades Slopes & Foothills	26,340	15%	82%	3%	-12%	-16%	+28%
5. Klamath Mountains	20,024	2%	49%	49%	-2%	-31%	+33%
6. Sierra Nevada	37,577	23%	58%	18%	-10%	-16%	+26%
7. Wasatch & Uinta Mountains	30,787	92%	8%	0%	-21%	+21%	0%
8. Southern Rockies	73,507	98%	2%	0%	-12%	+12%	0%
9. Middle Rockies	94,420	100%	0%	0%	-3%	+3%	0%
10. Idaho Batholith	56,361	92%	8%	0%	-19%	+19%	0%
11. Blue Mountains	28,209	53%	47%	0%	-39%	+35%	+4%
12. Canadian Rockies	71,401	100%	0%	0%	-6%	+6%	0%
13. Columbia Mountains / N. Rockies	142,425	81%	19%	0%	-22%	+19%	+3%
14. Thompson-Okanagan Plateau	41,937	96%	4%	0%	-19%	+19%	0%
15. Chilcotin Ranges & Fraser Plateau	38,458	100%	0%	0%	-9%	+9%	0%
Other	70,794	53%	35%	12%	-22%	+7%	+15%
Total	**824,536**	**74%**	**21%**	**5%**	**-15%**	**8%**	**7%**

Appendix C.

Chapter 4 Supplemental Information

Table S4.1 Land cover and associated surface roughness (Manning's M) values based on the dominant land cover of watershed.

Watershed	Dominant Land cover	Surface Type from Chow (1959) Table 5-6	Manning's n	Manning's M
Fort Nelson	young & old forest	D-2.d. 3-4	0.08	12
Blueberry	young forest	D-2.d. 3	0.06	17
Whiteman Creek	young & old forest	D-2.d. 3-4	0.08	12
Capilano River	subalpine	D-1.b. 1 or C.d. 2.	0.04	25

Table S4.2 Fort Nelson unsaturated/saturated zone parameters. McConachie soil – sphagnum peat over morainal till. Fine clastic sedimentary (mudstone, siltstone, shale) bedrock of the Fort St. John Group.

Depth below ground surface (m)	Layer	Density (Kg/m^3)	θs	θr	α (cm^{-1})	n	Sy	K_z (m/s)	K_{xy} (m/s)	Ss
0-0.2	O fibric	40	0.85	0.04	0.08	1.9	0.68	4.8E-5	4.8E-5	1E-4
0.2-0.4	O hemic	130	0.50	0.15	0.02	1.7	0.16	1.4E-5	1.4E-5	1E-4
0.4-0.6	O sapric	170	0.40	0.22	0.003	1.6	0.009	5.5E-7	7.0E-7	1E-4
0.6-2	C horizon	1500	0.35	0.068	0.016	1.31	0.062	2.7E-6	7.0E-6	1E-4
2-5	Saprolite	2200	0.20	0.068	0.008	1.31	0.02	1.0E-7	3.0E-7	1E-5
5-200	Bedrock	2400	0.12	0.068	0.008	1.31	0.01	1.0E-10	5.0E-10	1E-5

Table S4.3 Blueberry unsaturated/saturated zone parameters. Wonowon soil – morainal till. Dunvegan sandstone bedrock.

Depth below ground surface (m)	Layer	Density (Kg/m^3)	θs	θr	α (cm^{-1})	n	Sy	K_z (m/s)	K_{xy} (m/s)	Ss
0-0.2	A horizon	1310	0.45	0.067	0.02	1.41	0.23	2.7E-6	3.0E-5	1E-4
0.2-0.85	B horizon	1560	0.43	0.089	0.01	1.23	0.17	2.7E-7	5.0E-6	1E-4
0.85-1.5	C horizon	1420	0.36	0.07	0.005	1.09	0.1	2.7E-7	5.0E-6	1E-4
1.5-5	Saprolite	2200	0.27	0.05	0.03	1.45	0.2	2.0E-6	3.0E-6	1E-5
5-200	Bedrock	2400	0.25	0.05	0.008	1.45	0.2	5.0E-8	5.0E-8	1E-5

Table S4.4 Whiteman unsaturated/saturated zone parameters. Grant soil – morainal till. Trachyandesite bedrock of the Kitley Lake Member.

Depth below ground surface (m)	Layer	Density (Kg/m^3)	θs	θr	α (cm^{-1})	n	Sy	K_z (m/s)	K_{xy} (m/s)	Ss
0-0.1	A horizon	1300	0.41	0.065	0.075	1.89	0.2	2E-5	2E-5	1E-4
0.1-0.5	B horizon	1450	0.41	0.095	0.019	1.31	0.2	1.6E-5	5E-5	1E-4
0.4-0.75	C horizon	1600	0.41	0.065	0.075	1.89	0.2	1.1E-5	5E-5	1E-4
0.8-5	Saprolite	2400	0.15	0.05	0.0036	2.75	0.02	5E-7	6E-7	1E-5
5-200	Bedrock	2500	0.10	0.05	0.0036	2.75	0.01	3E-8	3E-8	1E-5

Table S4.5 Capilano unsaturated/saturated zone parameters. Sayres soil – colluvial underlain by igneous acidic bedrock. Mid-cretaceous unnamed quartz diorite bedrock.

Depth below ground surface (m)	Layer	Density (Kg/m^3)	θs	θr	α (cm^{-1})	n	Sy	K_z (m/s)	K_{xy} (m/s)	Ss
0-0.1	A horizon	1400	0.39	0.10	0.059	1.48	0.2	2E-6	5E-6	1E-4
0.1-0.8	B horizon	1450	0.39	0.10	0.059	1.48	0.2	2E-6	2E-6	1E-4
0.8-5	Saprolite	2700	0.05	0.01	0.0036	2.75	0.02	5E-7	5E-7	1E-5
5-200	Bedrock	2800	0.03	0.01	0.0036	2.75	0.01	1E-7	1E-7	1E-5

Table S4.6 **Mean annual values and absolute difference (°C) in mean annual temperature (Temp) and mean annual values (mm/year) and relative difference (%) in mean annual precipitation (Precip), peak snow water equivalent (SWE), annual runoff, actual evapotranspiration (AET), and groundwater recharge for 1980s baseline (1970-1999) versus 2050s (2040-2069) and 2080s (2070-2099) for representative concentration pathway (RCP) 4.5 and RCP 8.5.**

	Time Period	RCP	Fort Nelson		Blueberry		Whiteman		Capilano	
			Mean	Δ	Mean	Δ	Mean	Δ	Mean	Δ
Temp	1980s	--	-0.6	--	0.0	--	2.1	--	5.9	--
	2050s	4.5	2.1	+2.8	2.7	+2.7	4.8	+2.8	8.4	+2.6
	2050s	8.5	2.9	+3.5	3.3	+3.4	5.5	+3.4	9.1	+3.2
	2080s	4.5	2.8	+3.4	3.3	+3.3	5.6	+3.5	9.1	+3.2
	2080s	8.5	5.2	+5.9	5.8	+5.9	8.2	+6.1	11.4	+5.6
Precip	1980s	--	459	--	498	--	650	--	2346	--
	2050s	4.5	521	+13.5%	566	+13.7%	667	+2.6%	2440	+4.0%
	2050s	8.5	554	+20.7%	599	+20.3%	706	+8.6%	2524	+7.6%
	2080s	4.5	546	+19.0%	585	+17.6%	712	+9.5%	2576	+9.8%
	2080s	8.5	588	+28.2%	607	+21.9%	726	+11.7%	2594	+10.6%
SWE	1980s	--	123	--	124	--	312	--	398	--
	2050s	4.5	127	+4.0%	119	-3.8%	272	-12.9%	103	-74.1%
	2050s	8.5	132	+7.5%	123	-1.0%	252	-19.3%	77	-80.7%
	2080s	4.5	135	+10.0%	128	+3.3%	268	-14.0%	77	-80.6%
	2080s	8.5	140	+14.5%	101	-18.8%	162	-48.1%	31	-92.3%
Runoff	1980s	--	12	--	104	--	273	--	1588	--
	2050s	4.5	16	+27.8%	122	+17.6%	288	+5.7%	1668	+5.0%
	2050s	8.5	19	+57.6%	140	+34.5%	314	+15.1%	1729	+8.9%
	2080s	4.5	20	+60.3%	134	+28.7%	325	+19.0%	1773	+11.7%
	2080s	8.5	24	+96.3%	140	+34.8%	338	+23.9%	1785	+12.4%
AET	1980s	--	429	--	354	--	365	--	471	--
	2050s	4.5	479	+11.6%	395	+11.5%	364	-0.3%	471	+0.0%
	2050s	8.5	500	+16.4%	403	+13.8%	374	+2.3%	484	+2.8%
	2080s	4.5	491	+14.3%	397	+12.1%	371	+1.7%	483	+2.4%
	2080s	8.5	518	+20.6%	409	+15.5%	371	+1.7%	486	+3.2%
Recharge	1980s	--	288	--	194	--	234	--	774	--
	2050s	4.5	339	+17.6%	211	+9.2%	244	+4.4%	769	-0.6%
	2050s	8.5	368	+27.5%	221	+14.0%	258	+10.6%	783	+1.1%
	2080s	4.5	360	+24.9%	213	+10.0%	254	+8.7%	771	-0.4%
	2080s	8.5	394	+36.5%	229	+18.5%	264	+13.0%	742	-4.1%

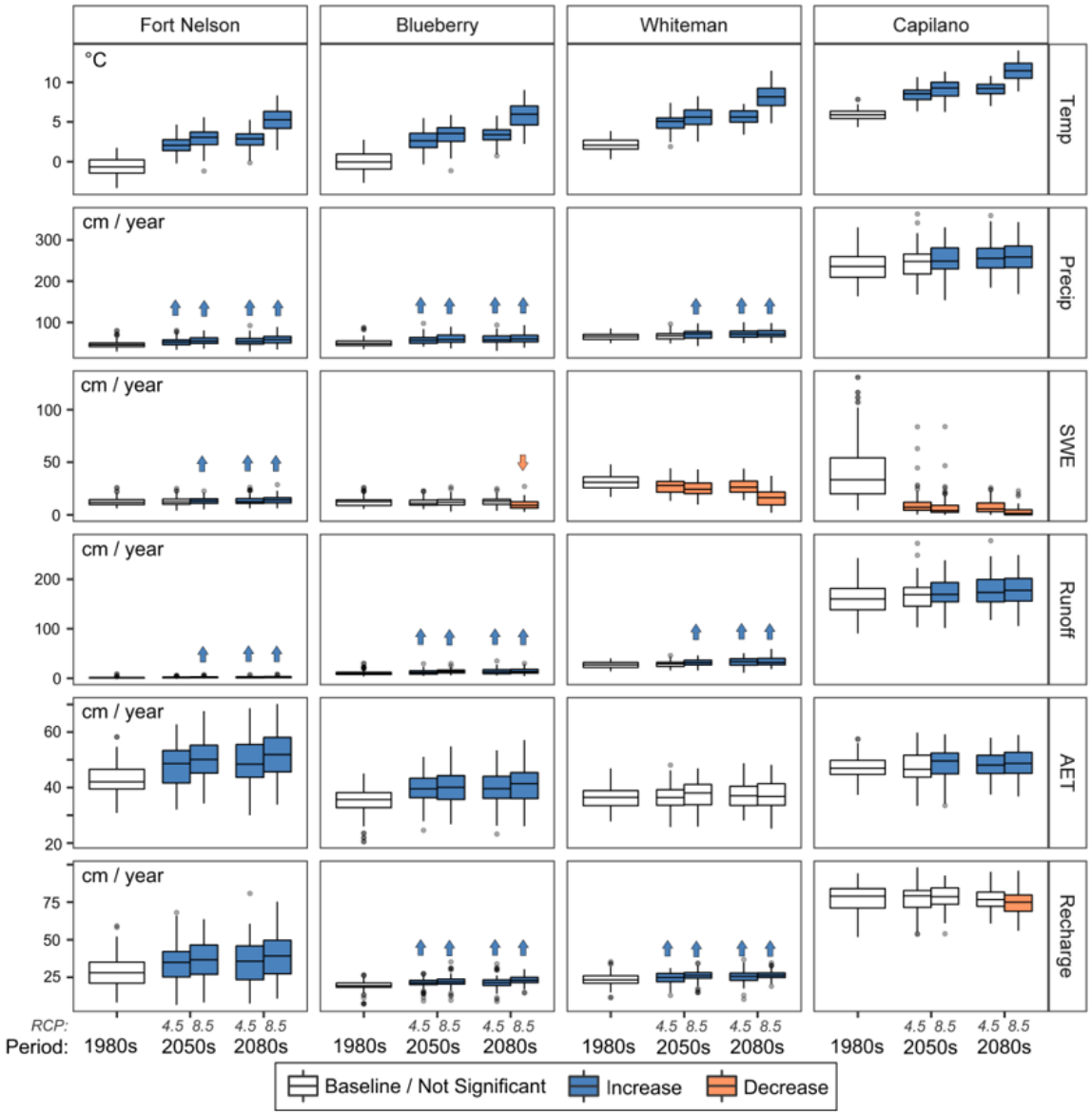

Figure S4.1 **Annual climate and water balance components for the 1980s baseline (1970-1999) versus 2050s (2040-2069) and 2080s (2070-2099) for representative concentration pathway (RCP) 4.5 and RCP 8.5, including mean annual temperature (Temp), annual precipitation (Precip), peak snow water equivalent (SWE), annual runoff, annual actual evapotranspiration (AET), and annual groundwater recharge. Blue and pink shading indicate a significant ($p < 0.05$) increase or decrease relative to the baseline period, as assessed with the two-sided Mann-Whitney U test. Arrows are added for clarity where boxplot shading is unclear.**

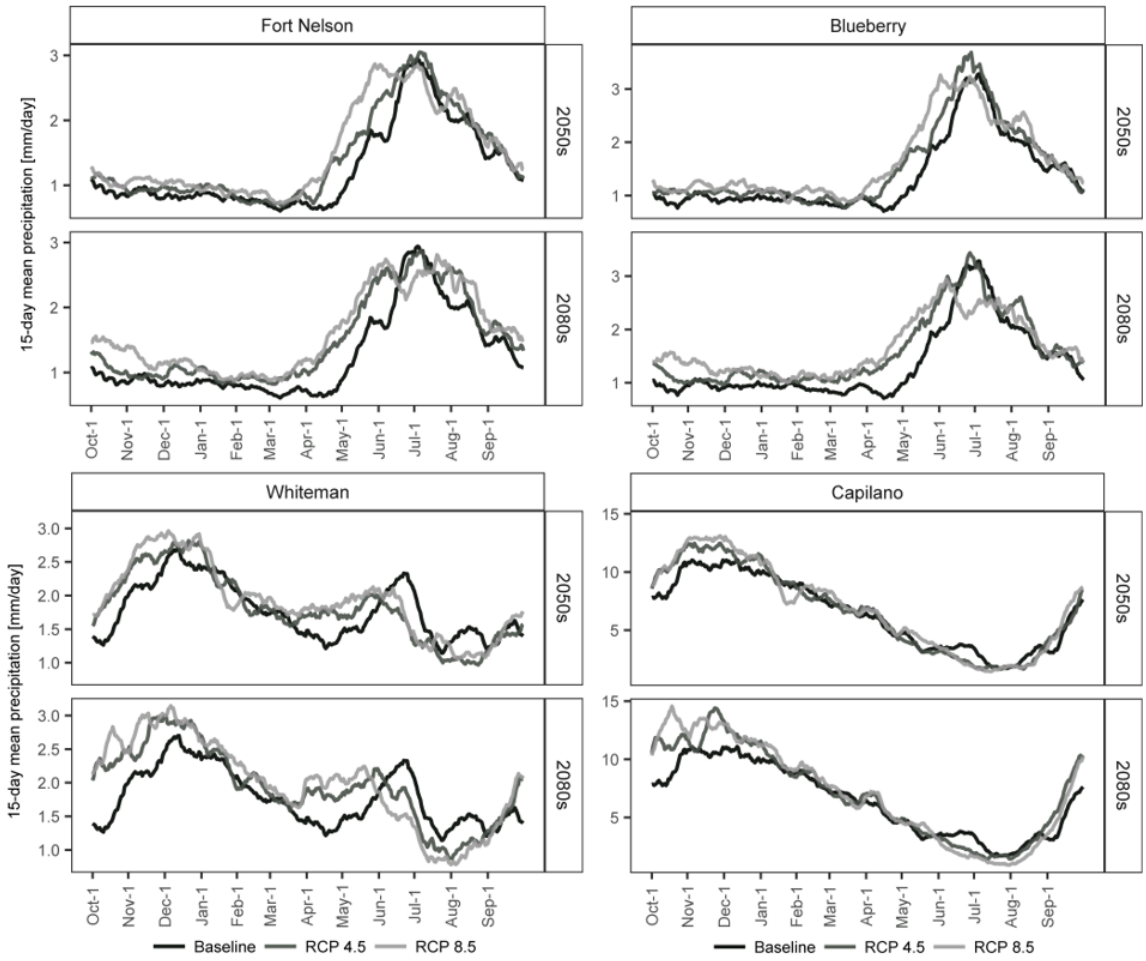

Figure S4.2 Smoothed 15-day mean precipitation rate for the 1980s baseline (1970-1999) versus 2050s (2040-2069) and 2080s (2070-2099) for representative concentration pathway (RCP) 4.5 and RCP 8.5.

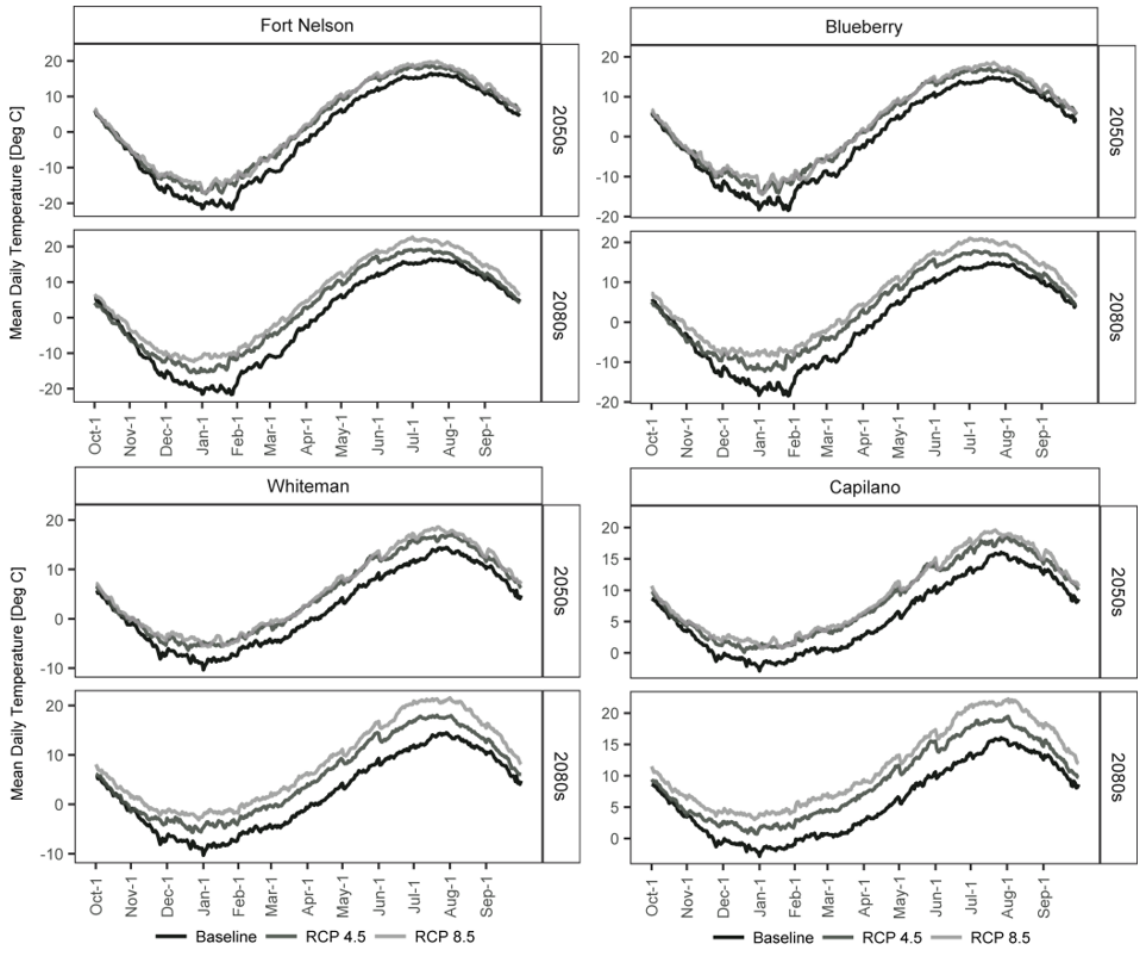

Figure S4.3 Mean daily temperature for the 1980s baseline (1970-1999) versus 2050s (2040-2069) and 2080s (2070-2099) for representative concentration pathway (RCP) 4.5 and RCP 8.5.

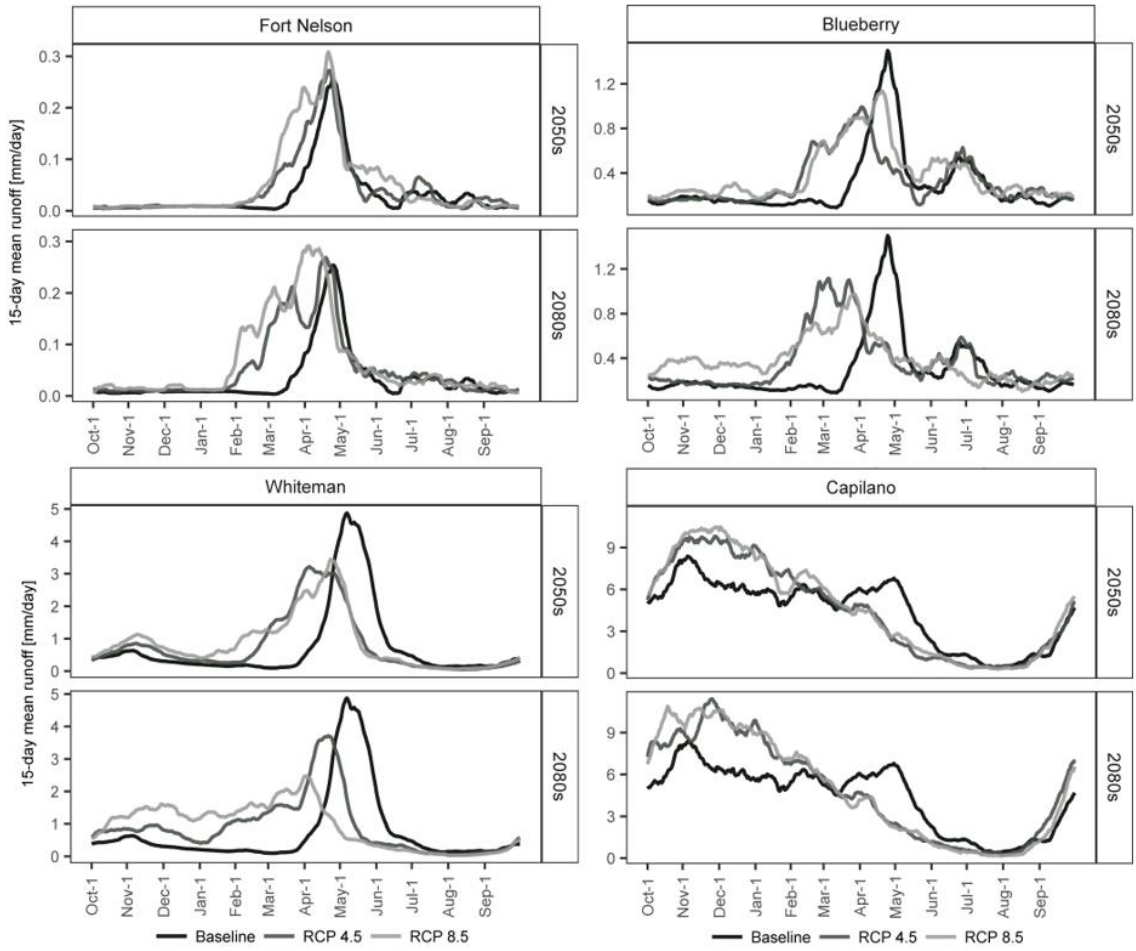

Figure S4.4 Smoothed 15-day mean daily runoff for the 1980s baseline (1970-1999) versus 2050s (2040-2069) and 2080s (2070-2099) for representative concentration pathway (RCP) 4.5 and RCP 8.5.

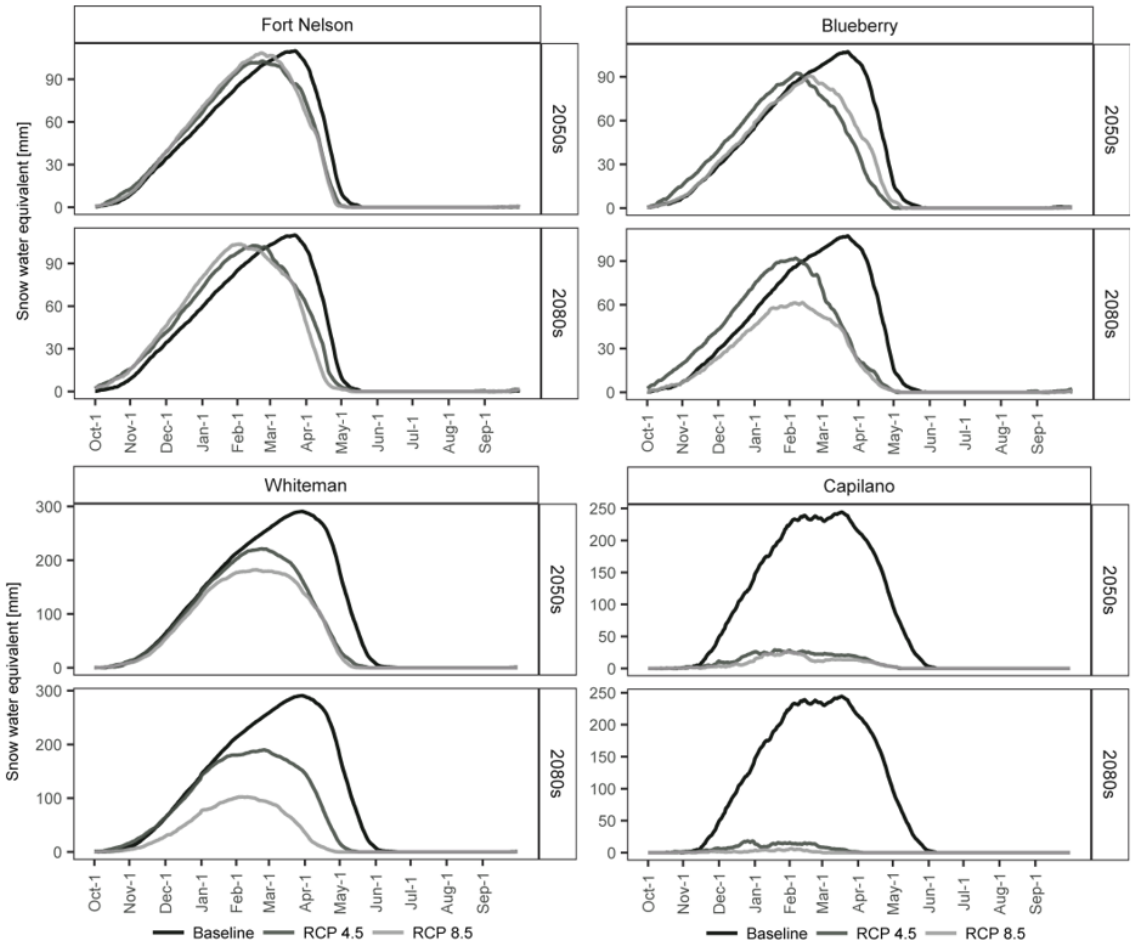

Figure S4.5 Mean daily snow water equivalent for the 1980s baseline (1970-1999) versus 2050s (2040-2069) and 2080s (2070-2099) for representative concentration pathway (RCP) 4.5 and RCP 8.5.

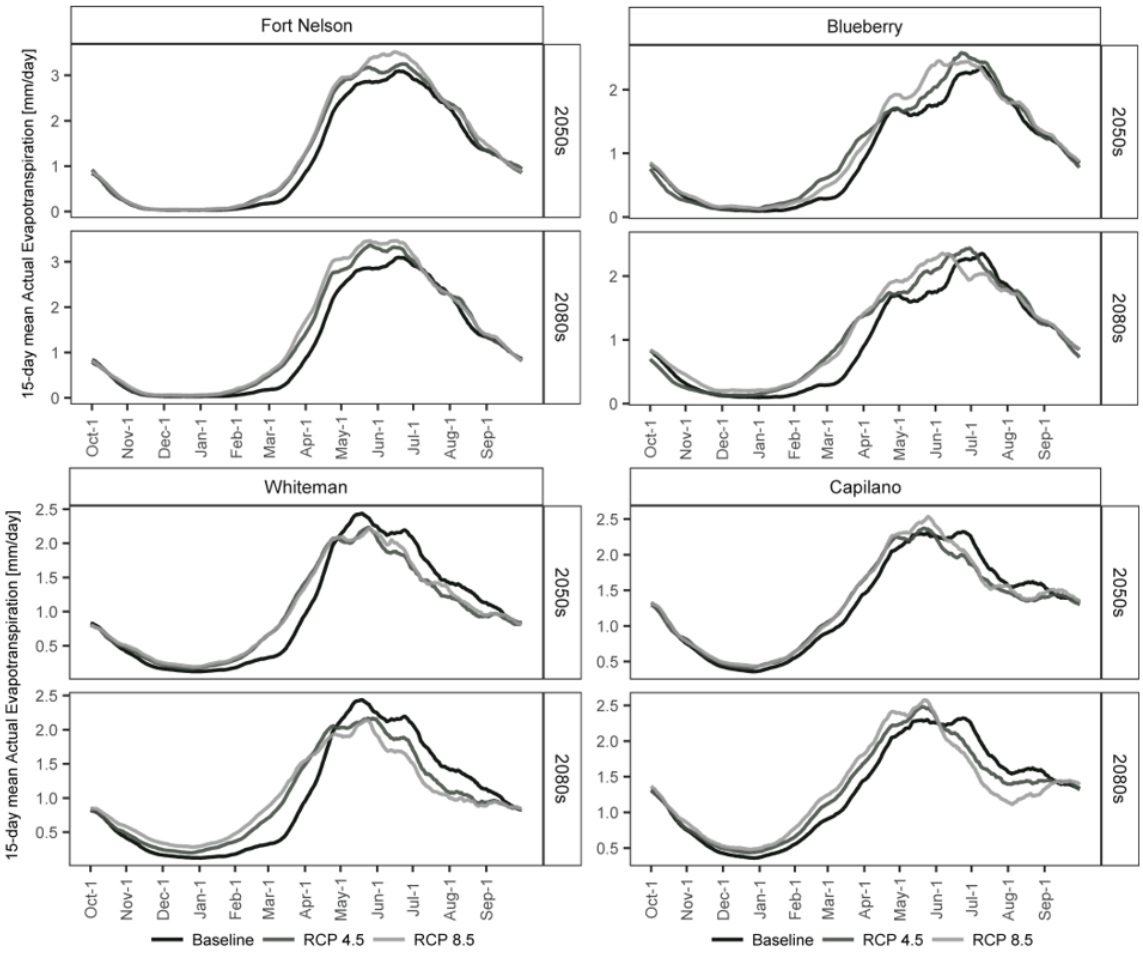

Figure S4.6 Smoothed 15-day mean actual evapotranspiration rate for the 1980s baseline (1970-1999) versus 2050s (2040-2069) and 2080s (2070-2099) for representative concentration pathway (RCP) 4.5 and RCP 8.5.

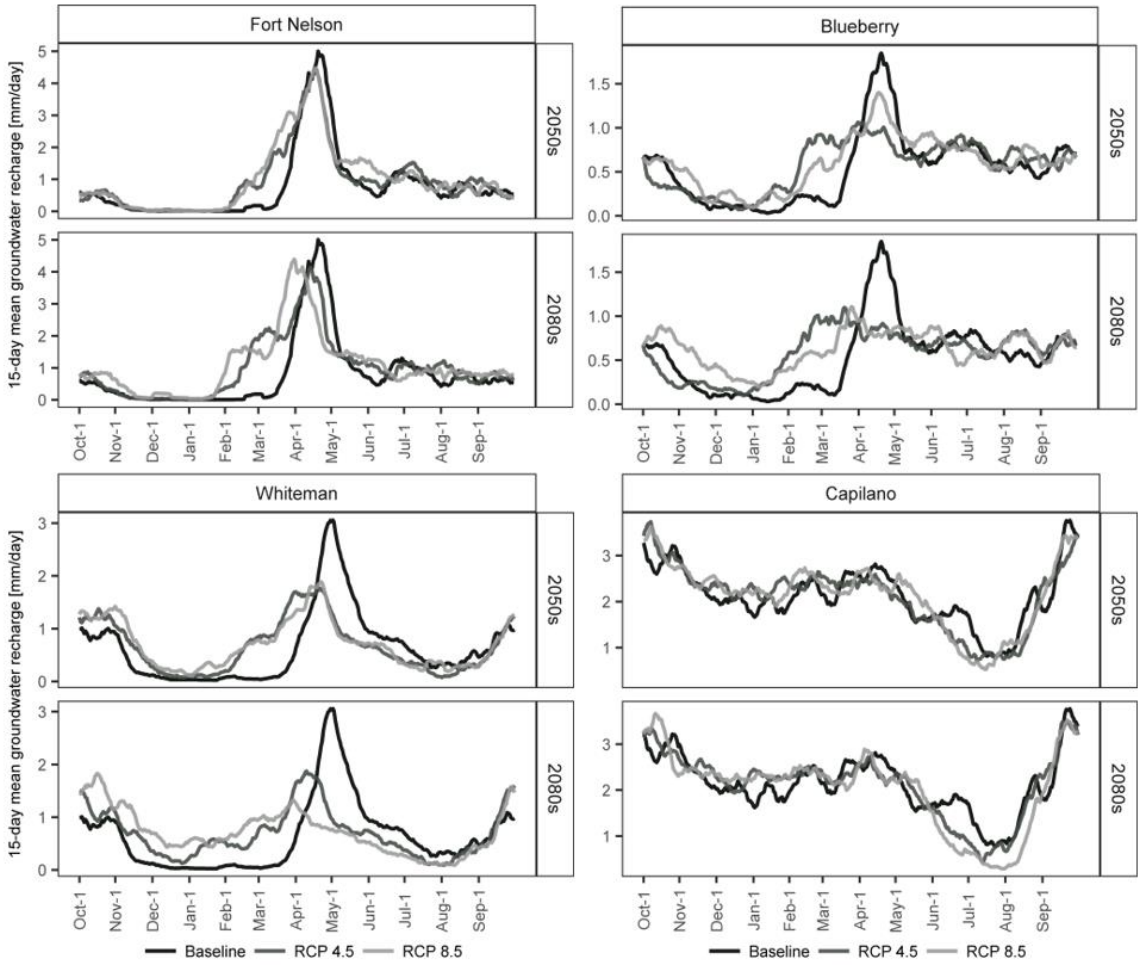

Figure S4.7 Smoothed 15-day mean groundwater recharge rate for the 1980s baseline (1970-1999) versus 2050s (2040-2069) and 2080s (2070-2099) for representative concentration pathway (RCP) 4.5 and RCP 8.5.

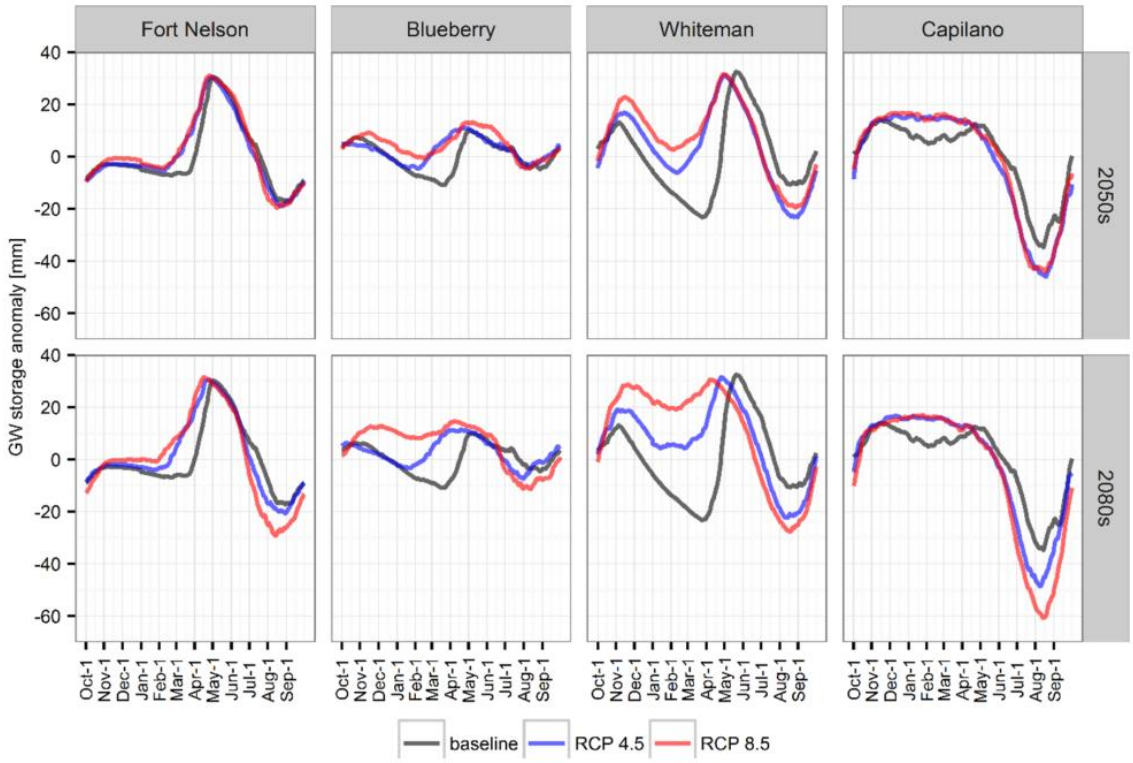

Figure S4.8 **Mean daily groundwater (GW) storage anomaly (calculated as the mean *daily* value minus the baseline mean *annual* value) for the 1980s baseline (1970-1999) versus 2050s (2040-2069) and 2080s (2070-2099) for representative concentration pathway (RCP) 4.5 and RCP 8.5.**

Table S4.7 Frequency (fraction of years) of dry (D), warm (W), and warm and dry (W&D) snow droughts. Baseline 1980s (1970-1999) versus 2050s (2040-2069) and 2080s (2070-2099) for representative concentration pathways (RCP) 4.5 and 8.5.

		Fort Nelson		Blueberry		Whiteman		Capilano	
1980s	D	0.16		0.16		0.22		0.07	
	W	0.08		0.09		0.07		0.30	
	W&D	0.30		0.26		0.22		0.21	
	RCP	***4.5***	***8.5***	***4.5***	***8.5***	***4.5***	***8.5***	***4.5***	***8.5***
2050s	D	0.04	--	0.01	--	0.01	--	0.01	--
	W	0.23	0.20	0.34	0.39	0.37	0.59	0.54	0.63
	W&D	0.27	0.19	0.29	0.19	0.33	0.19	0.41	0.34
2080s	D	--	--	--	--	--	--	--	--
	W	0.28	0.32	0.32	0.71	0.51	0.79	0.60	0.60
	W&D	0.22	0.08	0.22	0.04	0.20	0.13	0.40	0.40

Table S4.8 Mean severity (fraction below baseline normal) of dry (D), warm (W), and warm and dry (W&D) snow droughts. Baseline 1980s (1970-1999) versus 2050s (2040-2069) and 2080s (2070-2099) for representative concentration pathways (RCP) 4.5 and 8.5.

		Fort Nelson		Blueberry		Whiteman		Capilano	
1980s	D	0.20		0.18		0.17		0.45	
	W	0.16		0.19		0.12		0.47	
	W&D	0.21		0.22		0.23		0.56	
	RCP	**4.5**	**8.5**	**4.5**	**8.5**	**4.5**	**8.5**	**4.5**	**8.5**
2050s	D	0.31	0.03	0.16	0.23	0.29	0.16	0.70	0.79
	W	0.13	0.16	0.20	0.26	0.20	0.27	0.82	0.82
	W&D	0.23	0.22	0.27	0.23	0.25	0.29	0.82	0.88
2080s	D	--	--	--	--	0.34	--	0.51	--
	W	0.15	0.22	0.20	0.37	0.22	0.49	0.84	0.92
	W&D	0.23	0.23	0.27	0.49	0.31	0.53	0.84	0.95

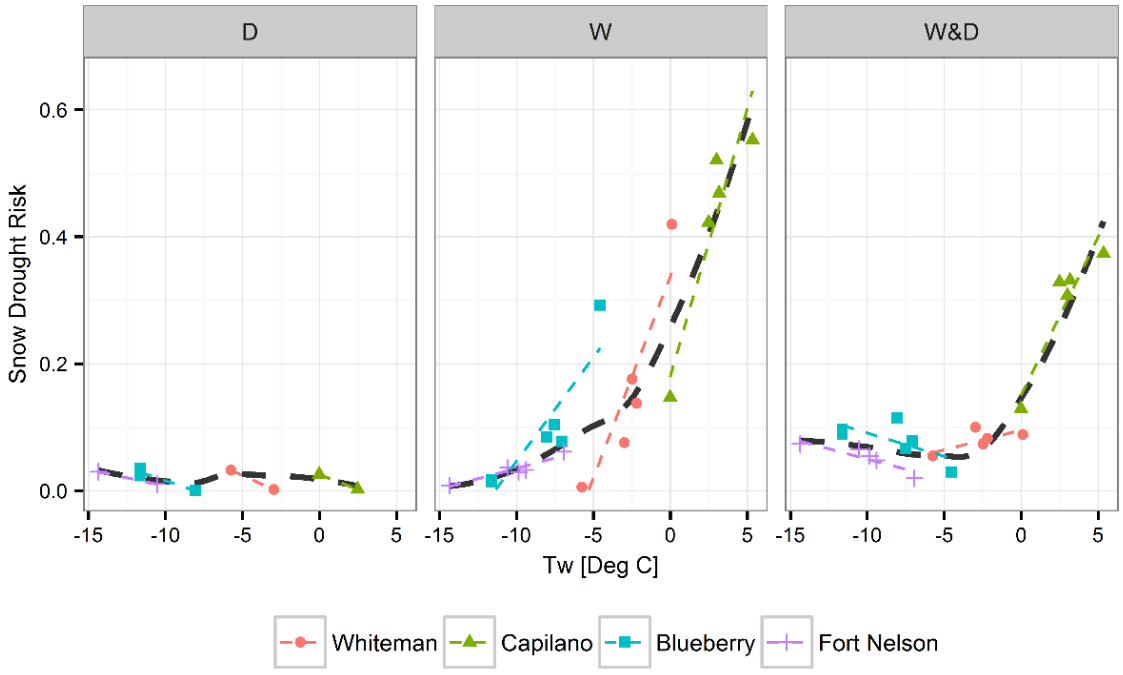

Figure S4.9 **Snow drought risk (frequency x severity) for dry (D), warm (W), and warm and dry (W&D) snow droughts versus the mean winter (1-Nov to 1-Apr) temperature (T_w). Linear trend lines plotted by watershed and local regression lines (dark gray) plotted for all data points to highlight the non-linear relationship between risk and Tw.**

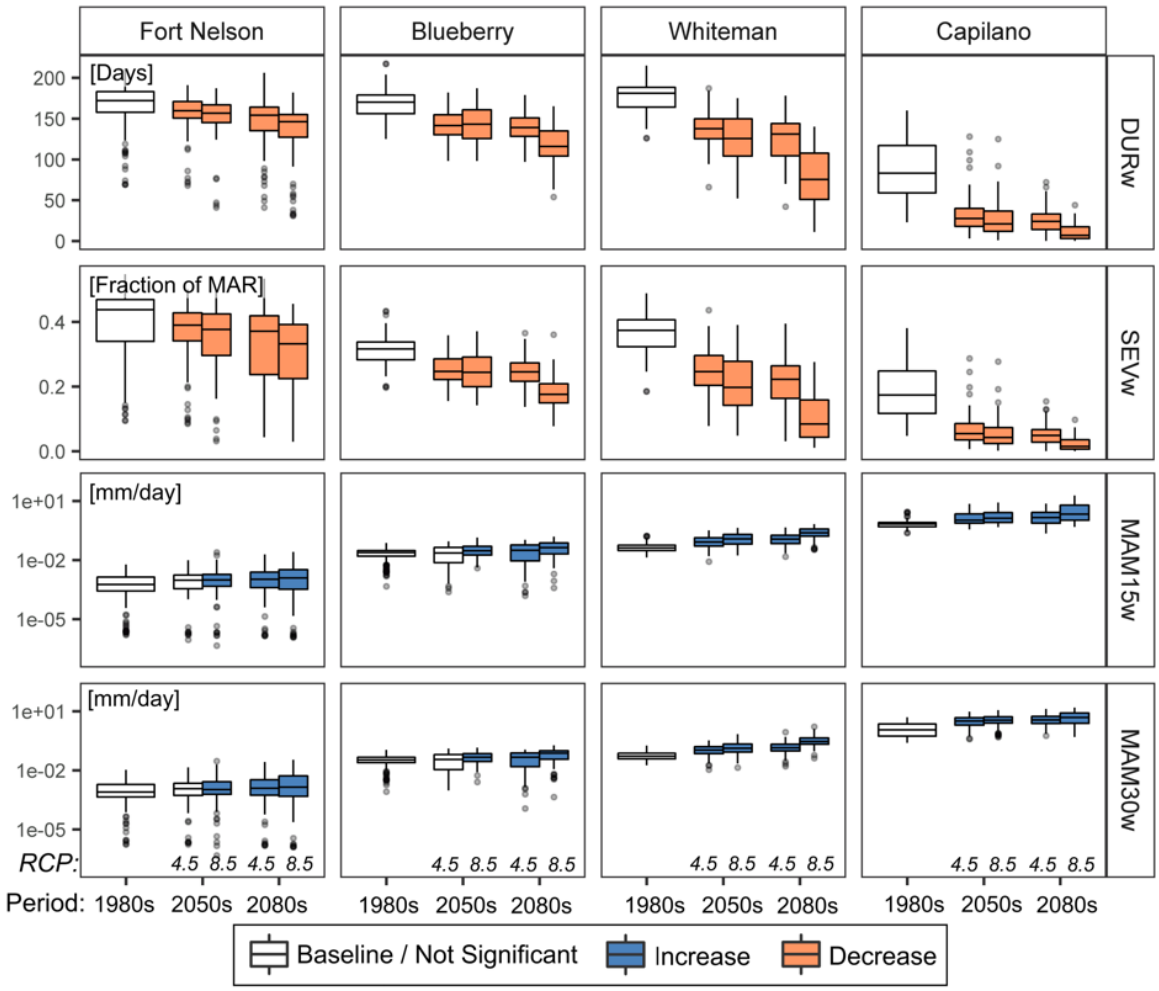

Figure S4.10 Winter low flow regime indicators for the 1980s baseline (1970-1999) versus 2050s (2040-2069) and 2080s (2070-2099) for representative concentration pathway (RCP) 4.5 and RCP 8.5. Blue and pink shading indicate a significant ($p < 0.05$) increase or decrease relative to the baseline period, as assessed with the two-sided Mann-Whitney U test. Figure 4.5 (in main text) shows summer low flow regime indicators.

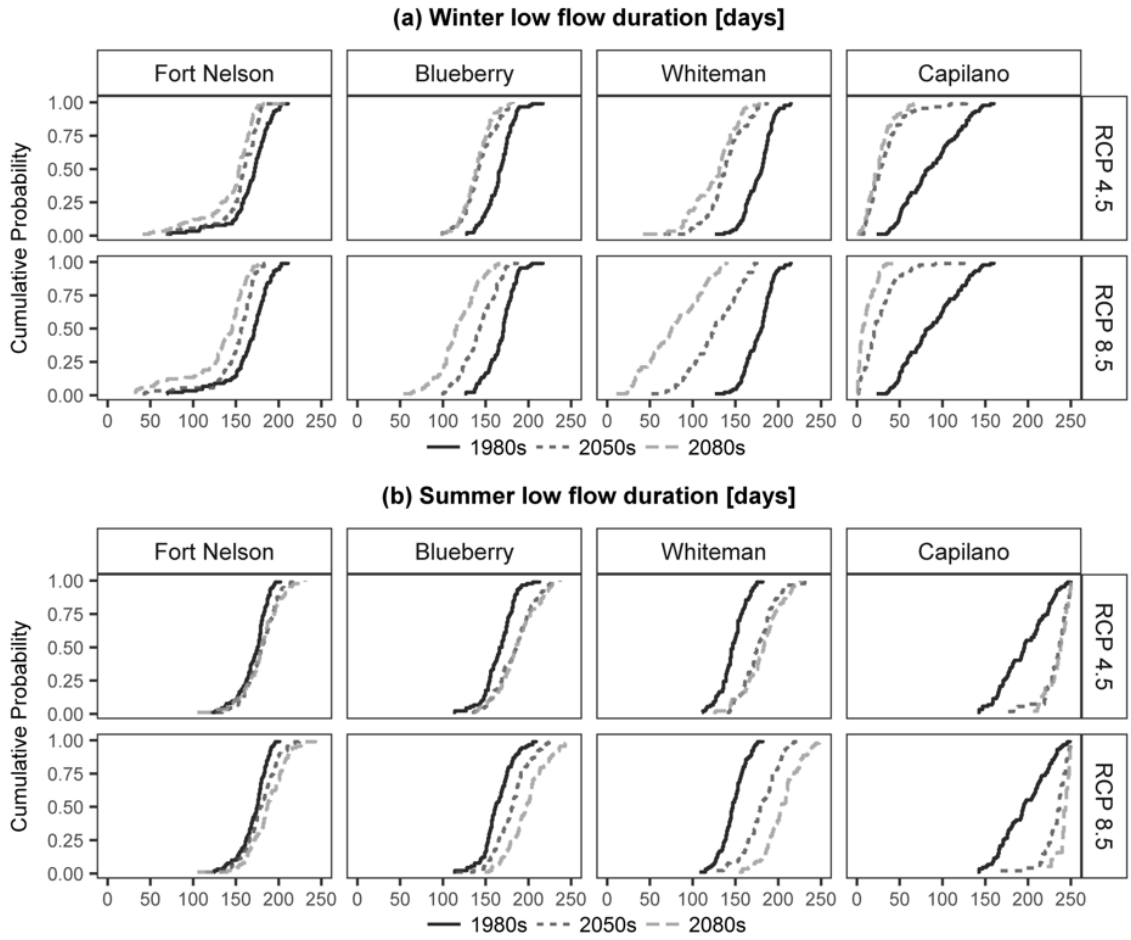

Figure S4.11 Empirical cumulative distributions for (a) winter low flow duration and (b) summer low flow duration for the 1980s baseline (1970-1999) versus 2050s (2040-2069) and 2080s (2070-2099) for representative concentration pathway (RCP) 4.5 and RCP 8.5. A shift to the right of the 1980s baseline indicates increased low flow duration, while a shift to the left indicates decreased low flow duration.

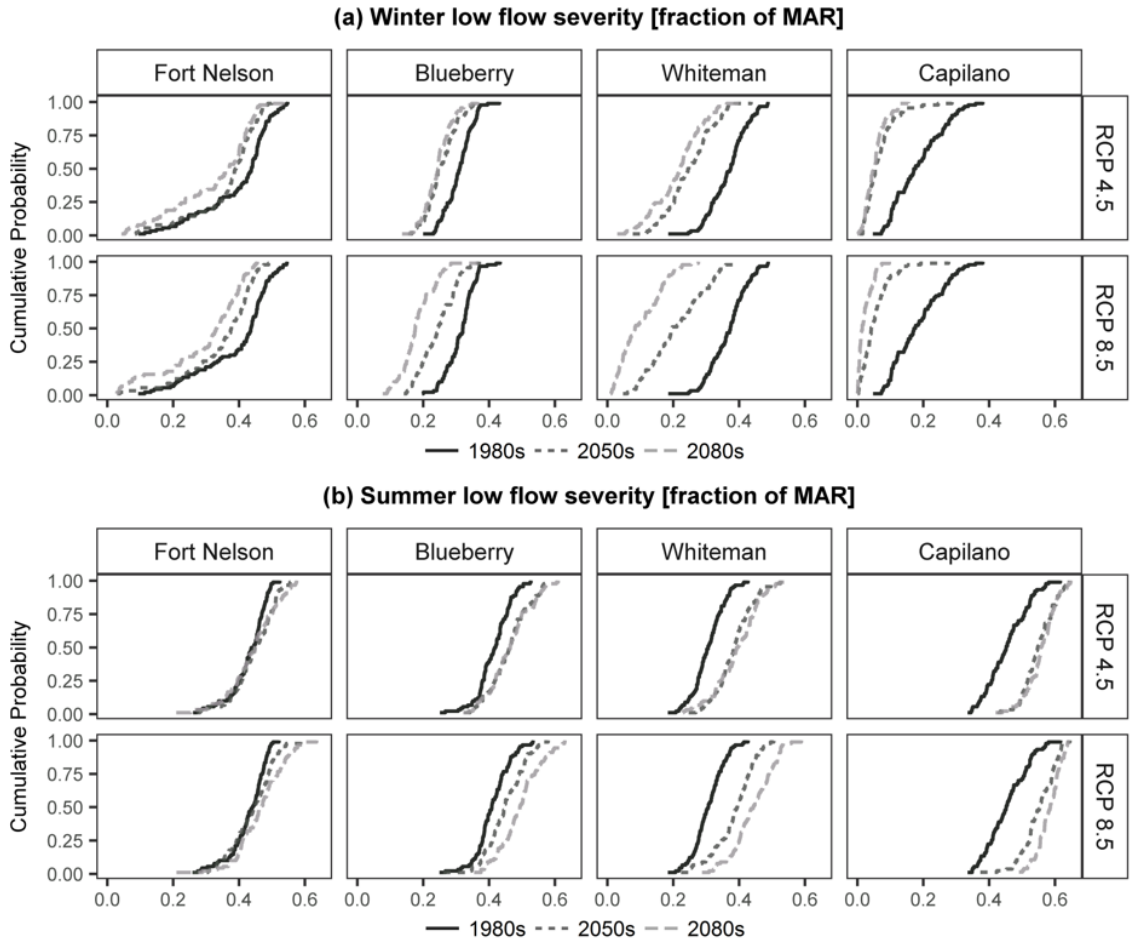

Figure S4.12 Empirical cumulative distributions for (a) winter low flow severity and (b) summer low flow severity for the 1980s baseline (1970-1999) versus 2050s (2040-2069) and 2080s (2070-2099) for representative concentration pathway (RCP) 4.5 and RCP 8.5. MAR = Mean Annual Runoff for the baseline period. A shift to the right of the 1980s baseline indicates increased low flow severity, while a shift to the left indicates decreased low flow severity.

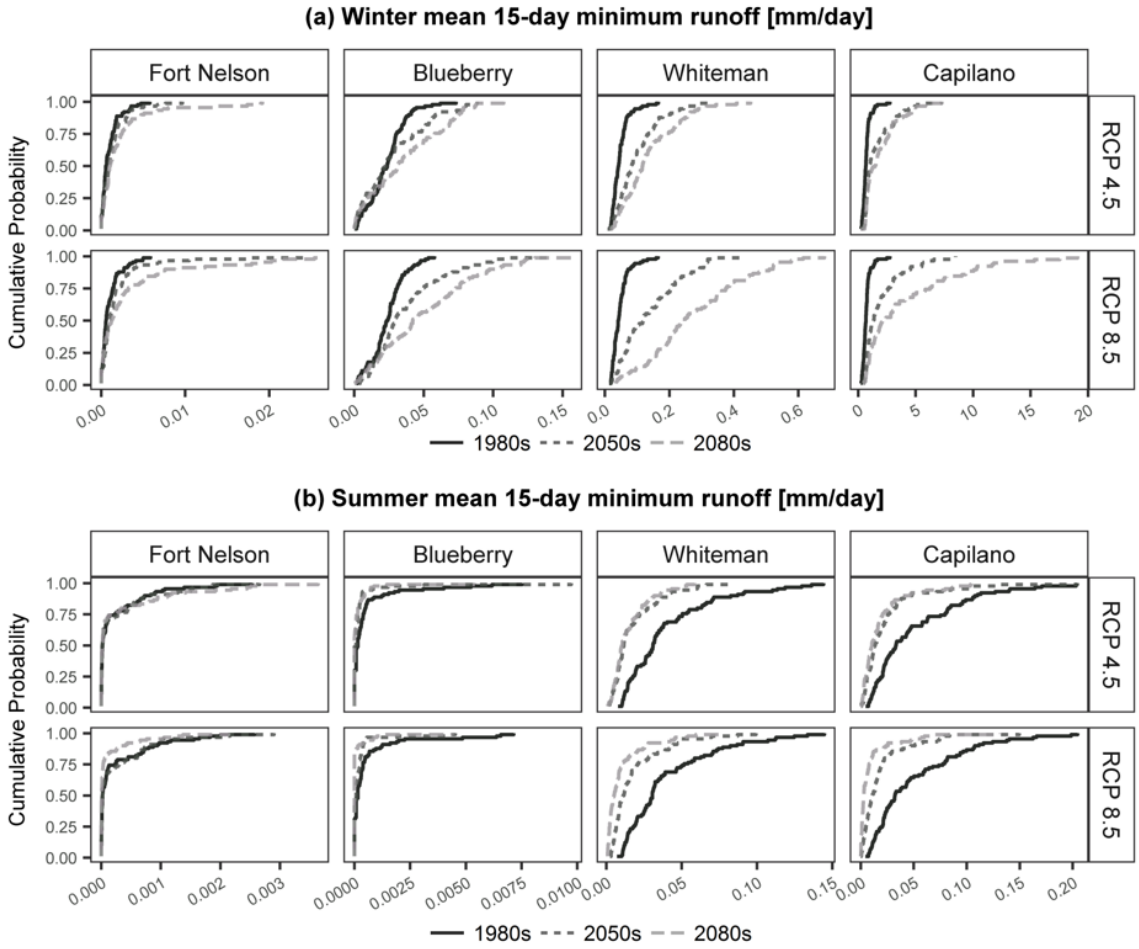

Figure S4.13 Empirical cumulative distributions for (a) winter and (b) summer mean 15-day minimum runoff for the 1980s baseline (1970-1999) versus 2050s (2040-2069) and 2080s (2070-2099) for representative concentration pathway (RCP) 4.5 and RCP 8.5. A shift to the left of the 1980s baseline indicates increased low flow severity, i.e. lower low flows, while a shift to the right indicates decreased low flow severity, i.e. higher low flows.

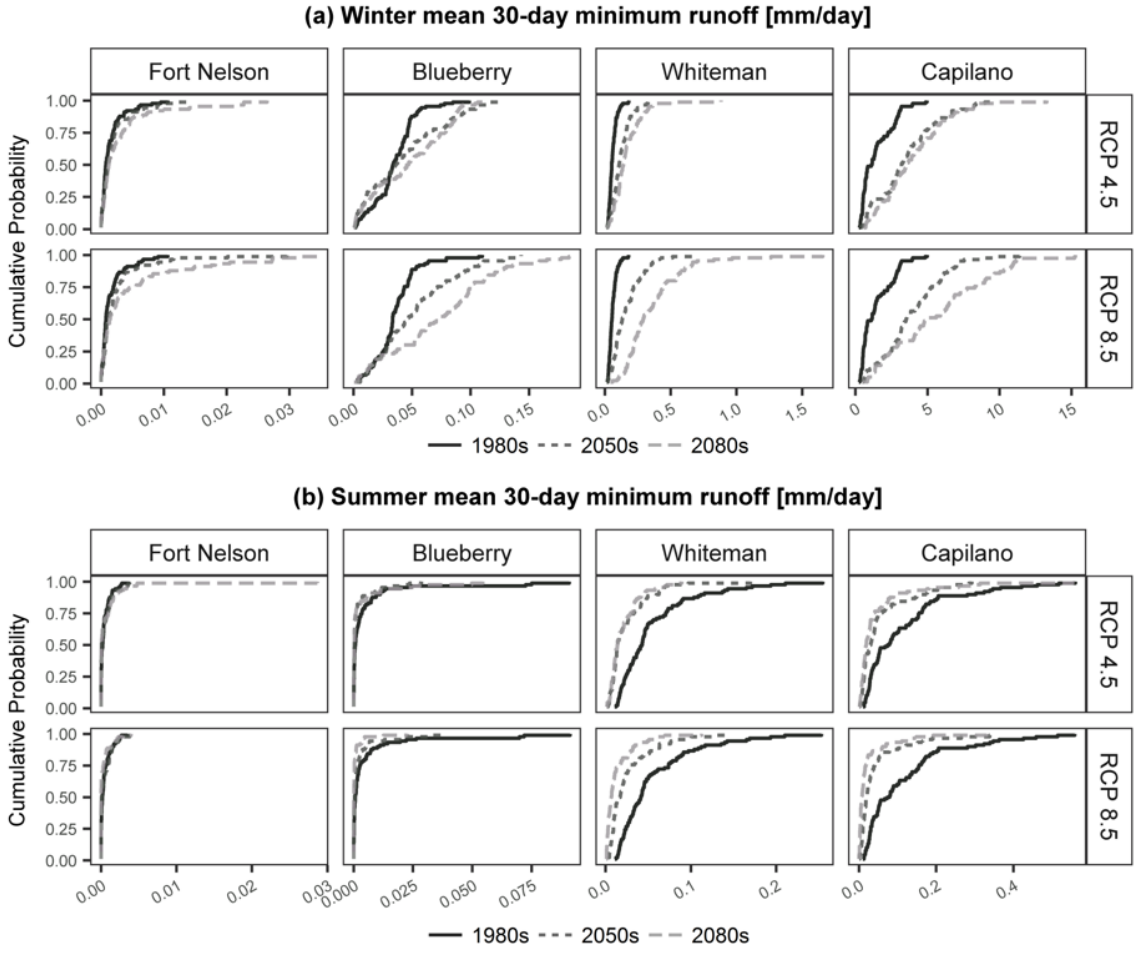

Figure S4.14 Empirical cumulative distributions for (a) winter and (b) summer mean 30-day minimum runoff for the 1980s baseline (1970-1999) versus 2050s (2040-2069) and 2080s (2070-2099) for representative concentration pathway (RCP) 4.5 and RCP 8.5. A shift to the left of the 1980s baseline indicates increased low flow severity, i.e. lower low flows, while a shift to the right indicates decreased low flow severity, i.e. higher low flows.

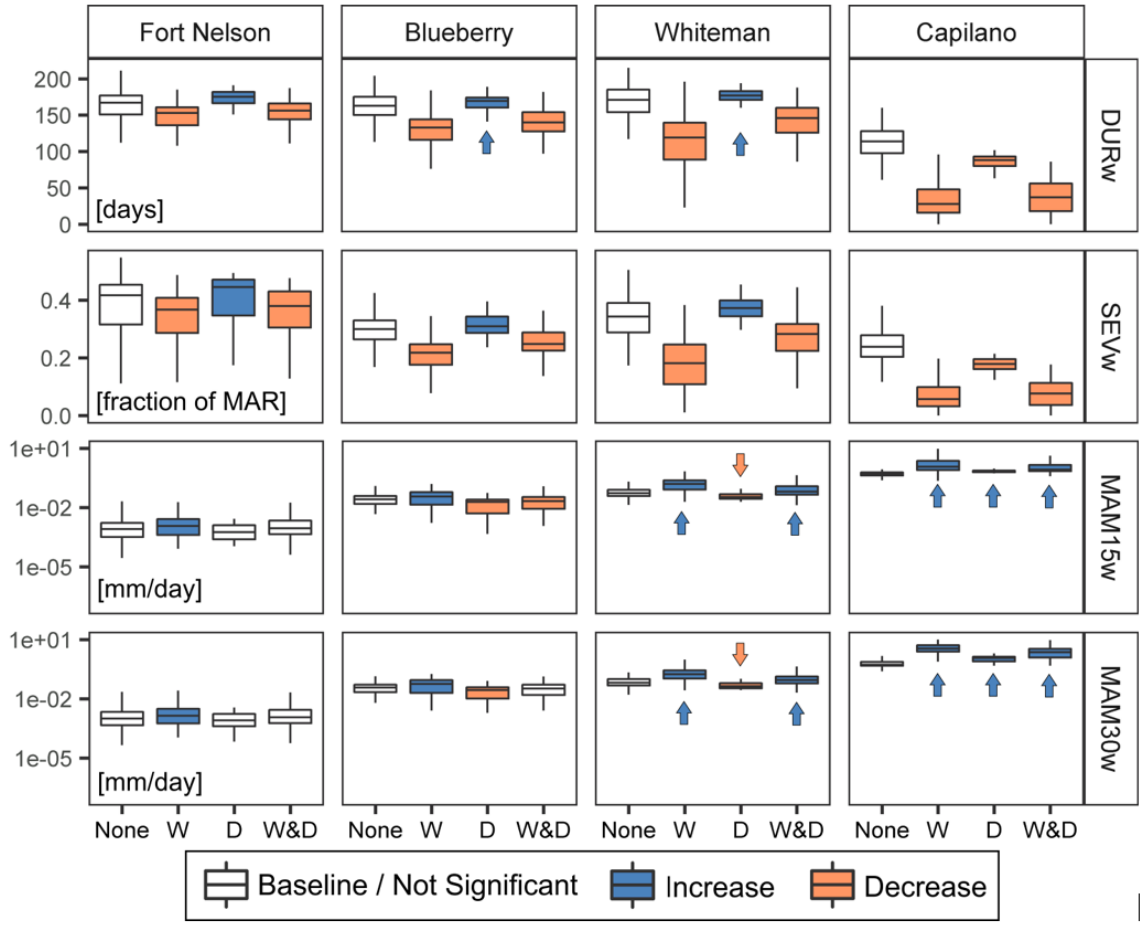

Figure S4.15 Snow drought impacts on winter low flows by snow drought type, including years without snow drought (None) and years with warm (W), dry (D), and warm and dry (W&D) snow droughts. Blue and pink shading indicate a significant ($p < 0.05$) increase or decrease relative to the baseline period, as assessed with the two-sided Mann-Whitney U test. Abbreviations are as in Table 4.2 Error! Reference source not found.**. Arrows are added for clarity where boxplot shading is unclear. Figure 4.6 (in main text) shows the summer low flow regime indicators.**

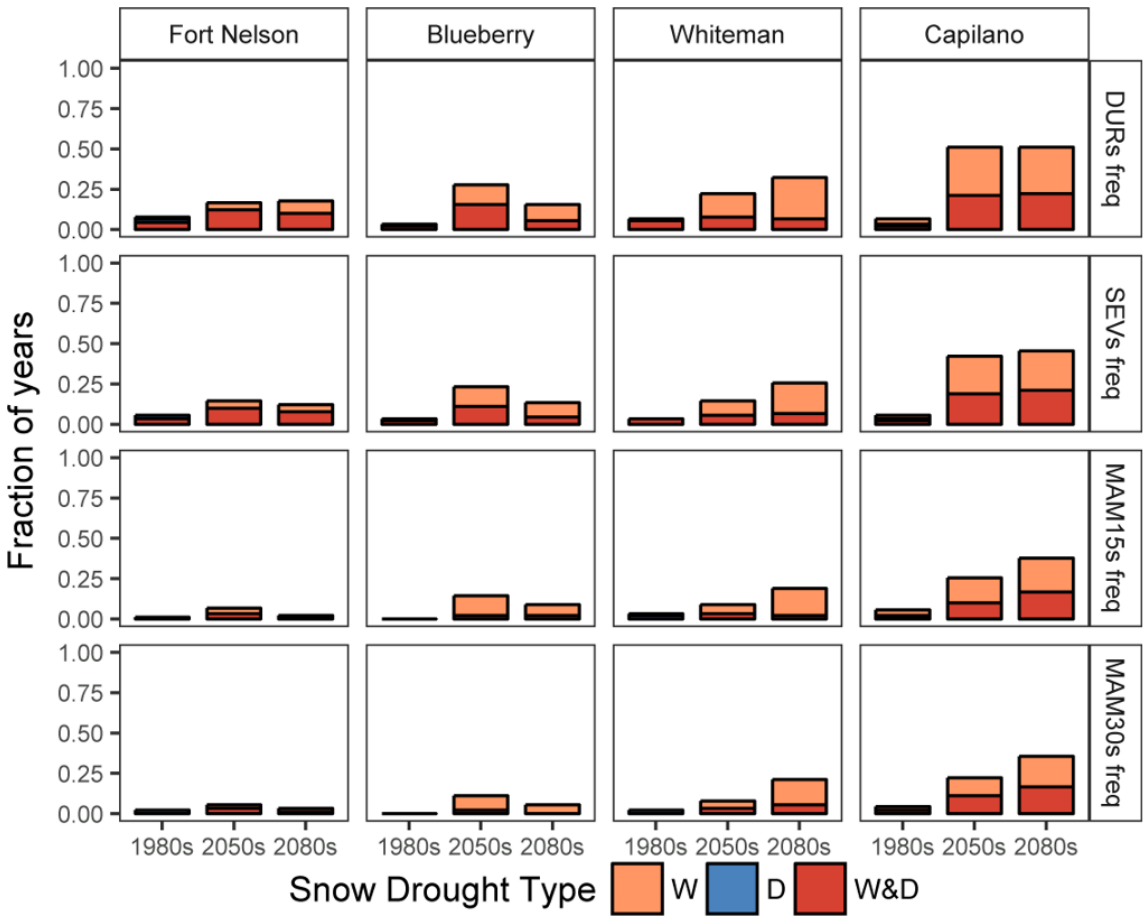

Figure S4.16 Frequency of snow drought propagation into summer streamflow drought, in the absence of summer precipitation deficit, by snow drought type: warm (W), Dry (D), warm and dry (W&D), RCP 4.5. Figure 4.7 (in main text) shows the same plot for RCP 8.5.

Appendix D.

Chapter 5 Supplemental Information: Daily to Hourly Climate Time Series Disaggregation

To disaggregate the daily downscaled climate projections to the hourly time series required for the Cold Regions Hydrological model, the observed hourly data were first subset to full days (24 hours) with no missing observations. For each day in the downscaled daily time series, one day of observed hourly data was then randomly selected based on temporal occurrence and precipitation amount. For example, for each day in the daily time series, a preliminary subset of hourly data was selected based on a 30-day centered window, i.e. from days of the year within ±15 days of the day of the year of respective daily downscaled data. The set of days of observed hourly data was then further subset to match precipitation of the daily data (binary: Yes or No). For days in the daily time series with precipitation, further subsetting of the set of days of observed hourly data was completed based on quartile matching of the daily precipitation amount. In this step, quartiles of daily precipitation were calculated from the subset of observed hourly data, and the set of days of observed hourly data was then subset to days with a precipitation amount within the quartile that matched (i.e. contained) the precipitation amount of the daily data. One day (24 hours) of the observed hourly data was then randomly selected from the final subset.

From the final selected 24 hours of observed climate data, hourly humidity and wind speed observations were used without transformation. The diurnal patterns of the hourly temperature and precipitation observations were used to disaggregate the daily time series to hourly as described in the following sections.

Temperature disaggregation

The observed hourly temperatures were transformed into a normalized diurnal temperature curve, ranging from 0 (minimum daily temperature) to 1 (maximum daily temperature) using Equation S5.1.

$$T_{norm} = \frac{(T - min(T))}{(\max(T) - min(T))} \quad [S5.1]$$

Where T is the set of hourly temperatures for the randomly selected day. The normalized diurnal temperature curve was then used to disaggregate the daily maximum and minimum temperature from the downscaled time series to hourly using Equation S5.2:

$$t = \left(T_{norm} \times \left(t_{d,max} - t_{d,min}\right)\right) + t_{d,min} \quad [S5.2]$$

Where t is the disaggregated temperature time series for one day. T_{norm} is the diurnal temperature curve from Equation S5.1, and $t_{d,max}$ and $t_{d,min}$ are the downscaled daily maximum and minimum temperature.

Precipitation disaggregation

For days with precipitation, the daily precipitation was disaggregated using Equation S5.3:

$$p = \frac{P}{\sum_1^{24} P} \times p_d \quad [S5.3]$$

Where *p* is the disaggregated precipitation time series for one day, and p_d is the downscaled daily precipitation, and P is the observed hourly precipitation.

Appendix E.

Chapter 5 Supplemental Information: Gauge Time Series Comparison

The plots below show observed daily runoff time series for the Beatton River (15,600 km^2; ID 07FC001) and two sub-watersheds: the Blueberry River (1,770 km^2; ID 07FC003) and St. John Creek (201 km^2; ID 07FC002). Only years with no missing data for all three watersheds are included. These plots show that the hydrographs of the two sub-watersheds (St. John Creek and Blueberry River) differ significantly from each other and from the Beatton River watershed in which they are contained. St. John Creek, the smallest watershed, consistently exhibits an earlier spring snowmelt peak and lower summer rain event peaks compared to the Blueberry and Beatton watersheds.

Similarity and error statistics between the three watersheds (Beatton, Blueberry, and St. John) are shown in Table S5.1. The Nash-Sutcliffe (1970) efficiency criterion (NSE) is often used to evaluate the performance of hydrological models; however, it puts greater emphasis on high flows. Therefore, the volumetric efficiency criterion (VE), which was proposed by Criss & Winston (2008) to overcome problems with NSE, is also reported in Table S5.1. For the calculation of NSE and VE, the smaller watershed was treated as the observed data and the larger treated as the simulated data. Thus, the similarity measures give an indication of how well the hydrograph of the larger watershed matches the hydrograph of the smaller watershed. The common error statistics root mean square error (RMSE) and mean absolute error (MAE) are also reported.

NSE values range from –Inf to 1, with 0 indicating the model predictions are as accurate as the mean of the observed data and 1 indicating a perfect match. VE represents the fraction of water delivered at the proper time. VE values range from 0 to 1 and, where 1 represents a perfect match. Negative values represent the volumetric mismatch (Criss & Winston, 2008).

The hydrographs of the two larger watersheds (Beatton and Blueberry) have the greatest similarity. Neither the Beatton nor the Blueberry hydrographs are a good fit with

the hydrograph for the small St. John Creek watershed, as indicated by the low NSE and VE values and high RMSE values in Table S5.1.

Table S5.1 Similarity statistics between Beatton, Blueberry, and St. John Creek hydrographs.

	Beatton (SIM) | Blueberry (OBS)	Beatton (SIM) | St. John (OBS)	Blueberry (SIM) | St. John (OBS)
Nash-Sutcliffe efficiency	0.59	0.35	0.04
Volumetric efficiency	0.44	-0.08	0.00
Root Mean Square Error [mm]	0.48	2.75	2.28
Mean Absolute Error [mm]	0.18	0.30	0.28

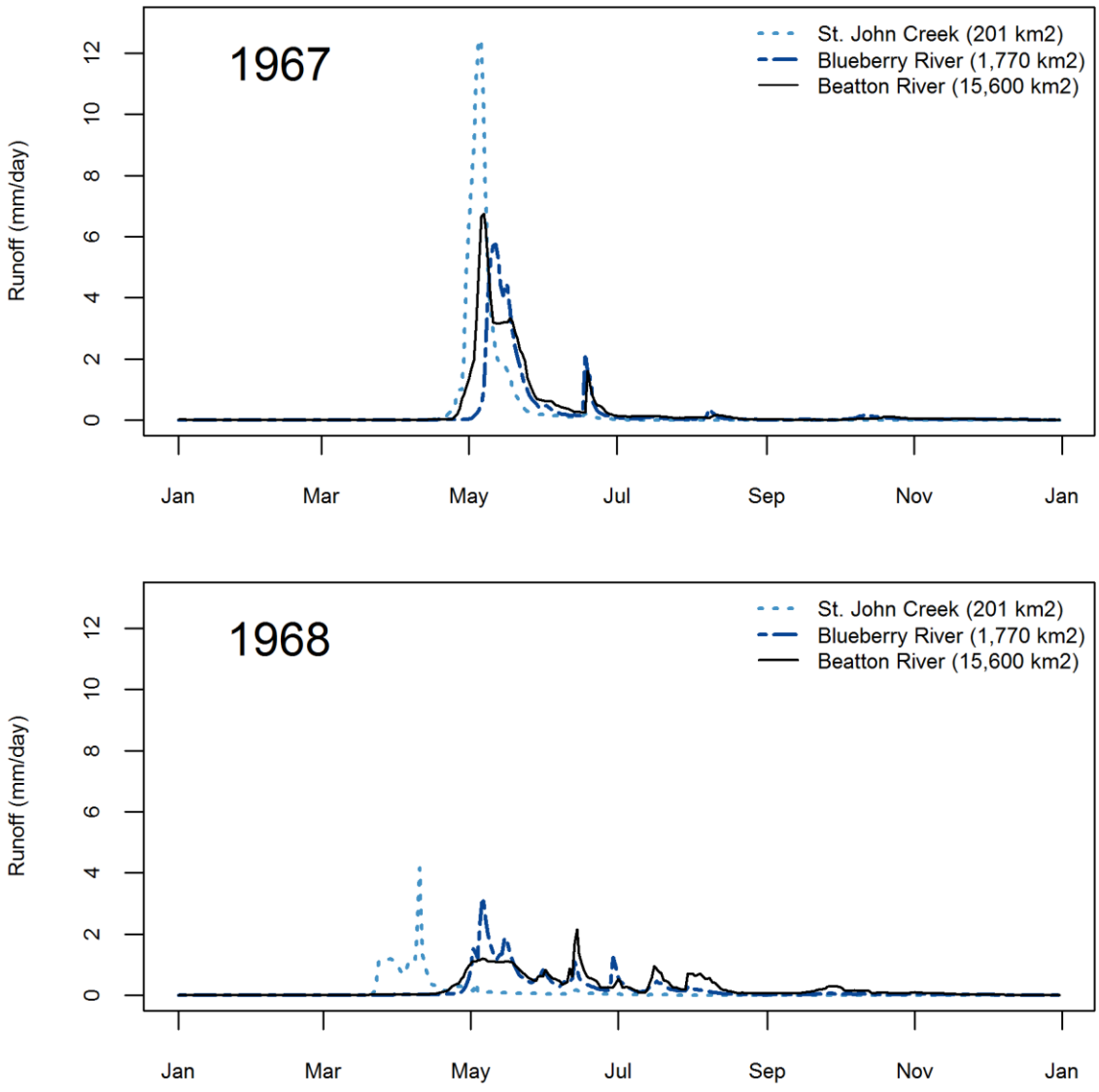
1967
St. John Creek (201 km2)
Blueberry River (1,770 km2)
Beatton River (15,600 km2)
Runoff (mm/day)
0
2
4
6
8
10
12
Jan
Mar
May
Jul
Sep
Nov
Jan
1968
St. John Creek (201 km2)
Blueberry River (1,770 km2)
Beatton River (15,600 km2)
Runoff (mm/day)
0
2
4
6
8
10
12
Jan
Mar
May
Jul
Sep
Nov
Jan

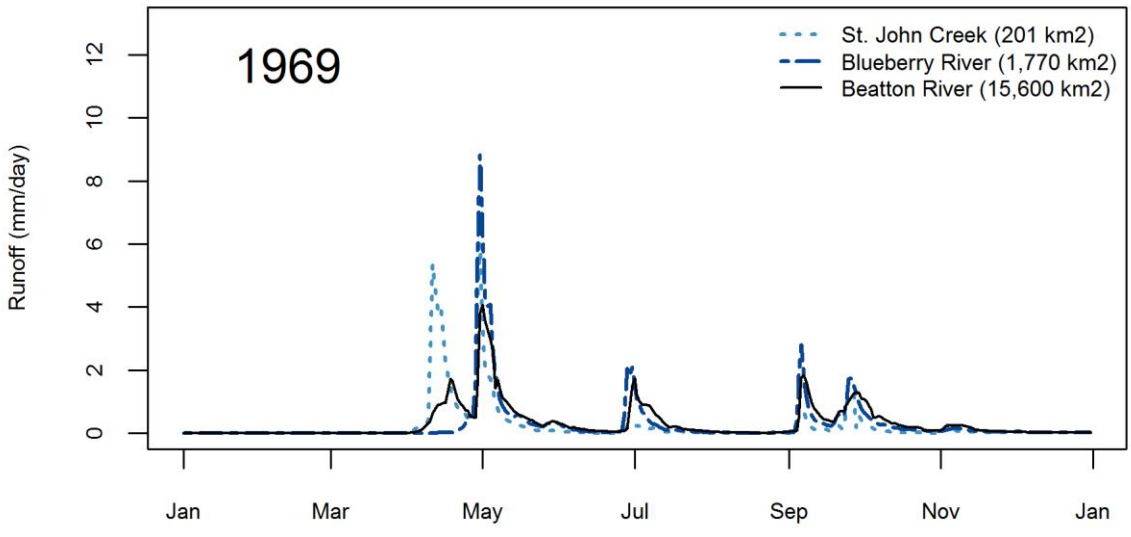
1969
St. John Creek (201 km2)
Blueberry River (1,770 km2)
Beatton River (15,600 km2)
Runoff (mm/day)
0
2
4
6
8
10
12
Jan
Mar
May
Jul
Sep
Nov
Jan

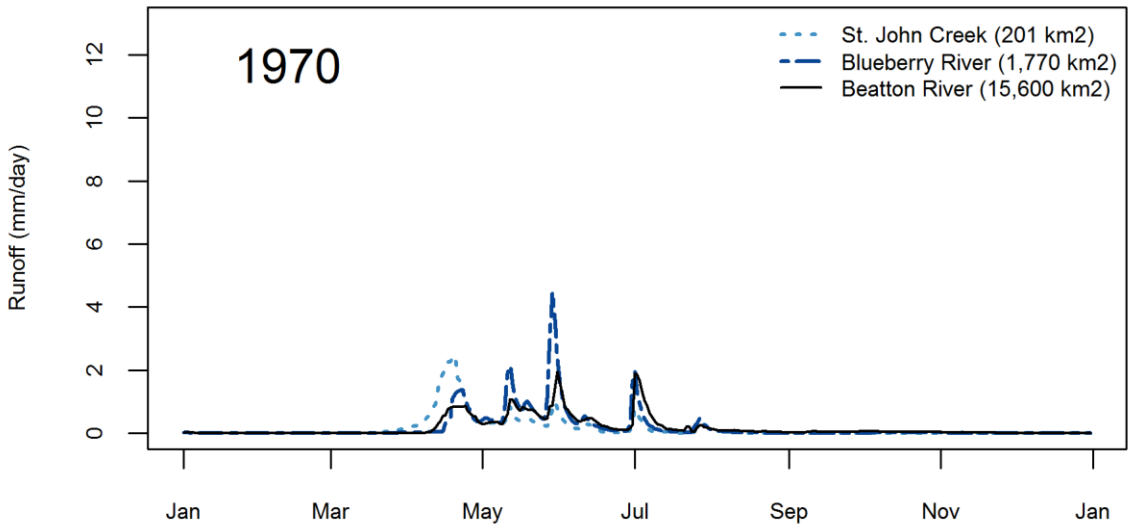
1970
St. John Creek (201 km2)
Blueberry River (1,770 km2)
Beatton River (15,600 km2)
Runoff (mm/day)
0
2
4
6
8
10
12
Jan
Mar
May
Jul
Sep
Nov
Jan

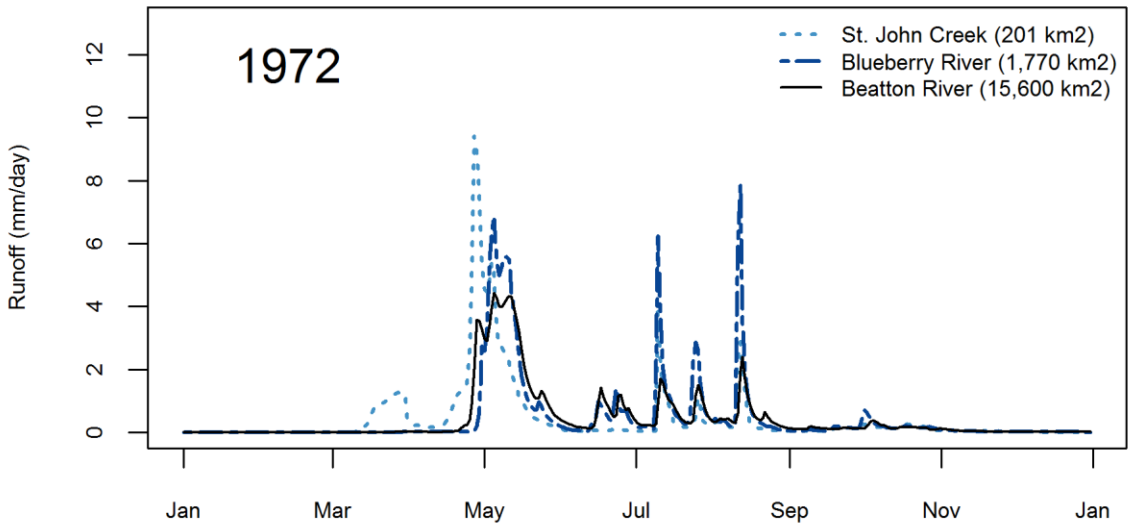
1972
St. John Creek (201 km2)
Blueberry River (1,770 km2)
Beatton River (15,600 km2)
Runoff (mm/day)
0
2
4
6
8
10
12
Jan
Mar
May
Jul
Sep
Nov
Jan

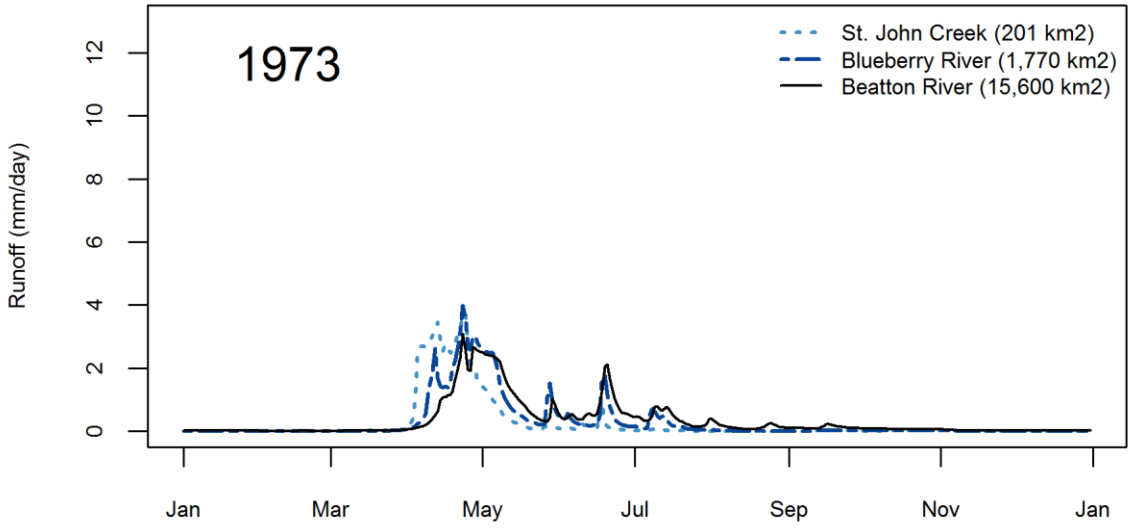
1973
St. John Creek (201 km2)
Blueberry River (1,770 km2)
Beatton River (15,600 km2)
Runoff (mm/day)
0
2
4
6
8
10
12
Jan
Mar
May
Jul
Sep
Nov
Jan